Aalto University
School of Engineering

Jenni Pekkarinen

# Assuring quality of injection molded products by validating design and manufacturability with injection molding simulation

Master's thesis submitted in partial fulfilment of the requirements for the degree of Master of Science in Technology

Espoo, November 24th, 2019

Supervisor: Professor Jouni Partanen
Thesis advisor: Vesa Palojoki, M.Sc. (Tech.)

Aalto University
School of Engineering

Aalto University, P.O. BOX 11000, 00076 AALTO
www.aalto.fi

**Abstract of master's thesis**

**Author** Jenni Pekkarinen

**Title of thesis** Assuring quality of injection molded products by validating design and manufacturability with injection molding simulation

**Master programme** Mechanical Engineering **Code** ENG25

**Thesis supervisor** Professor Jouni Partanen

**Thesis advisor** Vesa Palojoki, M.Sc. (Tech.)

**Date** 24.11.2019 **Number of pages** 151 **Language** English

**Abstract**

The purpose of this thesis is to assure quality of injection molded products by validating their design and manufacturability with injection molding simulation. Goal for this is to validate the product design already in its design phase and to recognize possible risks, in both product and mold designs, which could cause mold failure during injection molding.

To gain confidence to validate design choices based on injection molding simulation, equivalency between simulation and real molding process are studied with one of ABB's current product. For this study, the real molding parameters from production are used for simulation and cooling channels are constructed to imitate the real mold as close as possible. In addition, comparative studies with simplified cooling channels and with default process parameters are conducted to simulate the circumstances when product designer is designing a new product, mold construction and process parameters of which aren't yet known. One additional study was done to see the behavior of polypropylene in a mold constructed for PC-ABS and to analyze the possibility to use polypropylene instead of PC-ABS in already existing mold. Another part of this thesis concerned the possibility to predict mold failure from the simulation results. This study was done by simulating one existing product case where inserts were noticed to have cracks after first tests in molding trials.

The results show that simulation predicts more warping to the product than is seen in the real molding process. Reason for this unexpected high warpage was believed to be in the material data used. Studies with simplified cooling channels and process parameters showed quite consistent values and high differences weren't seen when compared to simulation done with real process parameters. Polypropylene had slightly higher displacements than PC-ABS, but by adjusting the process parameters, it could be most likely used in the mold designed for PC-ABS. Simulation of the mold insert failing case showed some high pressure differences on the insert base, which were analyzed to be the cause for inserts' cracking. High pressure differences resulted from the uneven filling pattern and gate locations. In order to decrease the risk for insert breaking, gate locations were moved, and changes were made to the product design to improve the melt flow pattern and to even the pressure differences. This study showed that by studying the filling pattern and pressure differences over the tool inserts, high risk areas can be identified even before mold construction.

**Keywords** injection molding, injection molding simulation, dynamic loads, mold failure

Aalto-yliopisto
Insinööritieteiden korkeakoulu

Aalto-yliopisto, PL 11000, 00076 AALTO
www.aalto.fi

**Diplomityön tiivistelmä**

**Tekijä** Jenni Pekkarinen

**Työn nimi** Ruiskuvalettavien tuotteiden laadun ja valmistettavuuden varmistaminen ruiskuvalusimuloinnilla

**Maisteriohjelma** Mechanical engineering **Koodi** ENG25

**Työn valvoja** Professori Jouni Partanen

**Työn ohjaaja** Diplomi-insinööri Vesa Palojoki

**Päivämäärä** 24.11.2019 **Sivumäärä** 151 **Kieli** Englanti

## Tiivistelmä

Tämän diplomityön tarkoituksena on tarkastella ruiskuvalettavien tuotteiden laatua ja valmistettavuutta ruiskuvalusimulaation avulla. Työn tavoite on varmistaa tuotegeometrian toimivuus ruiskuvalussa ja tunnistaa mahdolliset muottirikkoihin johtavat riskitekijät jo tuotesuunnitteluvaiheessa.

Diplomityössä tutkitaan ruiskuvalusimulaation ja ruiskuvaluprosessin vastaavuutta, jotta ruiskuvalusimulaation käyttämiseen osana tuotesuunnittelua saataisiin varmuutta. Simulaation ja ruiskuvaluprosessin tuloksia on verrattu keskenään tuotannossa jo olevan ABB:n tuotteen avulla, jonka ruiskuvaluparametrit sekä muottimalli ovat tiedossa. Lisäksi kyseistä tuotetta on simuloitu yksinkertaistetuilla jäähdytyskanavilla sekä simulaation antamilla oletusarvoisilla parametreilla, jotta voidaan tutkia tilannetta, jossa tuotesuunnittelijalla ei ole tietoa tarkoista prosessiparametreista tai muottikonstruktiosta. Lisätutkimus kyseiselle tuotteelle on tehty käyttämällä raaka-aineena PC-ABS:n sijaan polypropeenia. Tutkimuksen tarkoituksena on kartoittaa alustavasti olisiko prosessiparametreja säätämällä mahdollista valmistaa tuotetta polypropeenista PC-ABS:lle suunnitellussa muotissa. Diplomityön toinen osakokonaisuus koskee muottirikkoihin johtavien tekijöiden tunnistamista simuloinnin avulla jo ennen muottivalmistusta. Tämä tutkimustapaus koskee tuotetta, jonka muotti-inserteissä on havaittu halkeamia jo ensimmäisten koeajojen jälkeen. Tapauksessa tutkitaan eri tuotegeometrioita ja syöttöpaikkoja, jotta muotti-insertin rikkoutuminen vältettäisiin.

Tutkimusten tulokset osoittavat, että ruiskuvalusimulaatio ennakoi kappaleen kokemien vääntymien olevan suurempia kuin mitä oikeassa prosessissa nähdään. Suurten vääntymien syyksi arvioitiin simuloinnissa käytetyn materiaalin tietojen puutteellisuutta. Simuloinnit yksinkertaistetuilla jäähdytyskanavilla sekä oletusprosessiparametreilla eivät osoittaneet suuria eroavaisuuksia oikeilla kanavistoilla ja prosessiparametreilla saatuihin tuloksiin. Simulaatio käyttäen raaka-aineena polypropeenia osoitti hieman suurempia vääntymiä kuin PC-ABS, mutta tulosten perusteella polypropeenin käyttö muotissa olisi mahdollista prosessiparametreja säätämällä. Toisen tutkimustapauksen simulointi osoitti, että paine-erot muotti-inserttien yli olivat suuria, mikä oli luultavimmin syynä halkeamiin inserteissä. Korkeat paine-erot syntyivät kappaleen epätasaisen täyttymisen ja syöttöpaikkojen takia. Muottirikon riskin pienentämiseksi kappaleen geometriaa muutettiin ja syöttöpaikkoja siirrettiin, jotta kappale täyttyisi tasaisemmin. Tutkimus osoitti, että simulointi on hyödyllinen työkalu paine-erojen ja niiden synnyn tutkimiseen ja niistä aiheutuvien ongelmien ratkaisemiseen.

**Avainsanat** ruiskuvalu, ruiskuvalusimulaatio, dynaamiset kuormat, muottirikko

# Acknowledgements

*I would like to thank Vesa Palojoki for providing such an interesting thesis topic and acting as the advisor for this thesis. Thank you for all the guidance and help you provided throughout the work of this thesis. I want to thank professor Jouni Partanen for acting as the supervisor for this thesis and providing guidance and advices. Also, I would like to thank Janek Viman for providing an opportunity to work at ABB and gain important work experience during my studies.*

*I want to thank my family and friends who have encouraged and supported me during my studies and work of this thesis. Especially, thanks to my parents who have always encouraged me in my studies and to follow my dreams.*

*I would like to dedicate this thesis to my godfather's memory.*

Espoo, November 24th, 2019

Jenni Pekkarinen

# Table of contents

# Symbols

| | | |
|---|---|---|
| $A_{eff}$ | [$m^2$] | effective area |
| $A_h$ | [$m^2$] | cross-sectional area of hydraulic cylinder |
| $A_m$ | [$m^2$] | cross-sectional area of screw |
| $C_p$ | [J/K·kg] | specific heat of polymer |
| $D_h$ | [m] | diameter of hydraulic cylinder |
| $D_m$ | [m] | diameter of screw |
| $D_{max}$ | [m] | maximum cooling channel diameter |
| $D_{min}$ | [m] | minimum cooling channel diameter |
| E | [Pa] | elastic modulus |
| $F_{eject}$ | [N] | ejection force |
| $F_{friction}$ | [N] | friction force |
| $F_{normal}$ | [N] | normal force between surfaces of molding and mold |
| $H_{core}$ | [m] | core height |
| I | [kg $m^2$] | moment of inertia |
| L | [m] | length of one side |
| $L_{runner}$ | [m] | length of the runner portion |
| $L_{line}$ | [m] | length of cooling channel |
| $P_h$ | [Pa] | hydraulic pressure |
| $P_m$ | [Pa] | melt pressure |
| $\Delta P$ | [Pa] | pressure drop in runner |
| $\Delta P_{core}$ | [Pa] | pressure difference across the core |
| $\Delta P_{line}$ | [Pa] | pressure drop in cooling channel |
| R | [m] | radius of the runner portion |
| Re | | Reynolds number |
| $T_{eject}$ | [°C] | eject temperature |
| $T_{melt}$ | [°C] | melt temperature |
| $T_{solidification}$ | [°C] | solidification temperature |
| $\dot{V}_{coolant}$ | [$m^3$/s] | volumetric flow rate of coolant |
| $\dot{V}_{melt}$ | [$m^3$/s] | volumetric flow rate of polymer melt |
| Q | [$cm^3$/s] | flow rate of melt |
| $Q_{moldings}$ | [J] | heat energy |
| $\dot{Q}_{cooling}$ | [W] | cooling power |
| $\dot{Q}_{line}$ | [W] | cooling power per cooling channel |
| k | [Pa·s] | reference viscosity of polymer melt at melt temperature |
| $m_{moldings}$ | [kg] | mass of molded part(s) and runner(s) |
| n | | power law index of polymer melt at melt temperature |
| $n_{lines}$ | | number of cooling lines |
| r | [m] | gate radius |
| $r_v$ | [%] | volumetric shrinkage |
| s | [%] | linear shrinkage in one direction |
| $t_c$ | [s] | cooling time |
| $t_g$ | [m] | gate thickness |
| w | [m] | gate width |
| $\alpha$ | [1/K] | coefficient of thermal expansion |
| $\dot{\gamma}$ | [1/s] | shear rate |
| $\mu_{coolant}$ | [Pa·s] | viscosity of coolant |
| $\mu_s$ | | static friction coefficient between molding and core insert |

| | | |
|---|---|---|
| $\delta_{bending}$ | [m] | core bending |
| $\varepsilon$ | | thermal strain |
| $\rho_{coolant}$ | [kg/m$^3$] | density of coolant |
| $\sigma$ | [Pa] | tensile stress |
| $\emptyset$ | [°] | draft angle |
| $\emptyset_{core}$ | [m] | core outer diameter |
| $\emptyset_{inner}$ | [m] | core inner diameter |

**Conversions**

1 cm$^3$/s = 1·10$^{-6}$ m$^3$/s

# Glossary and abbreviations

| | |
|---|---|
| ABB | Asea Brown Boveri |
| DOE | Design of experiment |
| FEA | Finite element analysis |
| IM | Injection molding |
| IMM | Injection molding machine |
| PC-ABS | Polycarbonate-ABS |
| PP | Polypropylene |
| VIT | Visual inspection template |

# 1 Introduction

Injection molding (IM) is a repetitive process for manufacturing plastic parts with complex shapes and tight tolerances. It is widely used manufacturing method for mass produced plastic products. Injection molding is based on injecting molten plastic into a mold, where melt fills the mold cavity and produces product with the shape of the cavity. Injection molding involves an injection molding machine which is used to melt plastic and inject it to the mold. After part has solidified enough in the mold, it is ejected with automatic ejector system.

Injection molding simulation is an easy way to review the behavior of plastic part in the injection molding process. For instance, it can be used to validate completely new design choices and their manufacturability, or to review how changes e.g. for cooling system affect the process. Especially important to review part design with simulation is in cases where product design requires use of thin and long tool inserts. In these cases, simulation is helpful tool to evaluate the pressure levels and pressure differences over the inserts. Different studies have shown that injection molding simulation can predict behavior of plastic quite accurately and it has been used to simulate pressure loads on mold and to solve cases where mold failure has occurred. This thesis topic was selected to gain confidence to use simulation more as a tool to validate product design, and to gain knowledge of preventing mold failures occurring in the future.

## *1.1 Research problem and scope*

Purpose of this research is to assure quality of injection molded products at ABB Oy, Drives, by using injection molding simulation to validate product and mold design. Product design is important to validate with simulation in order to identify possible areas which can cause high stresses or high pressure differences to the mold, and which can lead to premature mold break.

Consistency between the simulation software and injection molding process is studied with an existing product to get confidence to make design choices based on the simulation results. In addition to this, effect of cooling system design is analyzed by comparing two different designs and their influence on the simulation results. Comparative study of cooling designs is done because in the product design phase the exact cooling channel design is not yet known, and most likely simplified cooling channels are used for the simulation. Therefore, it is important to compare how much difference it will cause to the results. Similar study is also done with the process parameters. Results with real molding parameters and results with default process parameters are compared in a simulation environment. As well, polypropylene's functionality in PC-ABS's mold is studied.

Another essential scope of this thesis is to study dynamic loads during injection molding to gain knowledge of the matter to help prevent mold failures. Goal of this part of the study is to be able to recognize the possible causes for mold failure with injection molding simulation before a mold construction. This would lead to improved product quality and time saving as the need to fix or replace a broken mold would decrease. Study of dynamic loads on mold is conducted with one case study where mold inserts have bent and cracked during the first molding trials. To decrease the risk for insert bending and cracking, effect of different design changes and gating locations are analyzed to find a solution which reduces the risk for tool failure.

## 1.2 Structure and implementation of the study

This master's thesis is divided into theoretical and practical part. Theoretical part contains a literature study which has two main sections. First one introduces the injection molding machine and the process. Furthermore, process parameters affecting each stage of the process are discussed. In addition to this, construction of the injection mold is reviewed. Second section of the literature study introduces how the process window for injection molding is defined and gives introduction to some of the parameters to be considered from the simulation results. These parameters are discussed in the literature study to assist in analyzing the simulation results.

Implementation of the practical part is done with two case studies. First of these case studies is an existing product at the ABB Drives. Product is used to compare the equivalence of simulation results and real manufacturing process. In addition to this, effect of cooling system to the simulation results is studied. Cooling system analysis consists of two different cooling system designs; one where cooling system is the same as used in the real mold and another where cooling system design is simplified, and what a product designer most likely would use to check product's processability with simulation. Also, process parameters' effect on the results are analyzed and polypropylene's behavior in a mold designed for PC-ABS is reviewed.

Second case study is related to dynamic loads on tool inserts. This case study consists of ABB's product which mold is being manufactured during the work of this master's thesis. Mold for this product has two separate beryllium copper tool inserts. These inserts are quite high and thin and fixed only from one end. During the first molding trials, inserts have cracked from the base, which has led to interruption of the trials. Furthermore, it was noticed that inserts had bent during the molding as the product had uneven wall thicknesses in the insert area. To study how high pressure levels and pressure differences are affecting during injection molding and causing the inserts to fail, product is analyzed with injection molding simulation. After the pressure differences are known, studies are made to find optimal combination of product geometry and gate locations, which reduces the risk for inserts' cracking.

## 1.3 Constraints of the study

Injection molding simulation software used in this master's thesis is Moldex3D R17. In this thesis the term injection molding simulation is used to refer to Moldex3D unless other is specified. Moldex3D has different levels available, based on the number of features they have. Throughout this thesis basic level, e-design, is used. This basic level restricts the capability to affect e.g. meshing, as there is only an automatic meshing tool available. In addition to the e-design level, core shift analysis and design of experiment analysis (DOE) options are included to the simulation license used in this thesis.

Simulation of the first case study product, is done based on parameters got from the molder and real molding circumstances are imitated as closely as possible with the simulation tools available. One of the studies in the first case study concerns study with alternative material, polypropylene. Purpose of this is to review if polypropylene could be used in a mold designed for PC-ABS, and not to define the exact process parameters which would give results similar to PC-ABS.

In the second case, tool insert failing problems are studied and analyzed with filling studies and core shift analyses. Only filling studies are done as the cracking problems are assumed to result from the filling phase when the part hasn't yet been filled. In this case only two of the studied designs were chosen into a closer analysis, as they were noticed to be the best options, and in addition to the filling analyses also core shift analyses were conducted. One of the designs was, based on the studies presented in this thesis, selected to the new molding trials to test if problems with tool inserts had been solved.

Materials used in the simulations are the ones the parts are being manufactured, or close to those by the rheological behavior. Trade names of the materials are not specified in this thesis because of privacy and they are only referred by general names, e.g. PC-ABS.

# 2 Stakeholders

This chapter describes the parties involved for the work of this thesis. First ABB Oy, Drives is introduced briefly, and then other parties involved to this thesis and their contribution are presented.

## 2.1 ABB Oy, Drives

ABB Oy is the market leader in the business of manufacturing drives and employs people in over 80 countries only for the drives business (ABB Oy, 2019). ABB Oy is divided into five businesses: electrification, industrial automation, robotics and discrete automation, power grids and motion. This master's thesis is written for ABB Drives which belongs to motion business unit. Examples of products manufactured and designed in motion business are electrical motors, generators and drives.

Plastic parts have big role at ABB Drives, as approximately 2000 tons of plastic is used yearly. If it is roughly estimated that 1,5 million drives are manufactured yearly and they each have 5-10 plastic parts, amount of plastic parts is approximately 7,5-15 million in a year. (Mäkelä, et al., 2019) This makes plastics and their manufacturing processes important sectors to know and to improve. According to Palojoki (2019) estimated amount of designed injection molded parts is approximately around 50 pieces in a year at ABB Drives R&D mechanics team. Most of the plastics used at ABB Drives are amorphous, for example PC and PC/ABS, and smaller share is reinforced semi-crystalline plastics like PA/GF, PBT/GF and PET/GF (Palojoki, 2019). Mainly all used plastics are flame retardant.

## 2.2 Other stakeholders

Injection molder of the IP21 cover provided the real process parameters and assisted analyzing the set-up sheet and simulation results of the first case. They also gave information of typical coolant rates used in injection molding, as this information wasn't available in the set-up sheet. Case 2 concerning tool insert failure was analyzed and solved together with the mold manufacturer. Plastlabs provided help and support for the Moldex3D software during this thesis work.

# 3 Injection molding

Injection molding is a repetitive process to produce plastic parts with complex shapes and tight tolerances. Furthermore, wide range of materials are available for injection molding. In injection molding process, plastic melt is injected into a mold under high pressure. Plastic melt takes form of the mold cavity and starts to cool and solidify. When plastic has cooled and solidified, mold is opened, and finished part is ejected automatically by pushing it out of the mold with ejector pins. Plastic melt is produced by heating and mixing plastic grains with a special screw in the injection molding machine. This screw is also used to inject the plastic melt into the mold. (Goodship, 2017 p. 1; Yang, et al., 2016 pp. 32, 34)

Injection molding is an old manufacturing process as the first injection molding machines were invented at the 1800 century. John Hyatt built, at 1869, a machine where steam was used to melt celluloid which was then injected with hydraulic plunger into a mold. This process was used to manufacture billiard balls. In 1872, a first injection molding machine was patented by John and Isaiah Hyatt (Goodship, 2017 p. 1). In 1951 William H. Willert developed a reciprocating-screw machine in which the modern machines base on (Yang, et al., 2016 p. 33). Nowadays injection molding machines can be electronic, hydraulic or hydraulic-electric where advantages of these two techniques are combined. (Kulkarni, 2010 p. 79)

## *3.1 Injection molding machine*

Injection molding machines (shown in figure 1) are specified by their shot capacity and amount of clamping force they can produce. An injection molding machine manufacturer ARBURG has machines which can produce a clamping force from 125 to 6500 kN (ARBURG, 2018). Shot capacity is the amount of plastic in weight or volume, that the machine screw can inject into the mold. Shot capacity is usually stated for polystyrene in the machine specification, and it should be noted that it differs for different materials. Term shot size is used to represent the amount of plastic needed to fill the mold cavity, and it is not a machine specific value. (Goodship, 2017 p. 33; Selke, et al., 2016 p. 288)

Injection molding machine (IMM) can be divided into four major components: injection unit, mold, clamping system and control unit. Purpose of the injection unit is to prepare the plastic melt and transfer it into the mold. Clamping system keeps the mold closed during injection and opens the mold when plastic has cooled, and molded part can be ejected. Control unit allows the machine operator e.g. to set the process parameters and monitor the process. (Goodship, et al., 2016 pp. 123-124, 126)

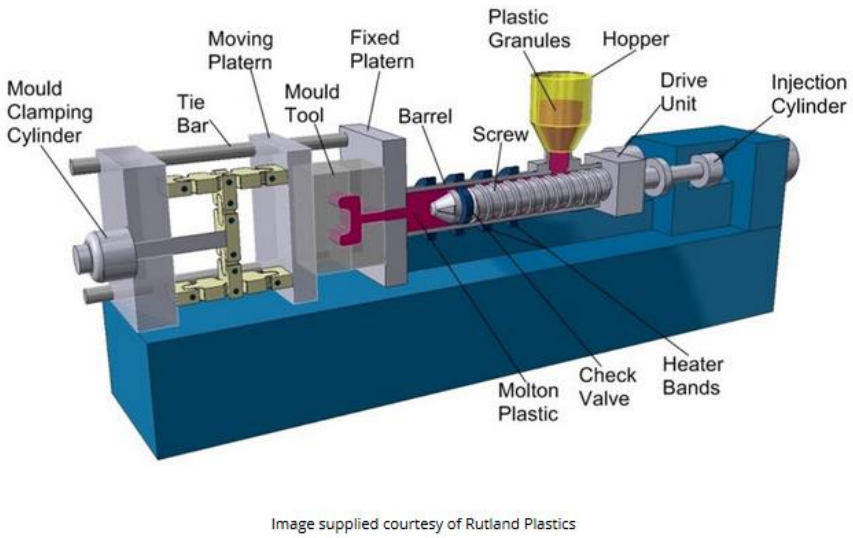


*Figure 1 Injection molding machine. (Pentagon Plastics LTD., 2019)*

**Injection unit**

Injection unit can be split into following components: hopper, heated barrel, drive unit, rotating screw and nozzle. These components are shown in figure 1.

Hopper is a container which stores the plastic material before plasticizing and feeds the plastic into the screw (Wang, et al., 2018 p. 88). Materials are usually as grains or powder in the hopper (Goodship, 2017 p. 1).

Barrel is a steel cylinder which consist of screw and heater bands. In the barrel, plastic material fed from the hopper, is melted with the heat generated by the heater bands as well as by the shearing action of the rotating screw. Approximately one third of the heat to the plastic is produced by the heater bands (Yang, et al., 2016 p. 36). Injection pressure in the barrel can vary from 14 to 205 MPa. (Rosato, et al., 2000 p. 4; Goodship, 2017 p. 34)

Drive unit, which produces movement of the screw, can be hydraulic or electronic (Wang, et al., 2018 p. 88). In an electronic drive unit, a servo motor produces the movement and in a hydraulic system, movement is produced by a hydraulic cylinder. Electric IMM's advantages over hydraulic are energy savings and accuracy. In electric IMM servomotors operate only when they are in use, when in hydraulic system hydraulic fluid is pumped constantly in the system. Using servomotors instead of hydraulic system, accuracy is improved as servomotors are capable to adjust faster on changes in processing parameters. In a hydraulic machine, hydraulic fluid flows through hoses and valves, which have losses and lead to power losses. Hydraulic machine is also liable to temperature changes in the environment which can lead to variation in the quality of finished parts. Injection molding machine can also be hydraulic-electric where usually clamping unit and dosing is done by electric drive system and injection is typically hydraulic. (Goodship, 2017 p. 103; Calhoun, et al., 2004 pp. 68-69)

Screw is used to transport, mix, plasticize and inject the plastic material. Hopper feeds the plastic grains into the rotating screw, which rotational movement shears the plastic and generates heat which starts to melt the plastic. This melt is then mixed and transported towards the tip of the screw by the rotational movement. When enough plastic melt is

produced in front of the screw, plastic melt is injected into the mold via nozzle. A standard screw type consists of three sections: feed, compression and metering (figure 2). Feed zone has the highest fight depth and this zone is used to soften the plastic granulates and to transport the compound towards the compression section. In the compression section, the fight depth decreases gradually towards the minimum fight depth of the metering section. This decrease in the fight depth forces the soften plastic granulates in contact with the heated barrel's inner wall and causes friction which generates more heat to melt the plastic. In the metering section, plastic melt's temperature increases more, and it is transported in front of the screw tip. In the front end of the screw a non-return valve allows the plastic to move only in front of the tip and not back from there. The melt in front of the screw tip forces the screw to move backwards and when it has reached predetermined position, rotational movement of the screw stops, and injection phase is started. In the injection stage, screw's movement is auxiliary instead of rotational as in the plasticization stage. (Kulkarni, 2010 p. 84)

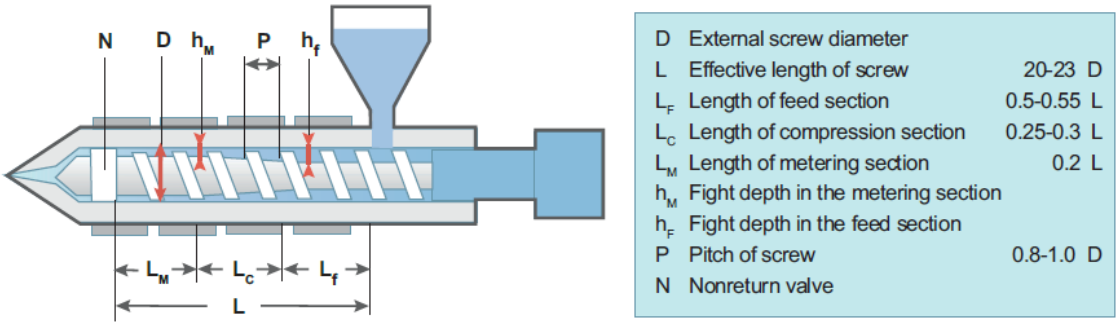


*Figure 2 Screw. (Wang, et al., 2018 p. 88)*

**Mold**

A two-plate, two cavity family mold is shown in figure 3. Two-plate mold has two mold plates which form the shape of the plastic part during injection molding: mold core and mold cavity insert plates. Between these two plates is the parting line from which the mold opens to eject the finished part. Two cavity mold produces two parts in one molding cycle as shown in figure 3. Ejection is done with the ejector pins which push the solidified plastic part out of mold. During an IM cycle, plastic melt enters to the mold by sprue and flows through runner(s) and gate(s) into the mold cavity. To cool the plastic melt, coolant circulates in the cooling channels in the mold core and cavity plates. (Kazmer, 2007 pp. 5-6)

Steel is usually used as a mold material as it can withstand high pressures during injection, and it has high thermal conductivity which promotes fast cooling. Aluminum is as well used in molds as its thermal conductivity is higher than steel's, but its strength is lower, and because of this, it is used mainly when batch sizes are small. (Francis, et al., 2016 p. 216) More about different mold types and mold materials is discussed later in chapter 3.3.

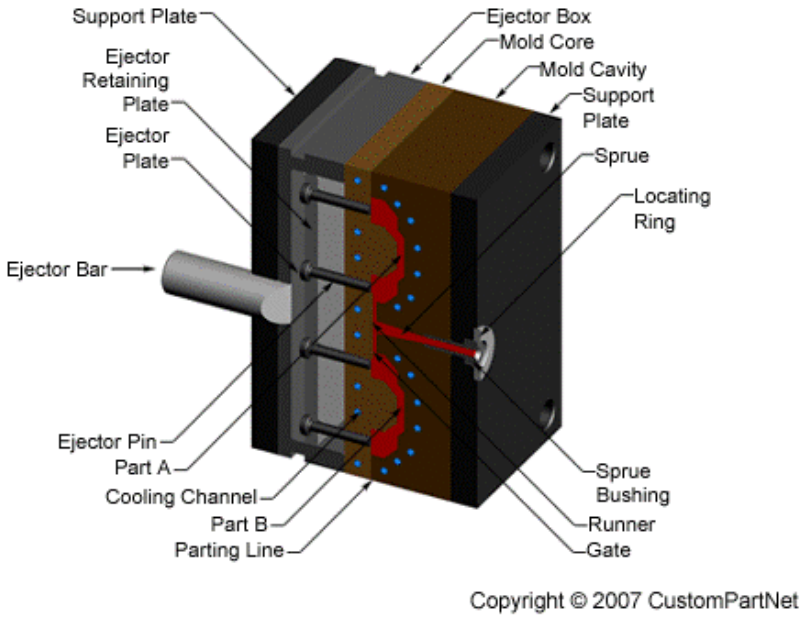


*Figure 3 Two-plate mold construction. (CustomPart.net, 2019)*

**Clamping unit**

Clamping unit has two purposes: to hold the mold in place during injection and to open and close the mold (Francis, et al., 2016 p. 214). Figure 4 shows construction of a clamping unit. Mold cavity is fixed to a stationary platen, which is fitted into the IMM, and mold core to a movable platen. Moveable platen is guided by four tie bars in each corner of the mold and clamping motor drives the moveable platen by ejector bars towards the stationary platen to close the mold. Clamping force of IMM can be from 0,1 to 100 MN. (Burkhardt, et al., 2011 p. 185; CustomPart.net, 2019)

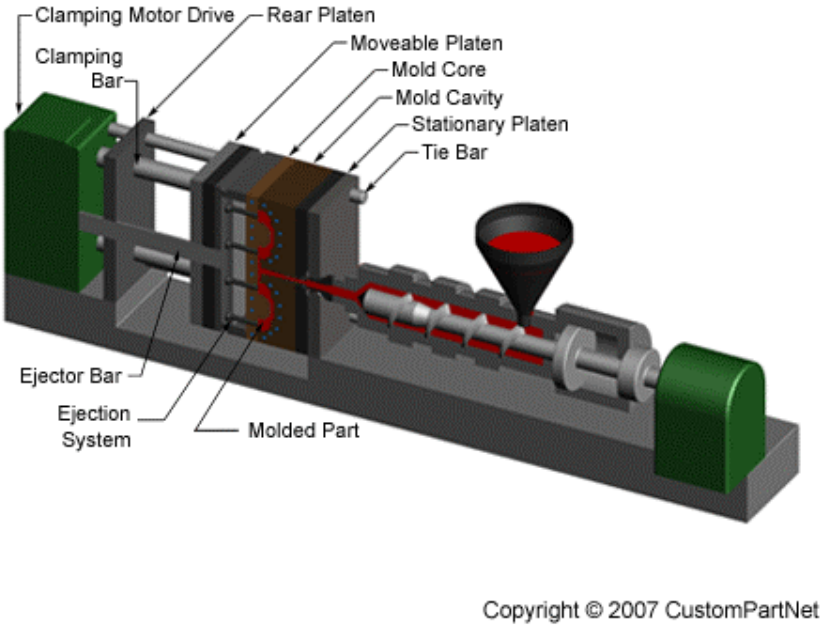


*Figure 4 Clamping unit. (CustomPart.net, 2019)*

## 3.2 Injection molding process

Injection molding process can be simply described with five different stages. These stages are:

1. Plasticizing
2. Injection
3. Packing
4. Cooling
5. Ejection. (Rosato et al, 2000, p.2)

### 1. Plasticizing

In the plasticizing phase (figure 5) the plastic grains from the hopper are fed into the screw and melted to homogenous compound. Melting results from heat from the heater bands around the barrel and as well from the friction between plastic and inner surface of the barrel, when rotation of the screw pushes the plastic towards the barrel wall. During the plasticizing, the plastic melt is transported in front of the screw to prepare enough melt for the injection. (Wang, et al., 2018 pp. 3, 6; Kazmer, 2016 p. 2)

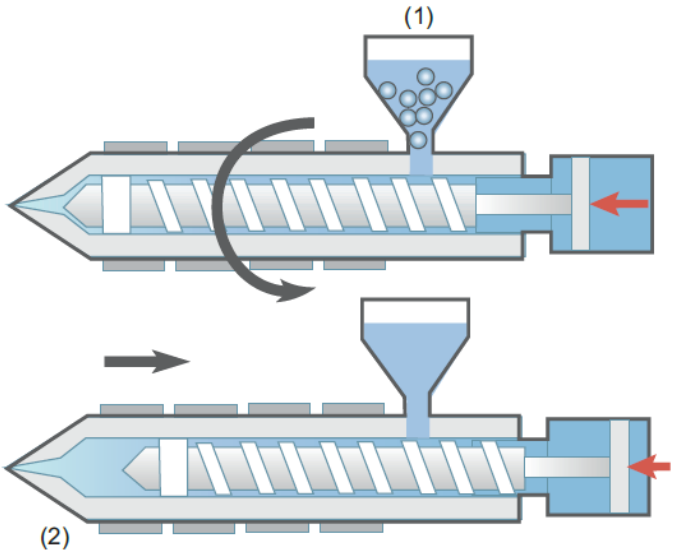


*Figure 5 Plasticizing stage. (Wang, et al., 2018 p. 94)*

Parameters affecting the plasticizing stage are barrel temperature, screw speed and back pressure. With barrel temperature and screw speed melt temperature is controlled. Screw speed should be set based on material being processed to produce a homogenous melt with desired temperature. With too high screw speeds heat damage can be caused to melt. Turning action of the screw brings plastic melt in front of the screw. This melt starts to pack against the screw and produces a small pressure. This pressure then pushes the screw backwards until pre-defined back pressure value is achieved and process will move on to injection stage. With higher back pressure value more shearing and mixing actions is achieved and more homogenous melt produced. However, with too high back pressure thermal degradation to the plastic can occur. (Goodship, 2017 p. 207; Kulkarni, 2010 pp. 138-139; Bryce, 1996 pp. 99-100)

### 2. Injection

During the injection (figure 6), plastic melt in front of the screw is forced into the mold cavity by axial movement of the screw. Plastic melt is injected into the mold cavity

through a nozzle and via sprue, runner(s) and gate(s). Melt starts to solidify as soon as it touches the cooler mold walls.

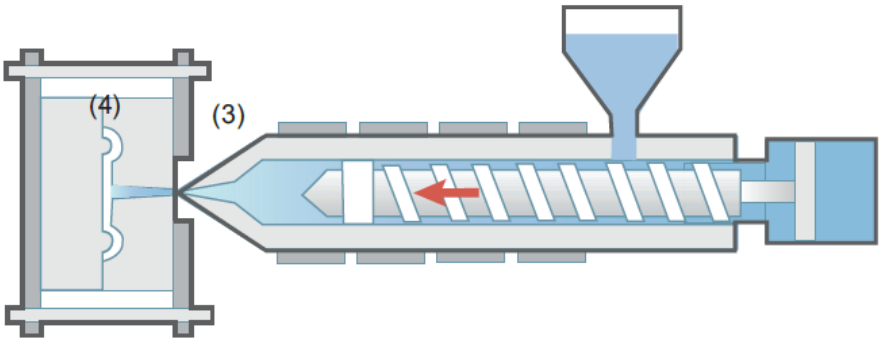


*Figure 6 Injection stage. (Wang, et al., 2018 p. 96)*

Parameters affecting injection stage are injection speed and injection pressure. Injection speed should be selected as high as possible to fill the mold quickly and to decrease the temperature and pressure differences in the part. Temperature of the plastic melt should as well be as high as possible to achieve low viscosity and easier material flow, which result in low pressure losses and differences inside the mold. (Goodship, 2017 p. 191)

Injection pressure is the amount of pressure applied to the plastic melt by the screw (Wang, et al., 2018 p. 112). In figure 7, injection pressure is presented with $P_m$ and hydraulic pressure applied to the screw with $P_h$. Injection pressure is proportional to the hydraulic pressure by equation (1). This equation shows that the square ratio of hydraulic cylinder diameter to screw diameter highly affects the amount of injection pressure. Injection pressure should be chosen as high as the cavity is needed to fill fast but not too high in order to avoid causing stressed parts which lead to warpage. (Goodship, 2017 p. 197)

$$P_m = P_h * \frac{A_h}{A_m} = P_h * \frac{\pi\left(\frac{D_h}{2}\right)^2}{\pi\left(\frac{D_m}{2}\right)^2} = P_h * \left(\frac{D_h}{D_m}\right)^2 \quad (1)$$

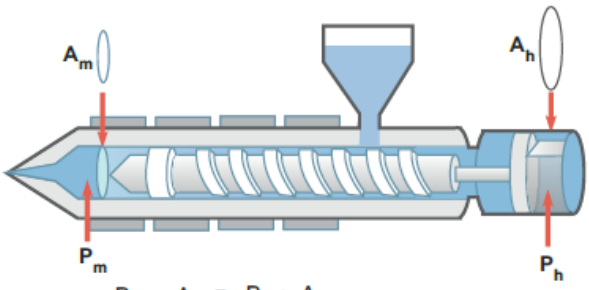


$P_m \cdot A_m = P_h \cdot A_h$

$P_m = P_h$ $\quad A_h / A_m$ = intensification ratio

| Melt Pressure (psi) | Intensification Ratio | Hydraulic Pressure(psi) |
|---|---|---|
| 5,000 | (7:1) | 714 |
| 6,000 | (8:1) | 750 |
| 7,000 | (9:1) | 778 |
| 8,000 | (10:1) | 800 |
| 9,000 | (11:1) | 818 |
| 10,000 | (11:1) | 909 |
| 10,000 | (7:1) | 1,429 |

*Figure 7 Injection pressure. (Wang, et al., 2018 p. 113)*

### 3. Packing

When molten plastic is injected into the mold cavity it starts to cool, and its molecules start to get closer to each other which causes volumetric shrinkage. To compensate this shrinkage, more plastic melt is injected into the mold cavity. This compensating action is called as packing (figure 8). After the packing stage, pressure of the plastic melt can be around 35 to 70 MPa which would force the plastic to flow out of the gate unless a certain amount of pressure would be still applied. This pressure is called as packing or holding pressure and it is applied by the injection screw until the gate is sealed. (Kulkarni, 2010 p. 106)

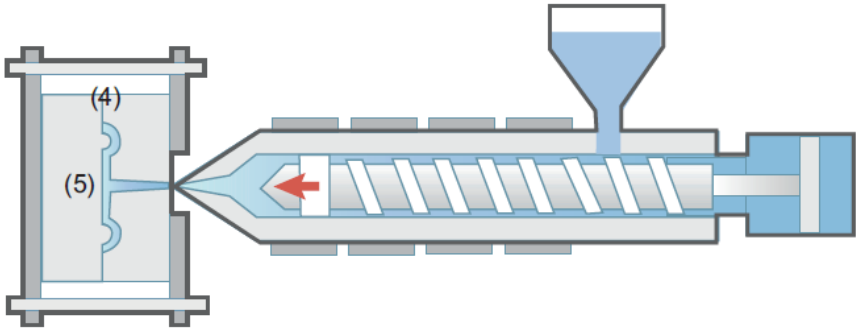


*Figure 8 Packing stage. (Wang, et al., 2018 p. 97)*

Parameters during packing and holding phase are packing pressure, packing time and mold temperature. After injection phase, there should be a melt cushion of 3-10 mm in front of the screw, to be able to produce the packing pressure. Packing pressure should be applied until the gate is sealed but excessively long packing time should be avoided as it will lead to high stresses in the molded part. Optimum packing time can be found with molding trials where packing time is constantly decreased until it leads to sink marks in the part. The shortest packing time where sink marks don't occur, is chosen. Optimal mold temperature depends on material but temperature distribution in the mold should be as uniform as possible to minimize the plastic shrinkage. With high mold temperatures, better melt flow, lower injection pressures and improved surface quality can be obtained. However, higher mold temperatures lead to longer cooling times which increases the cycle time and as well costs. (Goodship, 2017 pp. 209, 211-212)

### 4. Cooling

After the packing and holding phase, plastic is cooled in the mold until it has solidified enough to be ejected. During cooling (figure 9), the screw moves back and starts to prepare the next shot.

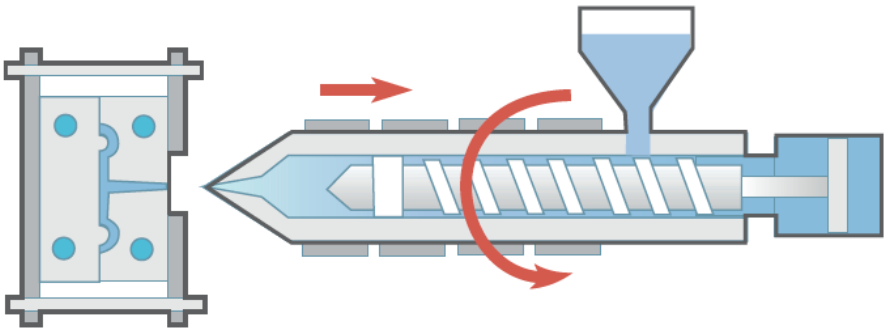

*Figure 9 Cooling. (Wang, et al., 2018 p. 98)*

### 5. Ejection

When the part has solidified enough, it can be ejected from the mold. Ejection is done by opening the mold and pushing the finished part out of the mold with ejector pins (figure 10).

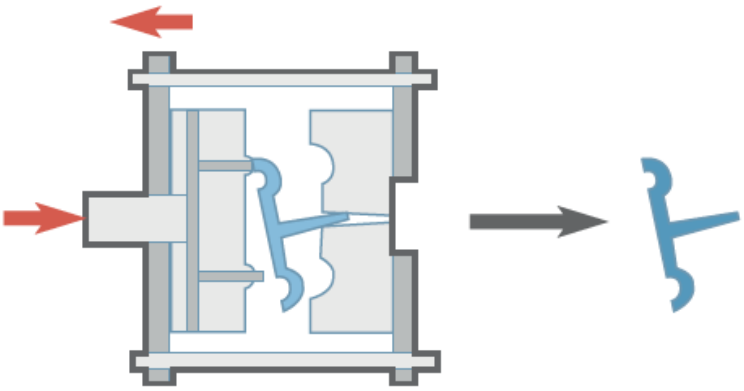

*Figure 10 Ejection. (Wang, et al., 2018 p. 99)*

**Injection molding cycle**

Figure 11 shows the injection molding cycle time for a part with 2 to 3 mm wall thickness (Wang, et al., 2018 p. 90) and how the cycle time is divided between different phases of the process. IM cycle starts from closing the mold which takes only second, and which is followed by the filling stage (4 seconds). After filling, more material is forced into the mold to control the volumetric shrinkage and holding pressure is applied (10 seconds). Next stage, the cooling stage, is the longest part of the cycle, approximately 18 seconds. After the part has cooled enough to be ejected, mold is opened, and solidified part ejected (2 seconds). As the figure 11 shows, cooling of the part takes the longest time of the IM cycle. Therefore, it is important to optimize the part design to avoid designing too thick sections which would increase the cooling time and the whole cycle time and to make sure that cooling is efficient.

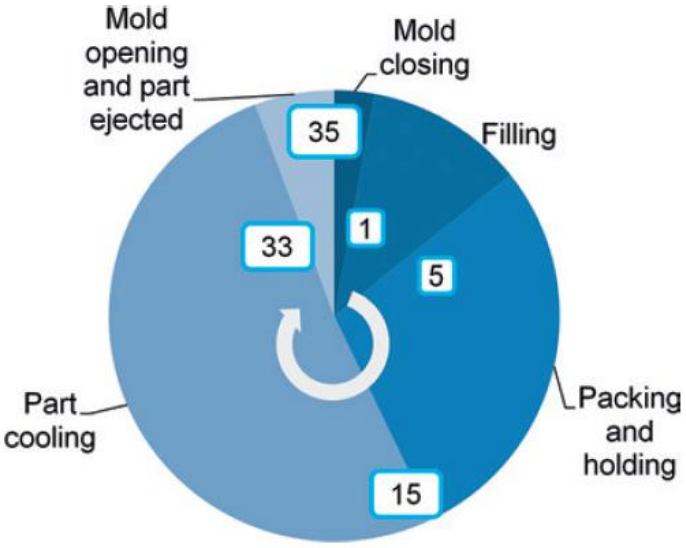


*Figure 11 Injection molding cycle time. (Wang, et al., 2018 p. 91)*

## 3.3 Molds

Three basic injection mold types are two-plate, three-plate and hot runner molds (figure 12). From these three mold types, the first two are called as cold-runner molds. In a cold-runner mold the runner system solidifies in every cycle and is ejected with the molded part. In a hot-runner mold this is opposite. Runner system is kept melt during the whole process by heating the runner system and runner system isn't ejected. Difference between the two-plate and three-plate mold is in the runner system ejection technique. In the two-plate mold the runner system is ejected with the part (figure 12 (a)) when in the three-plate mold there is an additional mold plate which allows the runner system to be ejected separately (figure 12 (b)). Three-plate molds give more freedom to the runner system and gating design, as the additional plate allows the runners to go through the plate without intersecting with the mold cavities (Kazmer, 2016 p. 149). Construction of the most commonly used two-plate mold was described more detailed in the section 3.1. (Kalpakjian, et al., 2014 p. 505)

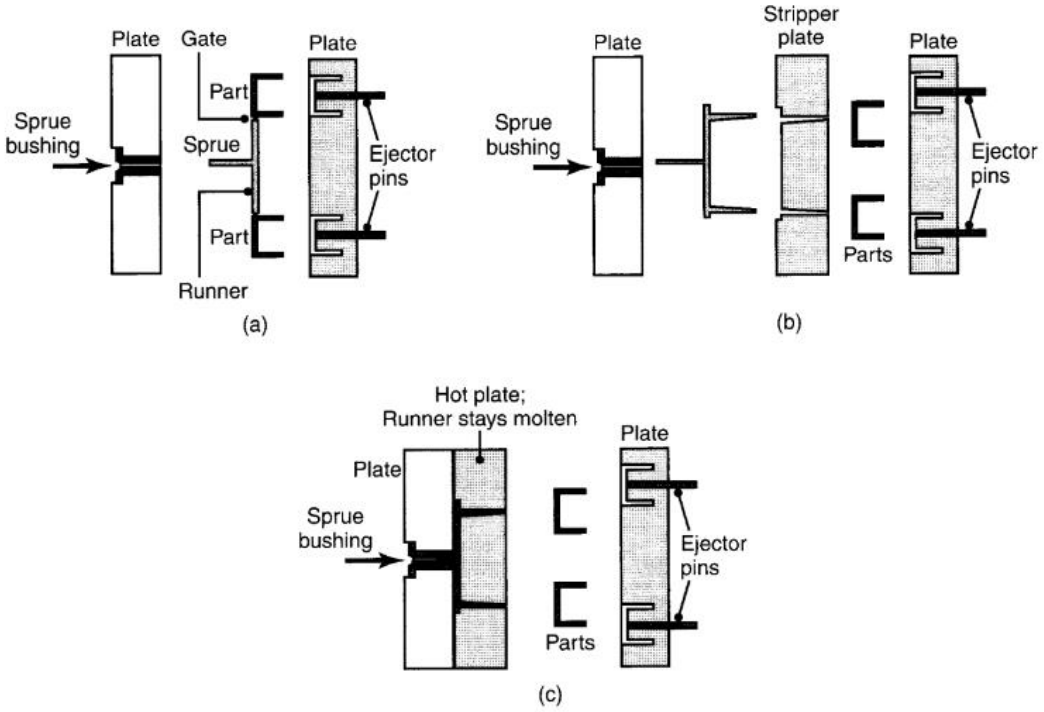


*Figure 12 Basic injection mold types: (a) two-plate mold, (b) three-plate mold and (c) hot-runner mold. (Kalpakjian, et al., 2010 p. 496)*

### 3.3.1 Materials

Mold material is chosen for every application based on the mechanical and thermal requirements. As well costs are important factor when deciding suitable mold materials. Table 1 shows some recommendations for core and cavity materials based on the number of injection molding cycles they need to last. This has a great impact to selection of core and cavity materials. Also, properties of plastic melt and injection molding process parameters, like injection pressure, affect this choice. When mold is intended to last only low number of molding cycles and low injection pressures are used, aluminum or copper can be chosen. With higher injection pressures and high number of cycles, steels are used, as they have higher strength and stiffness than aluminum. (Campo, 2006 p. 569)

*Table 1 Mold materials for core and cavity inserts. (Kazmer, 2016 p. 103)*

| | Low number of cycles ($n_{cycles}$ < 10,000) | Moderate number of cycles | High number of cycles ($n_{cycles}$ > 1,000,000) |
|---|---|---|---|
| Nonabrasive melt with low molding pressures | Al alloys | Al or Cu alloys | Cu alloys, P20, SS420 |
| Slightly abrasive melt or moderate molding pressures | Al or Cu alloys or 1045 | Cu alloys, P20, 4140, S7 | SS420, S7, D2, A6 |
| Highly abrasive melt | P20, S7 | D2, A6, H13 | H13 |
| High molding pressures | 1045, 4140, P20 | P20, S7 | D2, A6 |
| Highly corrosive melt | P20, SS420 | SS420 | SS420 |

Advantage of using copper or aluminum alloys over steel is their higher thermal conductivity (table 2). Table shows that ranges for thermal conductivity are quite wide, and for steel the best thermal conductor has a value over twice the one of the worst materials. Some examples of steels with different thermal conductivity are shown in the table 2 and it shows that with a choice of steel type the cooling time can be affected quite effectively. For aluminum, thermal conductivity is over twice as high as that of steel. Thus, aluminum mold conducts heat twice better than steel mold and decreases cycle times. As the heat properties are better for aluminum and copper alloys, complex cooling channels aren't necessarily needed which simplifies the mold design (Mennig, et al., 2013 p. 462). Differences in thermal conductivity and its influence on part cooling and material's behavior in the mold should be noted especially when using different mold material for prototyping than for mass production. In a research of Kelly, et al. (2011) copper mold inserts were compared to conventional tools steel inserts, and it was noted that use of copper inserts reduced cooling times. Cooling time was decreased up to 29% with copper inserts, when compared to inserts made of tool steel. Four different composition of the copper inserts were used, where copper content ranged from 85 to 96%. Research showed that with higher copper content, cooling time was decreased, which was due to increased thermal conductivity with higher copper content.

*Table 2 Thermal conductivities for steel, aluminum and copper alloys based on (Mennig, et al., 2013 p. 442).*

| **Mold material** | **Thermal conductivity (W/mK)** |
|---|---|
| Steel | 15-40 |
| Uddeholm Elmax (tool steel) | 15* |
| SLM 1.2344 (H13) (tool steel) | 25,6** |
| Industeel P20 (tool steel) | 35*** |
| Aluminum alloys | 110-220 |
| Copper alloys | 210-320 |

* (UL Prospector, 2013)
** (UL Prospector, 2017)
*** (UL Prospector, 2013)

In case of molding only low number of products, for example making prototypes, 3d printed inserts can be used. 3d printed inserts are easy to manufacture with low costs, but their strength and wear resistance are poor. Furthermore, surface quality of 3d printed inserts is quite rough which can cause small undercuts to the molded part and this way require more ejection force, which can lead breaking the mold insert. Thermal

conductivity of 3d printed polymer inserts is lower than metals, which leads to longer cooling times and increases the cycle times. (Kutz, 2017 p. 626)

Figure 13 shows average part production costs for four different mold constructions. With low production volumes (below 1000 parts), 3d printed inserts are more economical than steel or aluminum molds. When volume is increased over 1000 parts, 3d printed inserts have constant costs as they break eventually and need to be replaced with new one. This makes aluminum the best option for production volumes above 1000 but below 10000. After production volumes exceeds 100 000 parts, steel molds become the cheapest mold option as steel has better mechanical properties than aluminum or printed inserts.

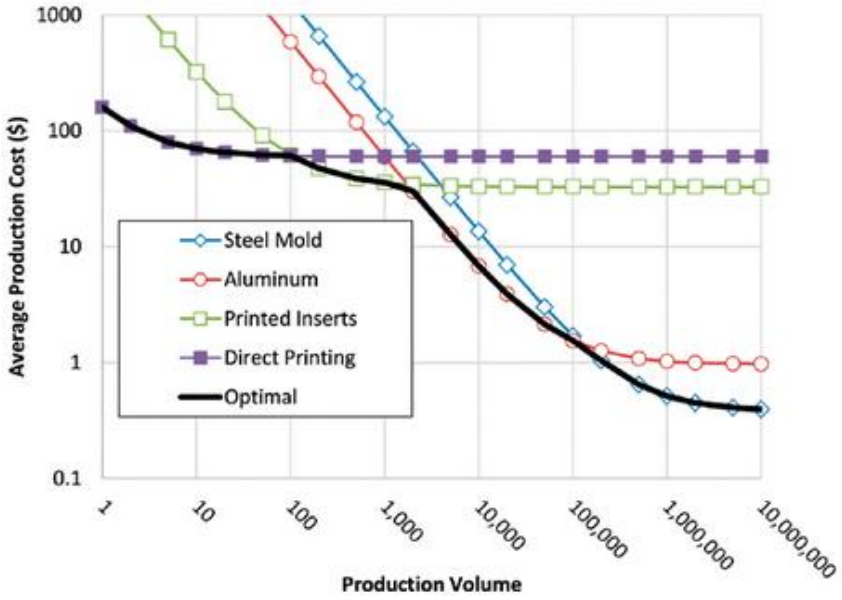


*Figure 13 Average part production costs for four different mold constructions. (Kazmer, 2016 p. 74)*

### 3.3.2 Cooling

Cooling of plastic is based on heat exchange between the mold and the coolant, which circulates in the cooling channels and transfers the heat out from the polymer melt. Heat is transferred from the mold by radiation, conduction and convection. In radiation, heat is transferred via electromagnetic waves and conduction is based on heat exchange via atoms and molecules. In convection, heat is transferred between fluid and solid surface, as in figure 14 where coolant circulates in cooling lines. (Wang, et al., 2018 pp. 238-239)

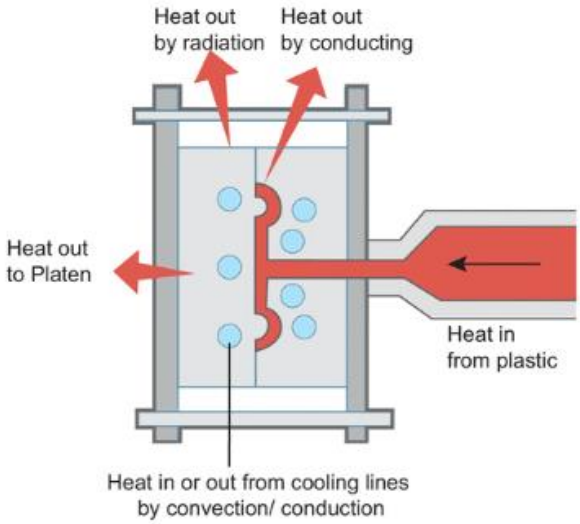


*Figure 14 Heat extraction from mold. (Wang, et al., 2018 p. 240)*

**Design rules for cooling channels**

Based on Wang, et al. (2018) following rules can be applied when designing cooling channels:

- Distance between cooling channels should be approximately three times the diameter of the cooling channel
- Distance of the cooling channels below and above part should be approximately two to three times of the cooling channel diameter
- Turbulent flow of the coolant.

Turbulent flow of the coolant is desired as it can provide better heat transfer than laminar flow. Turbulent flow is achieved in a round cooling line when Reynolds number is above 4000 (equation (2)). Equation (3) can be used to calculate maximum cooling channel diameter:

$$Re = \frac{4 * \rho_{coolant} * \dot{V}_{coolant}}{\pi * \mu_{coolant} * D_{max}} > 4000 \quad (2)$$

$$D_{max} = \frac{4 * \rho_{coolant} * \dot{V}_{coolant}}{\pi * \mu_{coolant} * 4000}, \quad (3)$$

where $\rho_{coolant}$ is density of the coolant,
$\dot{V}_{coolant}$ is the volumetric flow rate and
$\mu_{coolant}$ is viscosity of the coolant. (Kazmer, 2016 pp. 254-255)

Minimum cooling channel diameter is dependent of the allowed pressure drop in the cooling channel by equation (4)

$$\Delta P_{line} = \frac{\rho_{coolant} \cdot L_{line} \cdot \dot{V}^2_{coolant}}{10\pi \cdot D^5_{min}}, \quad (4)$$

where $L_{line}$ is the length of the cooling channel.

Minimum cooling channel diameter can be expressed with equation (5).

$$D_{min} = \sqrt[5]{\frac{\rho_{coolant} \cdot L_{line} \cdot \dot{V}_{coolant}^2}{10\pi \cdot \Delta P_{line}}} \quad (5)$$

Equations (3) and (5) are most suitable to estimate the cooling channel diameter when coolant is water, and in case of using non-water coolant, it should be noted that a turbulent flow might not be achieved, and other equations are needed to estimate the channel diameter. (Kazmer, 2016 pp. 255, 257)

Cooling power required from the cooling system is calculated with equation (6)

$$\dot{Q}_{cooling} = \frac{Q_{moldings}}{t_c}, \quad (6)$$

where $t_c$ is the cooling time and
$Q_{moldings}$ is the amount of heat energy to be removed from the moldings.

Amount of energy to be removed can be calculated with equation (7) where $m_{moldings}$ is the mass of molded part(s) and cold runner(s), $C_p$ is the specific heat of the polymer and $T_{melt}$ and $T_{eject}$ are melt and ejection temperatures (Kazmer, 2016 p. 252):

$$Q_{moldings} = m_{moldings} \cdot C_p \cdot (T_{melt} - T_{eject}). \quad (7)$$

If it's assumed that each cooling line removes same amount of heat, the amount of heat removed by one cooling line can be expressed with equation (8), where $n_{lines}$ is the number of cooling lines (Kazmer, 2016 p. 252)

$$\dot{Q}_{line} = \frac{\dot{Q}_{cooling}}{n_{lines}}. \quad (8)$$

Coolant needs to have stable and uniform temperature in order to cool the plastic evenly and to minimize possibility for shrinkage and warpage. Usually an increase of 1 °C is allowed in the coolant temperature, but when more accurate dimensional and geometrical tolerances need to be achieved, allowed temperature rise can be even lower. Volumetric flow rate of the coolant is directly proportional to the change in the coolant temperature as equation (9) shows and it determines how even temperature distribution can be achieved in the mold. (Kazmer, 2016 p. 253)

$$\Delta T_{coolant} = \frac{\dot{Q}_{line}}{\dot{V}_{coolant} \cdot \rho_{coolant} \cdot C_{P,coolant}} \quad (9)$$

### 3.3.3 Feed system

Feed system is used to transport the plastic melt from the injection molding machine to the mold. Feed system consists of runner(s) and gate(s). Two-plate cold runner, three-plate cold runner and hot runner are three commonly used feed system types. In a cold-runner system runner freezes in each process cycle and is ejected with the molded part,

when in hot runner plastic stays melt in the runner and doesn't need to be ejected. This is one of the advantages of using hot runner, as there is no need to fill the runner in every injection cycle or to wait it to be solidified (Kazmer, 2016 p. 153). A two-plate cold runner is used in two-plate mold which has one parting plane where the mold is opened into two sections. During the part ejection, solidified cold runner is also ejected with ejector pins. Three-plate runner is used in three-plate mold where there are two parting planes. This allows more design freedom to the runner system as the runner can travel in width and length direction at the parting plane. Runner system is disconnected from the part when the mold is opened from the first parting plane. After this, mold is opened from the second parting plane and both molded part and runner are ejected separately. Figure 12 under section 3.3 showed the differences between the construction of two- and three-plate molds and their runner systems. (Wang, et al., 2018 p. 205; Kazmer, 2016 pp. 146-151)

When designing feed system, type and routing of the feed system and diameters of runners and gates need to be determined. Pressure drops, shear rates, shear stresses and material utilization are matters to influence on sizing the runners and gates. Table 3 shows maximum values of shear stress and shear rate for various materials with the recommended runner diameter. (Kazmer, 2016 pp. 141-142)

*Table 3 Shear stress, shear rate and recommended runner diameter values for different materials. Table is collected based on (Wang, et al., 2018 pp. 78, 81).*

| | **Maximum shear stress (MPa)** | **Maximum shear rate (1/s)** | **Recommended runner diameter (mm)** |
|---|---|---|---|
| **ABS** | 0,30 | 50 000 | 4,7–9,5 |
| **PA66** | 0,50 | 60 000 | 1,5-9,5 |
| **PC** | 0,50 | 40 000 | 4,7-9,5 |
| **PC/ABS** | 0,40 | 40 000 | 4,7-9,5 |
| **PP** | 0,25 | 100 000 | 4,7-9,5 |
| **PS** | 0,25 | 40 000 | 3,1-9,5 |

Shear rate at gate can be calculated with equations (10) and (11) (Wang, et al., 2018 p. 78), which can also be used to check if the gate diameter is suitable for specific material. Equation (10) is used for round gates and (11) for rectangular gates. In these equations, $Q$ is flow rate of melt, $r$ is the gate radius, $w$ is the gate width and $t_g$ is the gate thickness.

$$\dot{\gamma} = \frac{4Q}{\pi r^3} \tag{10}$$

$$\dot{\gamma} = \frac{6Q}{wt_g^2} \tag{11}$$

Runner system should have a minimal pressure drop. This pressure drop shouldn't exceed 50% of the pressure required to fill the mold cavity. Other design rule is that pressure drop in the runner shouldn't be over 50 MPa. (Kazmer, 2016 p. 156) Pressure drop in every portion of the runner system can be estimated for power law fluids with equation (12) (Kazmer, 2016 pp. 163-164)

$$\Delta P = \frac{2kL_{runner}}{R}\left(\frac{\left(3+\frac{1}{n}\right)\dot{V}_{melt}}{\pi R^3}\right)^n, \quad (12)$$

where $k$ is the reference viscosity of the polymer melt at the melt temperature,
$n$ is the power law index of the polymer melt at the melt temperature,
$L_{runner}$ is the length of portion of the runner,
$R$ is the radius of portion of the runner and
$\dot{V}_{melt}$ is the volumetric flow rate of the polymer melt.

### 3.3.4 Dynamic loads in molds

During injection molding molds are exposed to high pressures which they need to bear multiple times. Forces in the mold cavities are typically from tens to thousands of tons (Kazmer, 2016 p. 381). One important factor in the structural design is the mold material. Figure 15 shows comparison of P20 steel and 6061-T6 aluminum when concerning number of cycles these materials can withstand when subjected to stress. Yield stress of P20 is almost twice the amount for 6061-T6. This means that P20 can withstand almost twice higher stress before plastic deformation occurs. Endurance stress, $\sigma_{endurance}$, for steel is 456 MPa and it is defined to be the stress that material will bear theoretically infinite number of stress cycles. For aluminum, there aren't endurance stress limit as aluminum can't bear any stress infinite cycles, as it will suffer eventually failure due to fatigue. This makes aluminum suitable for applications where number of molding cycles is quite low, and mold is subjected to low stresses. (Kazmer, 2016 pp. 385-386)

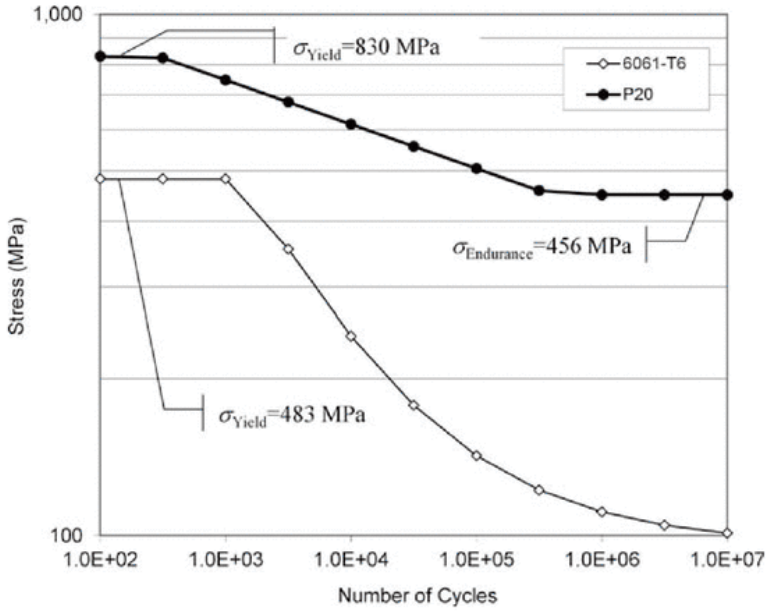


*Figure 15 Number of molding cycles steel (P20) and aluminum (6061-T6) can withstand when objected to stress. (Kazmer, 2016 p. 386)*

Core bending due to pressure difference over a core can be estimated with the equation (13) (Kazmer, 2016 p. 414)

$$\delta_{bending} = \frac{\Delta P_{core} \emptyset_{core} H_{core}^4}{8EI}, \quad (13)$$

where $\Delta P_{core}$ is the pressure difference across the core,
$\emptyset_{core}$ is the core outer diameter,
$H_{core}$ is the core height,
$E$ is the elastic modulus and
$I$ is the moment of inertia.

E.g. for a hollow core the moment of inertia is calculated with equation (14)

$$I = \frac{\pi}{64}(\emptyset_{core}^4 - \emptyset_{inner}^4), \tag{14}$$

where $\emptyset_{core}$ is the core outer diameter and
$\emptyset_{inner}$ is the core outer diameter.

### 3.3.5 Ejection forces

In order to eject plastic molding successfully, ejection force should be sufficient to eject the molding and it should be evenly distributed. Even distribution is important to avoid causing distortion to the part. (Kazmer, 2016 p. 331) Based on Kazmer (2016, p. 340) rough estimation of the amount of ejection force injection molding machine can provide is 2% of its clamp tonnage.

According to Kazmer (2016, pp. 334-336) equation for estimating ejection force can be derived as following. Friction force is calculated with equation (15)

$$F_{friction} = \mu_s \cdot F_{normal}, \tag{15}$$

where $\mu_s$ is the static friction coefficient between molding and core insert (see table 4), and
$F_{normal}$ is the normal force between surfaces of molding and mold (see figure 16).

*Table 4 Coefficient of static friction for some mold and polymer materials. (Kazmer, 2016 p. 335)*

| Polymer | P-20 Steel [4] | LaserForm ST-100 [3] | SL5170 Resin [3] |
|---|---|---|---|
| ABS | 0.40 | Not available | Not available |
| HIPS | 0.23 | 0.25 | 0.38 |
| HDPE | 0.35 | 0.54 | 5.47 |
| PA6 | 0.54 | Not available | Not available |
| PC | 0.31 | Not available | Not available |
| PP | 0.36 | Not available | Not available |

Based on the figure 16, ejection force can be expressed with friction force and draft angle (equation (16)):

$$F_{eject} = \cos(\phi) \cdot F_{friction} = \mu_s \cdot \cos(\phi) \cdot F_{normal}. \tag{16}$$

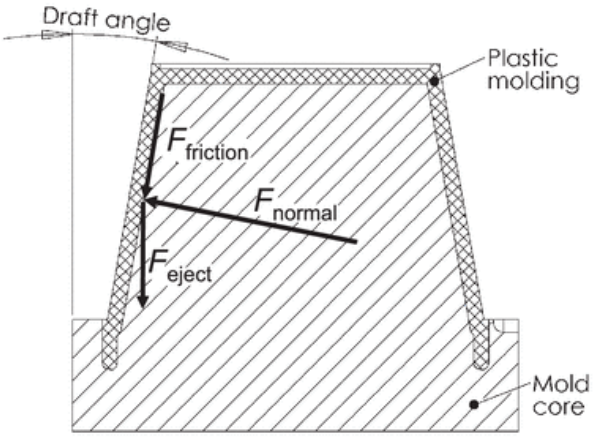


*Figure 16 Ejection, normal and friction force vectors. (Kazmer, 2016 p. 335)*

Normal force, $F_{normal}$, results from internal tensile stresses in plastic, which makes the plastic to stick into the core (equation (17)). This can be expressed as the multiplication of tensile stress and cross-sectional area of the plastic in which the stress acts (=effective area)

$$F_{normal} = \sigma \cdot A_{eff}. \tag{17}$$

Thermal contraction of the solidifying plastic melt is assumed to cause the tensile stresses into the molded part. This tensile stress, $\sigma$, can be expressed with Hooke's law of elasticity (equation (18))

$$\sigma = E\varepsilon, \tag{18}$$

where $E$ is the modulus of elasticity at room temperature
$\varepsilon$ is the thermal strain.

Thermal strain (equation (19)) is expressed with the coefficient of thermal expansion, $\alpha$, and temperature difference between the solidification and ejection temperatures:

$$\varepsilon = \alpha \cdot \left(T_{solidification} - T_{ejection}\right). \tag{19}$$

For the plastic cup shown previously in figure 16, this effective are is shown in figure 17.

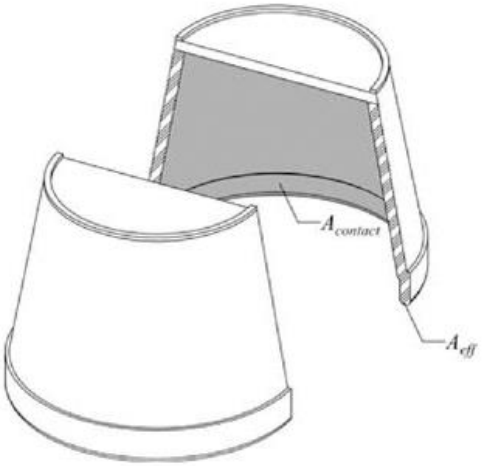


*Figure 17 Effective area of example part (plastic cup). (Kazmer, 2016 p. 337)*

Now the ejection force can be stated with equation (20)

$$F_{ejection} = \mu_s \cdot \cos(\phi) \cdot E \cdot \alpha \cdot \left(T_{solidification} - T_{ejection}\right) \cdot A_{eff}. \qquad (20)$$

# 4 Validating injection molding by simulation

This chapter describes how the different process parameters and the optimal process window for injection molding can be determined. Furthermore, different stages of the process and parameters are discussed with the simulation perspective. In the end of the chapter, previous research in the field of injection molding simulation is discussed and scope of the research cases of this master's thesis are presented.

## *4.1 Process window*

There are multiple process parameters in each phase of injection molding which affect the final part quality. For this reason, it is important to know the parameters which can produce acceptable parts. In figure 18, a schematic of process window is shown. If process parameters outside the green region are used, unacceptable part quality will result.

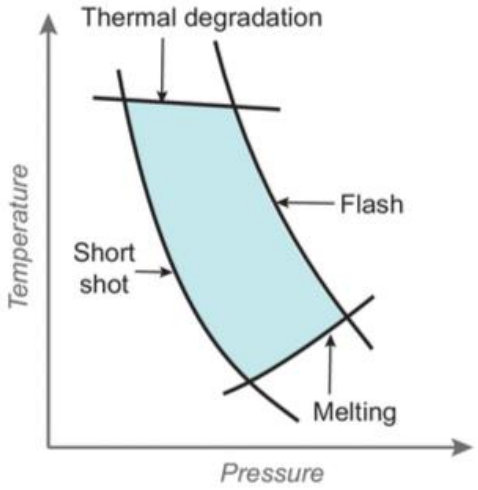


*Figure 18 Processing window. (Wang, et al., 2018 p. 93)*

Process to find the optimal parameters will start from dry cycles where operation of the mold is verified. After that, the molding trials are started first with low injection pressure and without any packing pressure to find the pressure needed to fill the cavity. Then the required packing time for the gate to freeze can be determined and finally the whole process will be optimized to find the most efficient combination of parameters. Flow chart to describe the setup process is shown in figure 19.

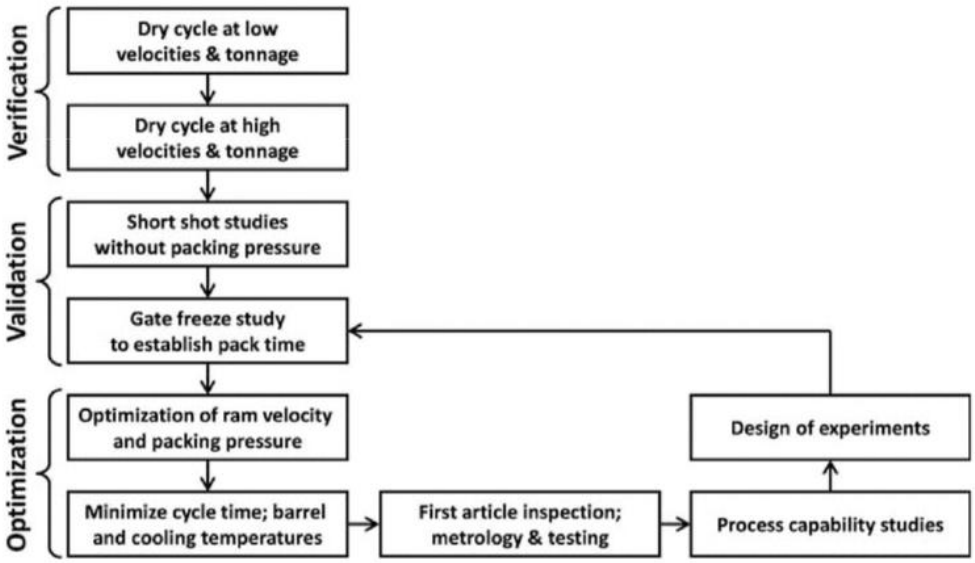


*Figure 19 Flow chart of determining process conditions for injection molding. (Kazmer, 2016 p. 470)*

Material suppliers provide range of guide values for molding different materials. These values are suggestive for the first molding trials. Proper injection pressure can be determined by starting the molding trials with the minimum injection pressure given by the material supplier. Barrel temperature should be set to minimum and packing pressure to zero (Kazmer, 2016 p. 471). Injection pressure is increased until the cavities are filled. When the injection pressure needed to fill the cavities is determined, 5-10% increase to this pressure can be used as the production injection pressure. With too high injection pressures flashing can occur. Suitable injection time can be determined by measuring weight of the injection molded parts. When part weight doesn't increase when injection time is increased, injection time is equal or above the solidification time. If injection time is below the solidification time, part weight will decrease and sink marks can occur. (Bryce, 1996 pp. 96-97; Goodship, 2017 p. 197)

Packing pressure can be set to be 80% of the injection pressure needed to fill the mold cavity (Kazmer, 2016 p. 294). Packing pressure should be applied until gate is sealed and melt plastic cannot flow back from the cavities. Proper packing time for a cold runner mold can be determined by decreasing the packing time until sink marks appear. Occurrence of sink marks is a sign that the gate hasn't freeze. When the sink marks have occurred, packing time is increased with 1 second intervals until sink marks aren't noticed in five cycles. This kind of study for an optimal packing time can only be done to cold runner molds as in hot runner systems the gate area doesn't freeze, and due to this weight of the part changes only little (Kulkarni, 2017 p. 260). For amorphous thermoplastics packing pressure should be reduced in the end of packing phase to prevent inducing high stresses inside the part and for semi-crystalline thermoplastics a constant holding pressure is usually preferred due to the crystallization process. (Bryce, 1996 p. 97; Goodship, 2017 p. 197)

Determining optimal process window for packing pressure and packing time for hot runner mold can be done by eliminating first the combination of parameters which cause defects e.g. short shots, sink marks, flashing and high stresses. After the set of parameters that can produce visual acceptable parts are found, DOE can be applied to find the parameters which results parts inside dimensional tolerances. Figure 20 shows a visual

inspection template (VIT) for a two-cavity screen model used in irrigation industry. This is an example case for which the process parameters are defined based on Kulkarni (2017, pp. 260-263). It is noted that there are three different process windows which produce visually acceptable parts. Window 3 is selected for a closer look for a DOE analysis to determine the process parameters which can produce dimensionally accepted parts. (Kulkarni, 2017 pp. 260-261)

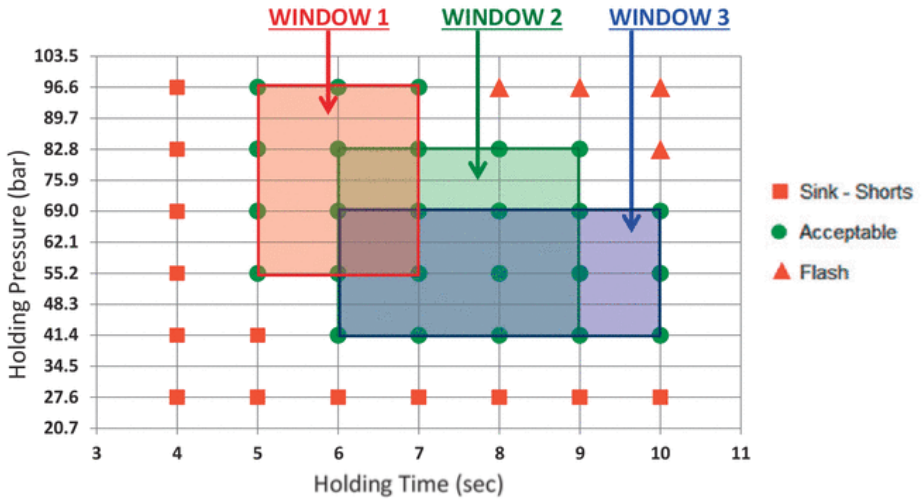


*Figure 20 Set of packing pressures and times which will cause acceptable/unacceptable parts based on visual evaluation. Red rectangular means that product has sink marks or short shot occurred, green circle means acceptable parts and red triangular indicates flashing. (Kulkarni, 2017 p. 261)*

Table 5 shows the set of parameters which are used in DOE analysis. The minimum and maximum values are selected for the DOE analysis. Dimensional tolerances for the part are $126{,}80 \pm 0{,}07\ mm$. (Kulkarni, 2017 p. 261)

*Table 5 Test sets for DOE. Table is formed based on (Kulkarni, 2017 p. 261).*

| Experience number | Hold time (s) | Hold pressure (bar) |
|---|---|---|
| 1 | 10 | 69,0 |
| 2 | 10 | 41,4 |
| 3 | 6 | 69,0 |
| 4 | 6 | 41,4 |

Results from the DOE analysis are shown in figure 21 where green lines represents the parts inside the tolerance, and red lines the unacceptable parts. Results of both cavities are plotted into the same figure, where the solid contour lines represent cavity 1 and dotted contour lines cavity 2. Process window is determined from the same figure by selecting the area where dimensions are under the dotted orange contour line (= the upper limit for cavity 2 to produce parts inside the tolerance). The center values of the process window should be selected as the process settings to achieve a robust process. Similarly, the effect of other parameters to the part quality can be taken account and process window for the whole injection molding process can be determined. (Kulkarni, 2017 p. 263)

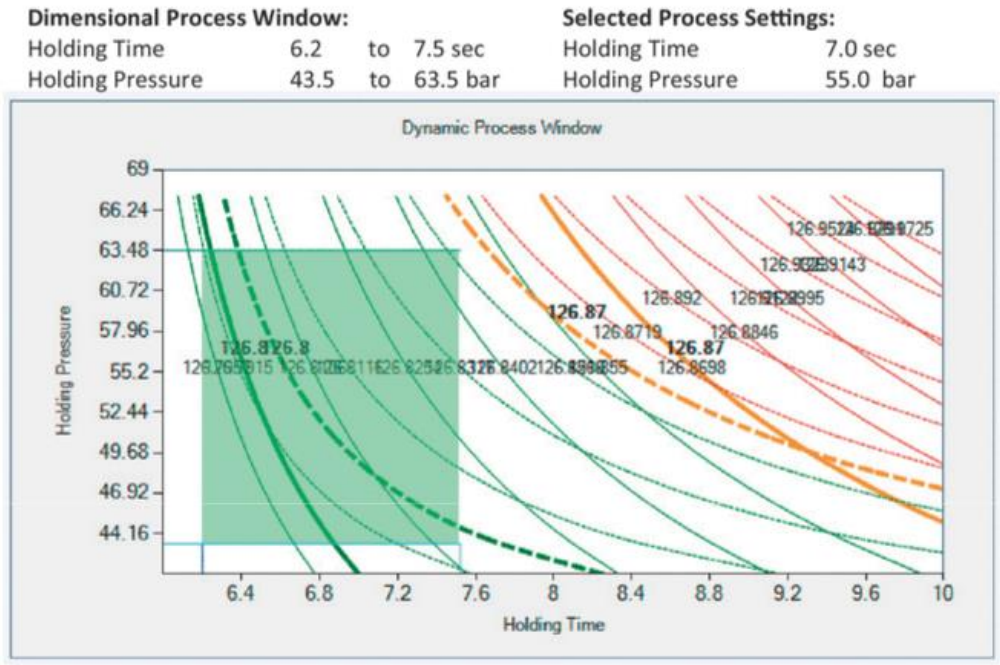


*Figure 21 Results of DOE for cavity 1 (solid contour line) and cavity 2 (dotted contour line). (Kulkarni, 2017 p. 263)*

Cooling time can be determined with molding tests where molding is conducted with different cooling time durations. With optimal cooling time, part dimensions are constant and inside tolerances in each cycle. After molding parts with different cooling times, critical dimensions of the parts are measured and presented in a same graph with the equivalent cooling times. From this graph, the optimal cooling time value can be determined by choosing an option which has the most dimensional accuracy. (Kulkarni, 2010 pp. 135-136)

*Table 6 Results of change in different parameters. Table is formed based on Bryce (1996).*

| Parameter | Change | Result |
|---|---|---|
| Injection pressure | Increase | Less shrinkage<br>Higher gloss<br>Less warp<br>Harder to eject |
| | Decrease | More shrinkage<br>Less gloss<br>More warp<br>Easier to eject |
| Back pressure | Increase | Higher density<br>More degradation<br>Fewer voids |
| | Decrease | Lower density<br>Less degradation<br>More voids |
| Melt temperature | Increase | Faster flow<br>More degradation<br>More brittle<br>More flashing |

| | | |
|---|---|---|
| | Decrease | Slower flow<br>Less degradation<br>Less brittle<br>Less flashing |
| Mold temperature | Increase | Longer cycle<br>Higher gloss<br>Less warp<br>Less shrinkage |
| | Decrease | Faster cycle<br>Lower gloss<br>Greater warp<br>Higher shrinkage |

## *4.2 CAE in injection molding*

In injection molding simulation software, the part geometry is a mesh of finite elements where the flow, pressure and temperature can be solved (Kazmer, 2016 p. 122). These simulation results can be used to predict filling pattern, pressure distribution, shrinkage and warpage. Subchapters here describes some of the simulation results and how they should be analyzed.

### 4.2.1 Filling and packing

Cavity filling analysis provides information of the required injection pressure to fill the cavity. Most injection machines can provide injection pressure of 200 MPa, but after taking account of losses in the runner system, 100 MPa is widely used maximum limit for the cavity filling pressure to assure that the injection molding machine can provide high enough cavity pressure to fill the mold. Using lower melt pressures, lower mold clamping forces are needed, and more safety margin is given e.g. for the pressure drop in the feed system. In the other hand, a very low filling pressures in the filling analysis can be a sign from too thick sections in a molded part, or incorrect process parameters. These parameters can be example melt or mold temperature as well as filling time. (Kazmer, 2016 pp. 109-111)

As previously mentioned in the section 3.3.3, the allowed shear stress and shear rate values differ for different materials. From the results of filling and packing analysis values of shear should be checked in order to avoid causing visual defects or thermal degradation to the material (Kazmer, 2016 pp. 198-199).

### 4.2.2 Shrinkage and warpage

Shrinkage can be divided into two cases: mold shrinkage and post-mold shrinkage. Mold shrinkage is defined to be the difference in dimensions between the mold cavity and the molded part 24 hours after ejection (Campo, 2006 p. 532). When shrinkage occurs 48 hours after molding, it is called as post-mold shrinkage. Post-mold shrinkage can occur when part is subjected to moisture or temperature. When small cycle times are targeted, cold molds are used to decrease the cooling time. This can lead to freeze stresses inside the part, which are relaxed during time and shown as post-mold shrinkage. (Fischer, 2003 p. 16)

Shrinkage can be expressed as linear or volumetric shrinkage. Linear shrinkage affects in one direction, when volumetric shrinkage influences in all three dimensions. If linear shrinkage in all dimensions is equal, then the shrinkage is isotropic. If the shrinkage values are not equal, shrinkage is anisotropic. Figure 22 shows two cubes which the one on the left has original dimensions, L, and the one in the right has experienced isotropic shrinkage. Original cube's each side has the length of L and shrunken cube's L(1-s), where the s corresponds to the linear shrinkage affecting each direction. Volume of the original cube was $L^3$, whereas the shrunken one can be expressed with $(L(1-s))^3$ or $r_vL^3$, where $r_v$ is the volumetric shrinkage. (Kazmer, 2016 p. 300)

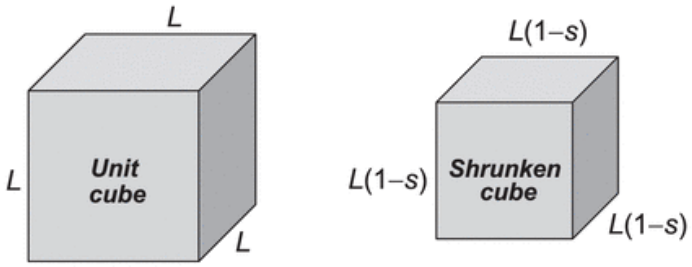


*Figure 22 Volumetric and linear shrinkage. (Kazmer, 2016 p. 300)*

Shrinkage is highly depended on the material being processed. For semi-crystalline polymers shrinkage is higher (usually from 1,0% to 4,0%) than for amorphous (usually from 0,3% to 0,7%) (Campo, 2006 pp. 533, 537). Shrinkage can be affected by adjusting the process parameters (figure 23). Use of high injection pressures and injection times can reduce the shrinkage as more plastic melt is injected into the mold cavity to compensate the already cooling and shrinking plastic in the cavity (Campo, 2006 p. 535). As well by increasing the packing pressure and time, shrinkage can be decreased due to increased packing of the mold cavity. Packing pressure profile has as well impact on the amount of shrinkage as usually high packing pressure is applied first to compensate the shrinkage far from the gate. When plastic near the gate starts to solidify, packing pressure is decreased. (Kazmer, 2016 pp. 312, 323)

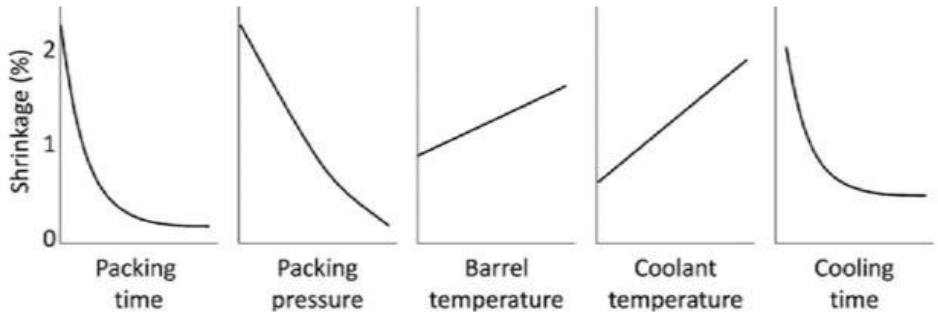


*Figure 23 Process parameters vs shrinkage. (Kazmer, 2016 p. 312)*

Warping is generated from non-uniform shrinkage which causes the part to bend or twist. This can be due to uneven cooling (in figure 24) or because of too low melt temperature. Temperature differences can occur e.g. in mold corners or near gates. Warping can also be developed because of problems with part or mold design. Dissimilar wall thicknesses and gating from a thin section of the part are examples of these cases. (Fischer, 2003 pp. 12-13)

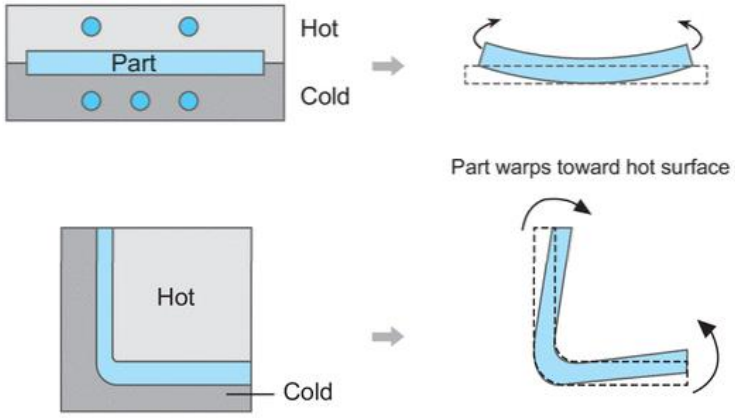


*Figure 24 Warpage because of uneven cooling. (Wang, et al., 2018 p. 285)*

### 4.2.3 Cooling simulation

Cooling takes about 70 to 80% of the lead time of an injection molded product, which makes it an important factor to optimize (Wang, et al., 2018 p. 237). Cooling analysis in the simulation software can be used as a tool to study if the cooling time is sufficient. Cooling time shouldn't be set too long as it will increase the process cycle time. Cooling time is sufficient when the whole part has achieved the eject temperature during the cooling time. Temperature differences in the part should be small in order to prevent uneven temperature distribution which will lead to warping of the part. This can be reviewed from the simulation results by studying the temperatures in the part and as well the cooling efficiency of the cooling channels. Coolant temperatures in the inlet and outlet point of cooling channel should be analyzed, and their difference shouldn't be higher than 3°C. If the temperature change in the cooling channel is above the 3°C, it can be sign of too low coolant flow rate. (Wang, et al., 2018 pp. 255, 257)

### 4.2.4 Venting

During injection of plastic melt into the mold cavity, plastic melt fills the cavity and replaces the air present in the cavity. This air needs to be removed from the cavity to avoid causing air traps. Location of air traps can be reviewed from the simulation results. Air traps can cause degradation of the plastic as the temperature in the cavity increases due to air compression in the cavity. This will cause burn marks to the final part. Other defect of air traps is short shot as the compressed air in the cavity can form a pocket which the plastic cannot get through. Trapped air can be removed for example with venting channels in the mold parting line (figure 25). Depths of these venting channels are small, usually from 0,01 to 0,04 mm, as the small depth will prevent the plastic melt to escape from the mold cavity. This is due to the skin layer (usually 0,01 to 0,02 mm thick) which forms when plastic melt flows into mold cavity and starts to solidify as soon as it touches to the mold walls which have lower temperature than the melt. Depth of the venting channel is depended on the plastic material, as smaller gap is needed for materials with higher flowability and bigger gap for materials with lower flowability. Based on (Wang, et al., 2018 p. 85) required venting gap for PA is approximately 0,005-0,015 mm and for PC approximately 0,01-0,03 mm. Air traps are possible to study with injection molding simulation to see their estimated placement. (Mennig, et al., 2013 pp. 37-38; Kazmer, 2016 p. 227; Wang, et al., 2018 p. 84)

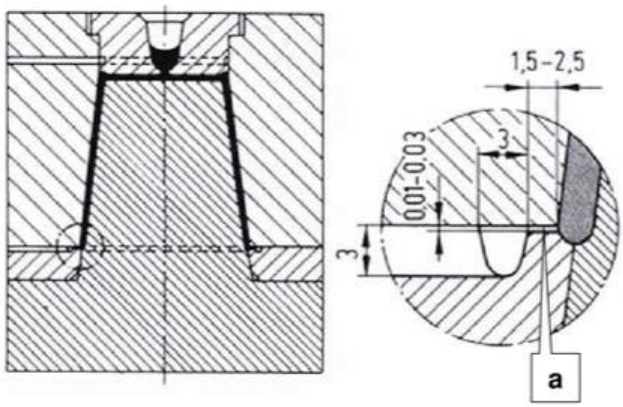


*Figure 25 Venting channel, a, in the mold parting line. (Mennig, et al., 2013 p. 38)*

### 4.2.5 Dynamic loads on mold/mold inserts

Studying dynamic loads on mold or mold inserts with computer aided tools can be done with finite element analysis (FEA) where the pressure loads are first determined with injection molding simulation. Other way to study dynamic loads on mold inserts with injection molding simulation is the core shift analysis in Moldex3D. Core shift analysis studies deflection of the mold inserts caused by uneven pressure distribution in the mold cavity during filling stage. Core shift in Moldex3D can be studied with one-way or two-way analysis where the difference is that the two-way analysis takes account the effect of deformation of mold insert(s) to the melt flow, whereas the one-way analysis doesn't take account the flow restricting effect of deforming mold inserts. (Moldex3D, 1995-2019)

## *4.3 Previous research and examples from industry*

There has been previous research on how well CAE injection molding simulation software's can predict the injection molding process. In a research by Gelotte, et al. (2007) comparison of injection molding simulation results to actual molded part was conducted. This research was concentrated on predicting the flow pattern and required injection pressures with Moldflow simulation software and validating these simulation results by molding with corresponding process values. Results of this research were that the simulation results of flow pattern were similar to the real experiments and the predicted injection pressures had some similar dependency as in the real case, but there was difference in the pressure levels. Noticeable is that the simulation was conducted by modelling only gate, and not taking account runner system and machine nozzle. This was one possible cause why the amount of required injection pressures differed in the simulation and in the real molding experiment, as the feed system creates pressure losses to the injection pressure.

Core shift in injection molding has been studied before by doing a core shift analysis with simulation or numerical method, and then comparing those results to real molding trials. One of these studies is by Dong-Gyu, et al. (2010), where the effect of four process parameters to core shift were studied, and optimal process conditions to minimize the core deflection were determined. Injection molding of the battery case was simulated with DOE to minimize the core deflection and to study which process parameter was the most domineering to the core shift. Initial mold temperature, injection time, injection pressure and holding time were varied during this research to find the optimal process conditions.

The optimal process condition was found when injection pressure was the lowest, and this was confirmed with molding trials. It was found out that injection pressure had the most effect to core shift, 76,3%, and injection time and initial mold temperature had only small effect. In a research by Kim, et al. (2013), an automotive part was studied with injection molding simulation in order to study the cause of mold failure. To confirm the accuracy of simulation software to predict the pressure profile, practical molding tests were conducted and melt pressure measured with piezoelectric pressure transducer. Measured pressure profile during molding of the part had similar profile to the one predicted by simulation. Stress analysis was conducted based on the maximum pressure from the simulation and it showed a stress concentration in the place where the actual mold has had fractures. With the fatigue life estimation made by the researchers, design changes to the mold were proposed to increase the mold's life estimation.

ABB has previous experience of tool insert deformation during injection molding. Below, figure 26 shows an example product from ABB which has had difficulties with the mold deformation leading eventually to mold failure. Cover is from R8 size drive and height of it is approximately 964 mm and width 297 mm. In the center of the part there is ribbed area which is manufactured with 103,4 mm long tool inserts. Thickness of these inserts is about 11,6 mm at the base and 6,7 mm at the tip. Cover is injection molded with four hot runner gates placed on top of the ribs. Results from the injection molding trials are shown in figure 27. Figure shows that wall thickness of the waved area is uneven due to bending of mold inserts. Because of this, after few molding cycles, fractures were discovered on the base of the tool ribs. This was later studied with simulating and it was noticed that the pressure difference over the tool inserts caused notable displacement to the tool insert, which are seen as uneven wall thickness in the part, as figure 27 shows. Pressure differences over the tool insert, causing the insert cracking, were approximately 5 MPa. Due to this previous case regarding mold failure, second case study of this thesis was selected to concern dynamic loads on mold inserts and insert deflection.

*Figure 26 Cover part of R8 drive.*

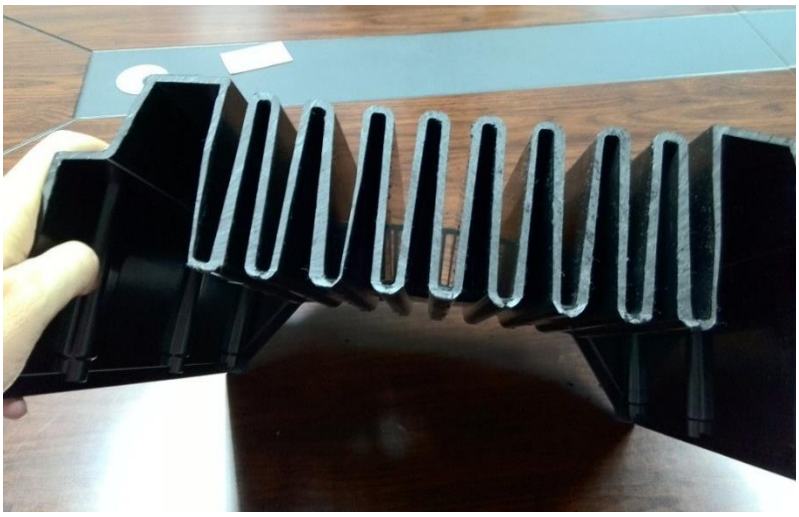

*Figure 27 Results after molding trials. Cross-section of the ribbed area. Some inserts have bent and caused uneven wall thickness.*

## 4.4 Research cases: Assuring product and mold design with injection molding simulation

This master's thesis consists of two separate research cases which are studied to gain knowledge to assure product and mold design by using an injection molding simulation software to verify design choices. Utilizing injection molding simulation more on product design and mold approval phase at ABB Drives will give a tool to validate the product and mold design before the mold construction and first molding trials. This will help to predict possible risk areas which could cause premature mold failures, even before a mold construction.

Practical study of this thesis is divided into two separate case studies. The first case study object is an existing product at ABB Drives, which is simulated to check how the simulation results correspond to results of real injection molding process. After verification of the simulation results, studies with simplified cooling channels and default process parameters are done. Also, an alternative material is studied for the same product. The primary material used for this product is PC-ABS and the alternative material studied is polypropylene. Second research case is related to dynamic loads in mold and especially on mold inserts. Product of this study is a gland box for a drive. Mold for this gland box is, during the work of this thesis, being constructed and first trials with the new mold have led to cracks in the tool inserts. To solve these problems, filling studies are done for the part to find out pressure levels causing the cracking. Effect of geometrical changes and different locations of gates are studied to find a solution which reduces the risk for insert failing.

### 4.4.1 Scope and goal of the study

Goal of this study is to assure quality of injection molded parts at ABB Drives, by gaining knowledge on the capability of injection molding simulation to predict behavior of the part and mold during the injection molding process. Study is divided into two separate case study from which the both concern existing products at ABB Drives. The second case studies dynamic loads in order to gain knowledge on predicting and preventing premature mold failures by solving a current tool insert failing problem. There have been

some premature mold failures at ABB because of high dynamic loads resulting from high pressure differences over mold inserts. Therefore, one part of the scope of this thesis is to gain information on how these premature mold failures could be prevented before a mold construction or first molding trials by injection molding simulation.

First case study is used to verify the simulation results with results from practical injection molding. For this case study, a product from ABB Drives is simulated with the real manufacturing parameters. Furthermore, the simulation model is constructed to imitate the real mold to ensure that the circumstances are as close to the real molding process as possible. When the simulation results have been confirmed, studies with simplified cooling channels, default process parameters and alternative material are conducted. Results with simplified cooling channels are compared with results of real cooling channels, as the exact cooling channel design is not known at the product design phase. Therefore, simplified cooling channels are constructed to imitate a situation where a new product is being simulated for the first time. For the same reasons, also a comparative study, with default process parameters (from Moldex3D) and simplified cooling channels, is done. Primary material for the cover is PC-ABS but due need to minimize the combustion gases in the future, alternative material for the cover could be polypropylene. Therefore, one simulation is done with polypropylene to see how much the results differ from PC-ABS's.

To prevent premature mold failures in the future, it is important to gain more knowledge of the dynamics loads during injection molding. Furthermore, knowledge on how possible risk areas in the mold could be identified with the simulation software, would help to prevent the mold breakdowns. Therefore, the second case study is about dynamic loads on mold inserts. Dynamic loads on mold inserts are studied with a practical problem case at ABB during the work of this master's thesis. Product of this case study is a gland box for a drive. Mold for this product is being constructed and in the first molding trials, mold inserts have had cracks and they have been noticed to bend during molding. These results as failed inserts but also as improper product quality due to uneven wall thickness in the product. To reduce the risk for insert bending and breaking, filling studies are made for the gland box. Filling studies are used to find out the pressure levels causing the inserts to fail. After this, few different part designs and gating locations are studied to find a one where pressure levels would be lower than with the initial design. In addition to filling studies, also core shift analyses are done for two of the most optimal cases to review predicted stress levels on the inserts and their estimated displacements during filling. Only filling analyses are done as the pressure differences during filling are assumed to be higher than in the packing phase as in the beginning of filling phase, there aren't any melt in the cavity to restrict the insert bending.

# 5 Simulations and practical experiments

This chapter contains the practical part of the thesis and is divided into two separate case study. First case is IP21 cover of ACS580-01 drive, an existing product at ABB. IP21 cover is used to verify the equivalence of simulation and injection molding process. Part is first simulated with the real process parameters. Results from this simulation are then compared to the real products to review dependency between simulation and real injection molding process. Simulation model for the first case study is constructed based on real mold construction which includes mold base, hot runner, gate and tempering channels. As this simulation model consists of real tempering channels which aren't known in case of simulating new product which mold hasn't been constructed, comparative study with simplified cooling channels is made to see how results from cooling analysis differ. For the same reason, a study with default process parameters (from Moldex3D) is done to see how results differ. Additionally, one study with alternative material, polypropylene, is done to see how it behaves when compared to PC-ABS. This is due the need to minimize IP21 cover's combustion gases in the future, and the possible alternative material could be polypropylene.

Second case study is related to dynamic loads on tool inserts and it concentrates on studying the pressure levels causing insert failure in a new mold constructed for ABB. Product of this case study is a gland box for a drive. Gland box has double walls which are manufactured with two quite high and thin beryllium copper inserts. During first molding trials, cracking occurred in the base of the inserts and it was noticed that inserts had bent during molding as the wall thicknesses of the gland box were uneven. This problem was tried to solve by adding two extra gates to even melt pattern and pressure differences over the inserts. However, also these molding trials resulted with cracks in the inserts and they bent as before. To solve these problems, four other possible solutions with some geometrical changes and different gating locations are studied to find the most optimal design for the new molding trials. Goal of this case study is in addition to solving the reasons for insert failing, also to gain knowledge of the pressure levels causing insert breaking, and comparing how different changes affect pressure differences over the insert.

## *5.1 Case 1: ACS580-01 R1 IP21 cover*

Object of this case study is an ACS580-01 R1 IP21 cover (figure 28) which is an existing product at ABB. Cover is used in ACS580-01 R1 IP21 drives (figure 29). Material of the cover is PC-ABS and its nominal wall thickness is 3,0 mm. Most of the surfaces are visible when assembled into a drive and therefore, good surface quality is required for the external surfaces. Standard DIN 16742 with tolerance group TG 4 is used to specify the accepted tolerances. Main dimensions of the product with tolerances are shown in figure 30 and more specifications of the part are collected to table 7.

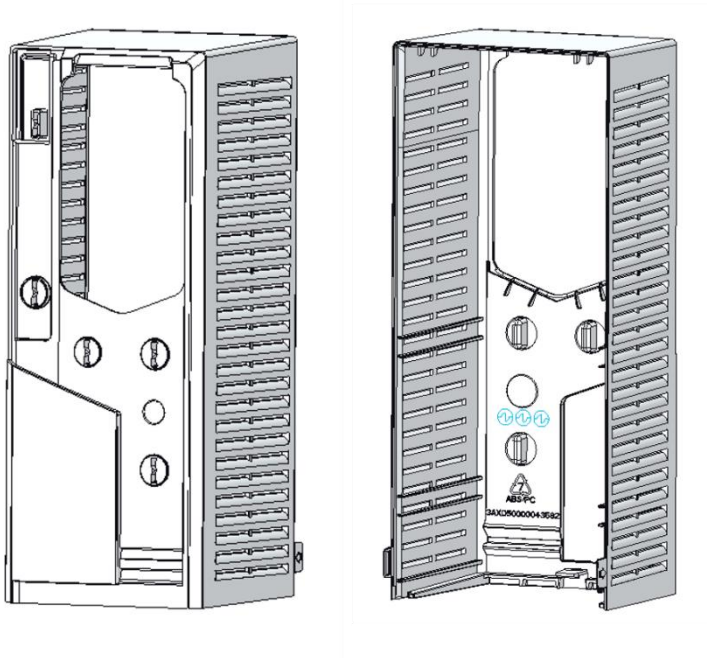

*Figure 28 3D schematics of the IP21 cover.*


*Figure 29 ACS580-01 drives, frame size R1-R4. R1 furthest on the right. (ABB Oy, 2019)*

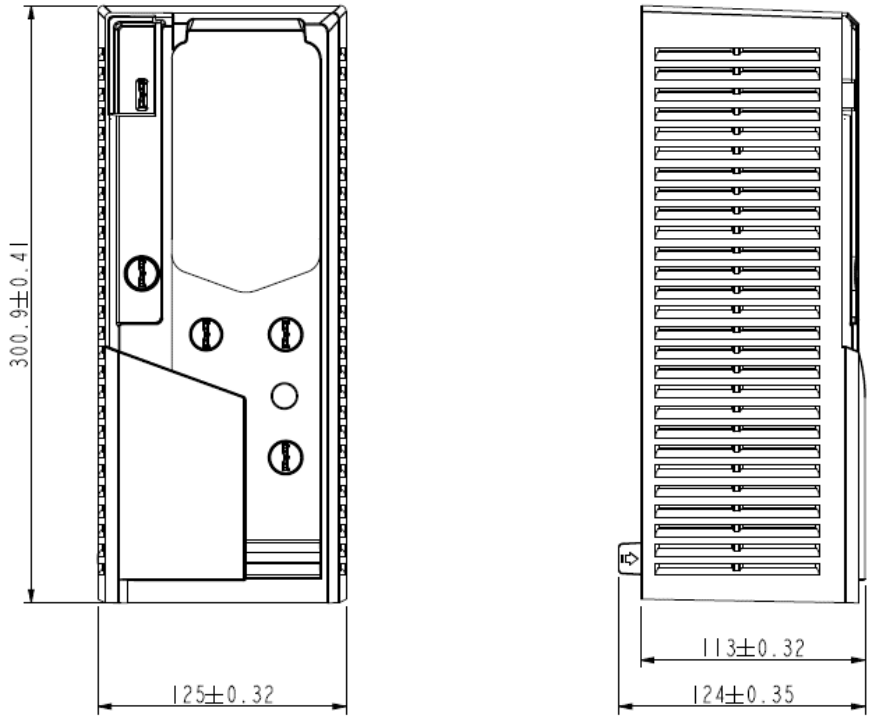


*Figure 30 Main dimensions of IP21 cover with tolerances based on tolerance group TG4 from standard DIN 16742 (2013).*

*Table 7 Specifications of the IP21 cover.*

| **Parameter** | **Value** |
|---|---|
| Nominal wall thickness | 3,0 mm |
| Volume | 259,2 $cm^3$ |
| Material | PC-ABS |
| General tolerance | DIN 16742 |
| Tolerance group | TG 4 |

IP21 cover is manufactured with one-cavity hot runner mold with 16 individual tempering channels. Size of the mold is 600x665x700 mm (maximum dimensions). Mold has one hot runner gate which placement compared to the part is shown in figure 31. Gating is on a non-visual surface as in the final assembly there will be a brand plate assembled on top of that surface. Gate diameter is 5 mm and runner diameter 8 mm. Length of the runner is 261 mm.

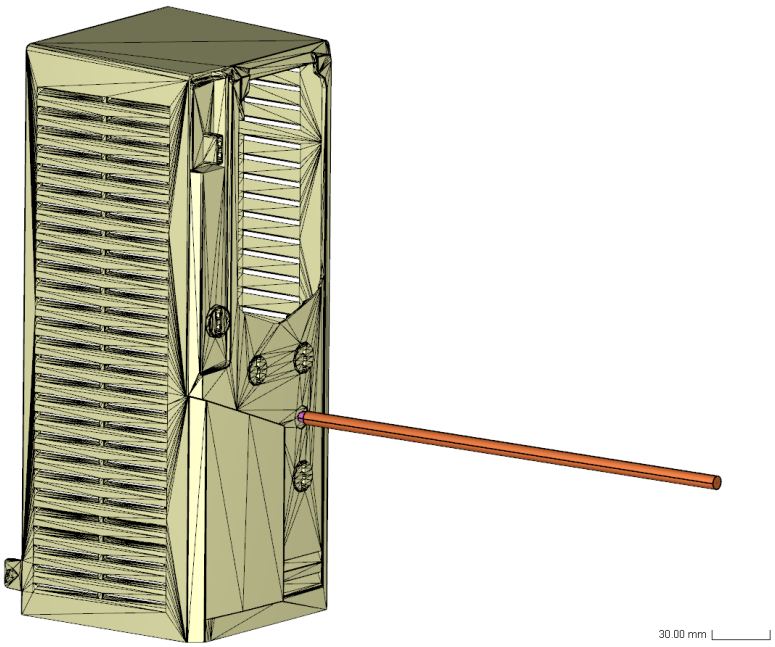


*Figure 31 Location of gate and runner.*

### 5.1.1 Object of the study

Object of this case study is first to analyze how results from injection molding simulation correlates to results seen in actual injection molding process. This is carried out by simulating IP21 cover with the process parameters used in its production. This product was chosen as it is an existing product at ABB and its behavior in injection molding is known. Also, a comparative study with simplified cooling channels is made to study how much simplification affects warpage results. This is done as usually in the product design phase the exact cooling channel design isn't known as the mold hasn't yet been constructed. Furthermore, one simulation is conducted with default process parameters from Moldex3D, to see the difference in results between default and real molding parameters. Another simulation is done by using polypropylene instead of PC-ABS, to see difference in their behavior and to analyze if polypropylene could be used in a mold designed for PC-ABS.

### 5.1.2 Hypothesis of the study

Based on previous research (presented in chapter 4.3) on how well the simulation programs are capable to describe and calculate injection molding process, it is assumed that simulation results will predict behavior of the product close to real. Still, some differences will result as the simulation software likely assumes the machine response and behavior more optimal than it is in the real process. Also, most likely some difference will be seen in cooling and warping results, as the mold base is modelled as a solid rectangular piece and no cavity or core pieces are included to the simulation model. In a real case mold consists of multiple mold plates, cavity and core pieces, slides and ejector pins. These are all excluded from the simulation model, which will affect cooling as interfaces of different elements are not taken account in the analysis. Some difference is assumed to be seen in the results of simplified cooling analysis when compared to results with real cooling channel design. Most likely the use of default parameters will have more effect on results than the cooling channel design. With polypropylene, shrinkage is expected to increase due to polypropylene's higher material shrinkage.

### 5.1.3 Real molding conditions in simulation

To study correlation between injection molding process and injection molding simulation, simulation model is created with the following objects:

- model of the IP21 cover
- cooling channels
- mold base
- hot runner channel
- hot runner gate.

Model of the IP21 cover was converted into a stl -file which was imported to Moldex3D. Stl -file was used in this case as it produced less problems with mesh than a stp -file. Cooling channels were constructed based on the real cooling channels in the mold. Channels were first formed in Creo as a surface model from the existing model of the mold and this file was exported to stp -file. This stp -file was then imported to Moldex3D, where channels were modeled again to make them compatible with Moldex3D. Without remodeling channels in Moldex3D, simulation software can't handle the cooling channels perfectly. One requirement for a cooling analysis is that the cooling channels inlets and outlets are on the mold base interface. If the cooling channels aren't modeled in the Moldex3D environment, the software can't place the channels inlets and outlets on the interface of the mold base. This will cause errors and performing cooling analysis isn't possible.

Some adjustments for shape and size of the cooling channels were required to make them compatible with the simulation software. Two cooling channels required changes for their shape as the simulation software couldn't operate with a channel which outlet wasn't orthogonal compared to the mold base. This was solved by forming one additional 90° turn to the channels. This change in the cooling channels is shown in figure 32. Figure 33 and figure 34 shows simulation model where cooling channels are assembled with the molded part. Figures also illustrate inlet and outlet points for each cooling channel. Diameters of the cooling channels are mostly 11 mm but, in few places, there are sections where diameter is 9, 10 or 16 mm.

Model of the mold base is simplified for the simulation and it is modeled as a solid rectangular piece, when real mold consists of several mold plates. Modeling the mold base with a solid piece, will likely cause some variation for the results of cooling analysis (when compared to real case) because the simulation software doesn't take account the heat exchange between the interfaces of the mold plates. Placement and dimensions of hot runner channel and gate are also based on the information of the real mold. Simulation model with part, mold base, hot runner, gate and cooling channels is shown in figure 35.

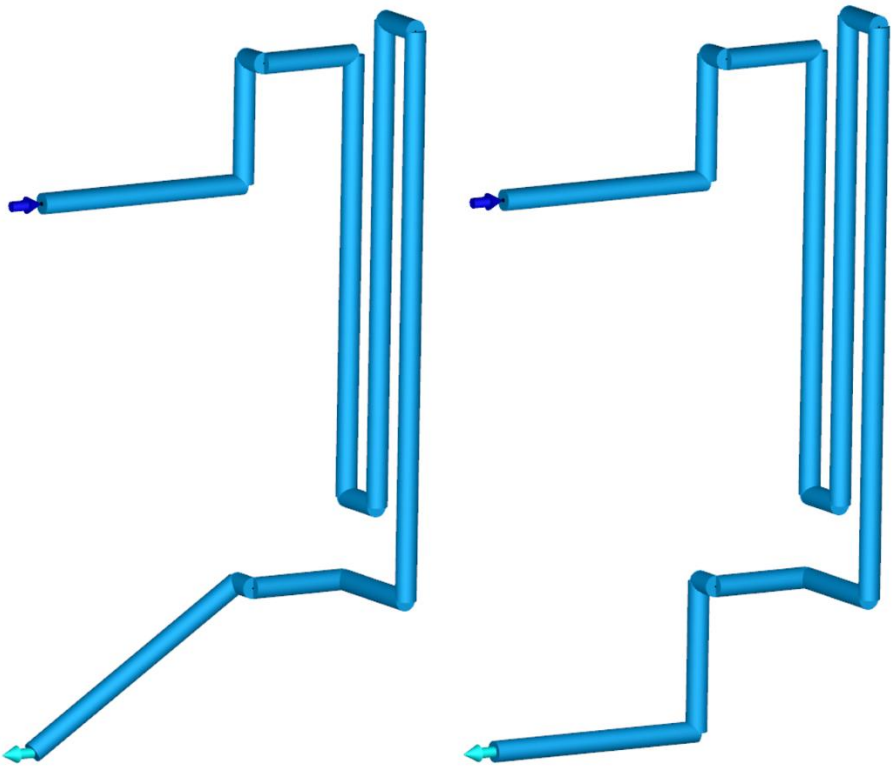

*Figure 32 Change for the cooling channel design. Original design on the left and modified on the right. One 90° turn was added to the outlet part of the cooling channel.*

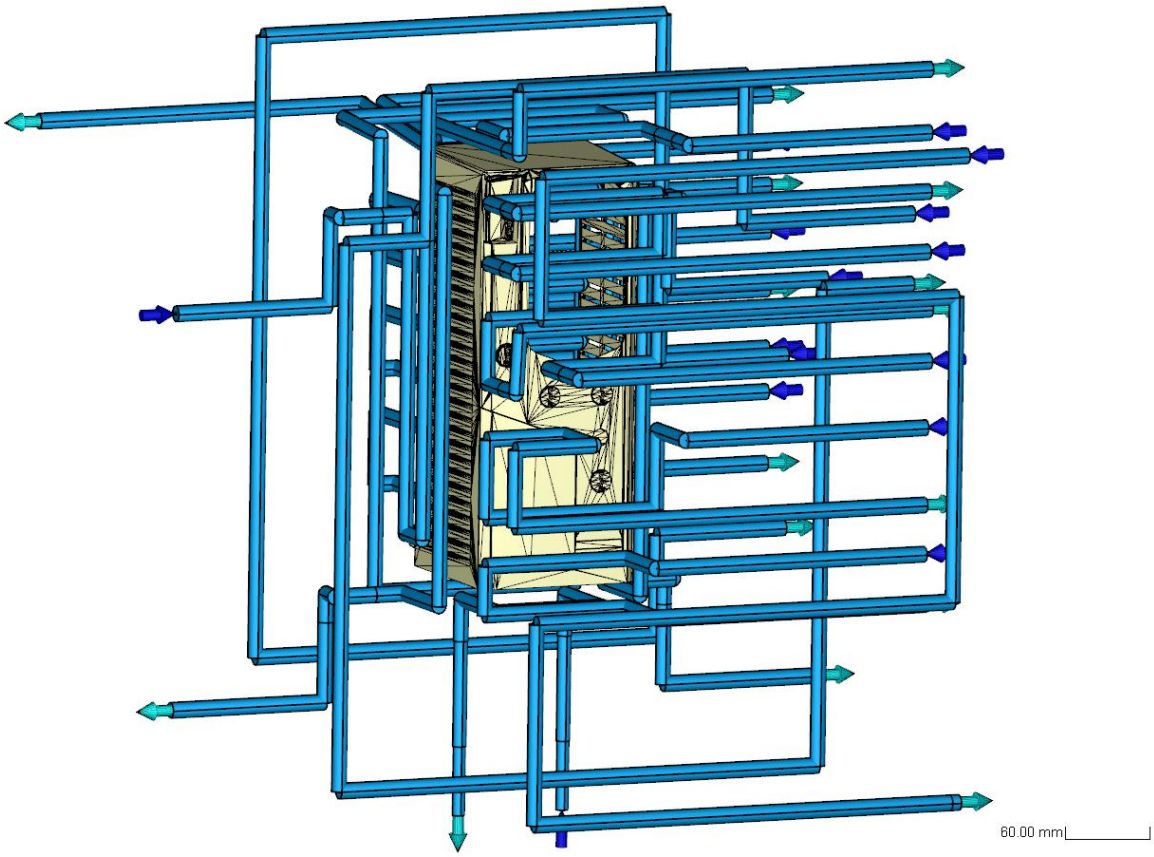


*Figure 33 Simulation model: cover with cooling channels (front view).*

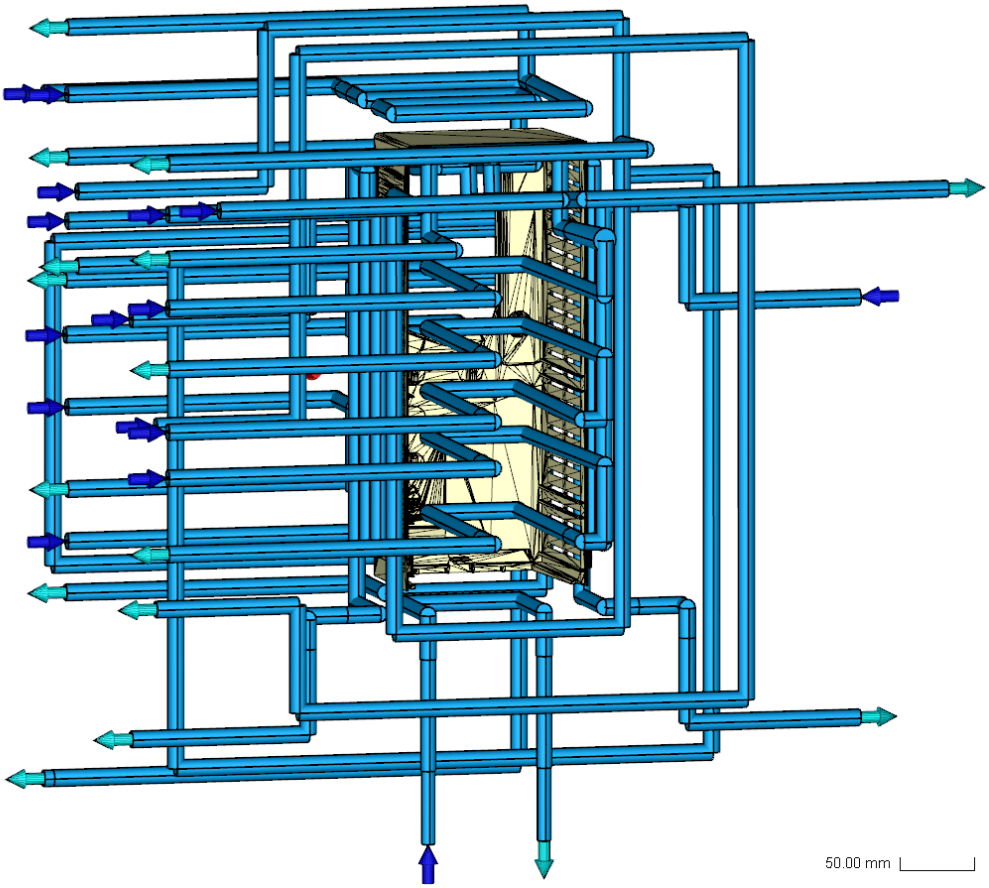


*Figure 34 Simulation model: cover with cooling channels (back view).*

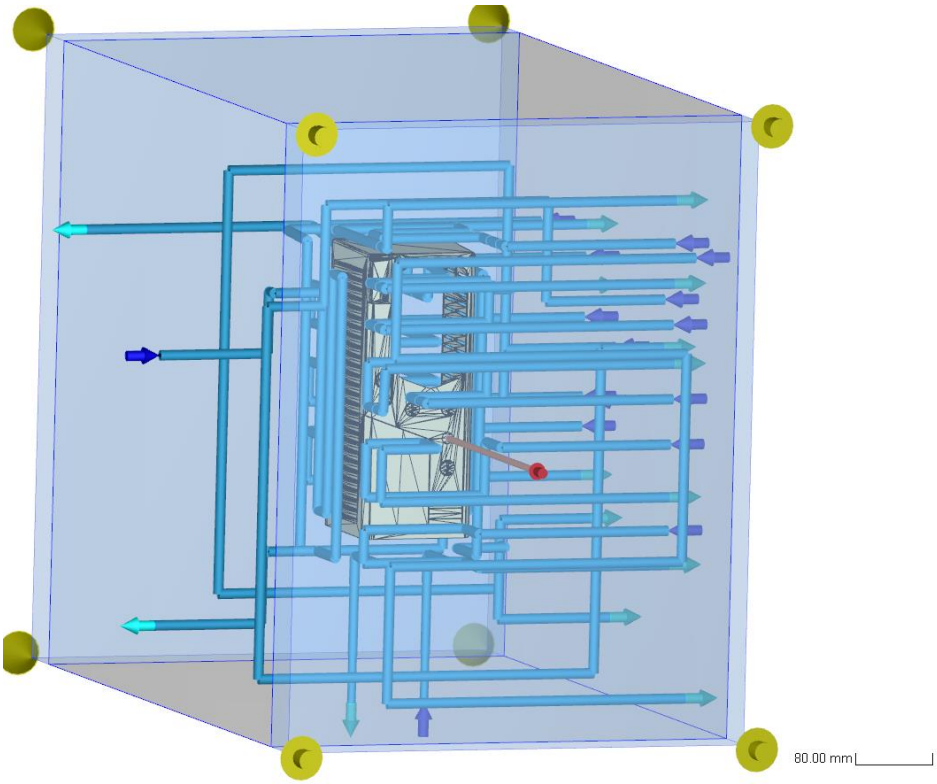


*Figure 35 Prepared simulation model consisting of part, mold base, gate, hot runner and cooling channels.*

Simulation model is meshed with an automatic meshing tool of Moldex3D. Meshing level can be set from 1 to 5, where level 5 has the most elements. For this case study, level 3 meshing is used as it produces a good mesh with good number of meshed elements (table 8). Level 3 meshing keeps simulation duration reasonable and its accuracy is enough as the simulations are inspected in a product designer point of view.

*Table 8 Number of mesh elements.*

| | **Solid mesh elements** | **Surface mesh elements** |
|---|---|---|
| **Part** | 825 302 | 15 590 |
| **Hot runner** | 18 944 | |
| **Total** | **844 246** | **15 590** |

Injection molding of the IP21 cover is simulated with the real molding parameters listed in table 9. These parameters are from the injection molder. Two parameters in the table differs in the simulation from the real molding parameters: filling and cooling times. Filling time is in the real molding process 5 s whereas in simulation it is 2,5 s. This results from incapability of the real molding machine to achieve the filling speeds defined. Due to this, injection happens in the real process slower than simulation predicts, as the molding machine in the simulation predicts more optimal process. Moldex3D's machine interface is used to place the parameters and choose the right injection molding machine, which is used to mold these parts at the injection molder. Cooling time was 22 s in the real molding parameters, but it was noticed from the simulation that part required more cooling time to solidify the plastic in the mold. Due to this, the cooling time was set to 35 s.

*Table 9 Process parameters from practical injection molding.*

| **Process parameter** | **Value** |
|---|---|
| Setting method | Machine mode 1 (by profile) |
| Injection molding machine | Haitian MA4700 II/2950 B |
| Material | PC-ABS |
| Mold material | P20 |
| Mold temperature | 65 °C |
| Melt temperature | 265 °C |
| Filling time | Real: 5 s<br>Simulation: 2,5 s |
| Filling pressure | 88,9 – 113,6 – 108,6 – 108,6 – 108,6 MPa |
| Filling speed | 18 – 20 – 28 – 32 – 20 mm/s |
| Screw position | 85 – 50 – 40 – 30 mm |
| VP switch over by ram position | 30 mm |
| Packing pressure | 64,2 – 59,3 MPa |
| Packing time | 3 – 4 s |
| Cooling time | Real: 22 s<br>Simulation: 35 s |
| Eject temperature | 70 °C |
| Coolant temperatures | 65 °C & 70 °C |
| Coolant flow rates | 120 $cm^3/s$ |

## Results

Filling pressure required to fill the part is 89,36 MPa in 2,552 s (figure 36). Filling pressures defined in table 9 are maximum limits which the sprue pressure during filling

cannot exceed. Filling time in the real process is 5 s and difference in filling times can be explained by the reason that in real molding process, injection molding machine doesn't reach as fast the specified injection speeds than the simulation predicts. As figure 36 shows, there is approximately 20 MPa pressure loss in the runner system. Also, pressure levels at the upper section of the part are lower than near the gate, as it's the last are to fill.

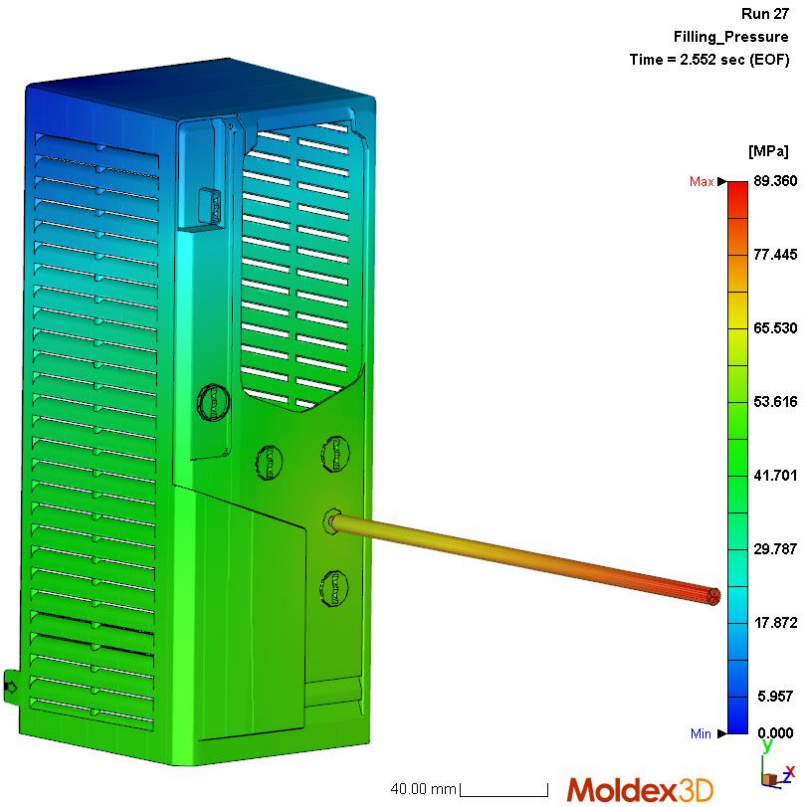


*Figure 36 Pressure distribution in part at the end of filling. Filling pressure required to fill IP21 cover is 89,36 MPa.*

Figure 37 shows pressure distribution inside the part after packing phase. Pressure levels near the gate are above 52 MPa when in one of the small snap fit elements further away from the gate, pressure level has already decreased to 8,2 MPa. Also, on top and side surfaces, pressure has already decreased to 35-40 MPa.

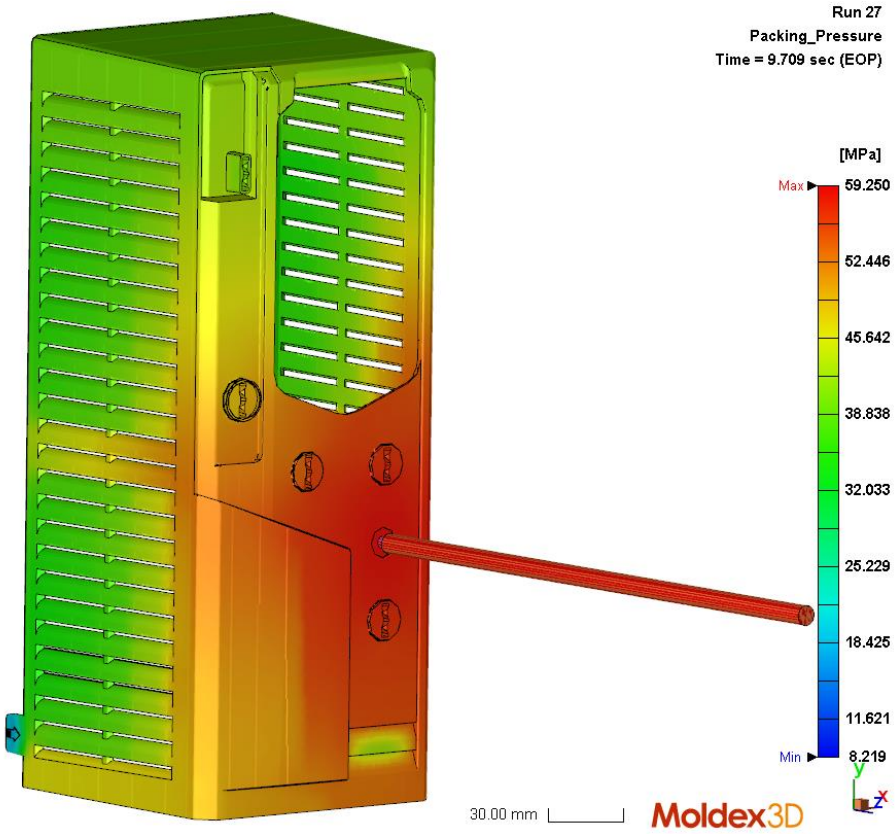


*Figure 37 Pressure distribution in part at the end of packing phase.*

Figure 38 shows cooling efficiency of each cooling channel. Cooling efficiency is defined to be the ratio of heat absorbed by one cooling channel to heat released from the part during molding cycle. Channels with the lowest efficiency rate (shown with blue, green and yellow) are used to control temperature of the mold and they locate further away from the part, which explains their negative cooling efficiency. Other cooling channels have efficiency between 2,69 % and 16,145 %. Best efficiency, 16,145 %, is on the side surfaces of the part. Cooling time for the part was defined to be 35 s. Temperature distribution after 35 s is shown in figure 39. Side surfaces and few parts of the top surface have reached close to the ejection temperature of 70 °C. However, in the back side of the part (figure 39 on the right) is noticed to have higher temperatures, about 90-100 °C. As there are areas where temperature differences are 20-30 °C, warping can be generated.

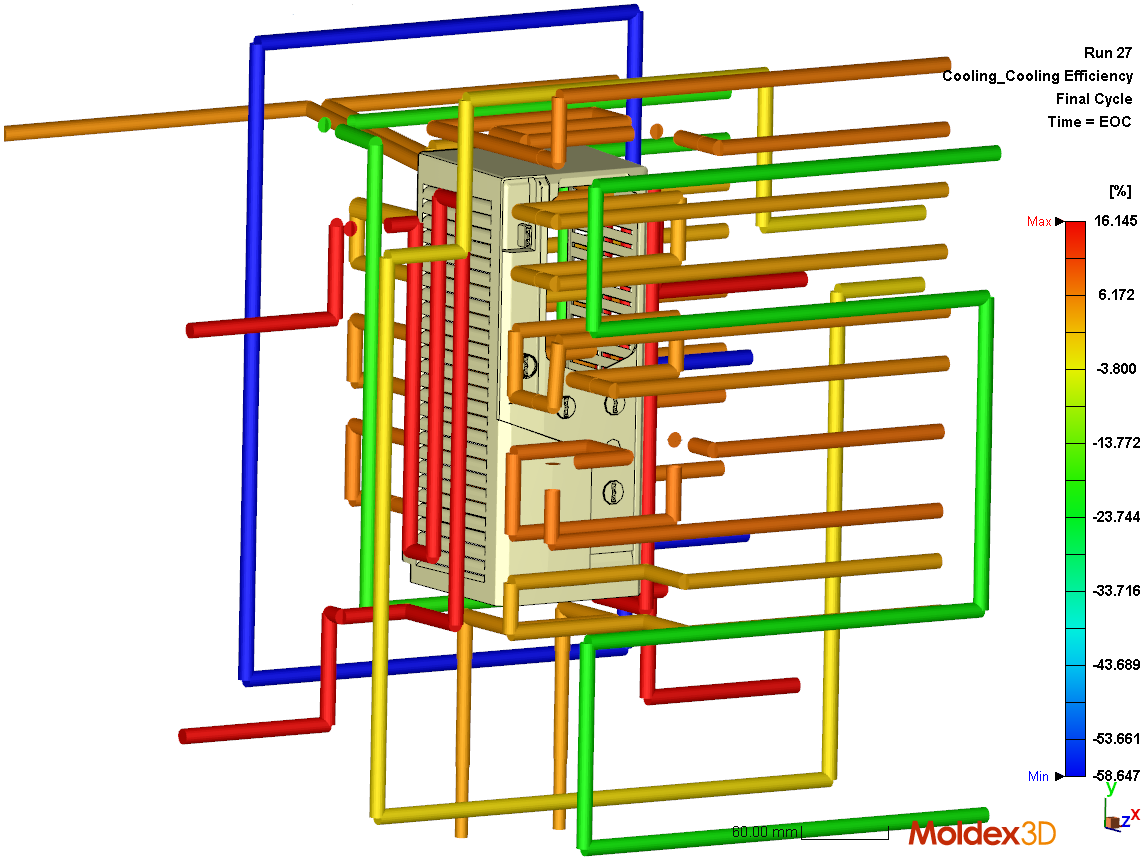


*Figure 38 Cooling efficiency of the cooling channels.*

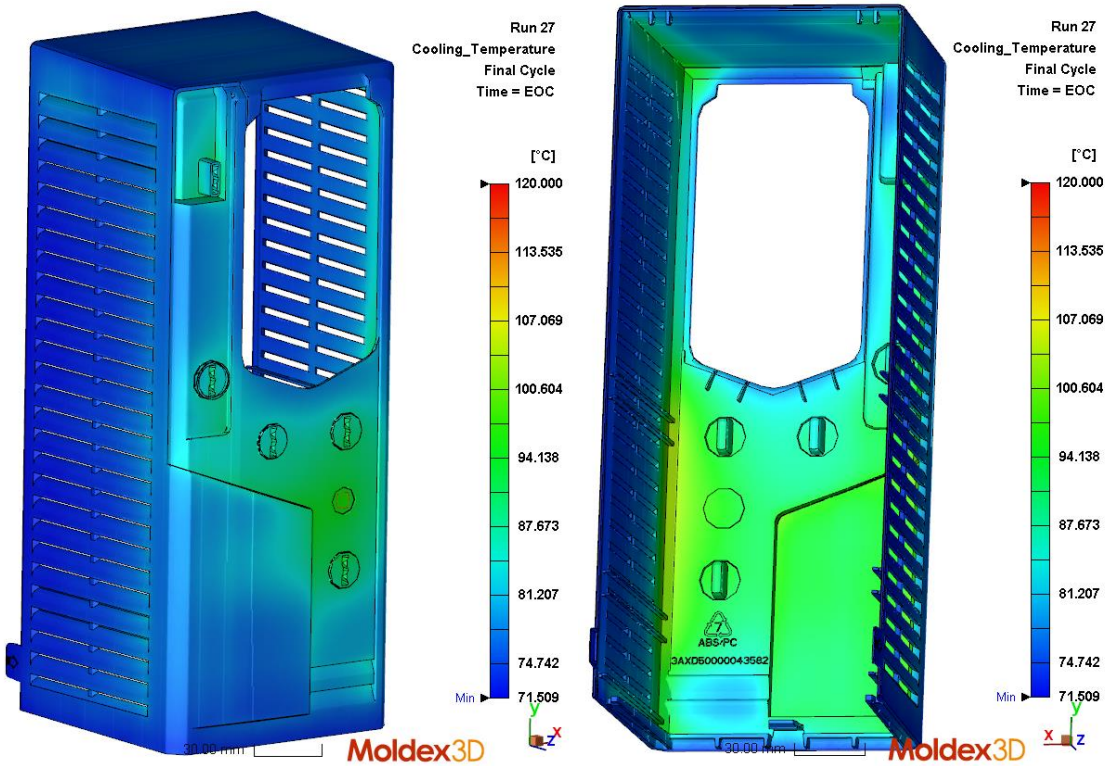


*Figure 39 Temperature distribution at the end of cooling on front and back sides. Maximum temperature is set to 120°C to illustrate better the temperature differences in the part.*

Figure 40 shows volumetric shrinkage resulting from part cooling down to room temperature after packing phase. Highest shrinkage is seen on the top surface of the part, whereas side walls has slightly lower shrinkage than other areas. As the shrinkage is uneven in the part, warping will most likely be seen on the top surface and side walls.

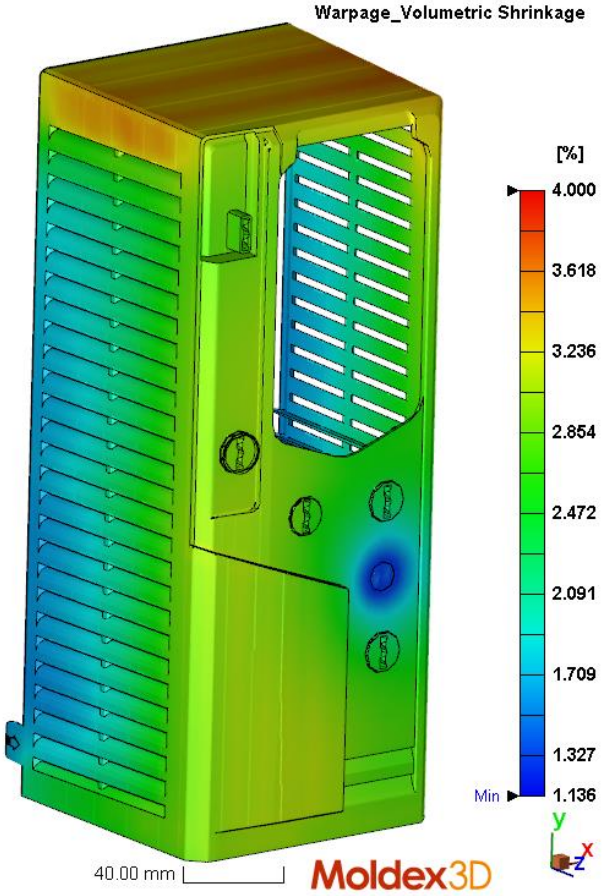


*Figure 40 Volumetric shrinkage when part is cooled after packing stage to room temperature.*

Displacement values in x-, y- and z-direction with 0,5% compensation factor are shown in figure 41 and figure 42. Displacement values are affected by all matters causing warpage. Compensation factor is used to review the results, as the mold is constructed based on 0,5% isotropic shrinkage.

In figure 30, main dimensions of the part were shown with allowed tolerances. In x-direction tolerance for the maximum width was ±0,32 mm and in y-direction, for height ±0,41 mm. From figure 41 it is seen that displacement values are over the tolerance limits, as based on the figure displacements predicted by the simulation are in x-direction from -0,835 mm to 0,458 mm and in y-direction from -0,806 mm to 0,817 mm. In x-direction, sidewalls have the highest displacements and they bend towards center of the part. As previously presented in section 4.2.2, warping is generated from uneven temperature distribution and part warps towards hotter section. In figure 39, sidewalls were noticed to have lower temperature, at the end of cooling, than the middle section. This can be one reason why the sidewalls bend towards the middle of the part. In y-direction there isn't as high temperature difference seen, which indicates that warping results more from uneven shrinkage.

Allowed tolerance in z-direction for the maximum depth is ±0,35 mm (defined in figure 30). Based on figure 42, displacements in z-direction would be from -0,377 mm to 0,932 mm. Maximum displacements are concentrated on one of the corners at the top surface of the part. In figure 39, some high temperature concentrations are located on the corners of the top surface. Overall, none of the results in x-, y- and z-directions fulfills tolerance limits and thus, correspond to results from real molding process. To find out what is causing these high displacements, displacements due to temperature and shrinkage differences are studied.

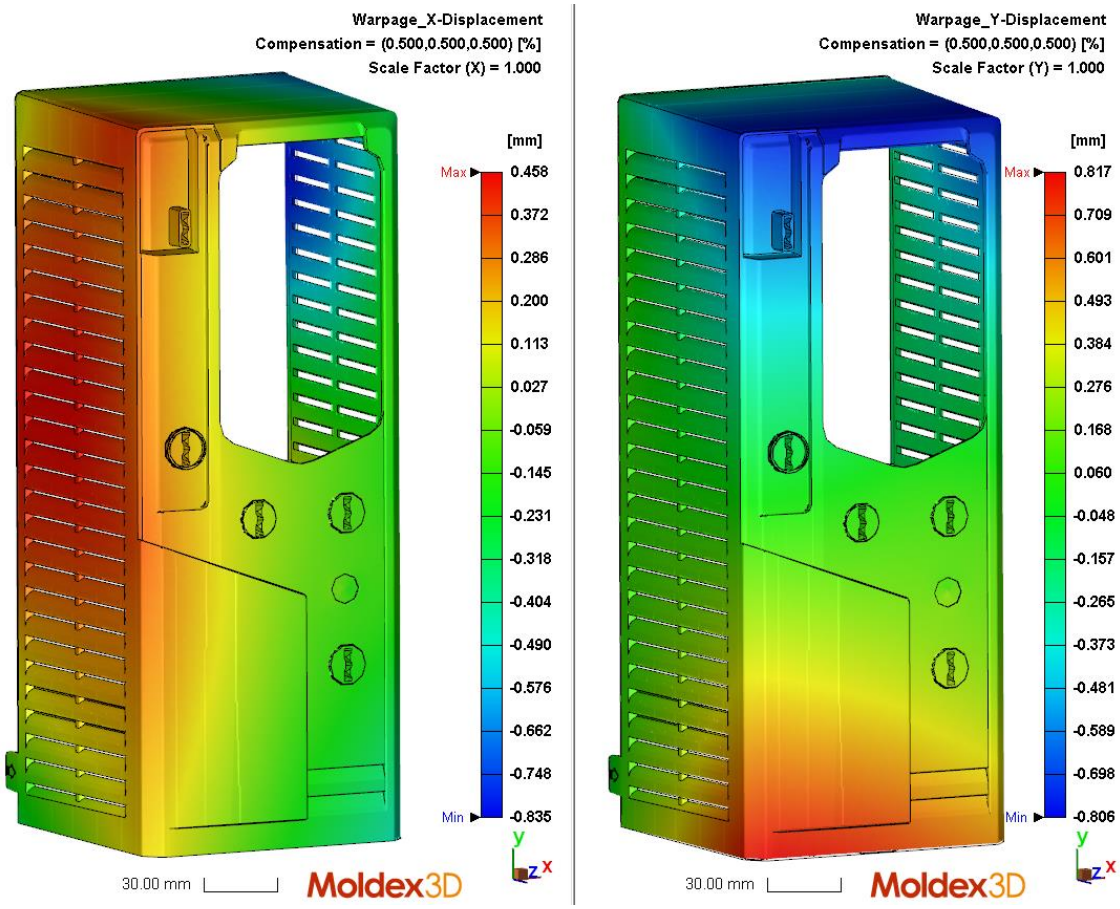


*Figure 41 Displacements in x- and y-direction with compensation factor 0,5%. Displacement in x-direction on left and y-direction on right.*

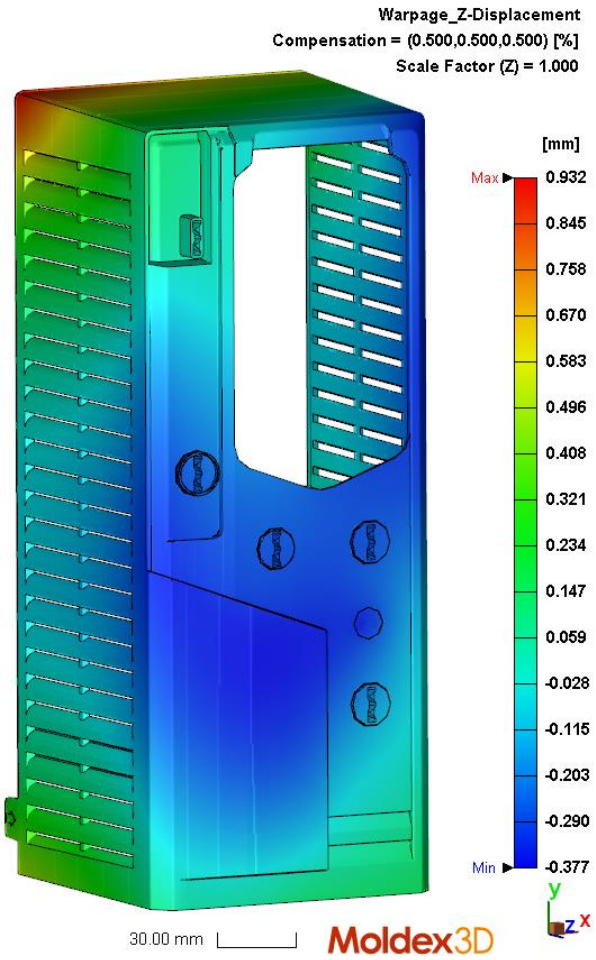


*Figure 42 Displacement in z-direction with compensation factor 0,5%.*

Thermal displacement values represent the displacement occurring after the part is ejected from mold and cooled down to room temperature (Moldex3D, 1995-2019). Thermal displacement values in x-, y- and z-direction are shown in figure 43 and figure 44. Range of thermal displacement in x-direction is from -1,592 mm to 1,595 mm. This is much higher than the tolerance ±0,32 allows. As it was predicted previously, based on temperature differences shown in figure 39, displacement in x-direction results greatly due to uneven cooling. Figure 38 previously showed that cooling efficiency was highest for the channels which located on part's sidewalls. Due to this, temperature on the sidewalls after cooling is lower than on other areas of the pat. This generates warping of the sidewalls.

In y-direction, thermal displacement values are inside the tolerance ±0,41 mm. As thermal displacement values aren't as high as values of displacement in y-direction, displacements are more likely to result from uneven shrinkage in the part. Thermal displacement in z-direction (figure 44) is almost inside the allowed tolerance ±0,35 mm.

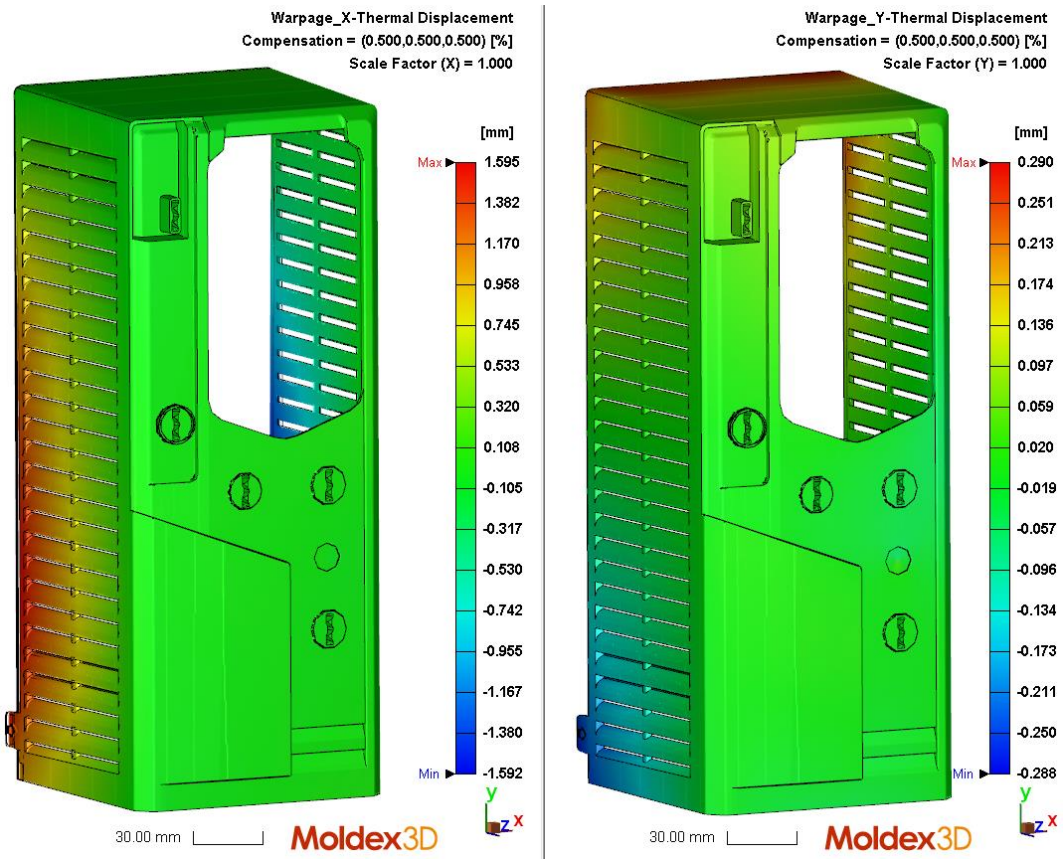


*Figure 43 Thermal displacement in x- and y-direction with 0,5% compensation factor. X-direction on left and y-direction on right.*

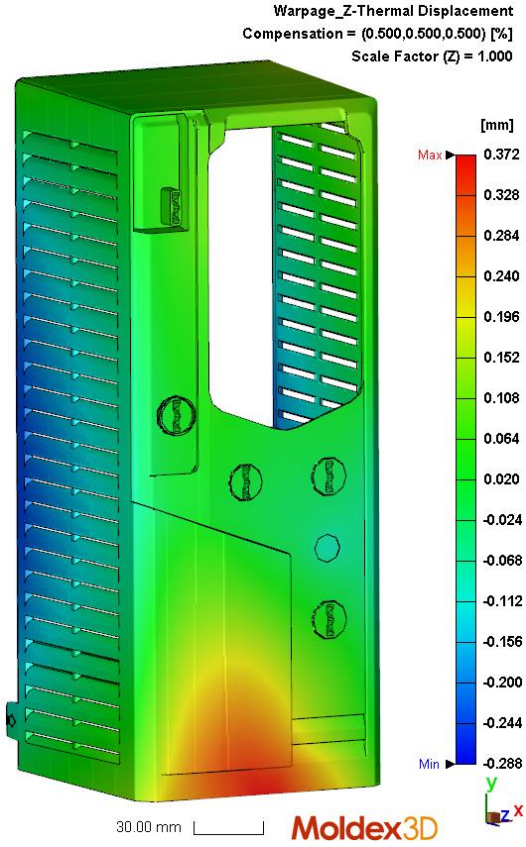


*Figure 44 Thermal displacement in z-direction with 0,5% compensation factor.*

Differential temperature effect displacement represents displacement due to uneven shrinkage, resulting from temperature differences, through the part thickness (Moldex3D, 1995-2019). Differential temperature effect displacements in x-, y- and z-directions are shown in figure 45 and figure 46. Compensation factor 0,5% is used to read these results.

Displacements in x-direction are from -0,457 mm to 0,512 mm and in y-direction from -0,705 mm to 0,800 mm. In x-direction highest values are on the sidewalls and in y-direction on top and bottom of the part. In z-direction displacements are lowest, from -0,396 mm to 0,226 mm. Displacements in all directions are noticed to expand the part in negative and positive direction quite evenly. These high displacements are explained by the compensation factor which expands the part by 0,5% and scales the displacement values higher due to this.

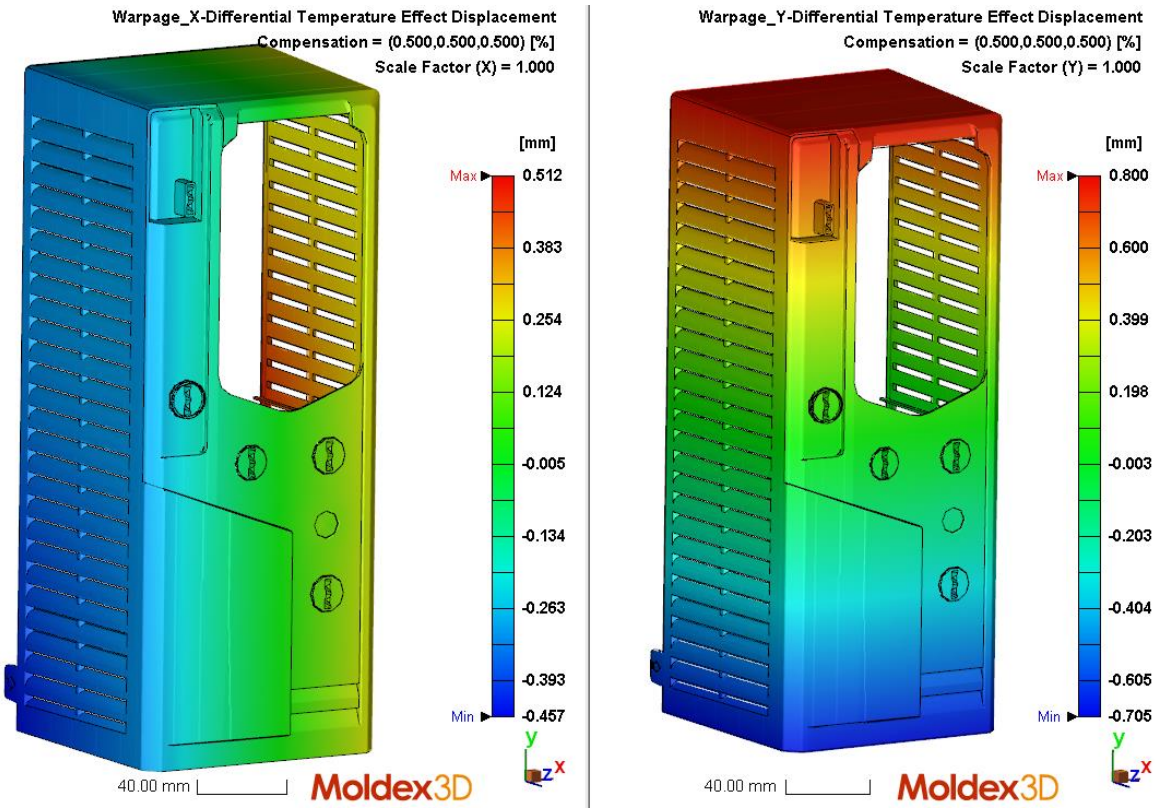


*Figure 45 Differential temperature effect displacement in x- and y-direction. X-direction on left and y-direction on right.*

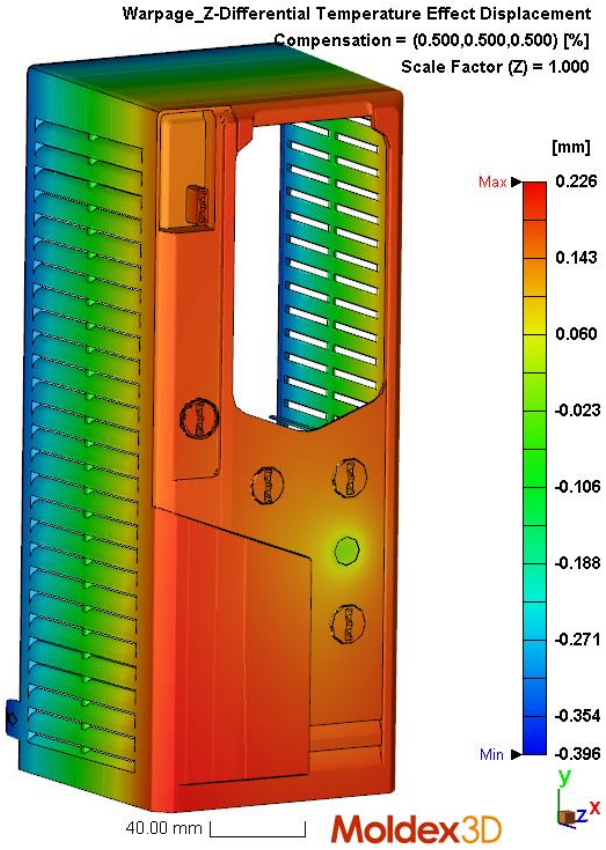


*Figure 46 Differential temperature effect displacement in z-direction.*

Differential shrinkage effect displacement results from uneven volumetric shrinkage distribution in the part (Moldex3D, 1995-2019). Differential shrinkage effect displacements in x-, y- and z-direction are shown in figure 47 and figure 48. Figures show that displacement values in each direction are quite high which means that there is uneven shrinkage through the part. In x-direction the highest displacements are located on the sidewalls and close to areas which had also high thermal displacement values and smallest shrinkage (refer to figure 40). In y-direction highest values are on the top and bottom. On the top surface high shrinkage value was seen in figure 40. In z-direction maximum displacement is 0,855 mm and located also on the top surface as with y-direction.

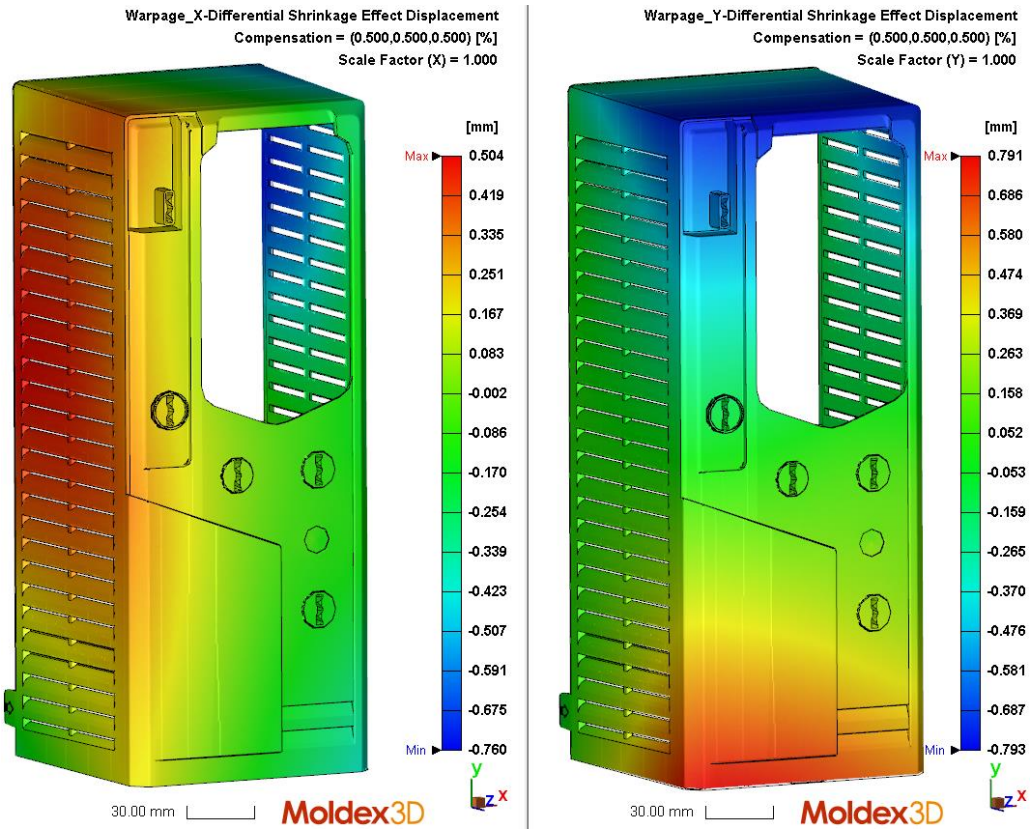


*Figure 47 Differential shrinkage effect displacement in x-and y-direction with 0,5% compensation factor. X-direction on left and y-direction on right.*

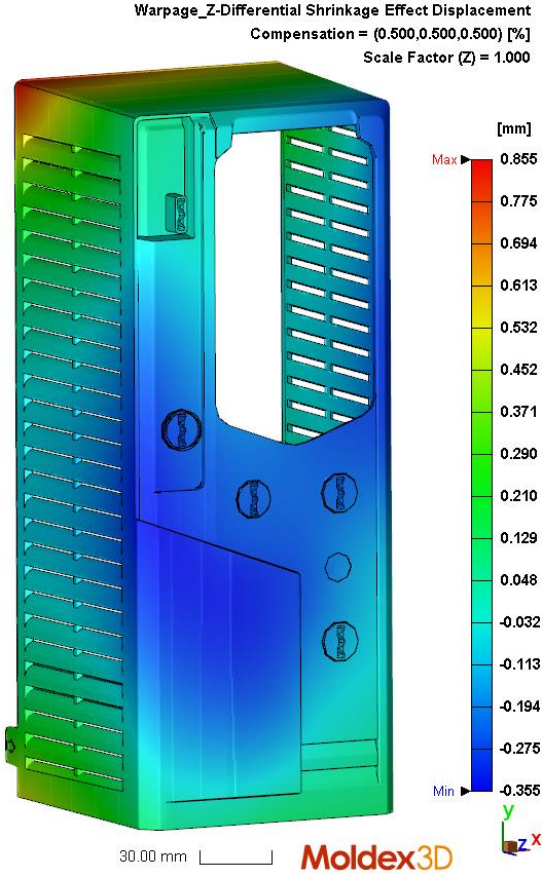


*Figure 48 Differential shrinkage effect displacement in z-direction with 0,5% compensation factor.*

Displacement values in x-, y- and z-directions (shown in figure 41 and figure 42) represented displacement for which all matters causing warpage, were taken account. These displacement values presented in three directions were all above the tolerance limits for the part. By analyzing different displacement values from the warpage analysis, it was noticed that the high displacement values were in y- and z-direction resulting more from uneven shrinkage than from unbalanced cooling. In x-direction also results of thermal displacement were high, which suggest unbalanced cooling. It was noticed from figure 39, showing temperature distribution in the part after cooling, that sidewalls had lower temperature than center of the part. This can be one reason for the high thermal displacement values on the side walls.

As the simulation model was constructed as close to the real molding situation as possible, by taking account the cooling channels and real process parameters, it was unexpected that displacements were such high. One difference between real process parameters and simulation results was seen in the filling time. In the real process parameters from the injection molder, the filling time was reported to be 5 s when simulation predicted this to be 2,5 s. As the injection happens in a real case twice slower than in simulation, pressure levels in the simulation are assumed to be higher than they are in real process. Though, this shouldn't affect the pressure differences inside the part. As mentioned in section 4.2.2, shrinkage can be reduced with higher filling times as more plastic melt is injected into the mold cavity to compensate the already cooling and shrinking plastic in the cavity. In figure 40, volumetric shrinkage was noticed to be uneven and at some areas also quite high. As the filling time in the simulation was half of the one in the real process, shrinkage can be more even, and values lower than this simulation predicts. During this study it was noticed that process parameters are reported differently by different companies which can sometimes be seen as insufficient and unclear reporting. Due to this, it would be recommended to have a form including all the necessary parameters and which would be sent from ABB to the injection molders to be filled.

Cooling channels were constructed based on 3D-model of the mold with Creo. However, they were brought to Moldex3D separately from the part model. This required that cooling channels needed to be placed on the right locations related to part in Moldex3D environment, which placing and measuring tools were noticed to be quite inaccurate. Due to this, it is recommended to place the cooling channels on right locations in 3D modelling environment and import the assembly as a stp -file to Moldex3D. Reason for bringing the part and cooling channels as separate files into Moldex3D was that cooling channels were imported as stp -file and part as stl -file to ease the meshing. This inaccuracy of placing the cooling channels might be one partial reason for uneven cooling but its effect should be relatively small and not cause as high displacement values as were seen. Cooling channels used in this simulation were handled with separate channels, whereas in real circumstances some of the channels would be chained together by hoses outside the mold. This can be one possible cause affecting the results, as the cooling efficiency, e.g. on the sidewalls, might not be as high as in this simulation, which could explain the high temperature differences in the simulation results. Simulation model also excludes materials and interfaces of different mold components, e.g. slides and mold plates, which affects the cooling results. Furthermore, coolant flow rate of 120 $cm^3/s$ was used in the analysis as the coolant flow rate used in the molder wasn't known. Flow rate of 120 $cm^3/s$ was selected based on experience of other injection molders.

As differences between the simulation model and the real circumstances weren't assumed to cause as high displacement values as results showed, material used in the simulation

was changed to another. Reason for the material change was doubt of insufficient material parameters in the Moldex3D library. However, with another PC-ABS material, results showed displacement values close to ones presented here, and material data in the first simulations was assumed to be sufficient to provide reliable results. Alternative PC-ABS was from the same manufacturer as the initial one. One possible cause for the high displacement values might be the process parameters used. Process parameters were reported as hydraulic pressures which were needed to convert to absolute pressures to set them to Moldex3D. Furthermore, it was unclear when the process parameters, provided for this thesis work, had been reported.

### 5.1.4 Cooling system analysis and results

As previously described, cooling system model for the simulation was constructed based on cooling channels in real mold. Object of this cooling system analysis is to compare a more simplified cooling system design to the one in the real mold. This is because in a case where product designer simulates new product, the exact cooling circuits are not yet known, and it is important to study how much simplification of the cooling system will affect the simulation results. Temperatures of the cooling channels were set to be same as in the original model in order to compare effect of channel design. Simplified cooling channels are shown in figure 49 and figure 50. There are 19 cooling lines in total which diameters are 11 mm. 14 of the cooling lines are on the front, top, bottom and side surfaces. The top and bottom lines are the same as used in the real mold but channels on the front and side surfaces are constructed with Moldex3D's automatic cooling channel tool. Five cooling lines are located inside the part at the same distance as the real ones. Cooling lines aren't chained outside the mold so cooling analysis results will give the most optimal situation. In a real situation, most of the channels would be connected to each other by hoses, to decrease the need for several tempering device. Temperatures of cooling lines in top, side and front surfaces are 65 °C and inside part, temperatures are 70 °C.

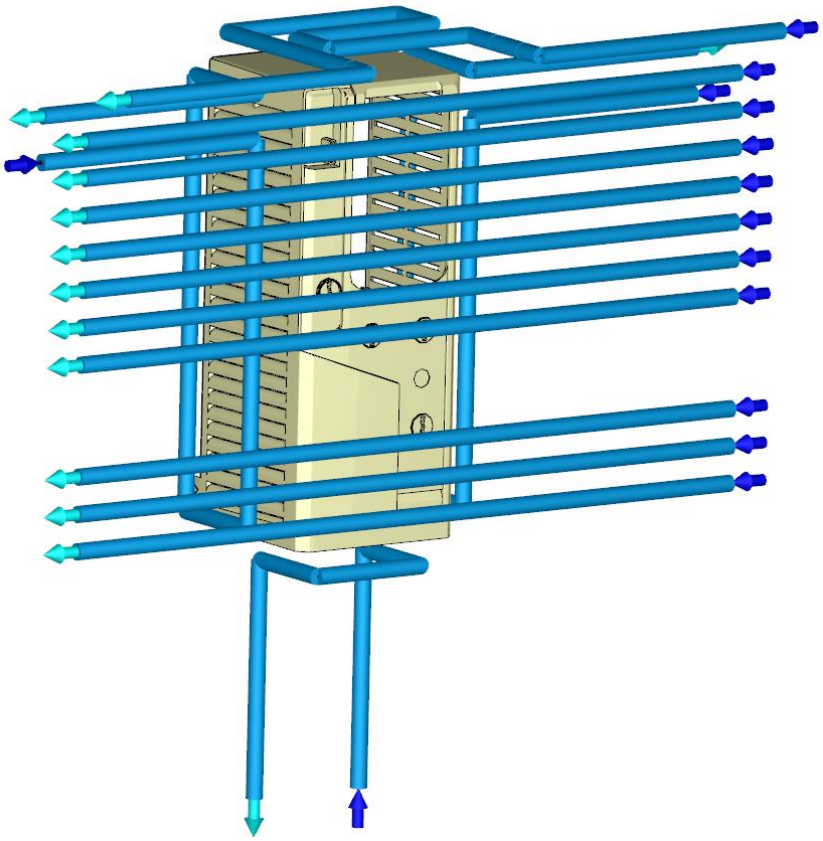

*Figure 49 Cooling channel group 1, temperatures 65 °C.*

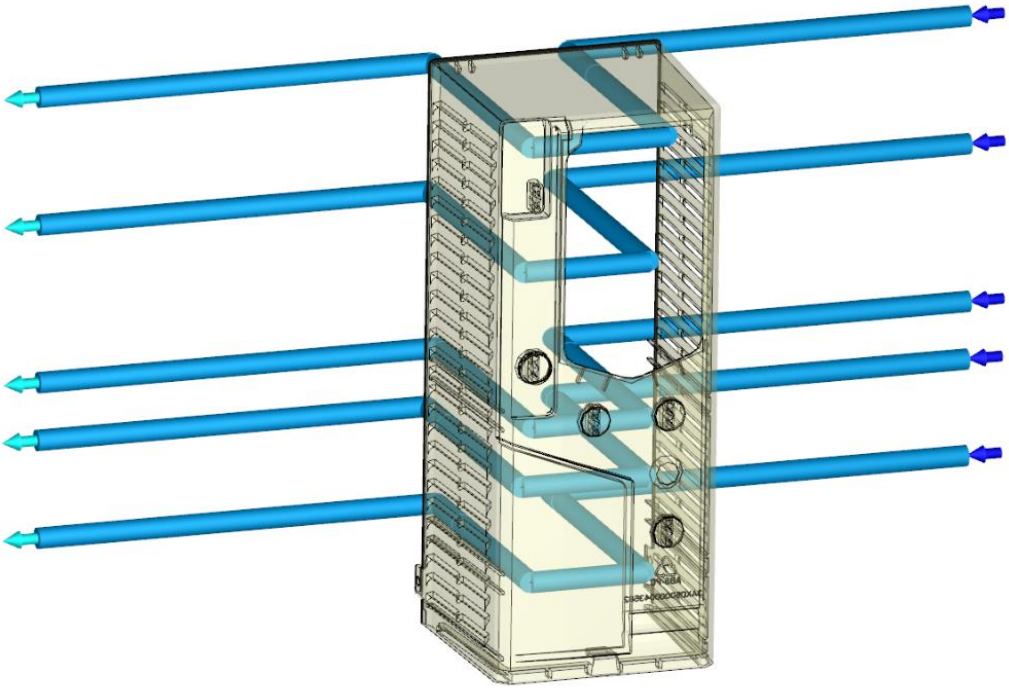

*Figure 50 Cooling channel group 2, temperature 70 °C.*

## Results

Cooling efficiency of both cooling channel designs are shown in figure 51. Cooling efficiency is defined to be the ratio of heat absorbed by one cooling channel to heat released from the part during molding cycle. Cooling efficiency with the real and simplified channels are close to same. Both models have cooling channels which efficiencies are negative. These channels are further away from the part, and their purpose is to control the mold temperature and not to absorb heat from the part. Cooling channel in the bottom of the part is the same in both cases. As the figure shows, in the simplified design, its efficiency is -100 %. This indicates that is so far away from the part that it doesn't absorb any heat from the part, and its purpose in the real mold is to control temperature of the mold parts and possibly also other cooling channels.

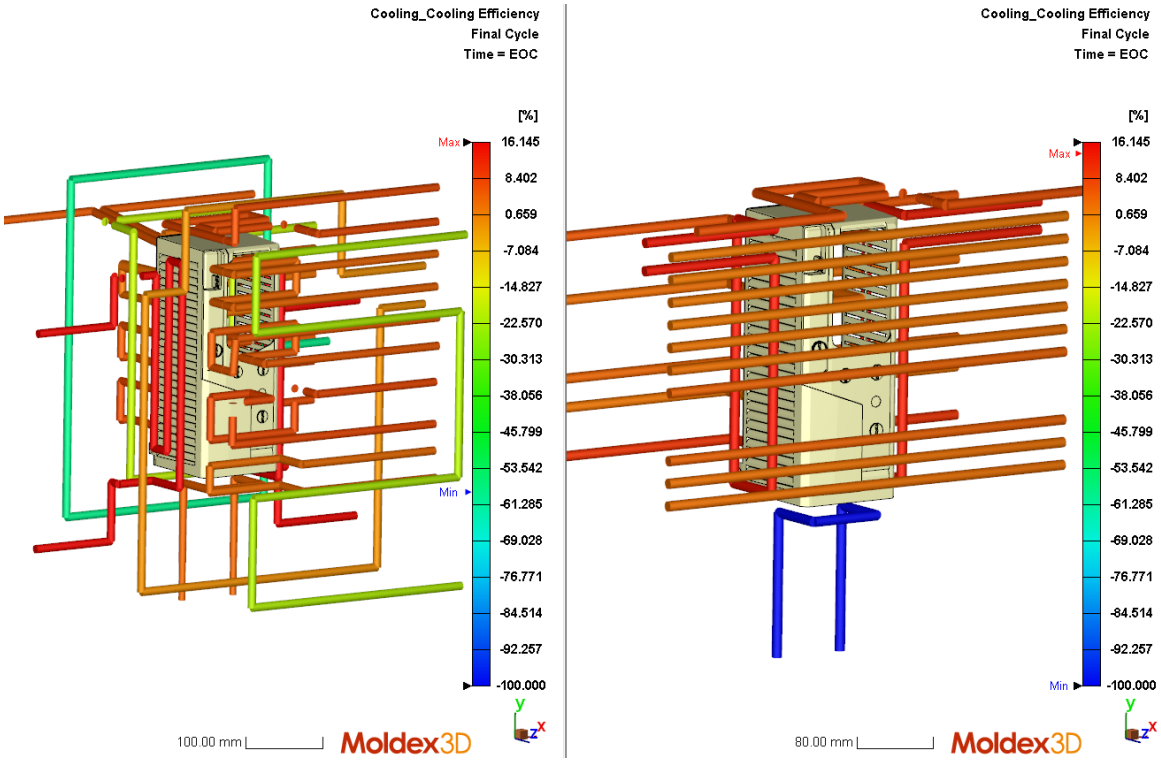


*Figure 51 Cooling channels' cooling efficiency. Results with real cooling channels on left and with simplified cooling channels on right.*

Temperature distributions in the part after cooling time are shown in figure 52 and figure 53. Figures show that on the front side of the part, temperature distributions are similar but with simplified cooling channels, temperatures on the sidewalls are slightly higher than with the real cooling channels. As the temperature distribution with the simplified design seems to be more uniform, warpage values should be lower than for the original design. Figure 53 shows back side of the part and on both cases, there is noticed to be higher temperature values than on the front surface. With simplified cooling channels, temperatures on the side walls seem to be higher also on the back side (when compared to results with real cooling channel design) which decreases temperature differences inside the part.

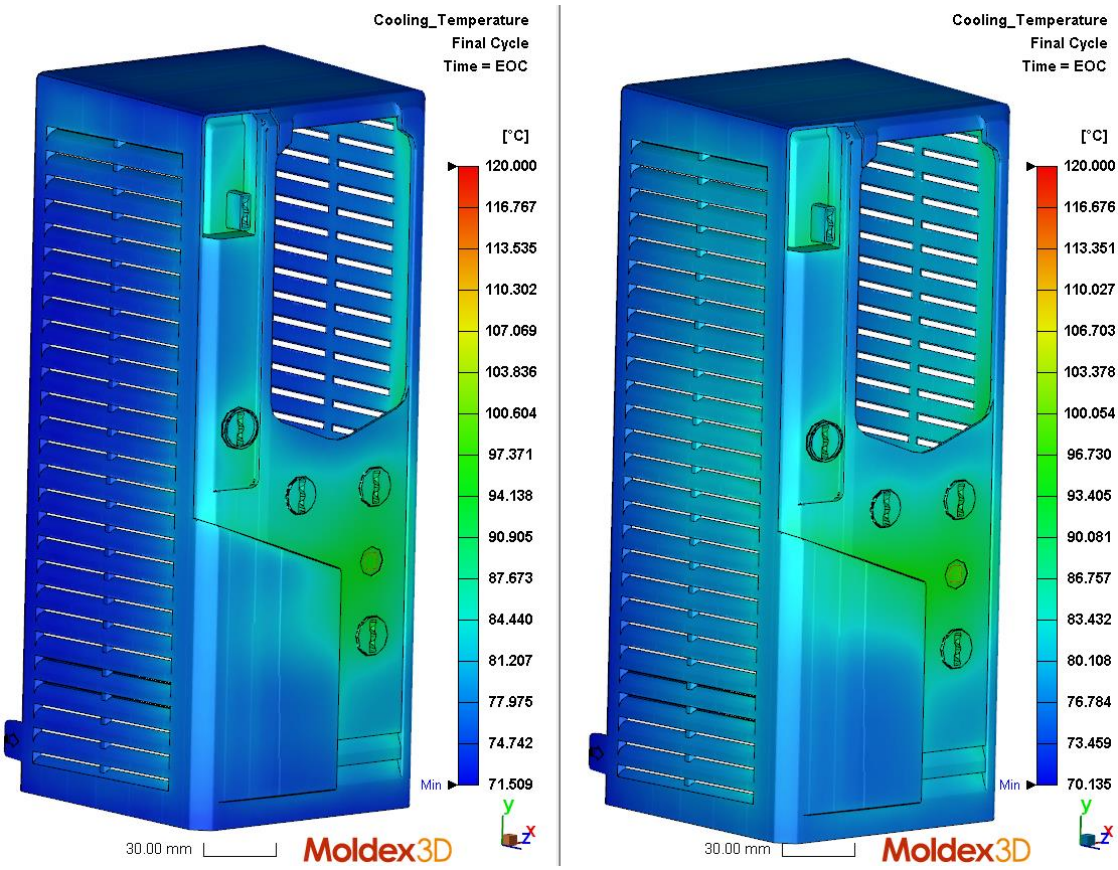


*Figure 52 Temperature distribution in the front side at the end of cooling. Results with real cooling channels on left and with simplified cooling channels on right.*

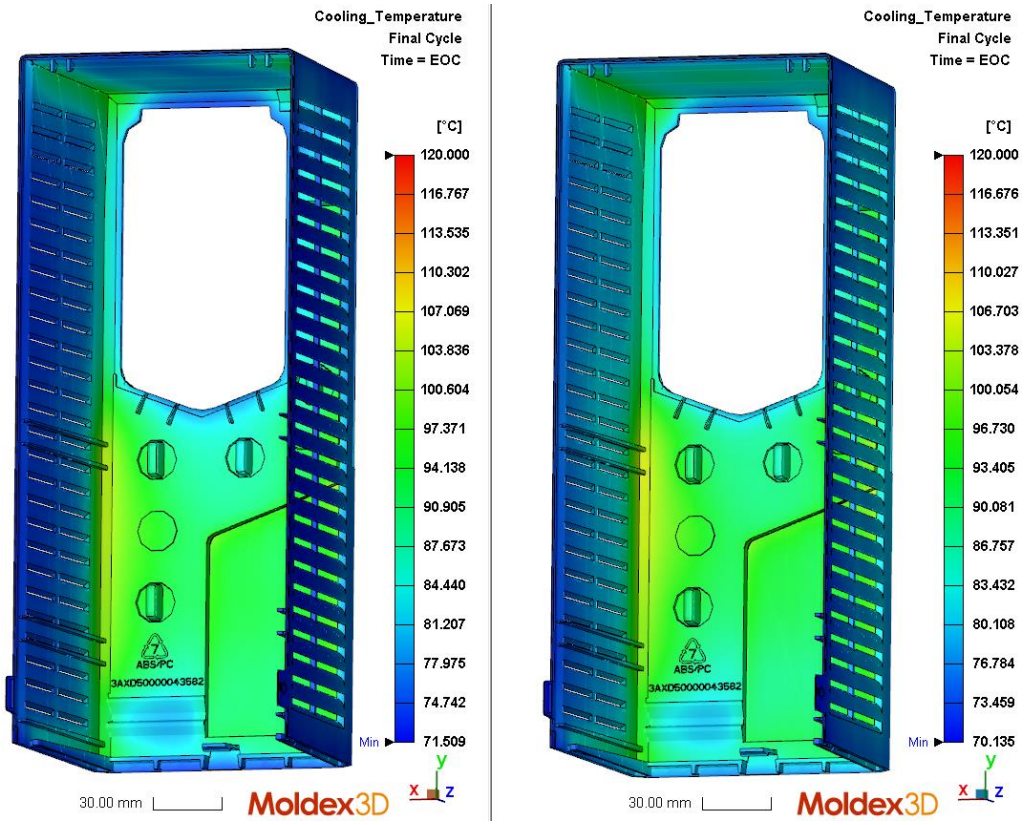


*Figure 53 Temperature distribution in the back side at the end of cooling. Results with real cooling channels on left and with simplified cooling channels on right.*

Displacements in x-, y- and z-direction with compensation factor are shown in figure 54-figure 56. Displacements with real cooling channels are on the left and corresponding values for simplified cooling channels design on the right. Displacements in all three direction are noticed to be close to same on both designs, which indicates that there is only a little difference between the cooling systems. Color range of the figures are also similar which means that displacements are located on similar areas.

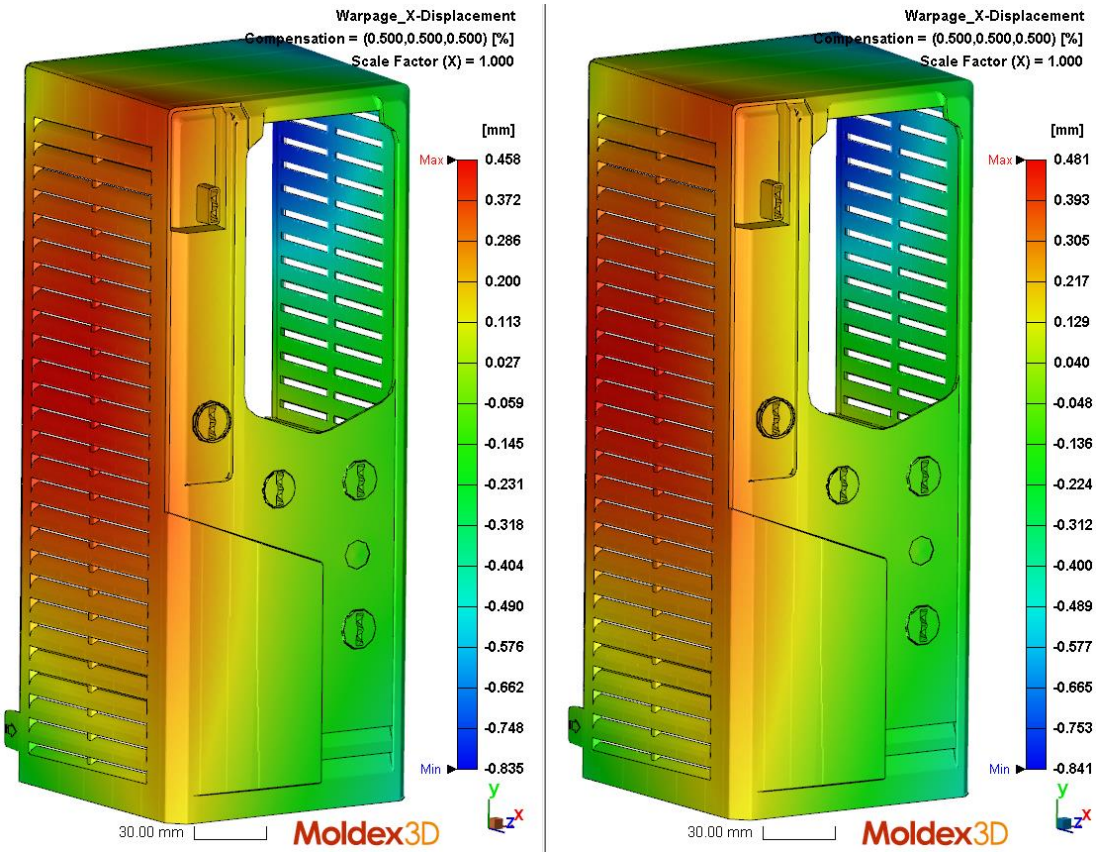


*Figure 54 Displacement in x-direction with 0,5% compensation factor. Results with real cooling channels on left and with simplified cooling channels on right.*

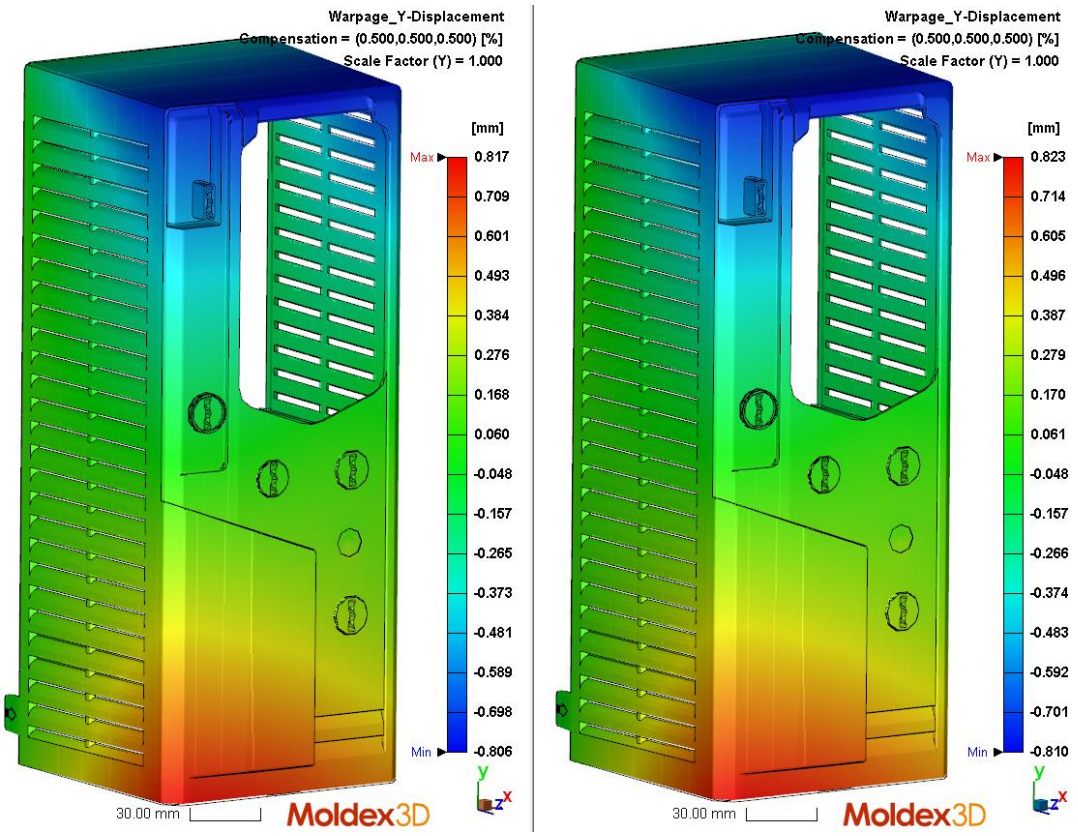


*Figure 55 Displacement in y-direction with 0,5% compensation factor. Results with real cooling channels on left and with simplified cooling channels on right.*

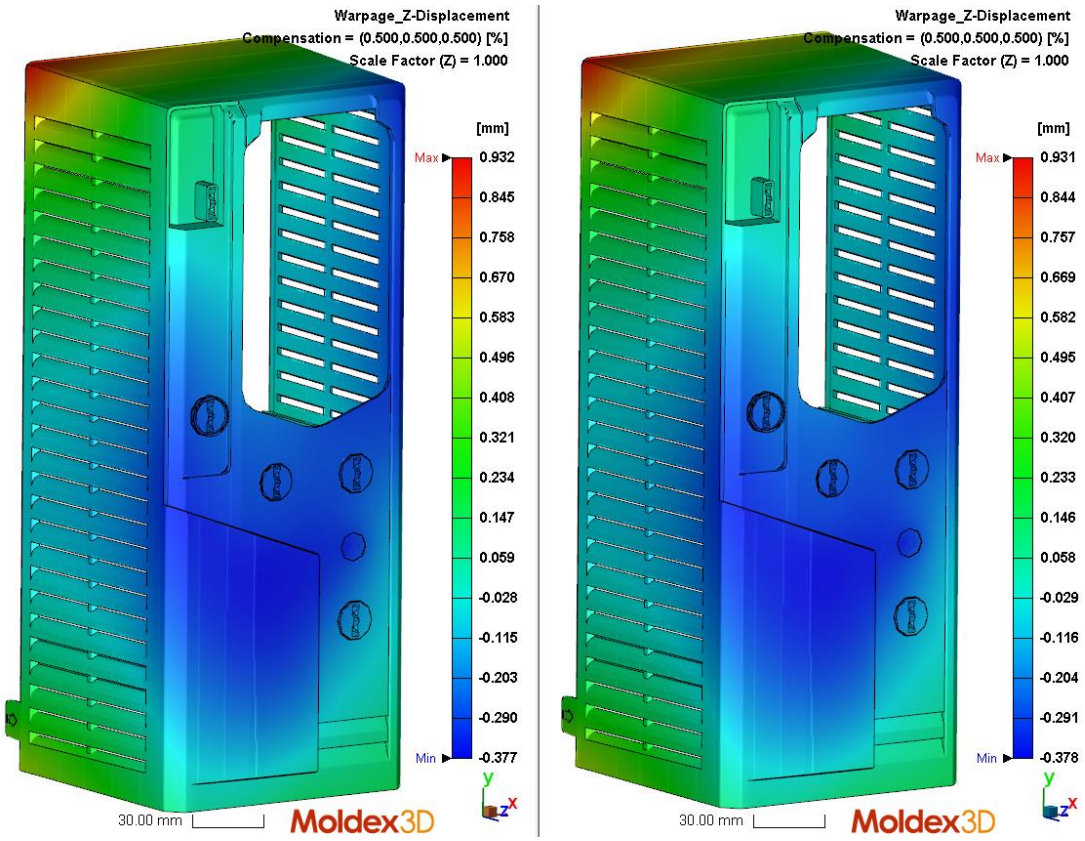


*Figure 56 Displacement in z-direction with 0,5% compensation factor. Results with real cooling channels on left and with simplified cooling channels on right.*

Thermal displacements in x-, y- and z-direction with 0,5% compensation factor are shown in figure 57-figure 59. Figures show that displacements due to uneven cooling are close to same on both designs in all directions. Figure 52 and figure 53 previously showed that with simplified cooling channels, sidewalls had slightly higher temperature at the end of cooling. This was expected to show in the displacement values but as figure 57 illustrates, displacements differ only by some hundreds of millimeters. However, it seems that in the design with simplified cooling channels, higher displacements are found on wider area. Figure 60 and figure 61 show distribution of total displacement as percentages in the part. Total displacement represents length of the total displacement vector i.e. takes account all directions. Comparison of figure 60 and figure 61 shows that higher displacements are noticed on slightly wider area with the simplified cooling channel design than with the original one. With the original one, total displacement between 0,839 and 1,904 mm is found from 28,52 % of the part. With simplified cooling channels, total displacement between 0,850 and 1,938 mm is in 31,35 % of the part.

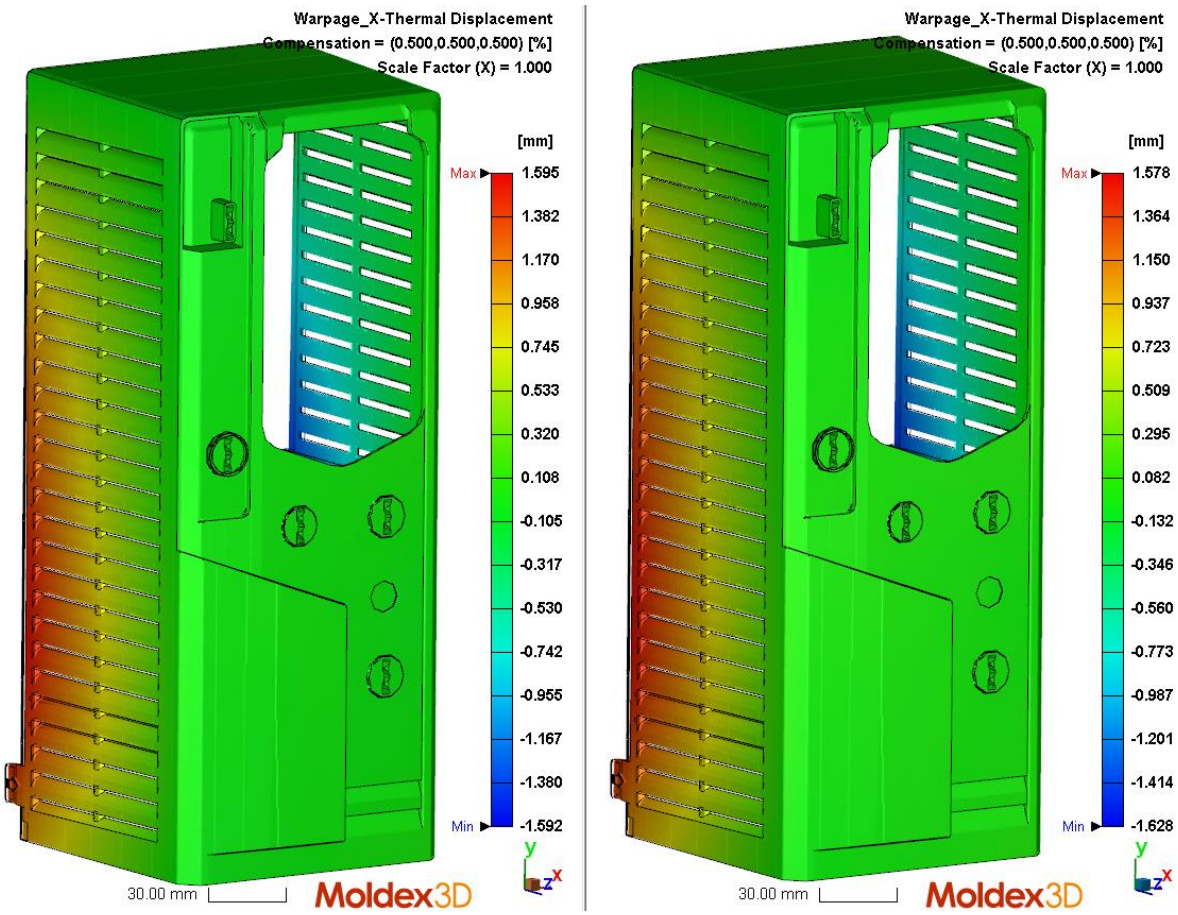


*Figure 57 Thermal displacement in x-direction with 0,5% compensation factor. Results with real cooling channels on left and with simplified cooling channels on right.*

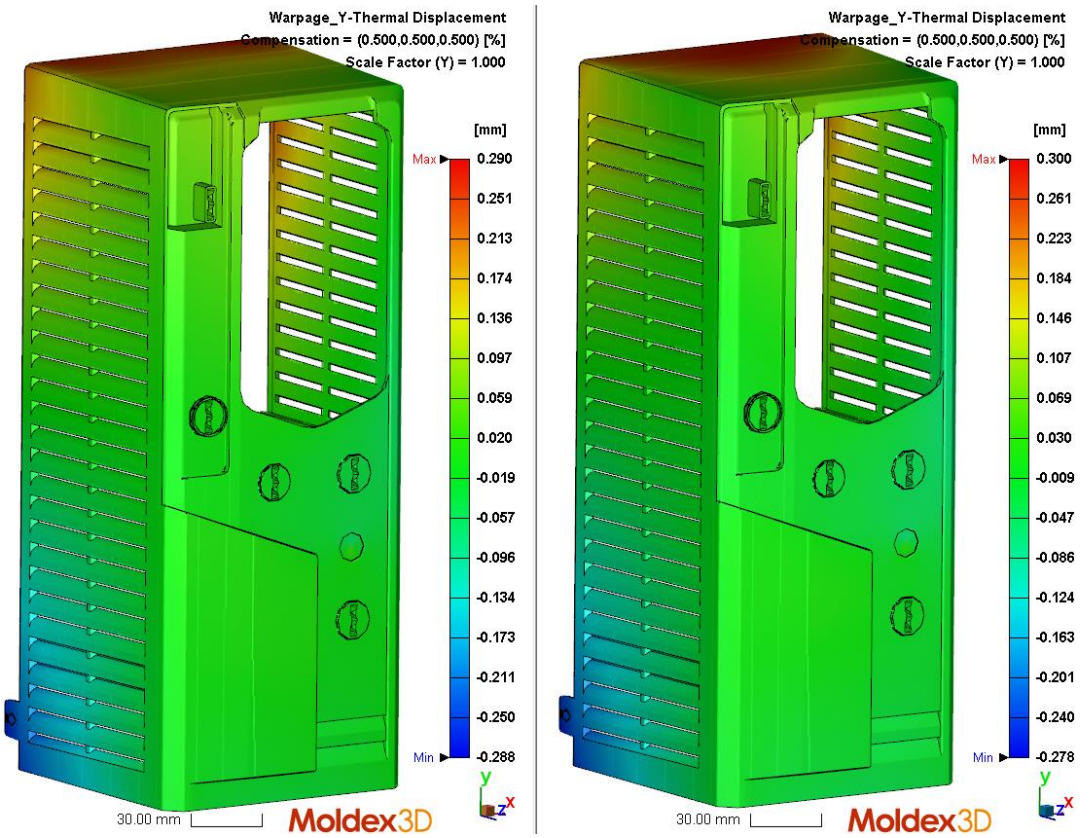


*Figure 58 Thermal displacement in y-direction with 0,5% compensation factor. Results with real cooling channels on left and with simplified cooling channels on right.*

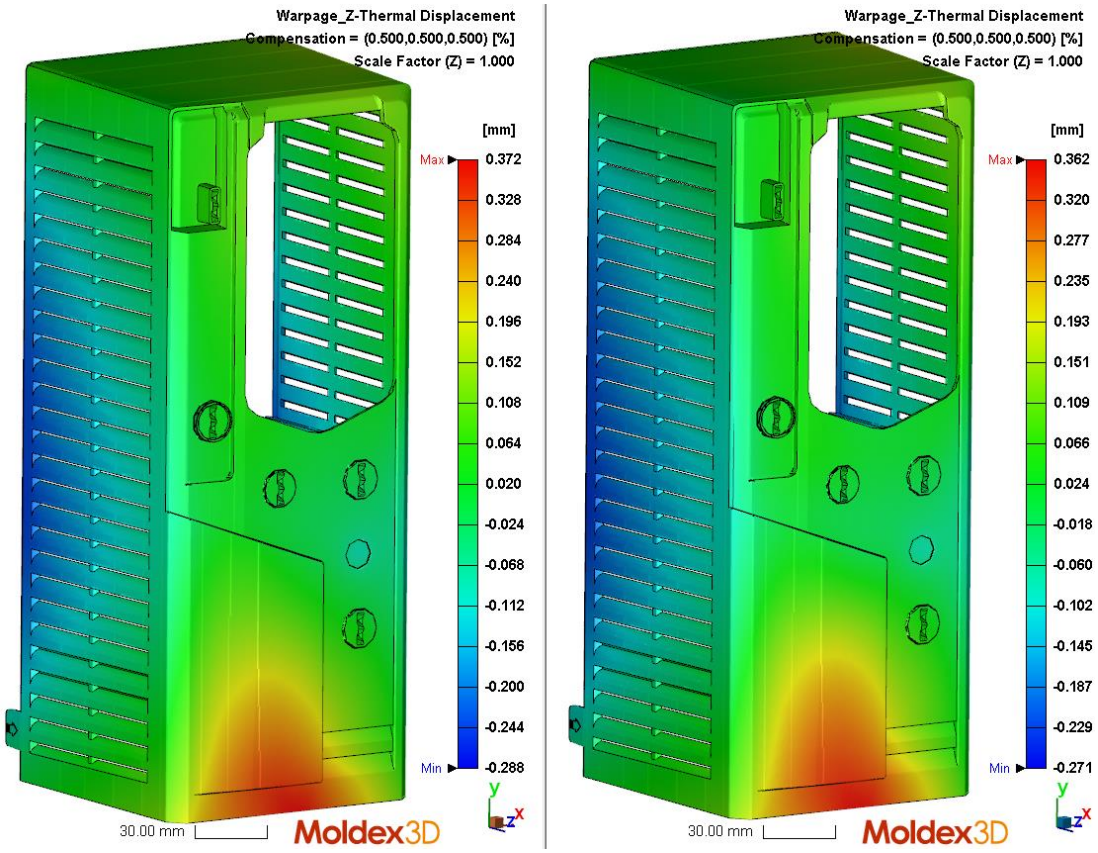


*Figure 59 Thermal displacement in z-direction with 0,5% compensation factor. Results with real cooling channels on left and with simplified cooling channels on right.*

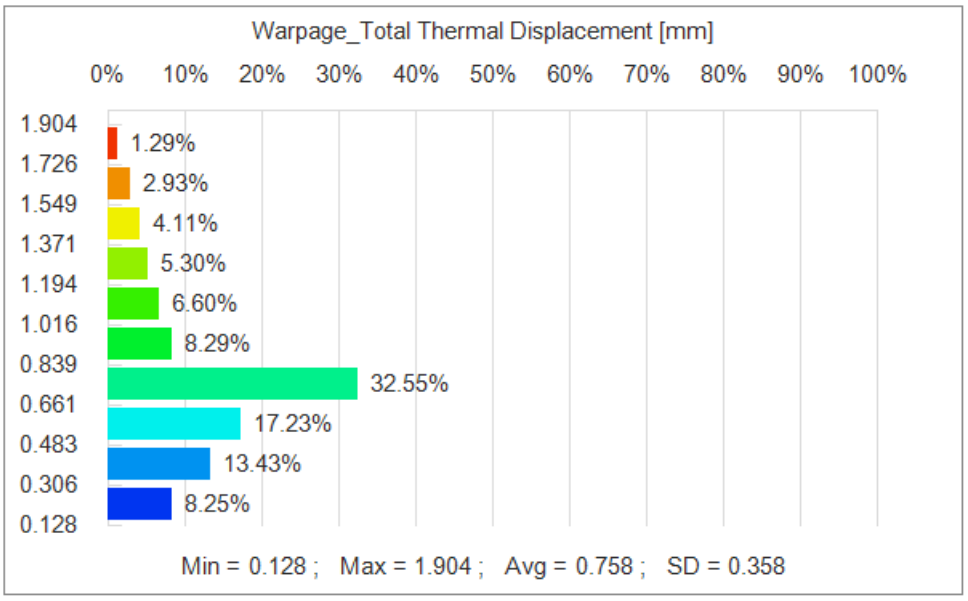


*Figure 60 Distribution of total displacement as percentages in the part with real cooling channels. Note that no compensation factor is taken account into these values.*

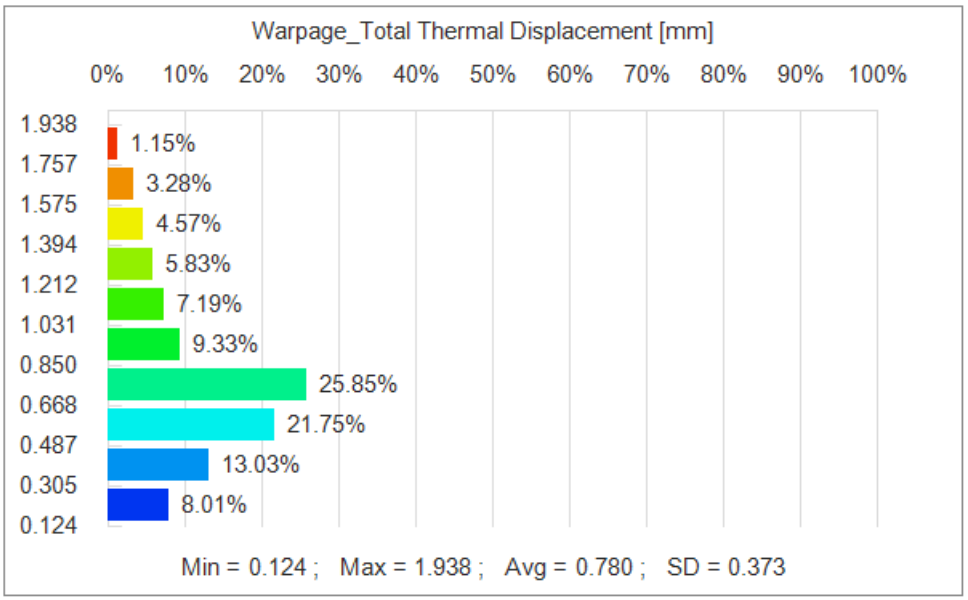


*Figure 61 Distribution of total displacement as percentages in the part with simplified cooling channels. Note that no compensation factor is taken account into these values.*

Figure 62 - figure 64 show the differential temperature effect displacement with 0,5 % compensation factor in x-, y- and z-directions. Figures show that values of displacement are the same and they are also located on same areas.

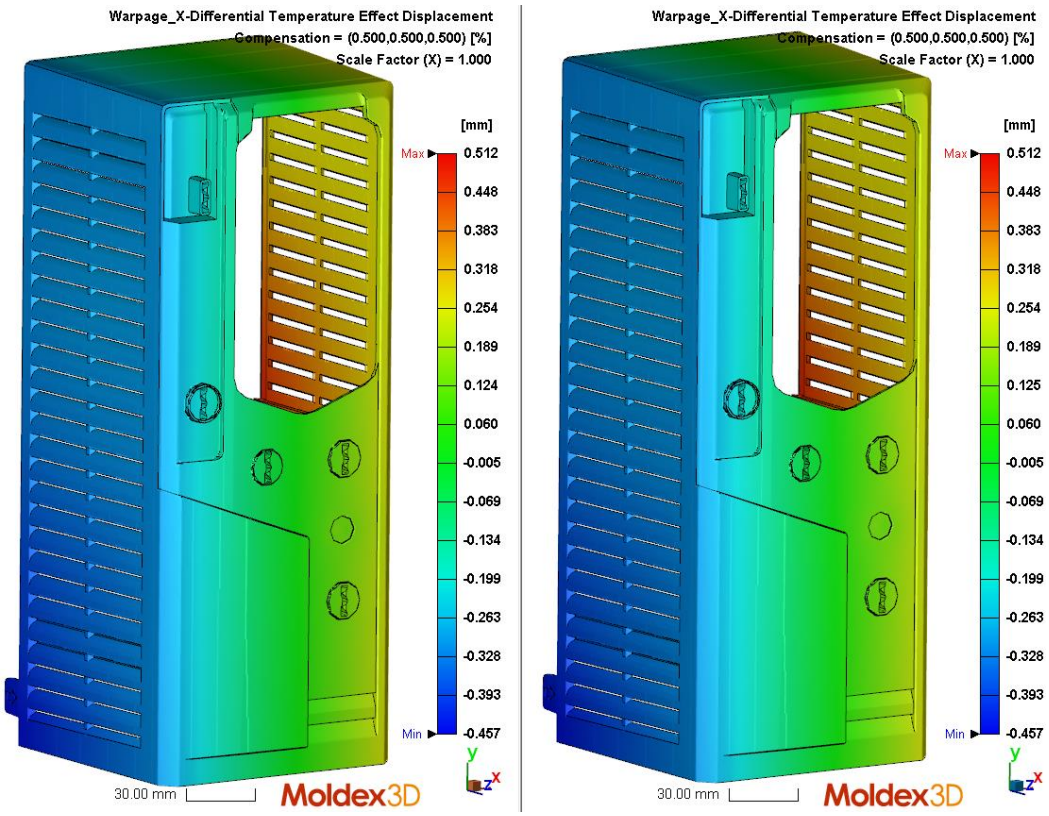


*Figure 62 Differential temperature effect displacement in x-direction with 0,5% compensation factor. Results with real cooling channels on left and with simplified cooling channels on right.*

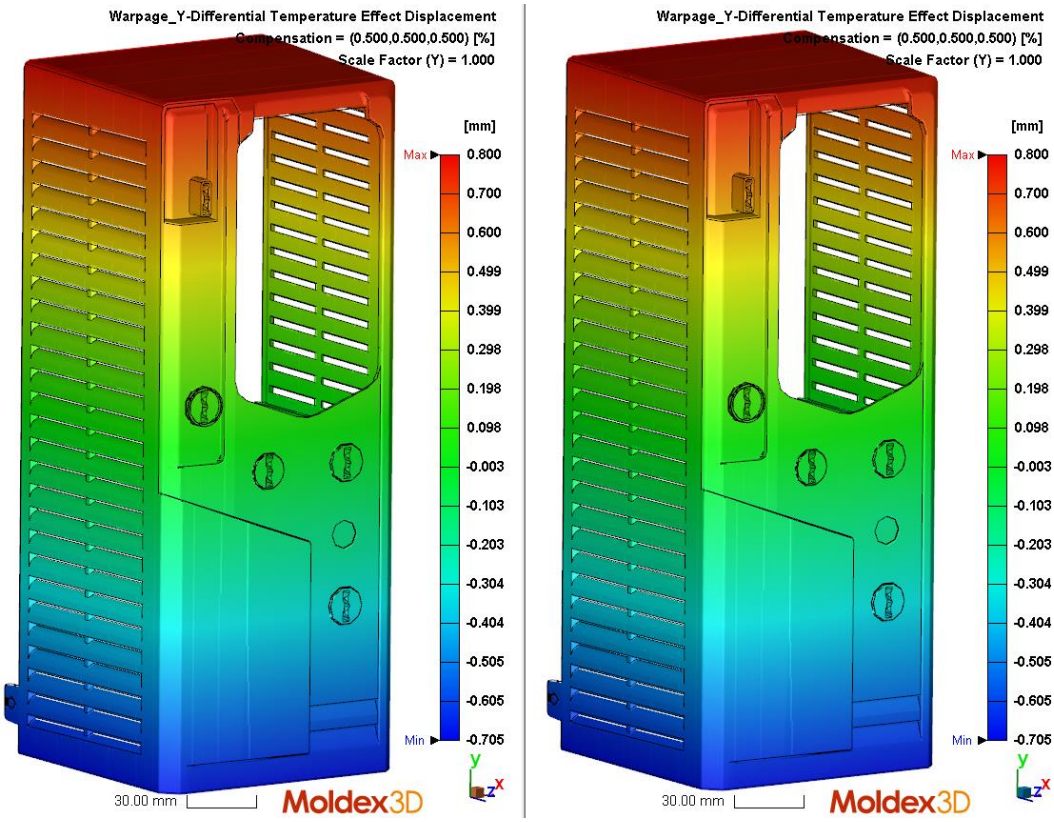


*Figure 63 Differential temperature effect displacement in y-direction with 0,5% compensation factor. Results with real cooling channels on left and with simplified cooling channels on right.*

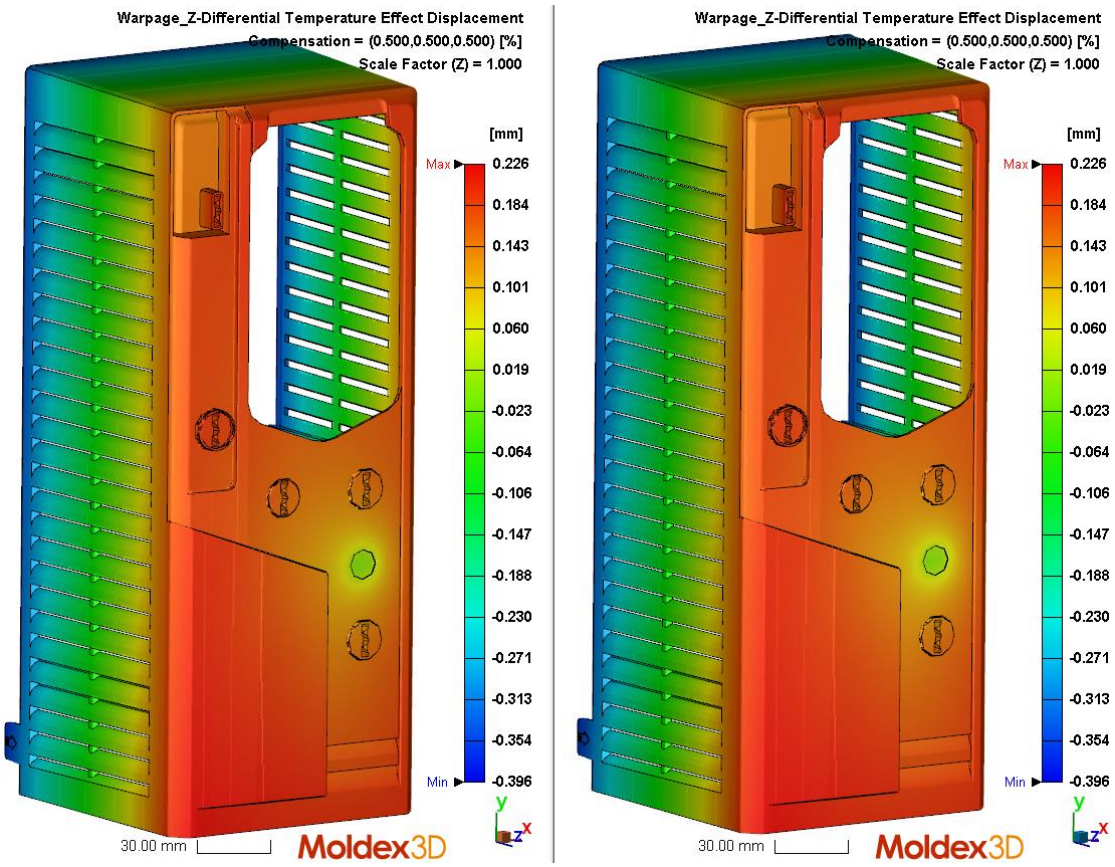


*Figure 64 Differential temperature effect displacement in z-direction with 0,5% compensation factor. Results with real cooling channels on left and with simplified cooling channels on right.*

Comparison of results with the real cooling channels and with simplified design, showed no big differences. Part temperature after cooling time showed some slight differences but they weren't seen in the results of warpage analysis. Slight difference was found from the distribution of thermal displacements. Values of thermal displacement with simplified cooling channels, were close to ones with original cooling channels but the displacements were noticed to be on slightly larger area. Based on results presented in this chapter, results of cooling and warping analysis don't differ much from simulation results with real cooling channel design. By doing separate cooling circuits on each side of the part and following rules for cooling channel design, good results can be obtained from the simulation.

### 5.1.5 Default parameters with simplified cooling channels

This study compares how much difference is seen in results when using real molding parameters, and when using default parameters from Moldex3D. This comparison is done as the exact process parameters aren't known at the product design phase. Simulation model used for this study is the same as in the previous study, with the simplified cooling channels. Default process parameters are listed to table 10. Mold, melt and eject temperatures were set to be the same as in previous cases.

*Table 10 Process parameters.*

| Process parameter | Value |
|---|---|
| Setting method | CAE mode |
| Material | PC-ABS |
| Mold material (mold plates) | P20 |
| Mold temperature | 65 °C |
| Melt temperature | 265 °C |
| Filling time | 2,38 s |
| Filling pressure | 238 MPa |
| Flow rate | 50 % |
| VP switch-over, by volume filled | 98 % |
| Packing pressure | 192,3 – 153,8 – 123,1 MPa |
| Packing time | 4,94 – 6,58 – 8,23 s |
| Cooling time | 35 s |
| Eject temperature | 70 °C |
| Coolant temperatures | 65 °C & 70 °C |
| Coolant flow rates | 120 $cm^3/s$ |

## Results

Filling pressure required to fill the cavity is 55,317 MPa. Pressure distribution at end of filling is shown in figure 65. Filling pressure is slightly lower than with the real process parameters.

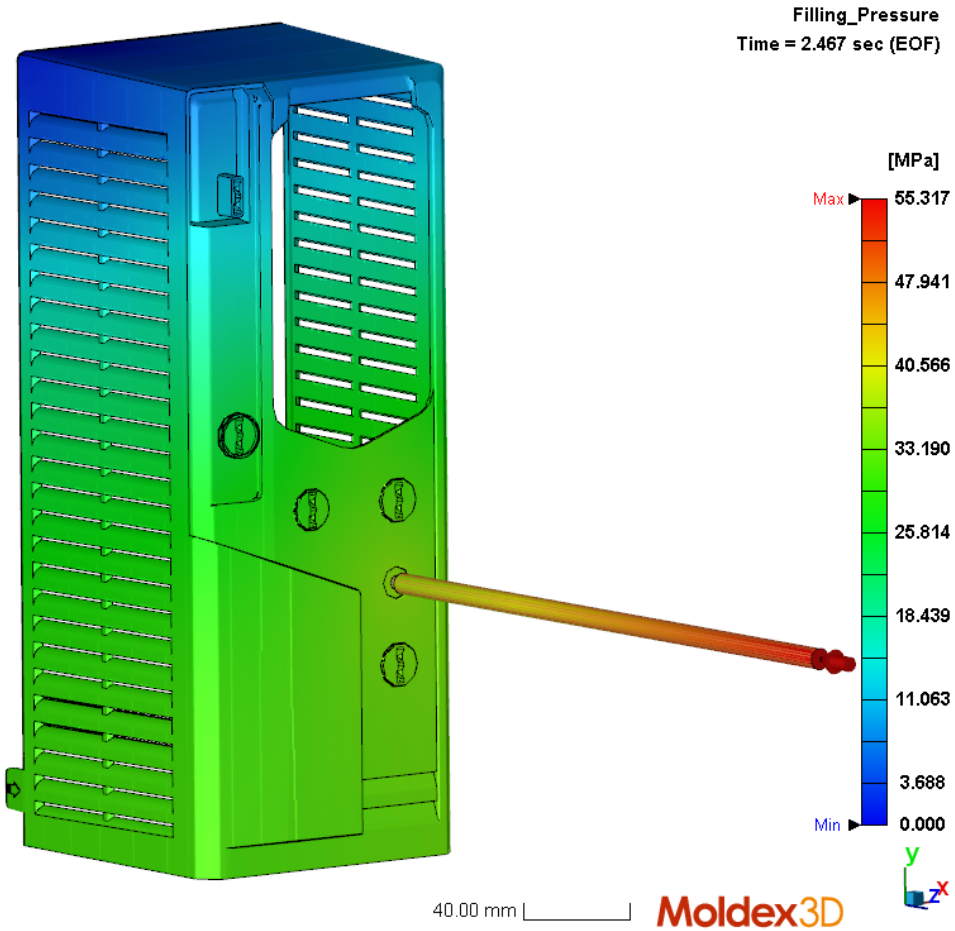


*Figure 65 Pressure distribution in part at end of filling.*

Pressure distribution in the part after packing time is shown in figure 66. Pressure differences in the part are similar to ones with real process parameters (compare to figure 37), with the difference that pressure levels are lower which is due longer packing time.

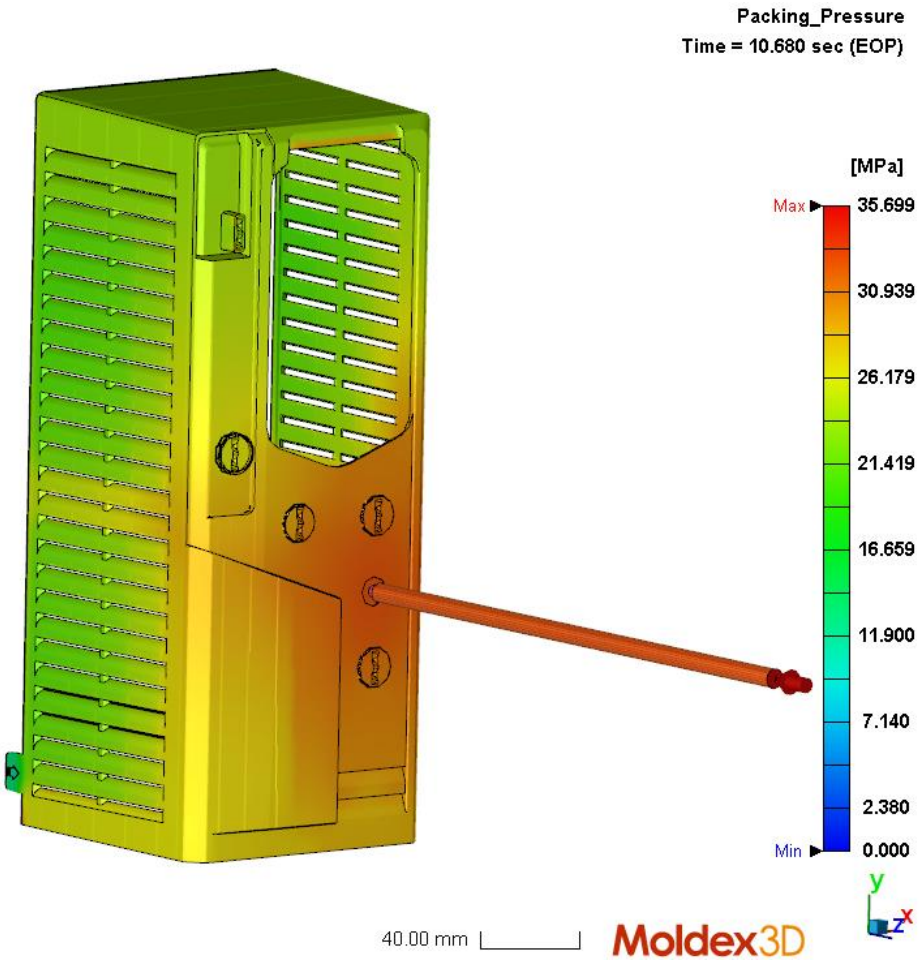


*Figure 66 Pressure distribution in part after packing stage.*

Figure 67 shows volumetric shrinkage of the part after packing stage when the part is cooled down to room temperature. Highest volumetric shrinkage is seen on the top surface as it is the last place to fill and have lower temperatures and pressures than other locations. Shrinkage is also slightly uneven on the side walls (light blue areas in figure 67), which can cause warping to the part.

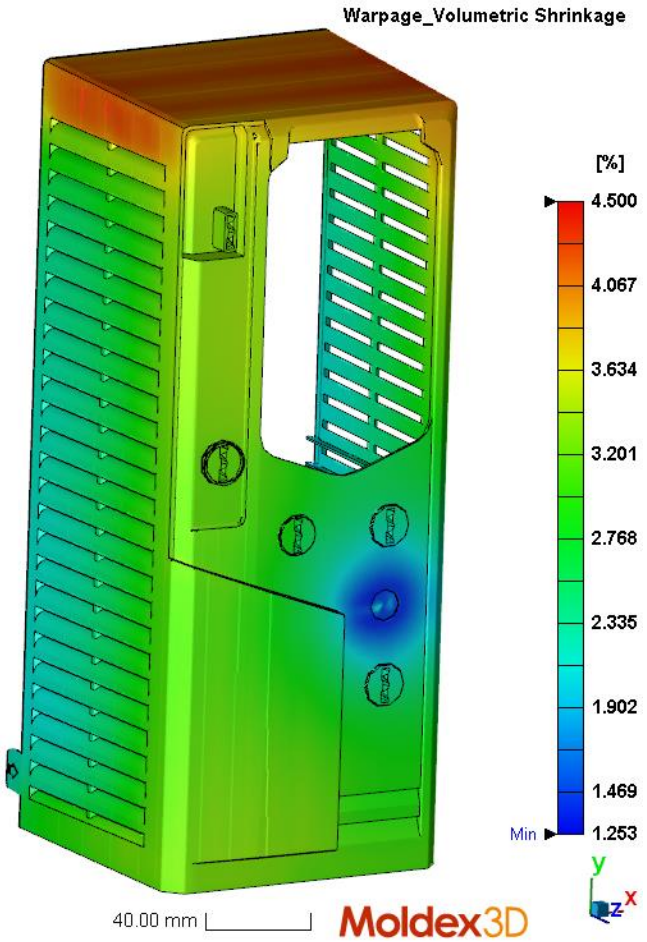


*Figure 67 Volumetric shrinkage when part is cooled after packing stage to room temperature.*

Displacement values in x-, y- and z-direction with real process parameters compared to default parameters are shown in figure 68 - figure 70. Compensation factor of 0,5% is used for all results, as the mold is constructed with 0,5% isotropic volumetric shrinkage. Figures of displacements in different directions shows that simulation with default parameters predicts higher displacement values than the real process parameters. However, differences between these values aren't enormous. Differences in maximum values are between 0,053 mm and 0,171 mm and in minimum values, 0,209-0,23 mm. When comparing locations of high displacements, it is noticed that on that matter, both cases predicts displacements to similar areas.

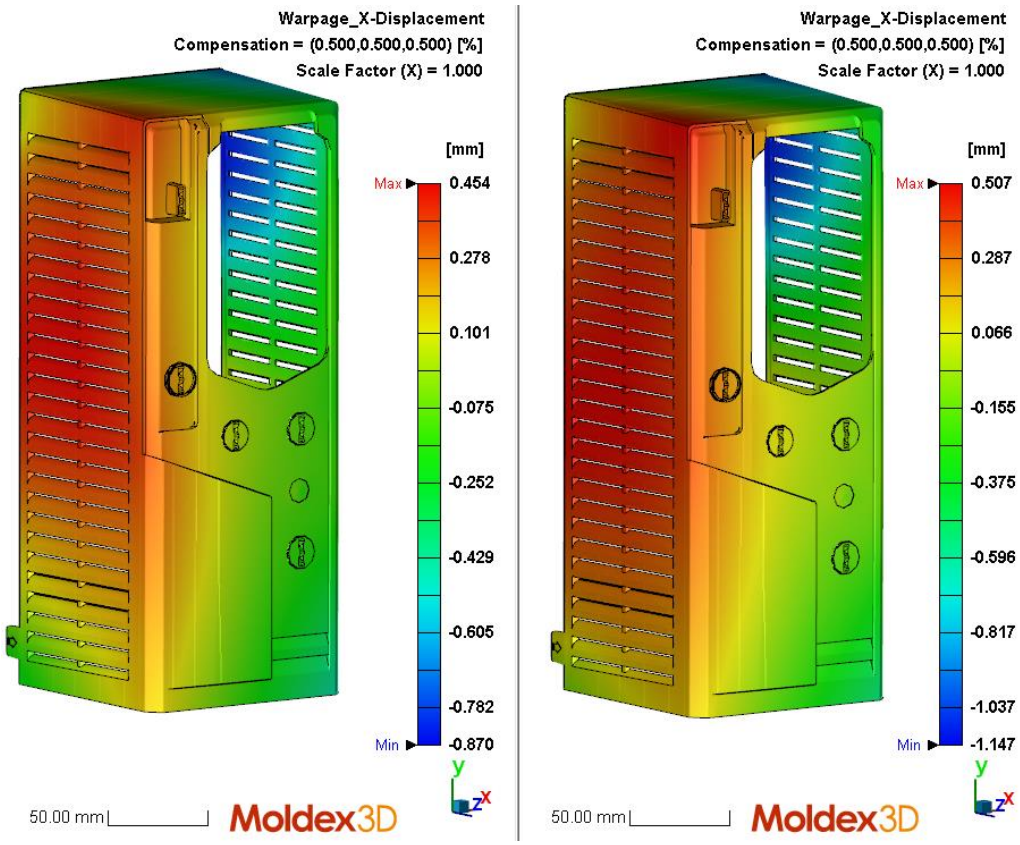


*Figure 68 Displacement in x-direction with 0,5% compensation factor. Results with real process parameters on left and with default process parameters on right.*

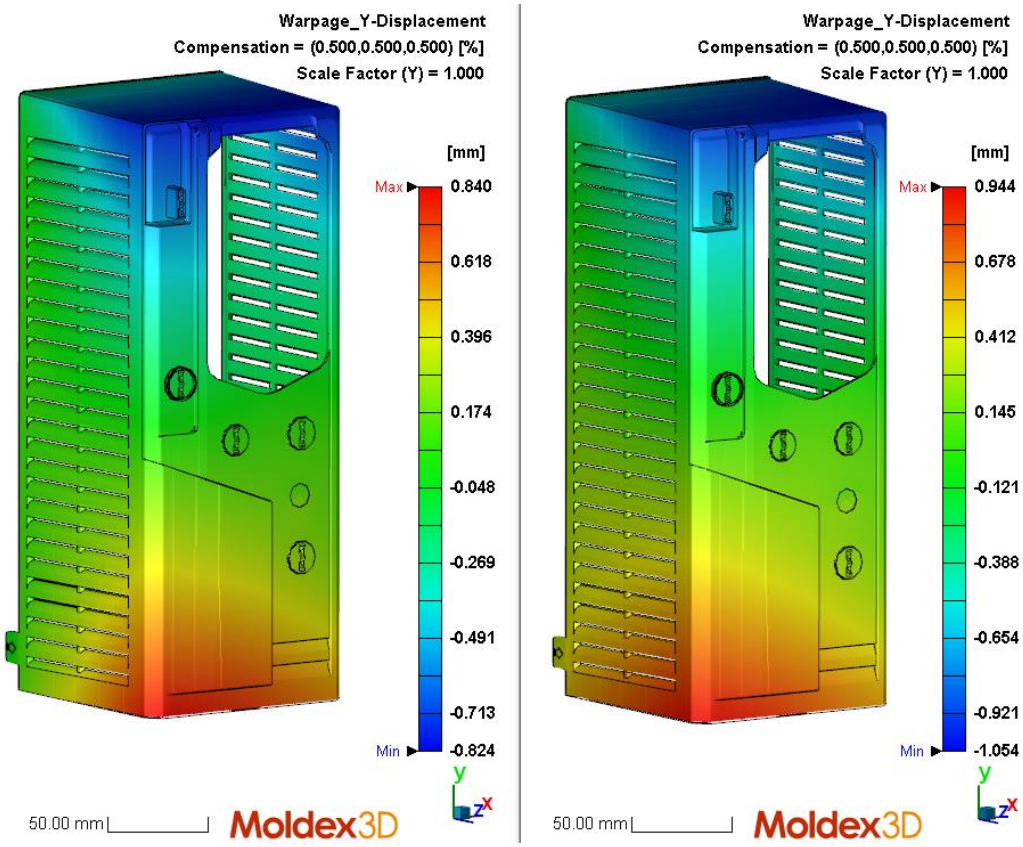


*Figure 69 Displacement in y-direction with 0,5% compensation factor. Results with real process parameters on left and with default process parameters on right.*

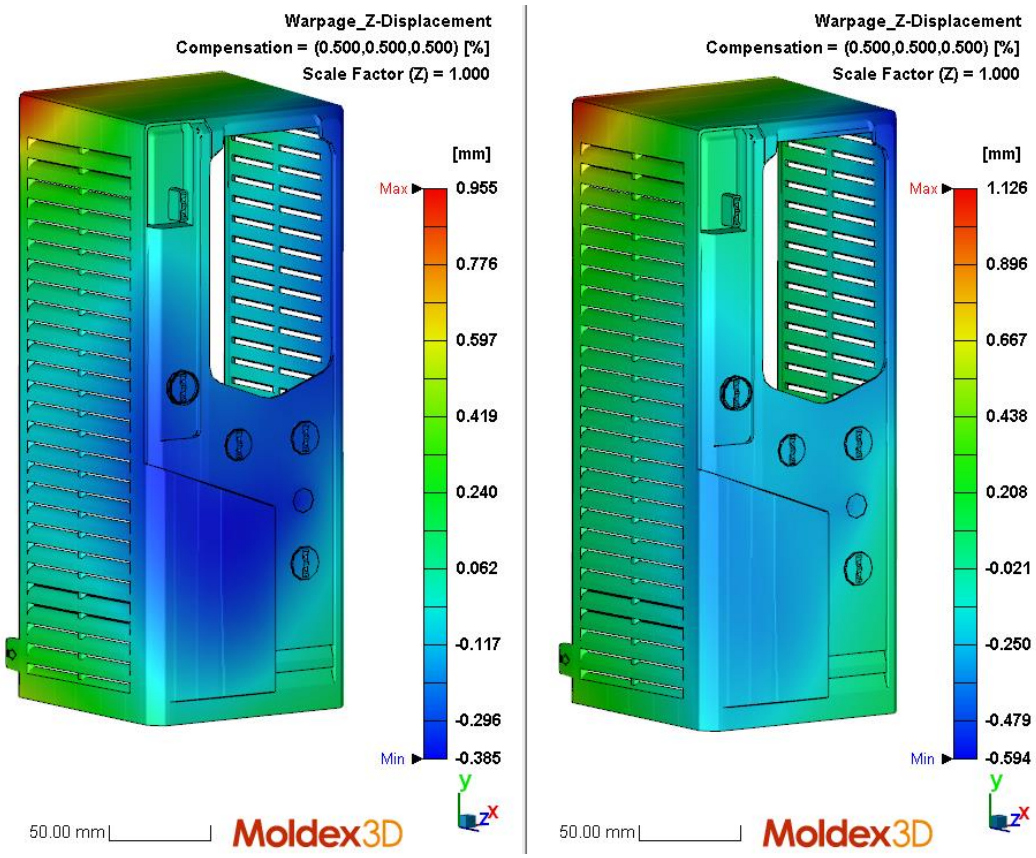


*Figure 70 Displacement in z-direction with 0,5% compensation factor. Results with real process parameters on left and with default process parameters on right.*

As the cooling channels in both studies were the same, warpage results related to temperature differences and distribution in the part aren't discussed here as the results are close to same. Displacements due to uneven shrinkage in the part are shown in figure 71 - figure 73. As previously, results with default process parameters predict higher displacement values. Differences in the results with real and default parameters are in the maximum values from 0,106 mm to 0,164 mm. In minimum values corresponding values are from 0,152 mm to 0,264 mm. As previously, results with default parameters predicts the highest displacement values on same areas as simulation with real process parameters.

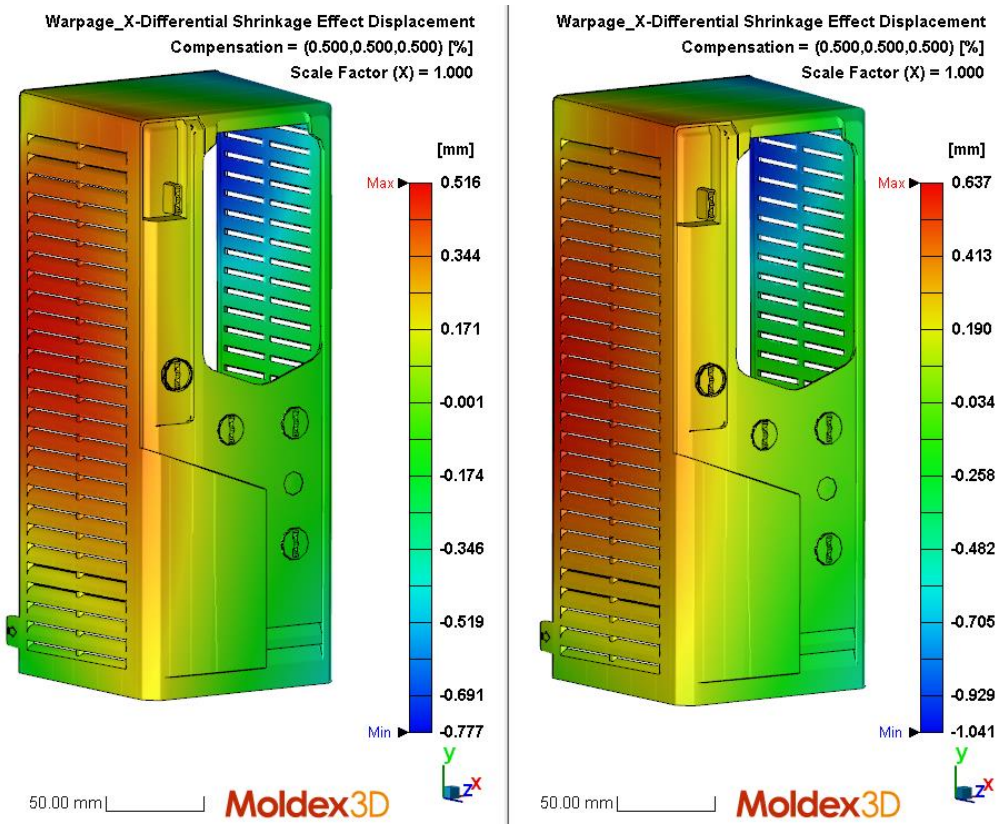


*Figure 71 Differential shrinkage effect displacement in x-direction with 0,5% compensation factor. Results with real process parameters on left and with default process parameters on right.*

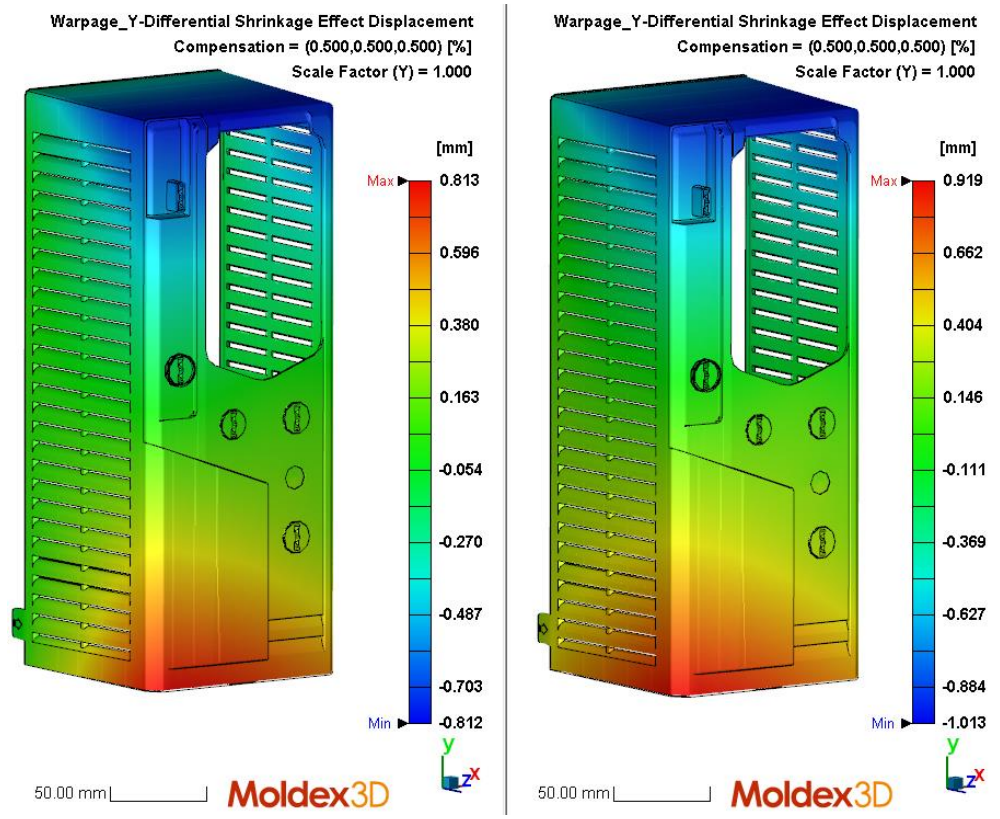


*Figure 72 Differential shrinkage effect displacement in y-direction with 0,5% compensation factor. Results with real process parameters on left and with default process parameters on right.*

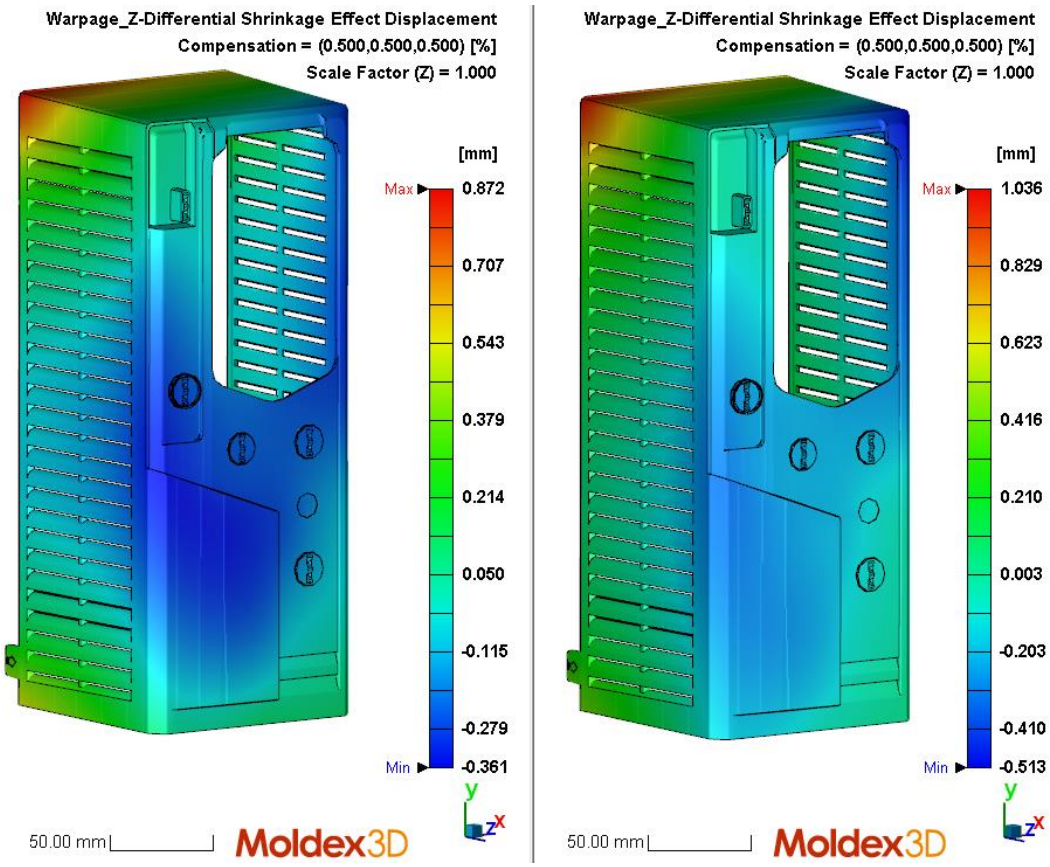


*Figure 73 Differential shrinkage effect displacement in z-direction with 0,5% compensation factor. Results with real process parameters on left and with default process parameters on right.*

When comparing results of displacement values in each direction with results of differential shrinkage effect displacement in corresponding direction, it is noticed that values are close to same. This predicts that displacement results from uneven shrinkage in the part and not from uneven cooling (which effect was in this case extinguish by using the same cooling channels and cooling parameters). Although results with default parameters predicted slightly higher displacement values, it predicted their locations on same areas as simulation with real process parameters. This will give confidence that simulation with default parameters will show areas where high displacements occur, close to simulation with real parameters. Based on these results, product designer can revise the geometry or wall thicknesses if simulation shows high displacements on some areas.

### 5.1.6 Polypropylene with default process parameters

This study analyses how polypropylene would work in the mold constructed for PC-ABS. This is studied by simulating the previous model, with the simplified cooling channels, with default process parameters for polypropylene. Polypropylene and PC-ABS has slightly different shrinkage behavior which will affect the results. The mold has been constructed with 0,5% volumetric shrinkage, and for the polypropylene used in this simulation, shrinkage is 0,5-0,8 %. Shrinkage is slightly lower than it is for most polypropylene grades, as the material is talc filled. Selecting polypropylene grade which shrinkage is close to shrinkage of the PC-ABS, makes it easier to get working in the same mold. Default parameters from Moldex3D are shown in table 11. Cooling time suggestion from Moldex3D was 14 s but as it has been noticed that default cooling times are usually

too short, cooling time was set to 35 s as with PC-ABS. Also, the eject temperature was adjusted from 100 °C to 70 °C as the default value 100 °C seems quite high based on experience at ABB.

*Table 11 Process parameters for polypropylene.*

| **Process parameter** | **Value** |
|---|---|
| Setting method | CAE mode |
| Material | PP |
| Mold material (mold plates) | P20 |
| Mold temperature | 55 °C |
| Melt temperature | 225 °C |
| Filling time | 2,38 s |
| Filling pressure | 140 MPa |
| Flow rate | 50 % |
| VP switch-over, by volume filled | 98 % |
| Packing pressure | 111,1 – 88,9 – 71,1 MPa |
| Packing time | 4,56 – 6,08 – 7,6 s |
| Cooling time | 35 s |
| Eject temperature | 70 °C |
| Coolant temperatures | 55 °C |
| Coolant flow rates | 120 $cm^3/s$ |

## Results

Filling pressure required to fill the part is 60,992 MPa. Pressure distribution after the filling phase is shown in figure 74. Figure 75 shows pressure distribution in part after packing phase. There is noticed to be high pressure differences inside the part and pressure differences are higher than in previous cases. Pressure in some areas of side walls is zero (seen as dark blue in figure 75) whereas near the gate, pressures are 30-36 MPa. These high pressure differences after packing stage are expected to be seen as high displacement values in warpage analysis.

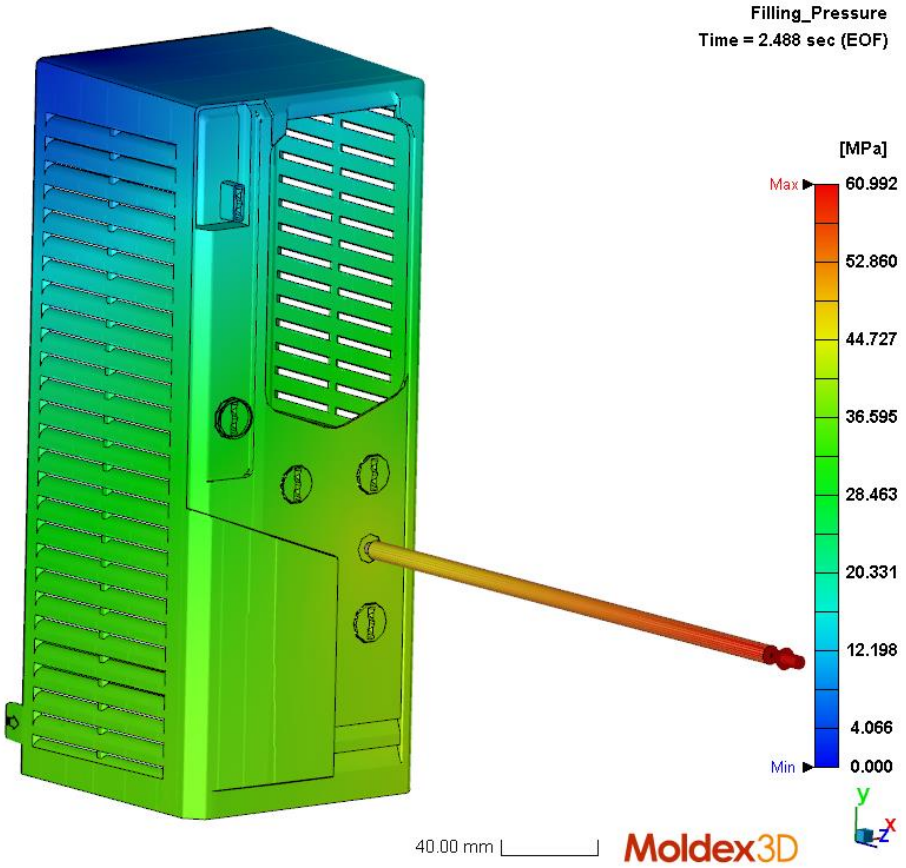


*Figure 74 Filling pressure with default parameters and PP as the material.*

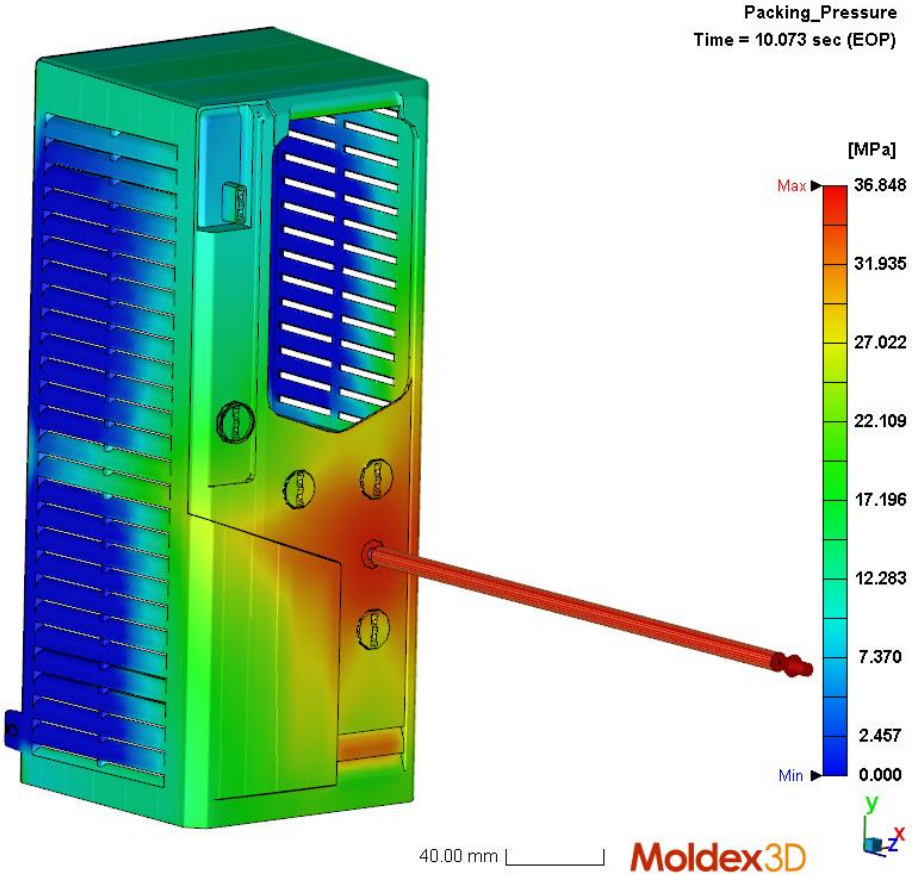


*Figure 75 Pressure distribution after packing phase.*

Cooling channels efficiencies are shown in figure 76. Coolant temperatures were set to 55 °C in each cooling channel. Cooling efficiencies are noticed to be lower on front surface of the part than inside the part. Highest cooling efficiencies are on the side walls cooling circuits, as also in previous cases. Temperature distribution in the part after cooling time is shown in figure 77. Temperature distribution on the outer surface seems to be quite even, but inside the part temperatures are higher. These high temperatures inside the part can cause the side walls to warp when part is cooled down to room temperature.

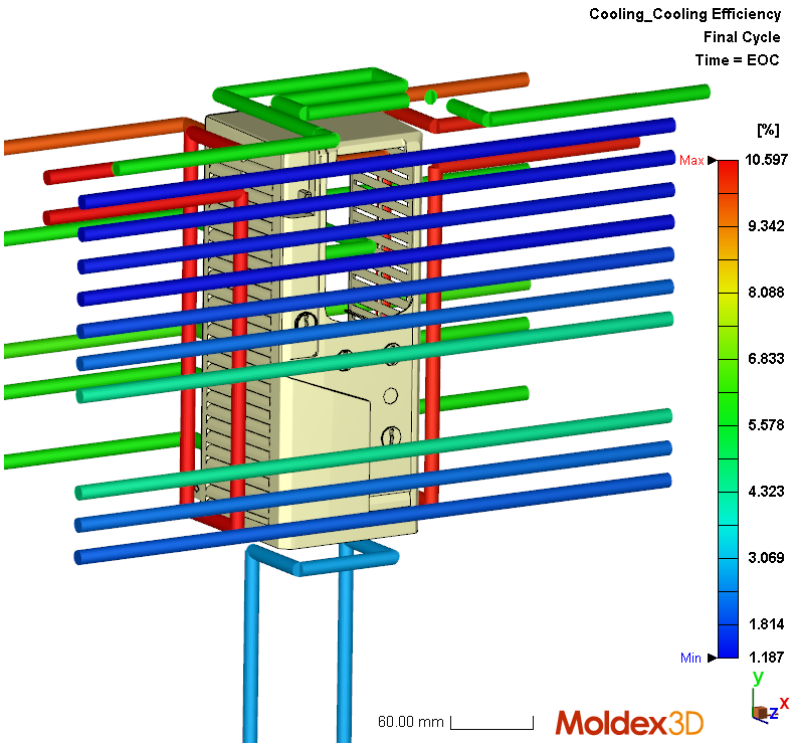


*Figure 76 Cooling channel efficiency.*

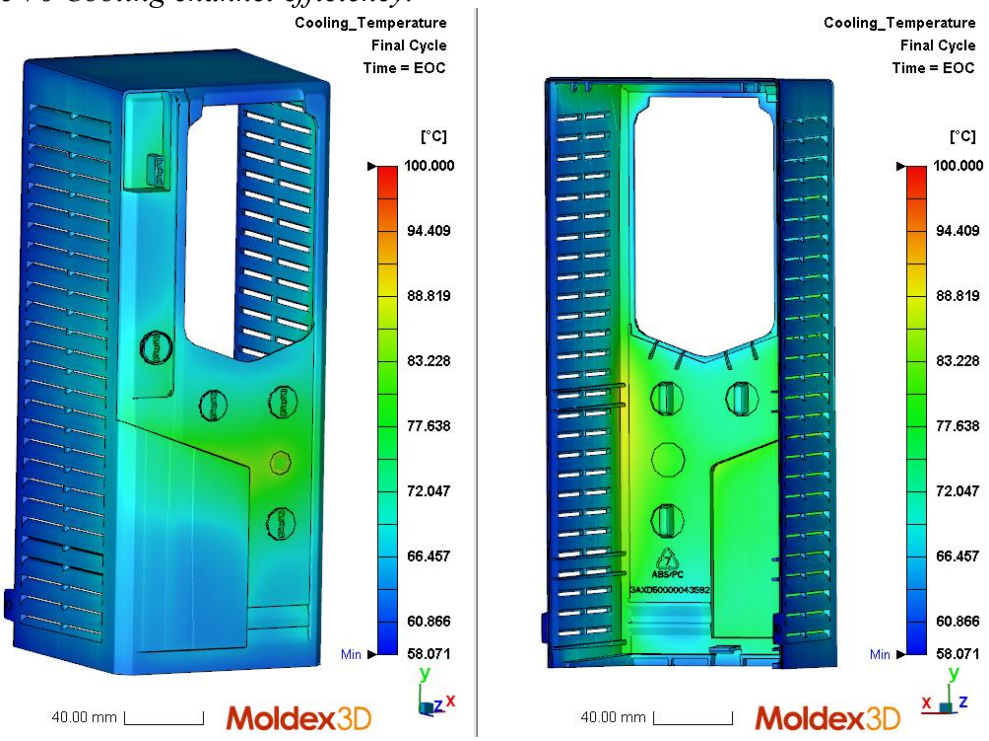


*Figure 77 Temperature distribution in part after cooling time.*

Figure 78 shows volumetric shrinkage when part is cooled down to room temperature after packing phase. Highest shrinkage is on the top surface but otherwise shrinkage seems to be more even than with PC-ABS and real process parameters (compare to figure 40 before).

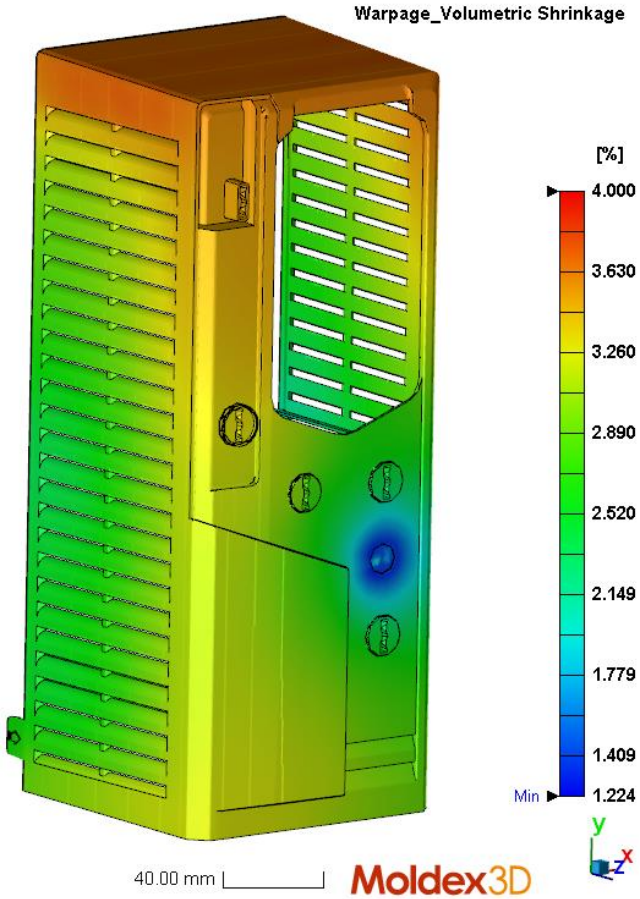


*Figure 78 Volumetric shrinkage when part is cooled to room temperature after packing phase.*

Displacements in x-, y- and z-direction are shown in figure 79 and figure 80. Figure 79 shows that displacements in x-direction are highest on the sidewalls and especially on the two fastening clips. Positive displacements are found on wider area than the maximum negative values which are concentrated only on the clip area. Tolerance limit for the maximum width was previously defined to be ±0,32 mm which is not fulfilled. In y-direction, maximum positive and negative values are found on top and bottom of the part. High displacements on the top surface are most likely generated from the uneven shrinkage which was seen in figure 78. Tolerance limit in y-direction was ±0,41 mm, which is half of the displacements seen in the simulation results. Figure 80 shows displacement in z-direction. Displacement values are from -0,363 mm to 0,696 mm. Highest displacement, 0,696 mm, is found from the top surface. Tolerance limit in z-direction was ±0,35 mm which means that the minimum displacement is close to be inside the tolerance, but highest displacement is about twice the tolerance limit.

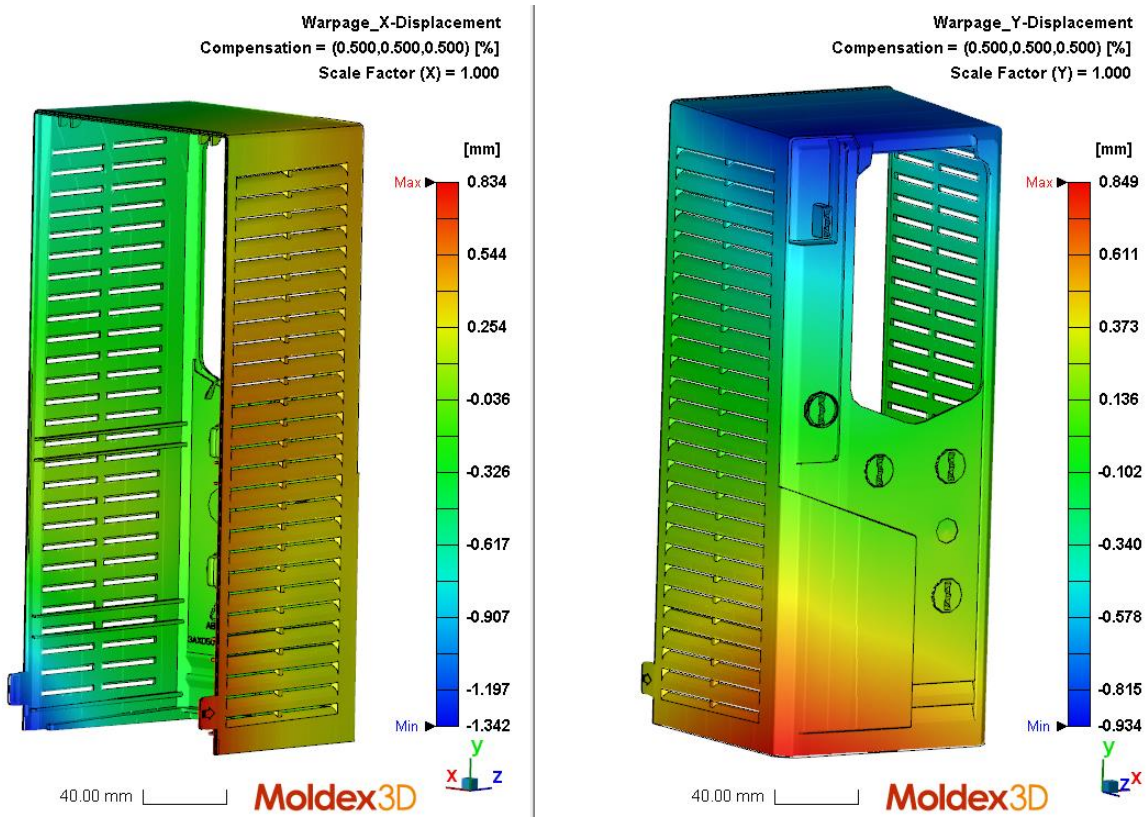


*Figure 79 Displacements in x- and y-direction with 0,5% compensation factor. Displacement in x-direction on left and y-direction on right.*

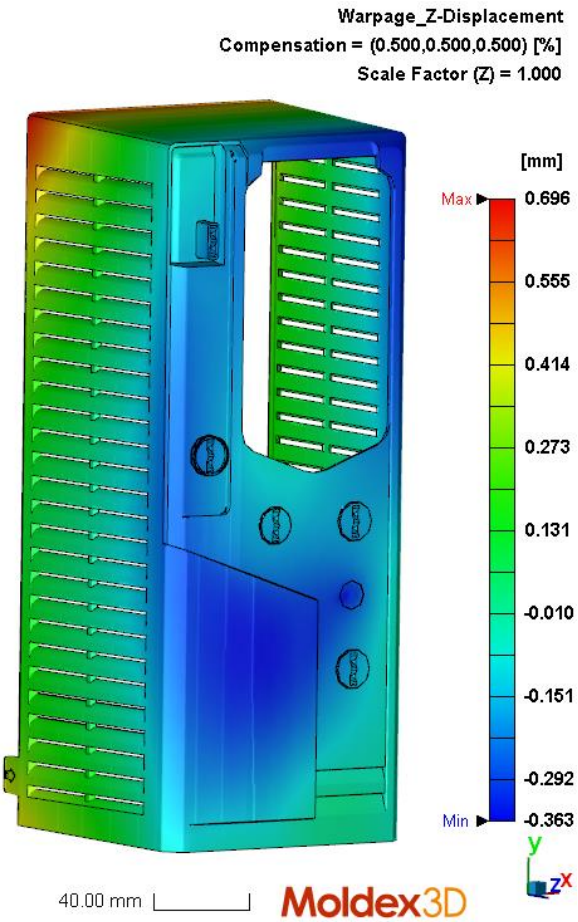


*Figure 80 Displacement in z-direction with 0,5% compensation factor.*

In order to study more which effect is causing the high displacements, also thermal displacement, differential temperature effect displacement and differential shrinkage effect displacement are reviewed to see which has the highest effect to the warpage. Thermal displacements in x-, y- and z-direction are shown in figure 81 and figure 82. Figure 81 shows that displacements in x-direction are high as the range is from -1,762 mm to 1,661 mm. Highest displacements are on the sidewalls. However, thermal displacement in y-direction seems more acceptable, as the range is from -0,313 mm to 0,362 mm and which is inside the tolerance, ±0,41 mm. Thermal displacement in z-direction (figure 82) is from -0,274 mm to 0,367 mm which is close to be inside the tolerance ±0,35 mm. Based on these results of thermal displacement, high displacement values in x-direction, noticed in figure 79, are highly resulting from unbalanced cooling. In y- and z-direction thermal displacements are inside the tolerances or really close to them.

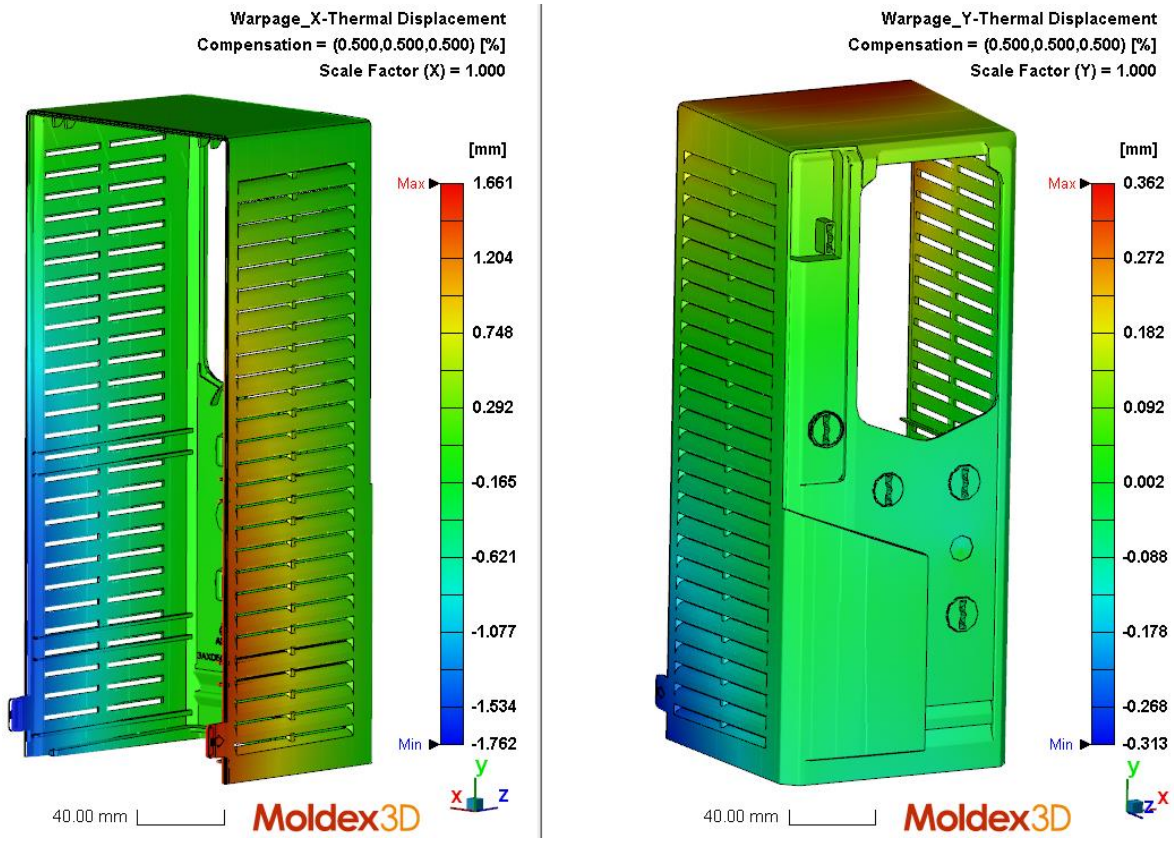


*Figure 81 Thermal displacement in x- and y-direction with 0,5% compensation factor. Displacement in x-direction on left and y-direction on right.*

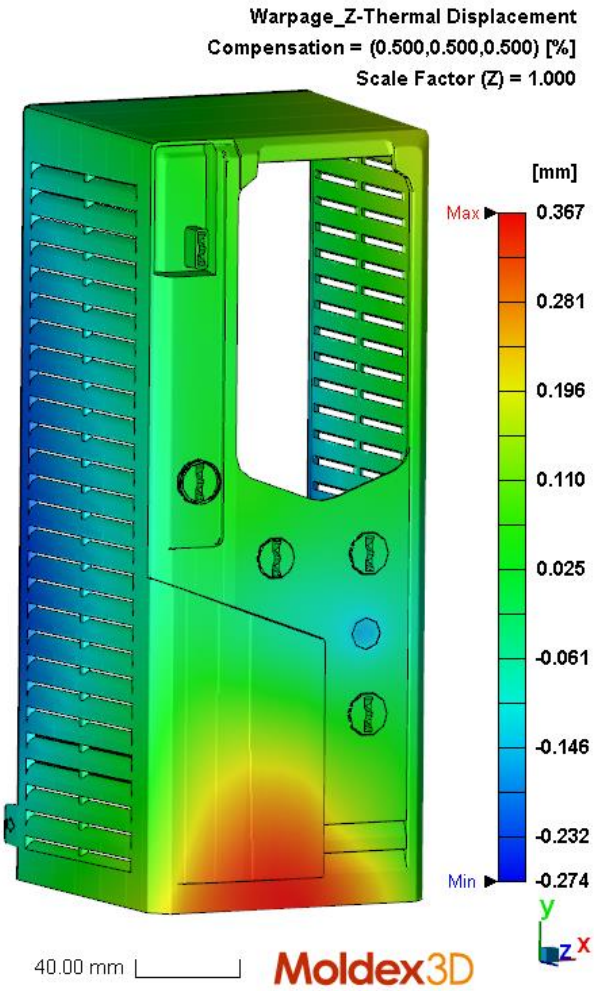


*Figure 82 Thermal displacement in z-direction with 0,5% compensation factor.*

Differential temperature effect displacement in x-, y- and z-direction with 0,5% compensation factor are shown in figure 83 and figure 84. In x-direction, range of displacement is from -0,438 mm to 0,550 mm, and in y-direction from -0,707 mm to 0,805 mm. These values are quite high and above the tolerances ±0,32 mm (x-direction) and ±0,41 mm (y-direction). In z-direction displacements are between -0,408 mm and 0,228 mm, close to be inside the tolerance ±0,35 mm.

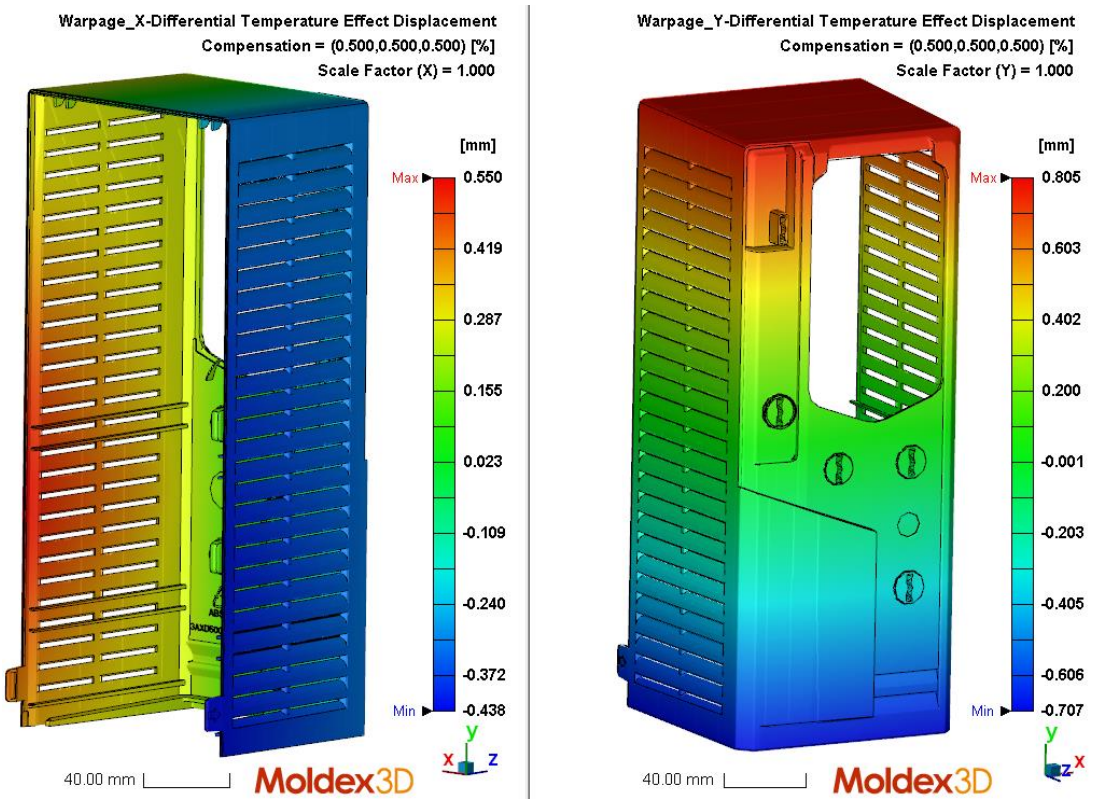


*Figure 83 Differential temperature effect displacement in x- and y-directions with 0,5% compensation factor.*

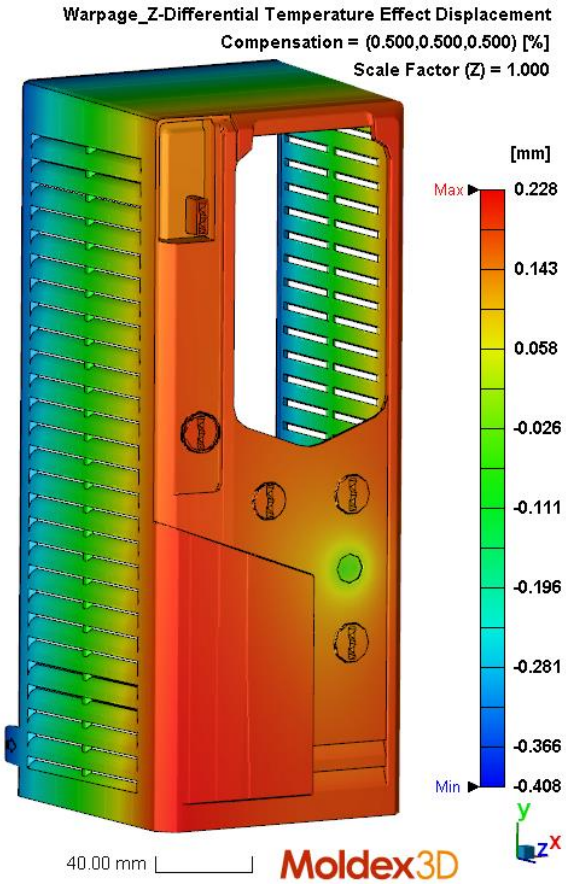


*Figure 84 Differential temperature effect displacement in z-direction with 0,5% compensation factor.*

Differential shrinkage effect displacement in x-, y- and z-direction are shown in figure 85 and figure 86. In x-direction displacement is from -0,651 mm to 0,501 mm when with PC-ABS and real process parameters it was from -0,760 mm to 0,504 mm. In y-direction values are -0,966-0,861 mm and with real parameters, -0,793-0,791 mm. In z-direction corresponding values are -0,323-0,690 mm and -0,355-0,855 mm. Displacements due to uneven shrinkage are in all directions close to values with PC-ABS and real process parameters. Highest displacements are noticed to be in y-direction which supports the shrinkage behavior seen in figure 78.

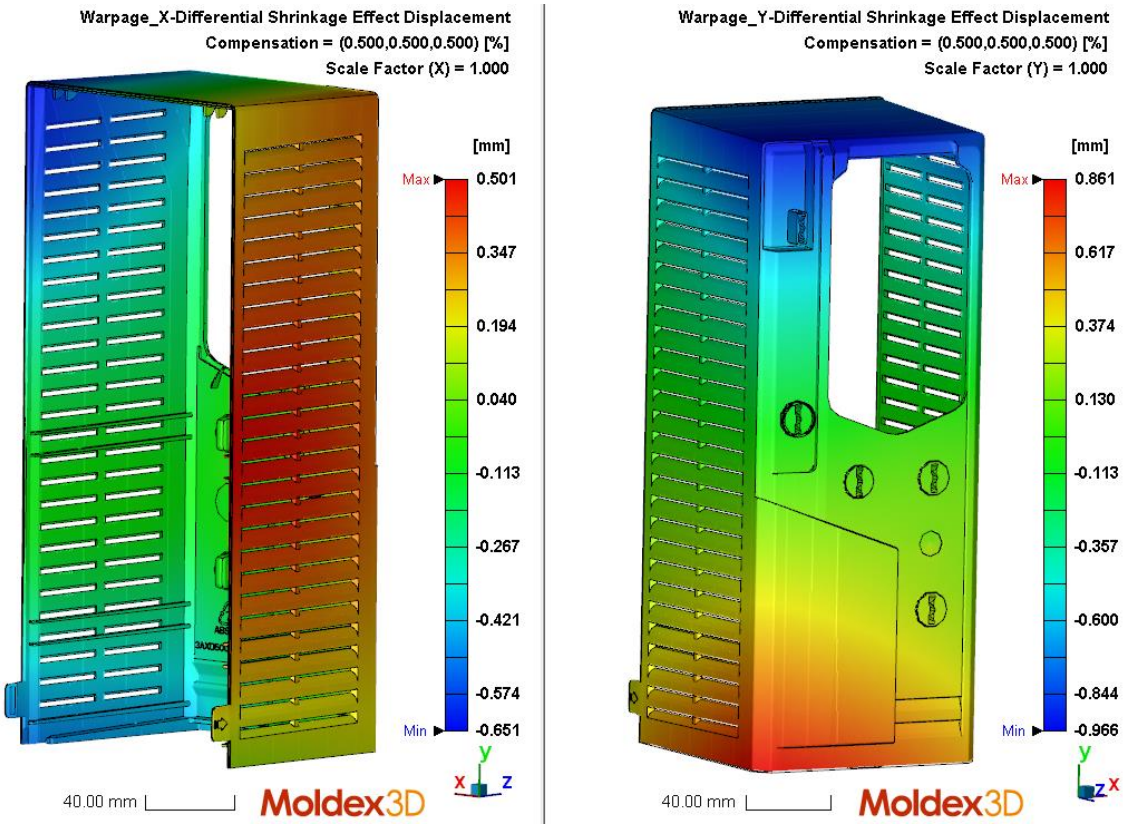


*Figure 85 Differential shrinkage effect displacement in x- and y-directions with 0,5% compensation factor. Displacement in x-direction on left and y-direction on right.*

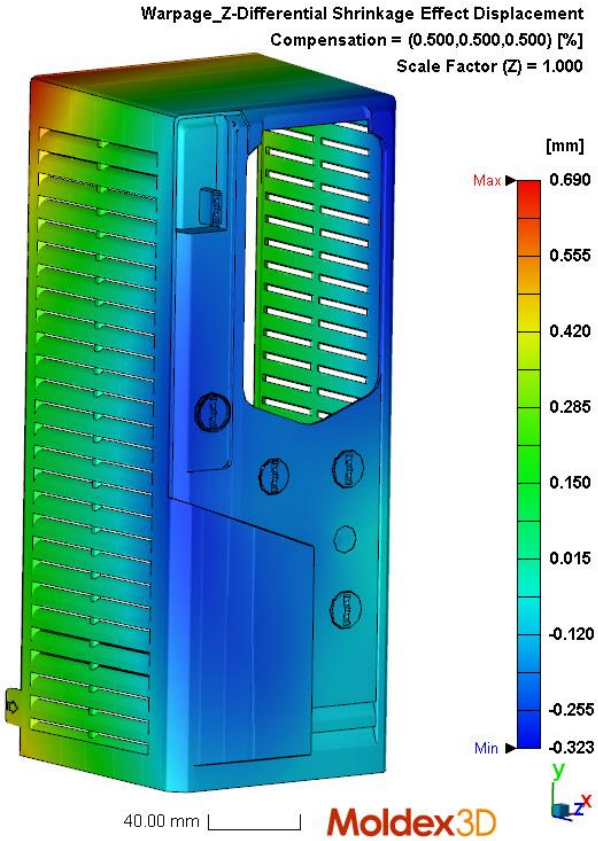


*Figure 86 Differential shrinkage effect displacement in z-direction with 0,5% compensation factor.*

Overall, when comparing displacement values of polypropylene (presented in figure 79 and figure 80) to ones of PC-ABS with real molding parameters (presented in figure 41 and figure 42), it is noticed that results are quite similar. Most difference is seen in x-direction, where displacement with polypropylene is almost twice the one for PC-ABS. However, in y-direction values are really close to each other and in z-direction polypropylene has smaller displacements than PC-ABS. Based on these results of total displacement, it could be possible to get the polypropylene to work in a mold designed for PC-ABS, by adjusting the process parameters. However, it should be noticed that for some reason, results from simulating PC-ABS with real parameters, never matched the tolerance limits set for the part. Due to this, before studying the alternative material more, some additional studies with the real parameters should be done to find out the cause for high displacements.

### 5.1.7 Conclusions

Results showed some inconsistency between simulation and what is seen after real molding process. These differences were estimated to result from some simplifications needed to do for the cooling system and used mold model for the simulation. Also, accuracy of PC-ABS's material data was questioned. However, studies with simplified cooling channels showed only little difference to the real molding conditions. With default parameters, as expected, displacement values were bit higher than with real process parameters. However, warpage was predicted on same areas than with the real process parameters. Use of polypropylene increased the displacements slightly, but by adjusting the process parameters, it most likely can be used in a mold designed for PC-ABS.

With simulation, it's easy to check how well the product geometry will work in injection molding and for example which areas require more cooling, and analyze if they could be improved by geometry changes. By multiple results of warpage analysis, it is possible to analyze more which factor is causing the warpage, e.g. either cooling system or uneven shrinkage. Simulation also gives a good tool to compare different designs, for example how diameter of cooling channels or cooling channel design affects to cooling time, and this way product designers have some estimation to judge the decisions. Results presented in this case study showed that quite accurate estimations can be get with simplified cooling system and by using default process parameters from Moldex3D. Default process parameters indicate slightly higher displacements, but their locations are predicted on the same areas as displacements with real process parameters.

### 5.1.8 Possible error sources

Simulation model for this case study was constructed based on real mold design which consists of mold plates, core and cavity pieces, hot runner system, cooling channels, slides, ejector pins and fasteners. For the simulation, the model was simplified to consist of solid mold model with hot runner and cooling channels. The mold dimensions were selected based on the real mold and it was modelled as a solid rectangular piece, which doesn't take account the heat exchange between different mold plates. Also, mold base material to the simulation was defined to be P20 when in real mold some of the mold pieces are different steel grade. These simplifications will affect the mold heat exchange properties. Hot runner system was modelled as close to real as possible, with the right runner and gate dimensions. Cooling system needed some changes and simplifications in order it to work in Moldex3D. Some of these changes were already mentioned in the chapter 5.1.3, where it was introduced that few of the channels needed changes to their shape/routing. Moldex3D also requires that inlets and outlets of the cooling channels are on the interface of the mold base. In order to fulfill this requirement, lengths of the channels needed to be changed slightly. This can cause small variation to the cooling analysis results and it should be noted that due to these reasons cooling channels used in the simulation don't correspond to the ones in the real mold with 100%. Other possible source for error comes from the placement of the molded part compared to cooling channels. Placing the part was done in the Moldex3D environment which is slightly inaccurate and can cause displacement of few millimeters between placement of the part in the simulation and in the real mold. Cooling channels weren't chained together outside the mold, as they would be in the real mold. This will affect to cooling efficiencies of the channels and also to coolant temperatures which can cause differences to results of cooling analysis. Issues stated here are possible sources for errors and they should be noted when analyzing the simulation results, but their effect is estimated to be small. Results from the simulation should be analyzed by acknowledging the fact that simulation provides estimation of the process in optimal conditions where the environment doesn't have any changes e.g. in temperature or humidity. In real molding process, the molding machine as well affects the process more, as machine have always slight delay to response to changes e.g. in pressure or flow rate.

Injection molding is also greatly impacted by material and especially in simulation it is important that material parameters are specified accurately. Displacement values with real process parameters were more than tolerances allow for the part. This was discussed with Moldex3D representatives who suspected that high displacements could result from inaccurate material data. PC-ABS used in this study was selected because it is an alternative material grade specified for this product. Simulation was run with different

PC-ABS grade to review if change in the displacements was seen. This alternative PC-ABS grade was from the same manufacturer as the initial PC-ABS and results showed similar behavior in the warpage analysis as the initial material.

## 5.2 Case 2: Gland box

This case study concentrates on studying mold insert deflection and cracking, and actions to decrease and prevent these issues. This mold insert failure is an ongoing problem during the work of this master's thesis, and goal of this thesis study is to compare the effect of different geometrical changes and gating point placements to reduce the insert deflection and cracking problems. Studying pressure variation over the tool insert will give knowledge for future to recognize possible areas which have risk for insert breaking, and gain information of the pressure difference values which are likely to cause bending or breaking problem.

Product of this case study is a gland box shown in figure 87. As the figure shows, product has double sidewalls which are manufactured with two tool inserts (see figure 88). Material of gland box is PC-ABS and tool inserts are made of beryllium copper. Beryllium copper is used as it has better thermal conductivity than steel and use of it will decrease the cooling time. Disadvantages are its lower strength and stiffness properties.

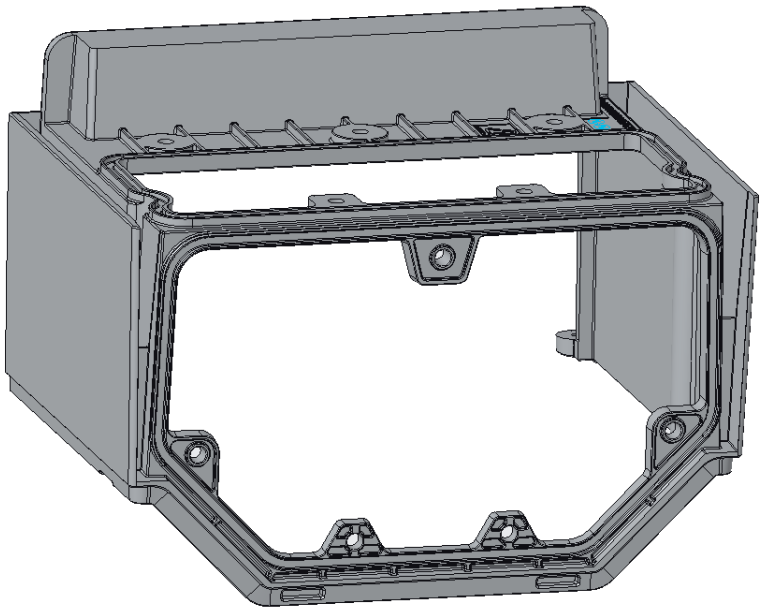

*Figure 87 3D schematic of the gland box.*

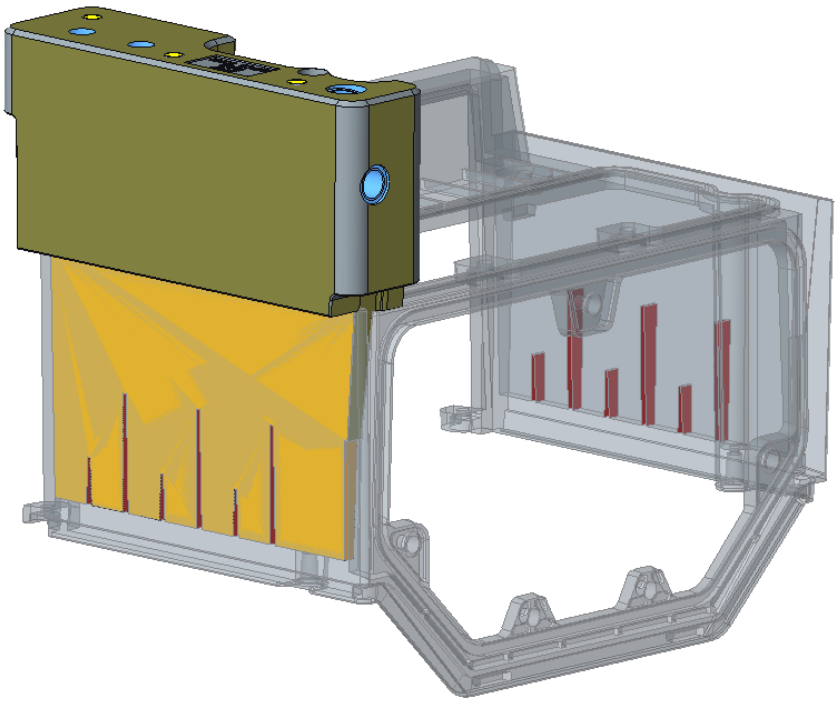

*Figure 88 Part with one tool insert. Inside the double walls there are six ribs (highlighted with red) to support walls of the part as well as help the plastic melt to flow on part's outer wall.*

Dimensions of the gland box and tool inserts are shown in figure 89 and figure 90. Figure 90 shows that 75,4 mm of the insert's height is unfixed during the injection molding. Thickness of the insert is at the base approximately 7,8 mm and 3,8 mm in the insert tip.

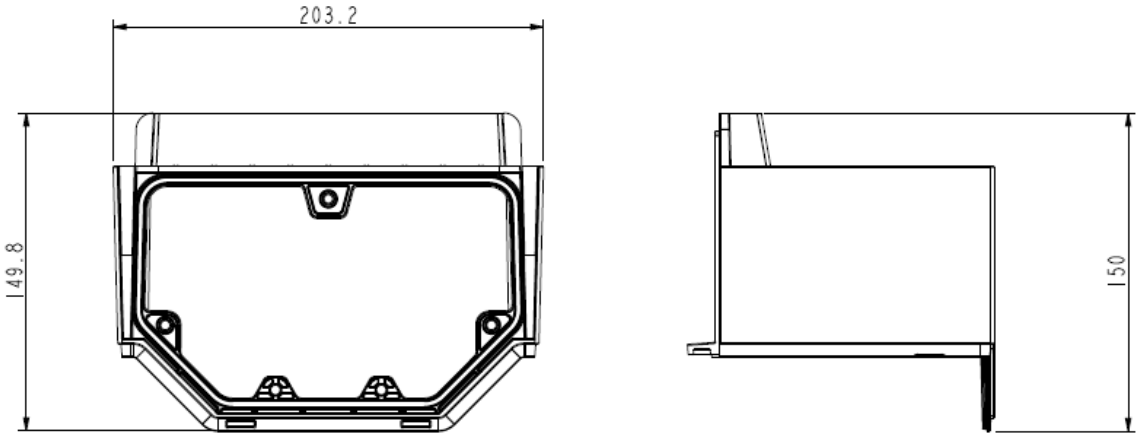


*Figure 89 Main dimensions of the gland box.*

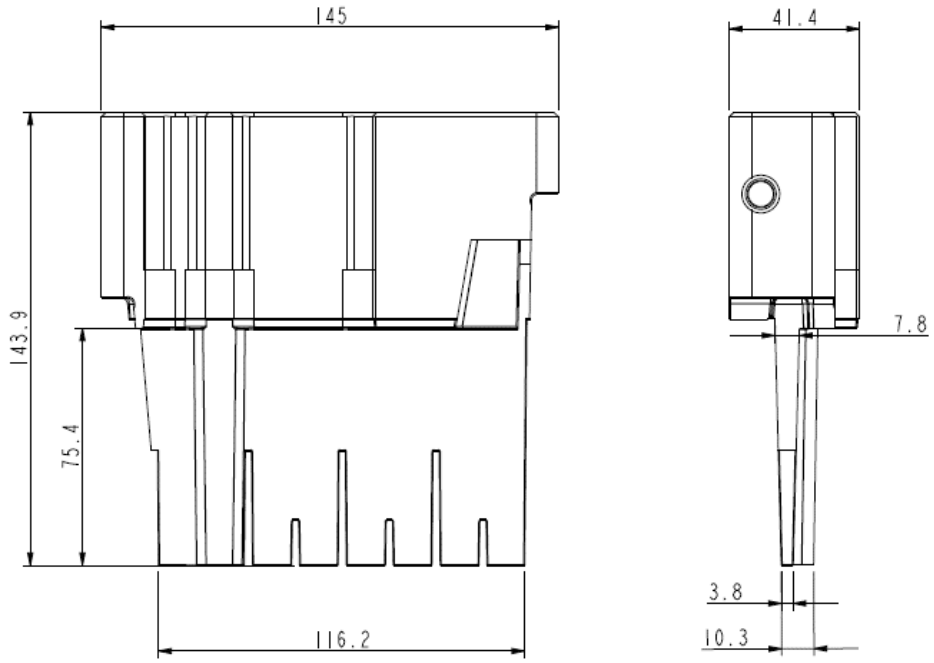

*Figure 90 Dimensions of tool insert.*

### 5.2.1 Object of the study

Object of this case is to study reasons for tool insert failure and means to prevent failure occurring in the future. It is also valuable to get information of how high pressure differences are causing the insert failing, as this can be used as a reference in future when similar inserts are used. Figure 91 shows tool inserts attached to the mold and figure 92 shows a closer view of the insert base where cracking has occurred. Cracking occurs already after few molding cycles which indicates that cracking results most likely from high pressure differences over the insert and high stress concentrations during filling. It is assumed that failing of the insert is caused during filling stage instead of packing as the pressure differences over the tool insert should be highest then when there aren't yet any material in the cavity. As the mold has already been constructed, there are limitations for the gating locations, which is why gating points presented later are chosen for this study.

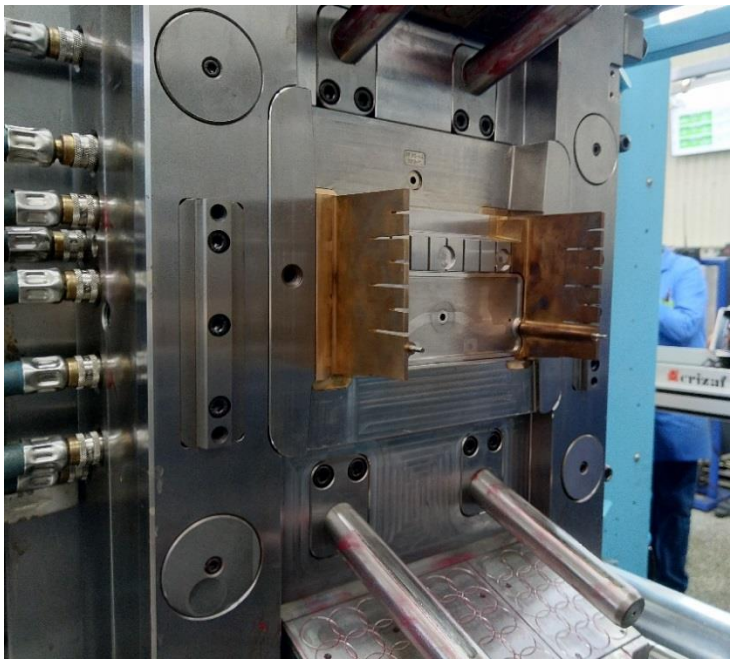

*Figure 91 Real mold with the tool inserts. (Palojoki, 2019)*

*Figure 92 Tool insert where cracking has occurred in the base of the insert. Red arrow points to the area where the cracks are seen. (Palojoki, 2019)*

Overall, six different part geometry and gating point configurations are studied to find out the one where possibility for insert failure would be the smallest. First two cases are constructed based on the test moldings done already and which are known to cause cracking in the insert base. They are analyzed to identify the melt flow behavior and pressure variation inside the mold. These results give approximated values to the pressure variation which are causing cracking. After these studies, some changes to part geometry and gating locations are made, to study how these changes affect the melt flow and pressures. Object is to find a solution of part geometry and gating points which gives balanced melt flow and has only small pressure variations over the tool insert.

### 5.2.2 Hypothesis of the study

Tool insert bending and cracking is assumed to be due to the pressure differences over the tool insert during filling. As material of the tool inserts is beryllium copper, strength and stiffness of the inserts are lower than for similar steel ones. Cracking happens in the base of the tool inserts where there is only a small radius which is assumed to cause high stresses on that area. Injection points of the feed system are only on one side of the tool inserts which will produce a higher pressure to the gating side when melt hasn't yet flowed on the other side of the insert.

### 5.2.3 Simulations and results

This chapter consist of six different studies for the previously presented gland box. Frist two of these studies were first test molded and they both resulted with failed tool inserts. Tool inserts had cracks in the base area, and they had bent during injection molding as the gland box's wall thickness was uneven in the area where the tool inserts affect it. Aim of the first two studies is to simulate the behavior of plastic in the failed cases in order to find out how high pressure differences are causing the inserts to fail. Eventually, some changes to part geometry and gating locations are made to analyze how these would affect pressures concentrating to the inserts.

All simulation models consist of part model and gating points. Runner system or gates are not specified for the simulation and only melt inlet points are defined (with diameter of 3 mm). Most, or all the rounds are excluded from the part for the simulation to make meshing of the part easier and increase its quality. Meshing of the part models is done with level 4 of Moldex3D. Unless other specified, process parameters used for the simulation are as following in table 12.

*Table 12 Process parameters for the studies.*

| Parameter | Value |
|---|---|
| Filling time | 1,8 s |
| Maximum filling pressure | 172 MPa |
| Flow rate | 50 % |
| Injection pressure | 100 % |
| VP switch over by volume filled | 98 % |
| Melt temperature | 260 °C |
| Mold temperature | 70 °C |

#### 5.2.3.1 Initial part design, 2 gating points

First simulation model was constructed with the initial part design and with two gating points. Rounds were excluded from the simulation model as they are so small that they are hard to mesh with the automatic meshing tool. Gating points of the part are shown in figure 93, and as shown they are located on the round surface of the part and pointing towards the tool inserts of the mold. Figure shows also meshing of the part which consist of 34 606 surface mesh elements with 1 332 610 solid mesh elements.

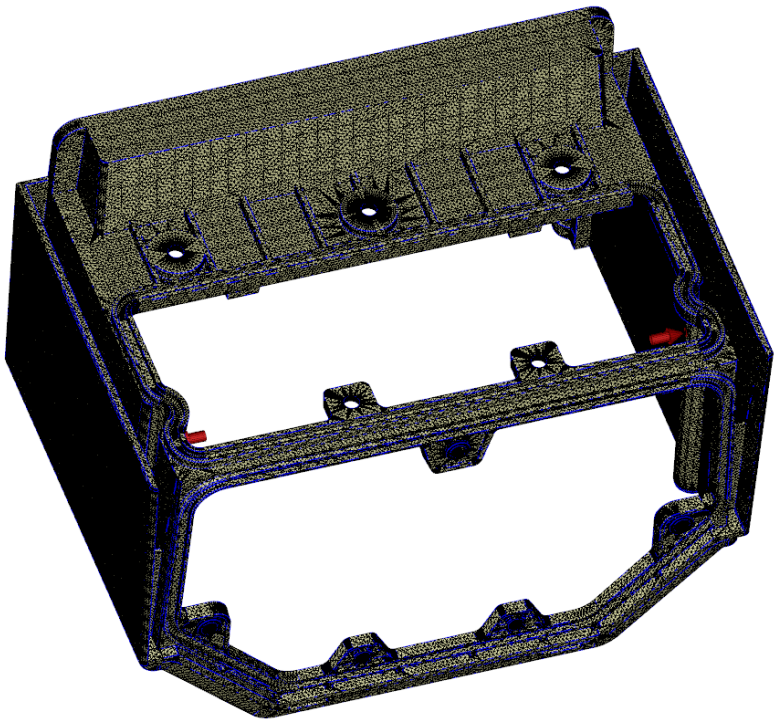

*Figure 93 Meshed part with two gating points (shown with red arrows).*

## Results

Pressure required to fill the part is 64,533 MPa and filling time is 1,910 s (figure 94). Highest pressures are near the gate (shown as red) and lowest pressures are on the area where part is filled at last (shown as blue). Melt flow time can be seen in figure 95, which shows that the inner wall is mostly filled when plastic starts to flow to the outer wall. This indicates high pressure differences on the insert base, which can be the cause of cracking problem. It takes roughly 0,3 seconds, minimum, to the plastic melt to reach on the outer wall through the ribs. From there, plastic starts to flow on horizontal and vertical direction, but it takes about 1,3 seconds until the outer wall opposite to the gating points is completely filled. This means that pressure differences near the gating points can be high and they will affect most of the filling time to the tool insert. Last areas to fill are in the middle of the part and as well on the leftmost corner of part's outer wall.

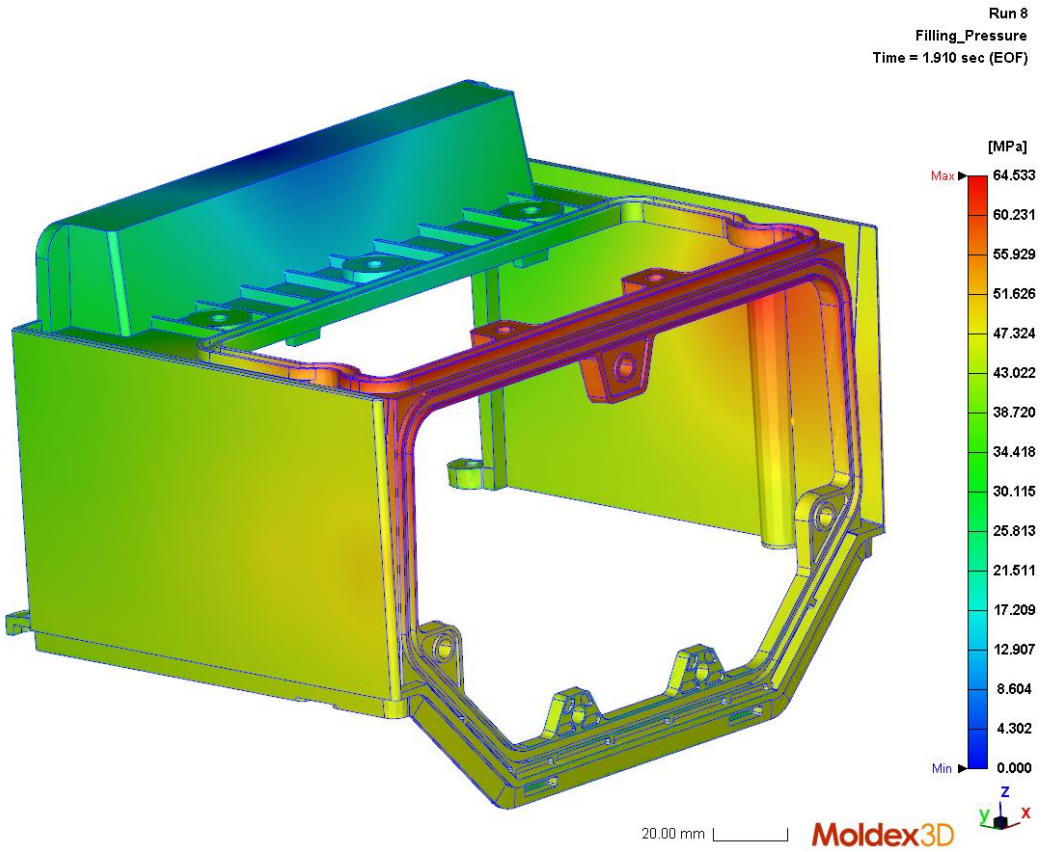


*Figure 94 Pressure required to fill the part is approximately 65 MPa.*

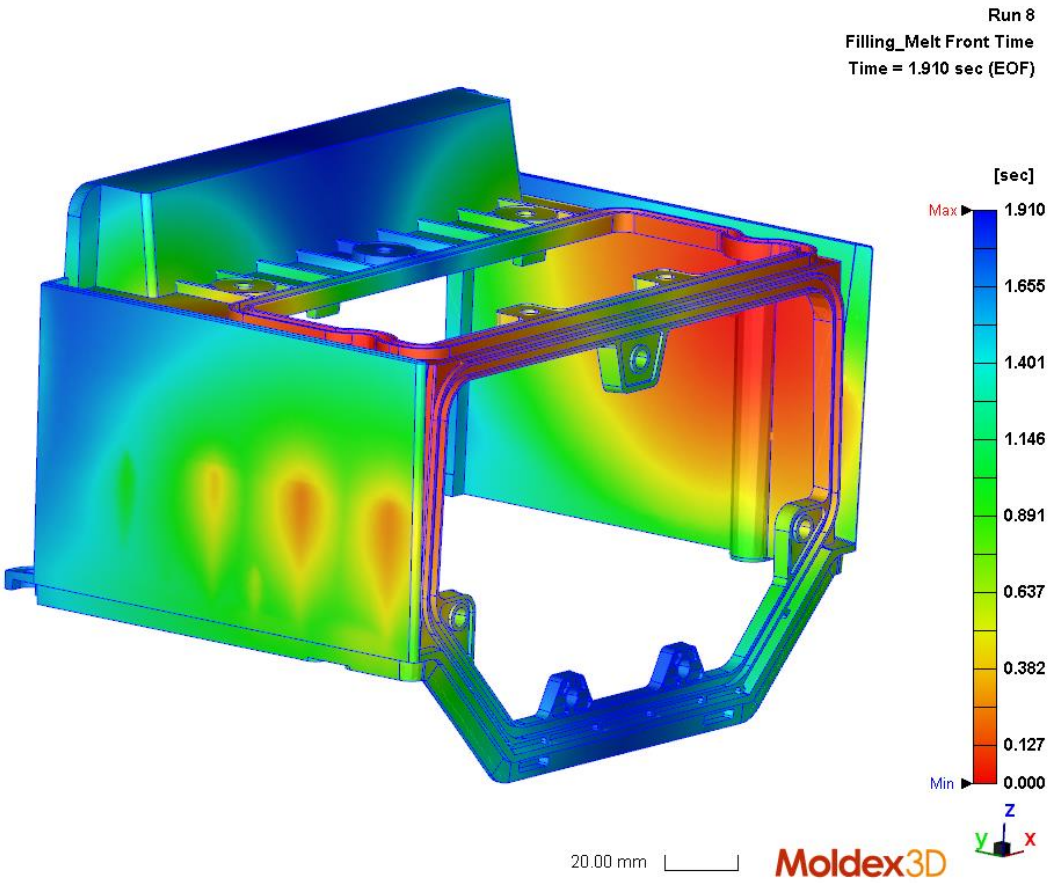


*Figure 95 Melt flow time.*

In order to study more how high pressure differences concentrate on the tool insert due to the uneven filling pattern shown in figure 95, 12 probe pairs are attached to the part to see the behavior of pressures in these exact locations, and find out the pressures concentrating on the tool insert. Only half of the part is studied as the part is symmetrical. Figure 96 shows location of the probe pairs. Probes 1 to 5 are on the tool insert base area and probes 6 to 12 are attached further away from the tool inserts fixed surface. As these probes are further from the fixed point, smaller load will bend the insert easier. Furthermore, insert tip area has multiple cuts due to ribs in the part which weakens the insert tip. Probes named "IN" are attached on part's inner wall which is in contact with tool insert's inner surface. "OUT" named probes are on the opposite side on the outer wall of the part, and on its outer surface. "OUT" probes were attached on the outer surface as the pressure difference through the wall can be assumed to be negligible.

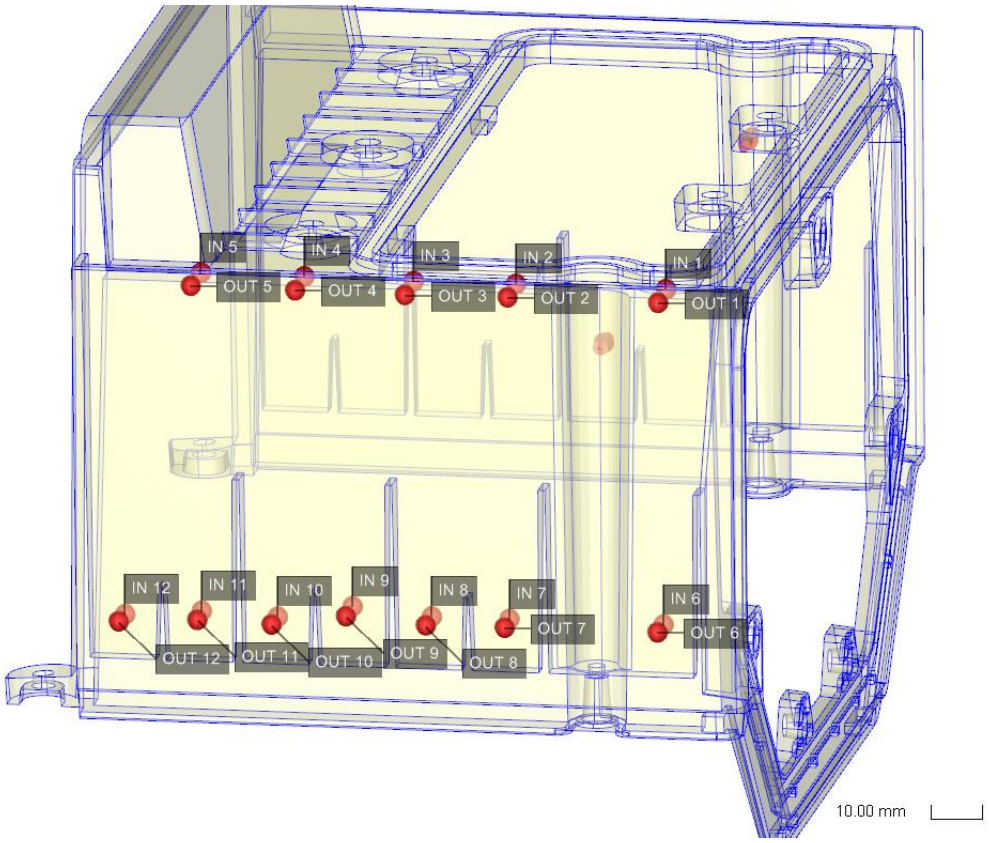


*Figure 96 Probe locations.*

During the first 0,508 s of filling, melt has filled approximately half of the inner wall (figure 97) and melt has started to flow on the outer wall through the higher ribs. However, pressures near the gating area are around 12 MPa without melt on the outer wall to even the pressure distribution. On time step 0,832 s, pressures have increased to 16 MPa and melt front hasn't yet reached on insert's base in the outer wall (figure 98). Nevertheless, melt has started to fill the outer wall from the bottom and pressure differences on probes 6-9 are between 0,5 MPa and 2,2 MPa.

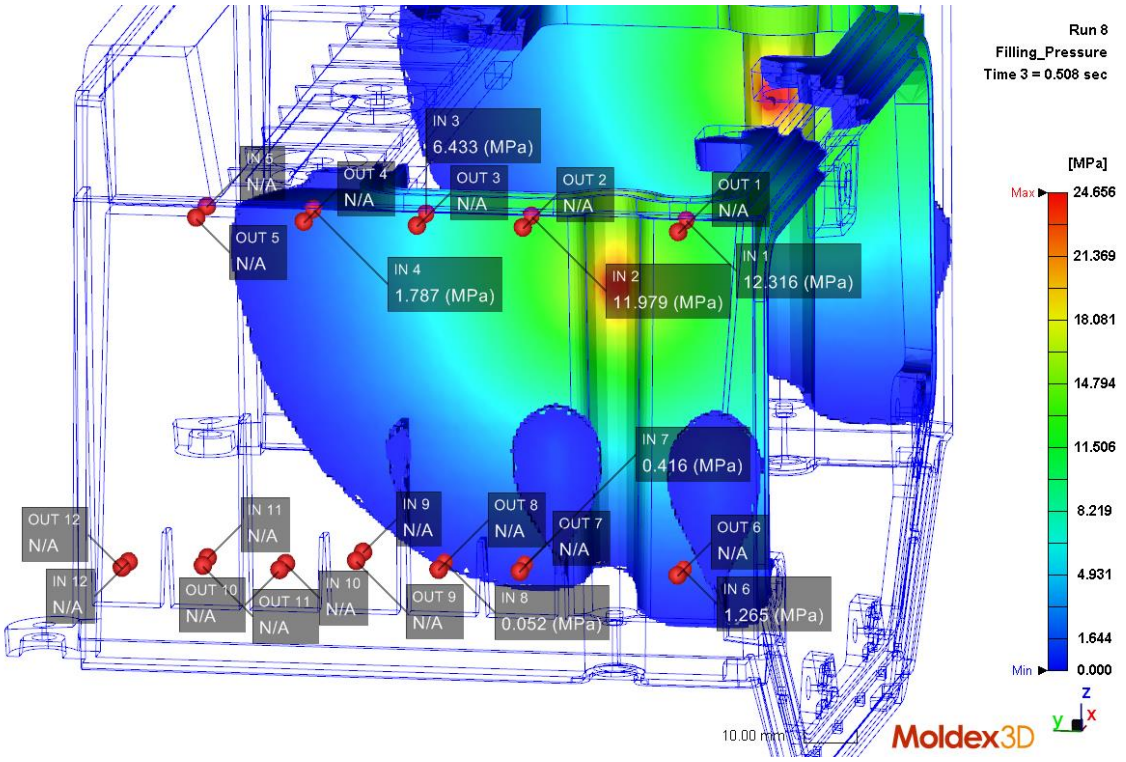


*Figure 97 Filling pattern and pressures at time step 0,508 s.*

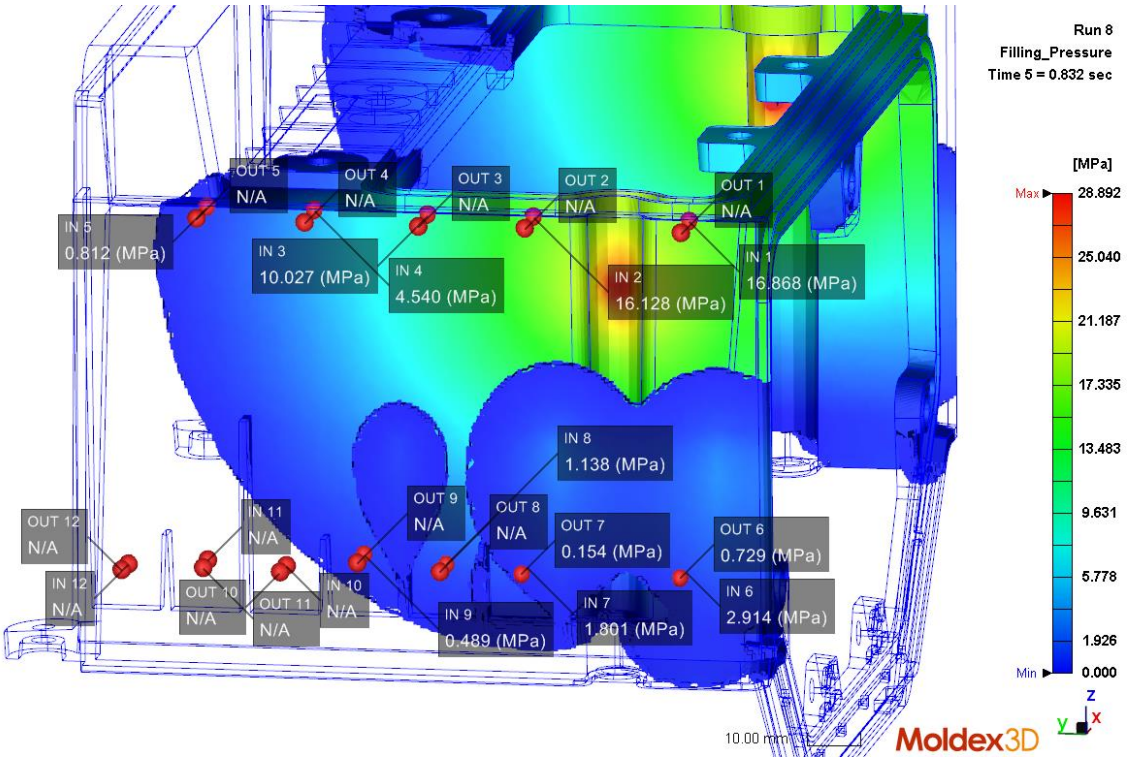


*Figure 98 Filling pattern and pressures at time step 0,832 s.*

On time step 1,150 s, melt has almost filled the inner wall (figure 99). Pressure differences of probes 1 and 2 have increased to 24,8 MPa and 21,7 MPa, as the melt front hasn't still reached the probes on the outer wall. Pressure differences of probes 6-10 haven't increased and are between 0,4 MPa and 1,8 MPa. Melt front hasn't yet reached on location of probes 11 and 12. On 1,498 s, melt has reached on all other probes than OUT 4, OUT 5 and OUT 12. Pressure differences of probes 1 and 2 have slightly decreased (to 21,9

MPa) as the melt has filled the outer wall (figure 100). Pressure differences on probes 6-12 are roughly around 1,5 MPa.

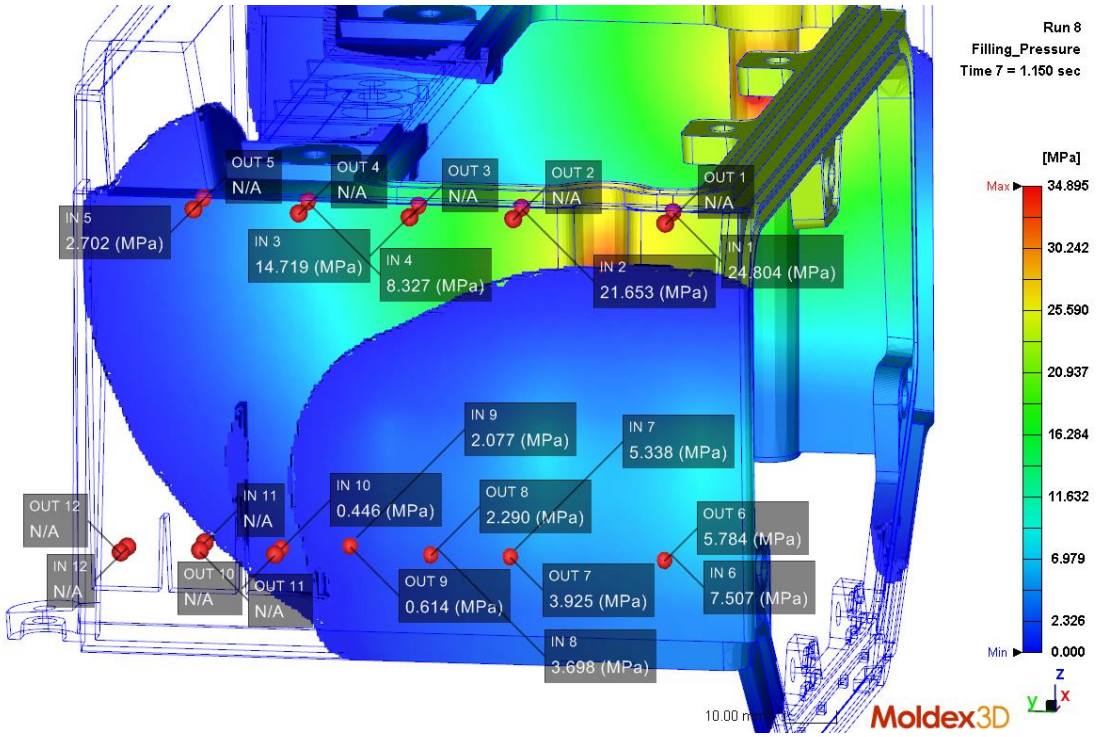


*Figure 99 Filling pattern and pressures at time step 1,150 s.*

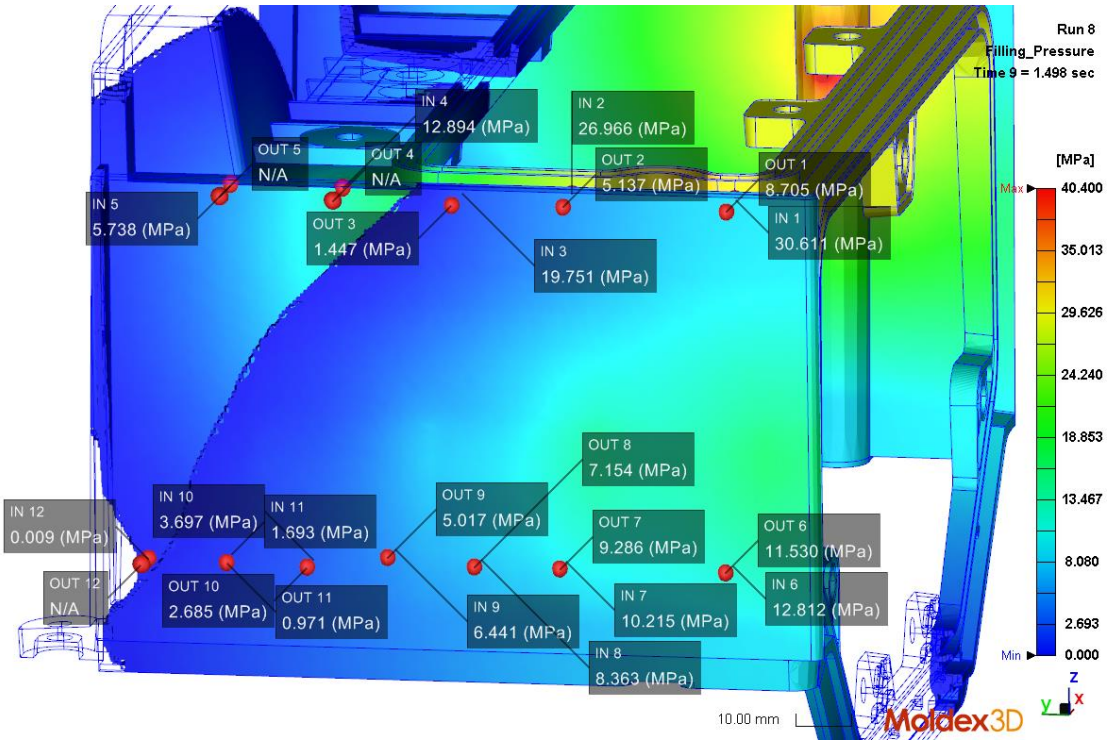


*Figure 100 Filling pattern and pressures at time step 1,498 s.*

Figure 101 shows the pressure distribution at 1,640 s. It is noted that the last area to be filled is around probe 5 in the outer wall. Pressure differences on probes 1-5 are from 8,6 MPa to 22,2 MPa and at the rib area approximately 0,9-1,7 MPa. At the end of filling (figure 102), pressure differences have decreases as the outer wall is completely filled.

Also, it is noted that probes 4, 5 and 12 have higher pressure on the outer than on the inner wall, which results most likely from the fact that they locate in places which fill last.

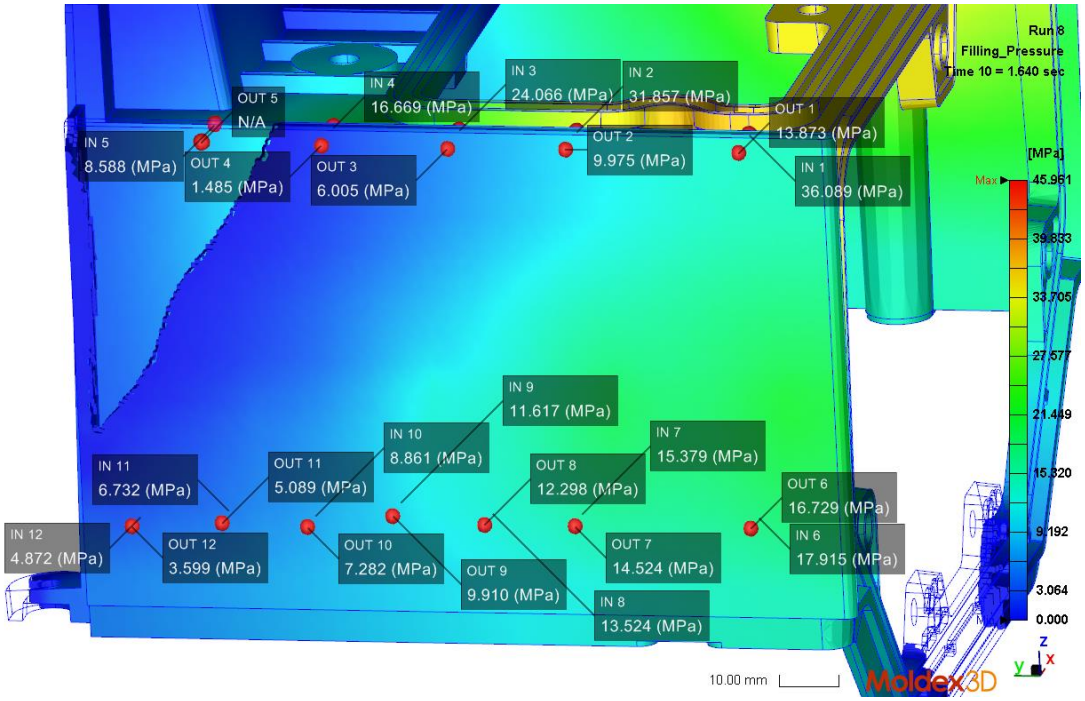


*Figure 101 Filling pattern and pressures at time step 1,640 s.*

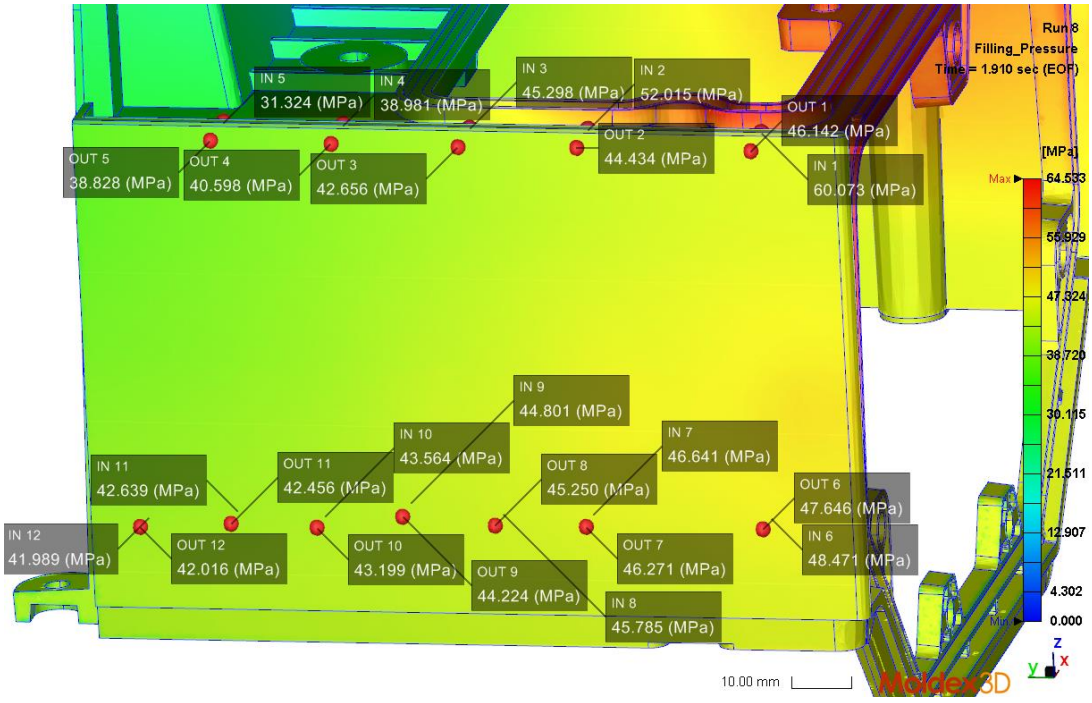


*Figure 102 Filling pattern and pressures at end of filling (EOF).*

Pressure differences at six different time steps are collected into table 13 based on figure 97 - figure 102 presented previously. Positive value means that pressure in the inner wall is higher than in the outer wall. Table shows that melt has reached at least one probe of each probe pair at 1,498 s. Highest pressure differences are found from the insert base (from probes 1 and 2), and most of the filling time pressures there are close to 20 MPa.

This means that pressure load on tool insert's base is almost the whole filling time 20 MPa or close to it. At the end of filling, pressures in the outer wall on probes 4 and 5 have increased higher than pressures in the inner wall. This results from the fact that inner wall has been filled between 1,640 s and EOF, when the outer wall isn't yet filled, and filling pressure is only increasing pressure on locations where filling is not completed. Probes 6-12 have quite small variation in pressure differences and values are mostly below 2 MPa. This indicates that both inner and outer wall are filling at quite same time. Insert cracking is assumed to result from the high pressure differences (near 20 MPa), over the inserts.

*Table 13 Pressure differences (as MPa) of probes 1-12 at six different time steps. Values bare based on figure 97 - figure 102. Positive value means that pressure in part's inner wall is higher than pressure in outer wall.*

| | **t = 0,508 s** | **t = 0,832 s** | **t = 1,150 s** | **t = 1,498 s** | **t = 1,640 s** | **t = EOF** |
|---|---|---|---|---|---|---|
| **$\Delta P_1$** | 12,3 | 16,9 | 24,8 | 21,9 | 22,2 | 13,9 |
| **$\Delta P_2$** | 12,0 | 16,1 | 21,7 | 21,8 | 21,9 | 7,6 |
| **$\Delta P_3$** | 6,4 | 10,0 | 14,7 | 18,3 | 18,1 | 2,6 |
| **$\Delta P_4$** | 1,8 | 4,5 | 8,3 | 12,9 | 15,2 | -1,6 |
| **$\Delta P_5$** | N/A | 0,8 | 2,7 | 5,7 | 8,6 | -7,5 |
| **$\Delta P_6$** | 1,3 | 2,2 | 1,7 | 1,3 | 1,2 | 0,8 |
| **$\Delta P_7$** | 0,4 | 1,6 | 1,4 | 0,9 | 0,9 | 0,4 |
| **$\Delta P_8$** | 0,05 | 1,1 | 1,4 | 1,2 | 1,2 | 0,5 |
| **$\Delta P_9$** | N/A | 0,5 | 1,5 | 1,4 | 1,7 | 0,6 |
| **$\Delta P_{10}$** | N/A | N/A | 0,4 | 1,0 | 1,6 | 0,4 |
| **$\Delta P_{11}$** | N/A | N/A | N/A | 0,7 | 1,6 | 0,2 |
| **$\Delta P_{12}$** | N/A | N/A | N/A | 0,009 | 1,3 | -0,03 |

#### 5.2.3.2 Initial part design, 4 gating points

In order to get the plastic melt flowing better into part's outer wall to prevent high pressure differences over the tool insert, two additional gates were added (placement shown in figure 103). Otherwise, the same model is used for the study as the one presented in previous section 5.2.3.1. This design also resulted as insert failing in the molding trials. Meshing of the part consisted 34 606 surface mesh elements with 1 332 610 solid mesh elements.

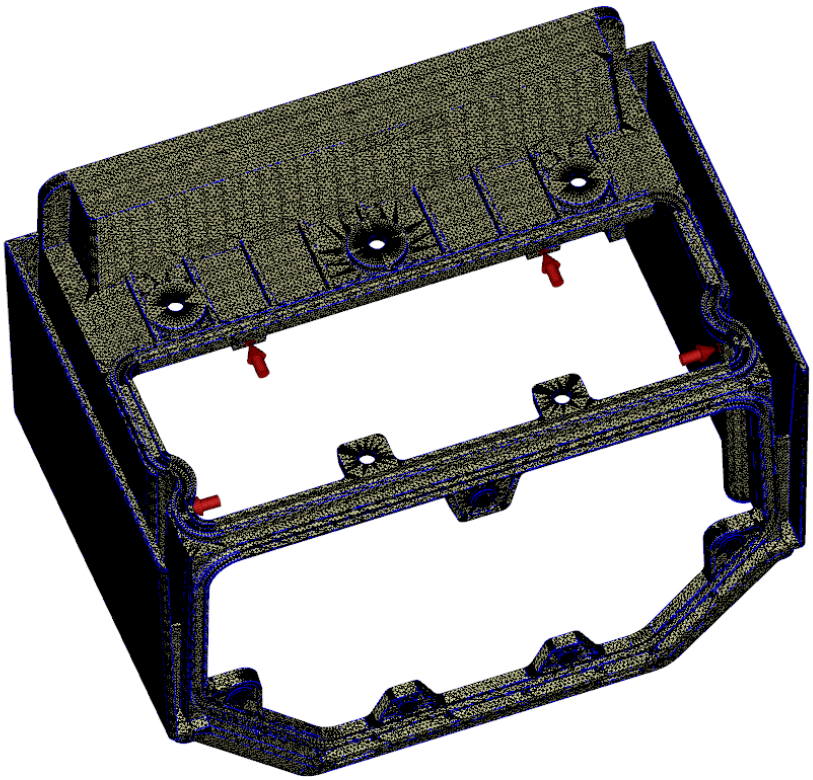

*Figure 103 Meshed part with four gating points (shown with red arrows).*

## Results

Pressure required to fill the part is 77,386 MPa (figure 104) and filling time is 1,870 s. Figure 104 shows that pressure is highest near gating points (shown as red) and lowest pressure is shown at blue. Melt front time is shown in figure 105 and it shows filling pattern of the part. As expected, areas near gating points are being filled first and the outer wall is noticed to be filled last. It takes about 0,5 seconds, until plastic starts to flow on the outer wall through the first higher ribs. Approximately at the same time, plastic starts to flow on outer wall from the leftmost corner due to the two added gating points. Melt flow in the outer wall seem to be moving behind the flow in the inner wall and last areas to be filled are on the outer wall. This melt pattern will most likely show as high pressure differences in the insert base area.

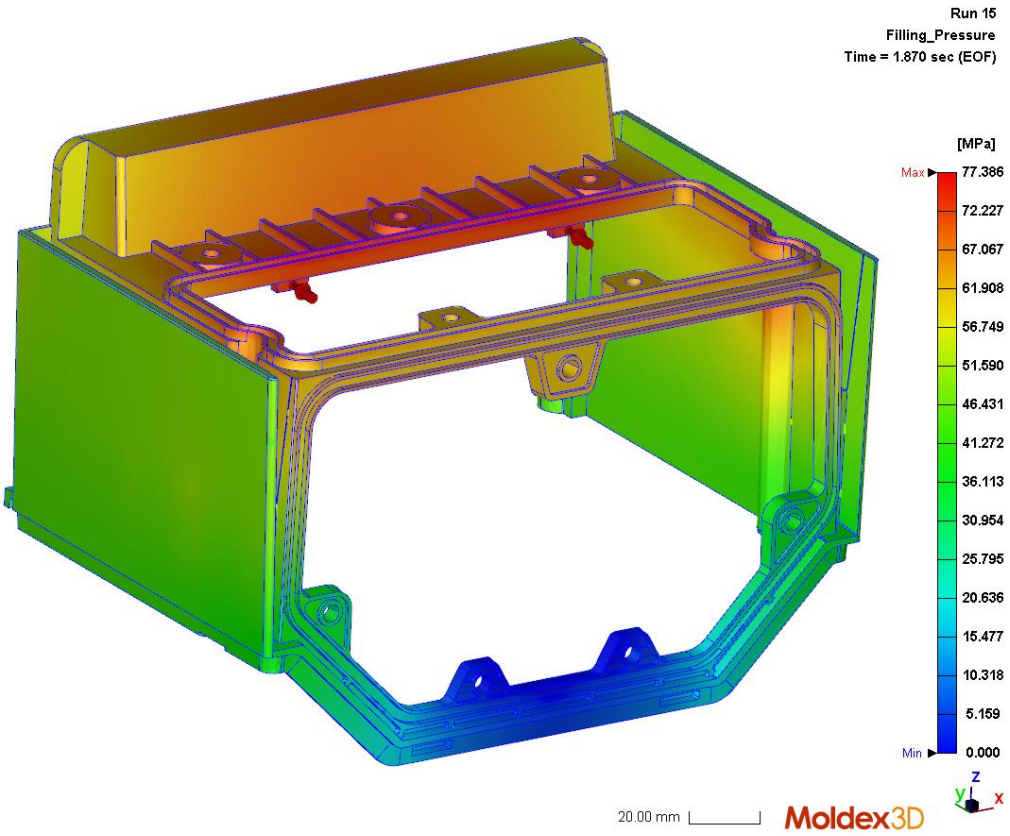


*Figure 104 Filling pressure is approximately 77 MPa and filling time is 1,870 s.*

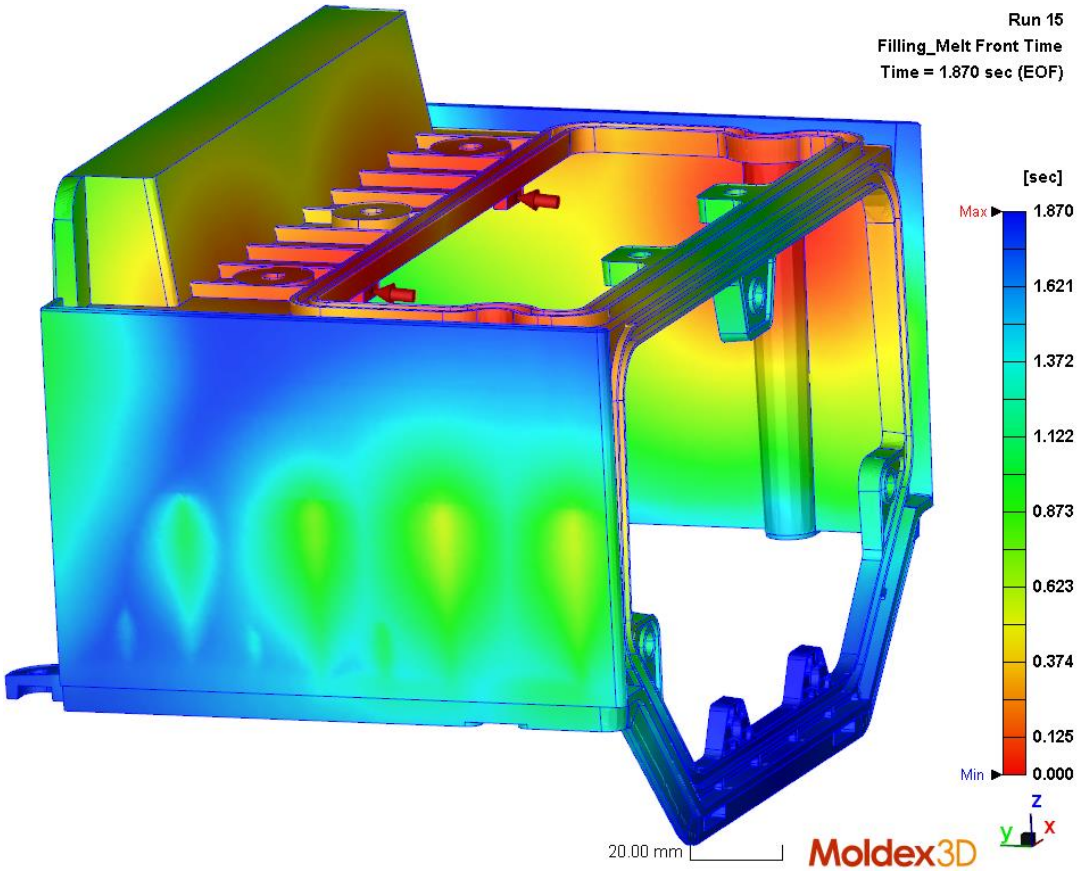


*Figure 105 Melt front time.*

To study more the flow behavior and pressure differences, 12 probe pairs are attached on locations shown in figure 106. Only half of the part is studied as the part is symmetrical. Probes 1 to 5 are on the tool insert base area and probes 6 to 12 are attached to further away from the tool insert's fixed surface. As these probes are further from the fixed point, smaller load will bend the insert easier. Furthermore, insert tip area has multiple cuts due to ribs in the part which weakens the insert tip. Probes named "IN" are attached on part's inner wall which is in contact with tool insert's inner surface. "OUT" named probes are on the opposite side on the outer wall of the part, and on its outer surface. "OUT" probes are attached on the outer surface as the pressure difference through the wall can be assumed to be negligible.

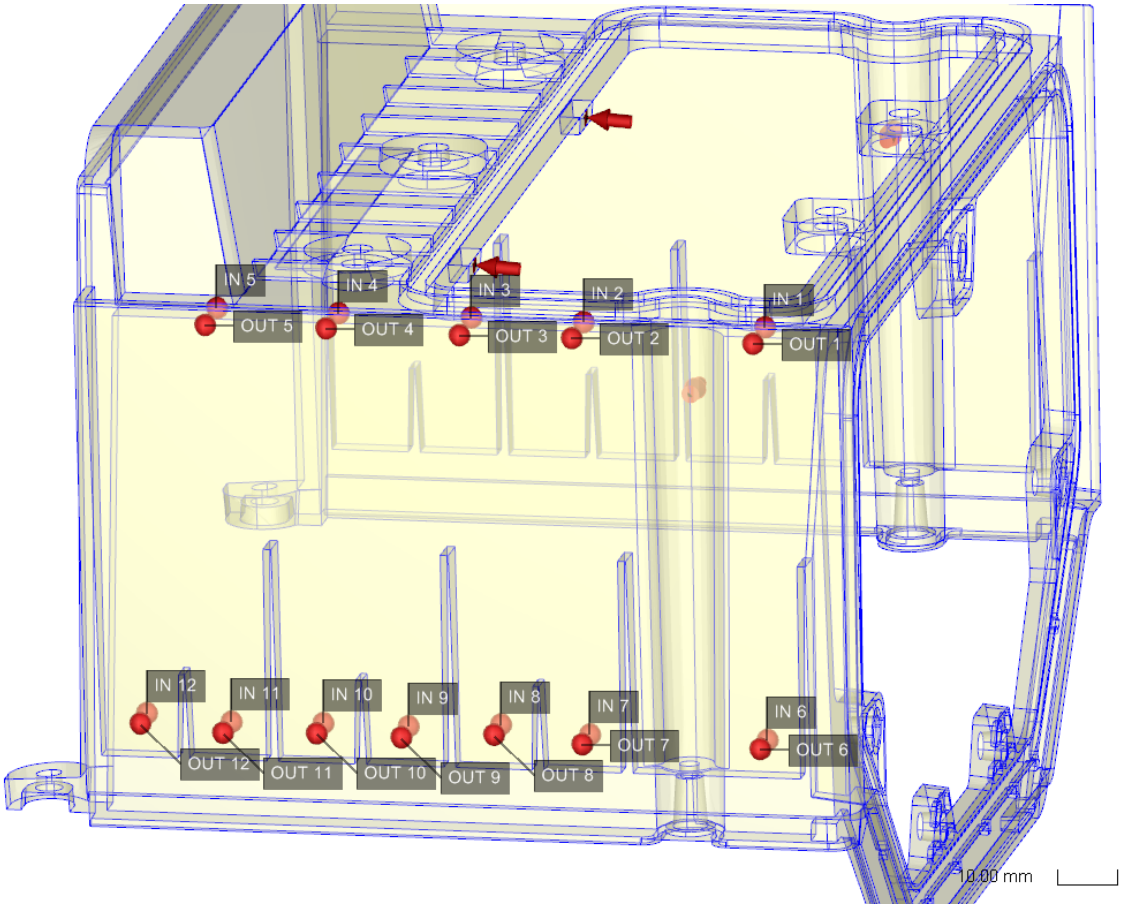


*Figure 106 Probe locations.*

After 0,494 s of filling (figure 107), melt has reached on probes IN 1 - IN 5 in the inner wall. Furthermore, melt has reached first ribs and is starting to flow on the outer wall. Pressure differences on probes 1-5 are from 0,3 MPa to 5,7 MPa depending on how close gating points the probes are. At 0,848 s (figure 108), approximately half of the inner wall is filled and melt front has reached on probe IN 6. Pressure differences of probes 1-5 have increased to 3,6 MPa - 12,8 MPa.

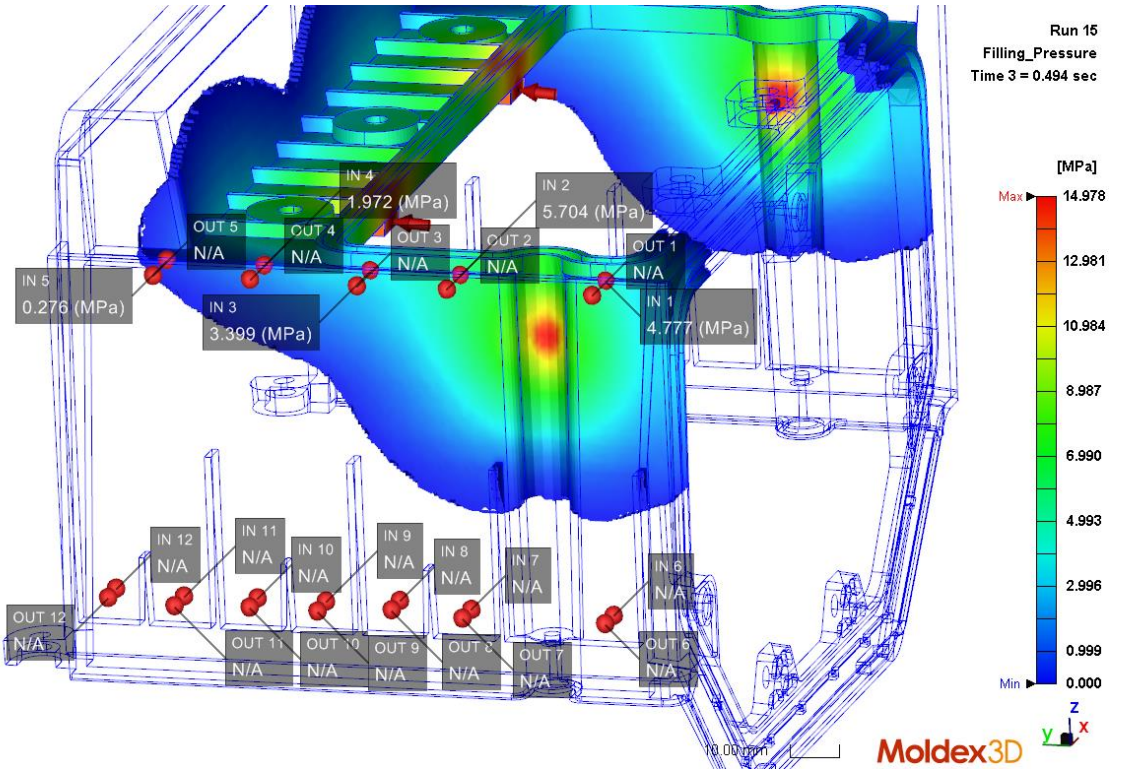


*Figure 107 Pressures on probes at 0,494 s.*

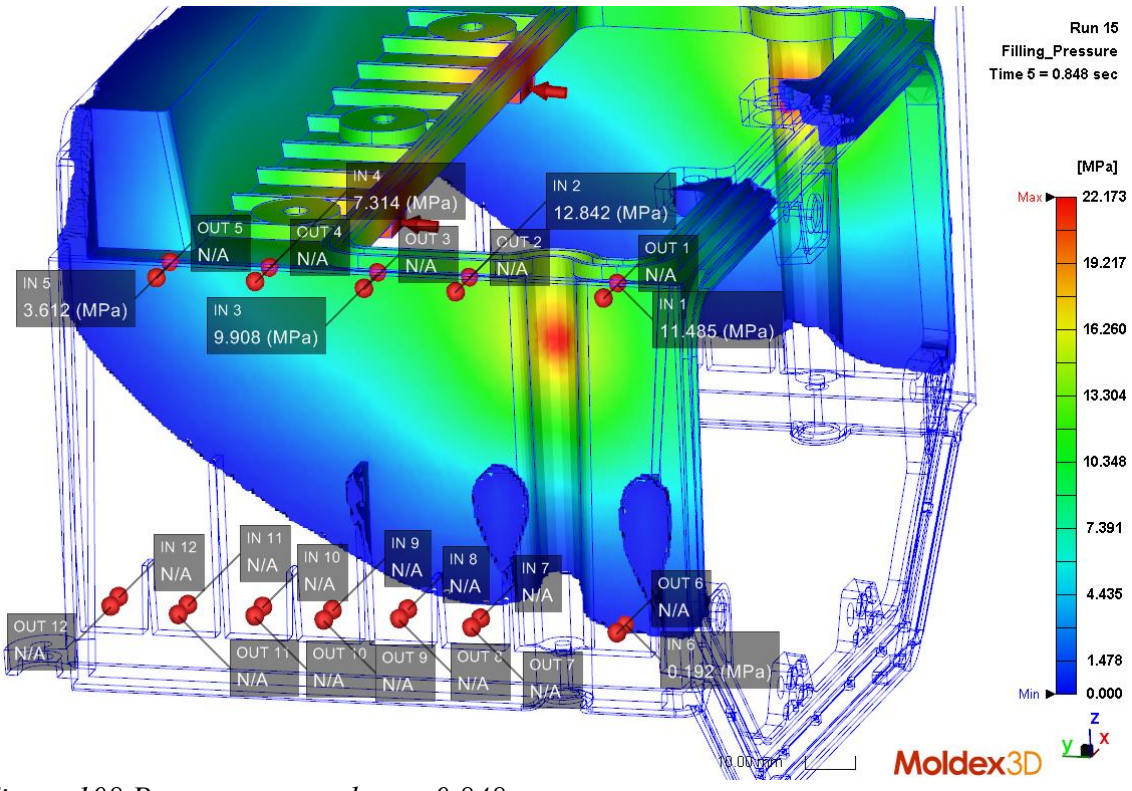


*Figure 108 Pressures on probes at 0,848 s.*

At 1,151 s, melt has started to flow on the outer wall through the first three ribs, but it hasn't yet reached any of the probes OUT 6 - OUT 12 (figure 109). Therefore, pressure differences on probes 6 - 12 are 0,06 MPa - 1,3 MPa. On the tool insert base, pressure differences have increased to 10,1 MPa - 19,4 MPa. At 1,490 s, pressure differences have increased more as the flow hasn't reached the upper part of the outer wall (figure 110).

Now the pressure differences in probes 1-5 are from 15,2 MPa to 25,4 MPa. For probes 6-11, pressure differences are from 0,1 MPa to 1,2 MPa. Melt has started to flow towards upper part of the outer wall, but it hasn't yet filled the whole inner wall or reached probes 12.

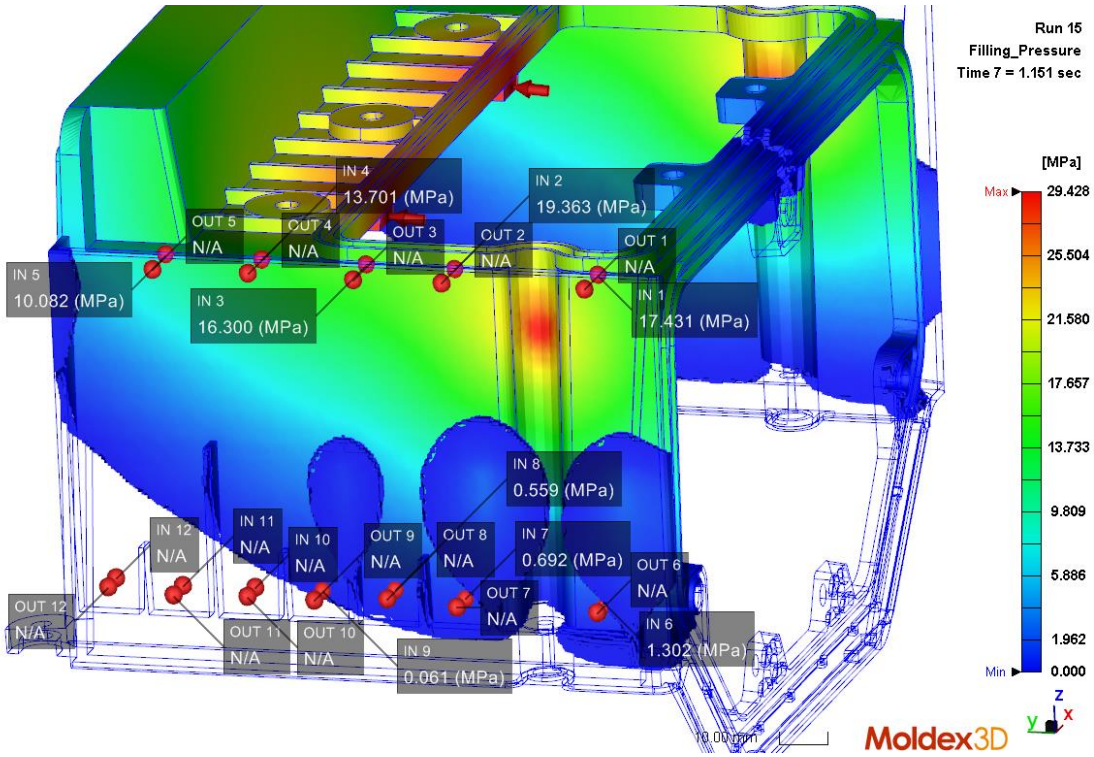


*Figure 109 Pressures on probes at 1,151 s.*

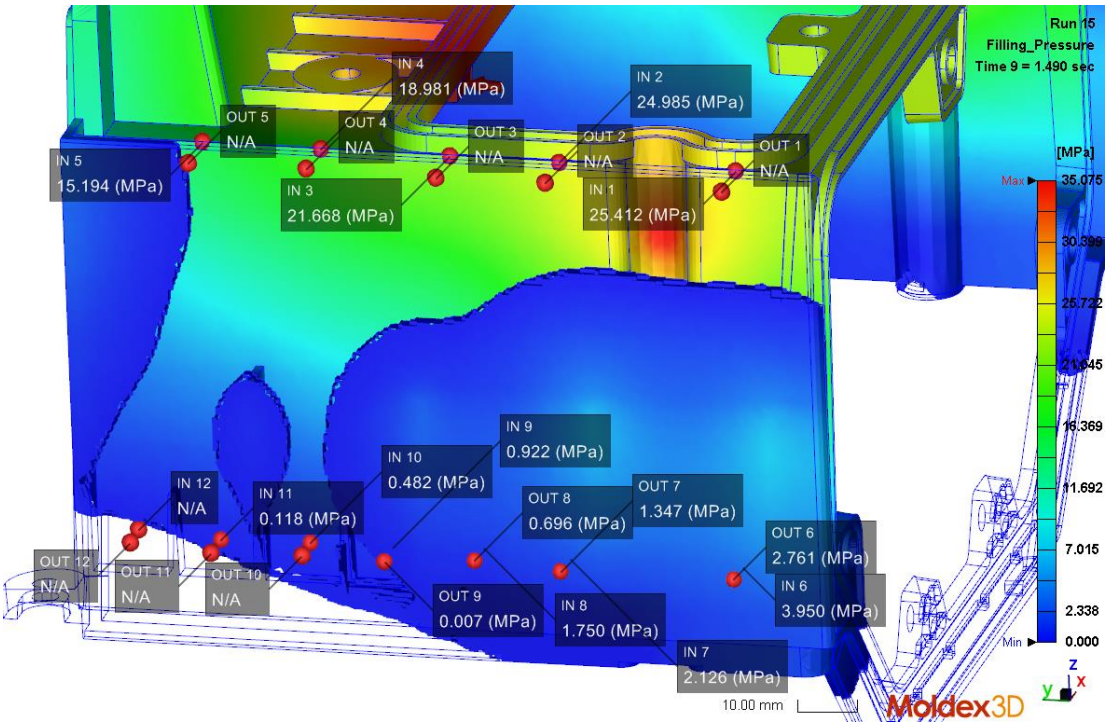


*Figure 110 Pressures on probes at 1,490 s.*

After 1,650 s, small part of the inner wall is still not filled and two melt fronts at the outer wall are starting to get closer to each other. Additionally, upper part of the outer wall is

not filled and pressure differences in tool insert's base are from 16,9 MPa to 27,9 MPa. Probes 6-12 have pressure difference from 0,6 MPa to 1,2 MPa. At 1,870 s, melt has filled the whole part and pressure differences on each location have decreased (figure 112). Pressure differences at the end of filling on probes 1-5 are from 11,6 to 17,9 MPa and on probes 6-12 from 0,2 MPa to 0,4 MPa. As the outer wall is filled from the upper part between 1,650 s and 1,870 s, almost the whole filling time there is a pressure load approximately 20 MPa concentrating on the tool insert base where the cracking occurred.

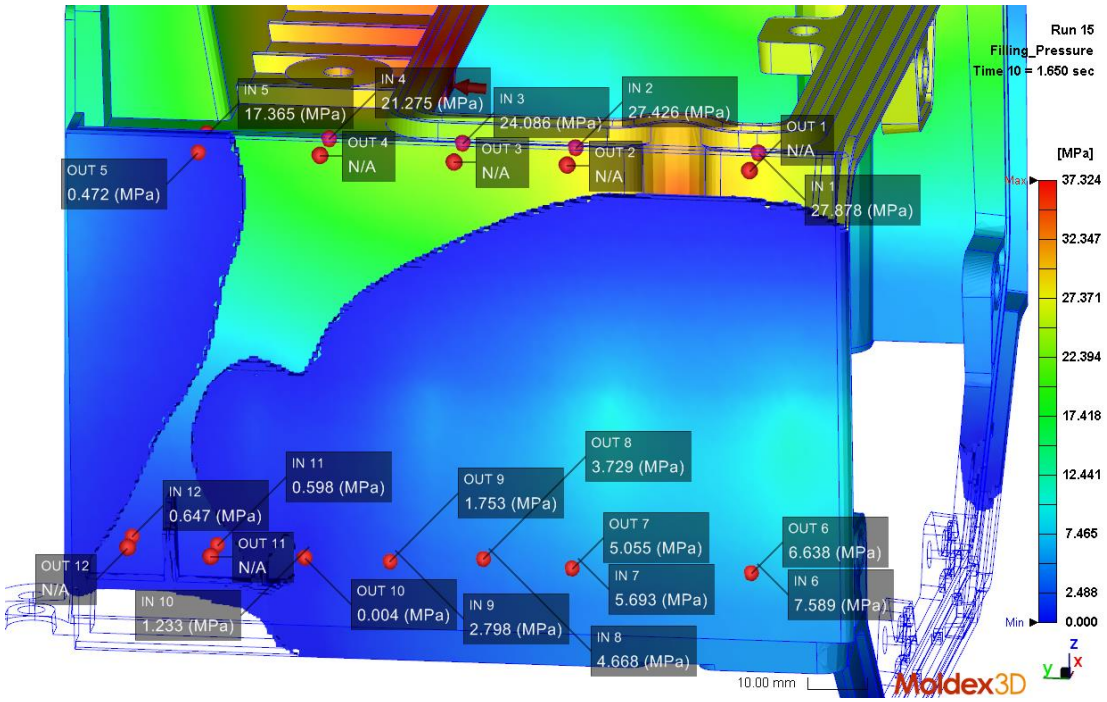


*Figure 111 Pressures on probes at 1,650 s.*


*Figure 112 Pressures on probes at end of filling.*

Pressure differences on probes 1-12 at six different time steps are collected to table 14 based on figure 107 - figure 112. Positive values in table means that pressure in the inner

wall is higher than in the outer wall. Table shows that at 1,650 s, melt front has reached at least one probe of each probe pair. Highest pressures can be found from probes 1-5 as they are nearest to the gating points and probes 6-12 have considerably smaller values. Overall, pressure differences on probes 6-12 are quite even and small which indicates that melt reaches both inner and outer wall (at the location of probes) at same time. At the end of filling, probe 6 has negative pressure difference which means that pressure in the outer wall is higher than pressure in the inner wall. Reason for this is that inner wall has been filled on that location before the outer wall has been filled. Therefore, pressure only at the outer wall has increased. Table shows that between 1,490 s and 1,650 s, pressure differences on insert base are high, above 20 MPa, which is probable cause for the insert bending and cracking.

*Table 14 Pressure differences (in MPa) at probes at six different time steps. Table is collected from figure 107 - figure 112. Positive value means that pressure in the inner wall is higher than in the outer wall. EOF refers to end of filling.*

| | **t = 0,494 s** | **t = 0,848 s** | **t = 1,151 s** | **t = 1,490 s** | **t = 1,650 s** | **t = EOF** |
|---|---|---|---|---|---|---|
| **$\Delta P_1$** | 4,8 | 11,5 | 17,4 | 25,4 | 27,9 | 16,2 |
| **$\Delta P_2$** | 5,7 | 12,8 | 19,4 | 25,0 | 27,4 | 17,9 |
| **$\Delta P_3$** | 3,4 | 9,9 | 16,3 | 21,7 | 24,1 | 16,9 |
| **$\Delta P_4$** | 2,0 | 7,3 | 13,7 | 19,0 | 21,3 | 15,2 |
| **$\Delta P_5$** | 0,3 | 3,6 | 10,0 | 15,2 | 16,9 | 11,6 |
| **$\Delta P_6$** | N/A | 0,2 | 1,3 | 1,2 | 1,0 | -0,3 |
| **$\Delta P_7$** | N/A | N/A | 0,7 | 0,8 | 0,6 | 0,3 |
| **$\Delta P_8$** | N/A | N/A | 0,6 | 1,0 | 0,9 | 0,4 |
| **$\Delta P_9$** | N/A | N/A | 0,06 | 0,9 | 1,0 | 0,2 |
| **$\Delta P_{10}$** | N/A | N/A | N/A | 0,5 | 1,2 | 0,2 |
| **$\Delta P_{11}$** | N/A | N/A | N/A | 0,1 | 0,6 | 0,2 |
| **$\Delta P_{12}$** | N/A | N/A | N/A | N/A | 0,6 | 0,3 |

#### 5.2.3.3 Modified part design, 2 gating points

Initial geometry of the part (presented in previous sections), caused the inserts to crack. Due to this, following geometry changes were made (illustrated in figure 113):

1. wall thickness of inner wall was decreased which respectively gives freedom to make the tool insert thicker
2. one additional rib added
3. thickness of the end walls increased
4. increased radius for the insert base and ribs of the part.

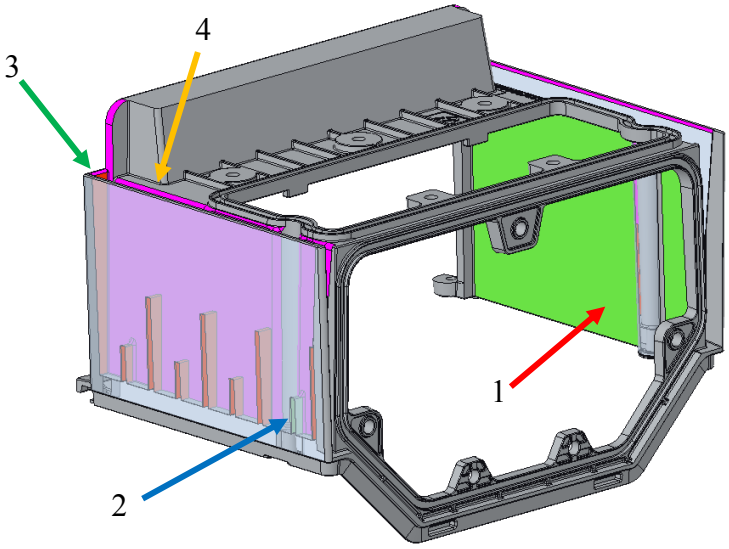


*Figure 113 Changes made to the original geometry: 1. wall thickness of inner wall decreased, 2. additional rib added, 3. thickness of the end walls increased and 4. radius added to the base of the inserts and to the ribs (not shown in the figure).*

These changes were expected to restrict the plastic flow in the inner wall and ease the flowing to the outer wall to even the pressure variation inside the part. As well, decreasing thickness of the inner wall gives possibility to make the tool insert thicker. Simulation model had rounds in the tool insert area, but other rounds were excluded from the model to simplify it. Changes described above had been made to a stp -file which was then imported to Creo to exclude most of the rounds. After this, model was again converted into a stp -file which was imported into Moldex3D, and it was noted that meshing accuracy wasn't as good as with previous models. This can result from multiple stp -file conversion of the model, or from some of the rounds left to the model. Meshing was done with level 4 and model consist of 22 412 surface mesh elements and 1 453 092 solid mesh elements. Gating points are in the same place as in the initial design, (in section 5.2.3.1). Figure 114 shows the meshed model with the gating points.

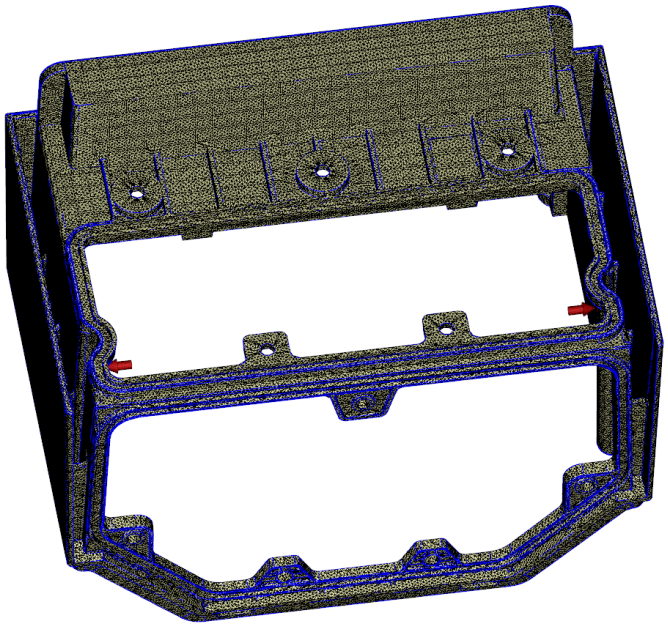

*Figure 114 Meshed model with gating points (red arrows).*

## Results

Pressure required to fill the part is 50,313 MPa and filling time 1,965 s (figure 115). Highest pressures are found near the gating points and lowest pressures are on the middle of the part, as that area fills last. Melt front time is shown in figure 116 which illustrates how the melt flows inside the part. Inner wall fills before outer wall, which will most likely generate high pressure differences over the tool insert at the base area. Melt starts to flow on the outer wall after 0,2 seconds through the higher ribs, but it takes about 1 second for the melt to reach on top of the outer wall. One of the last areas to be filled is seen at the leftmost part of the outer wall.

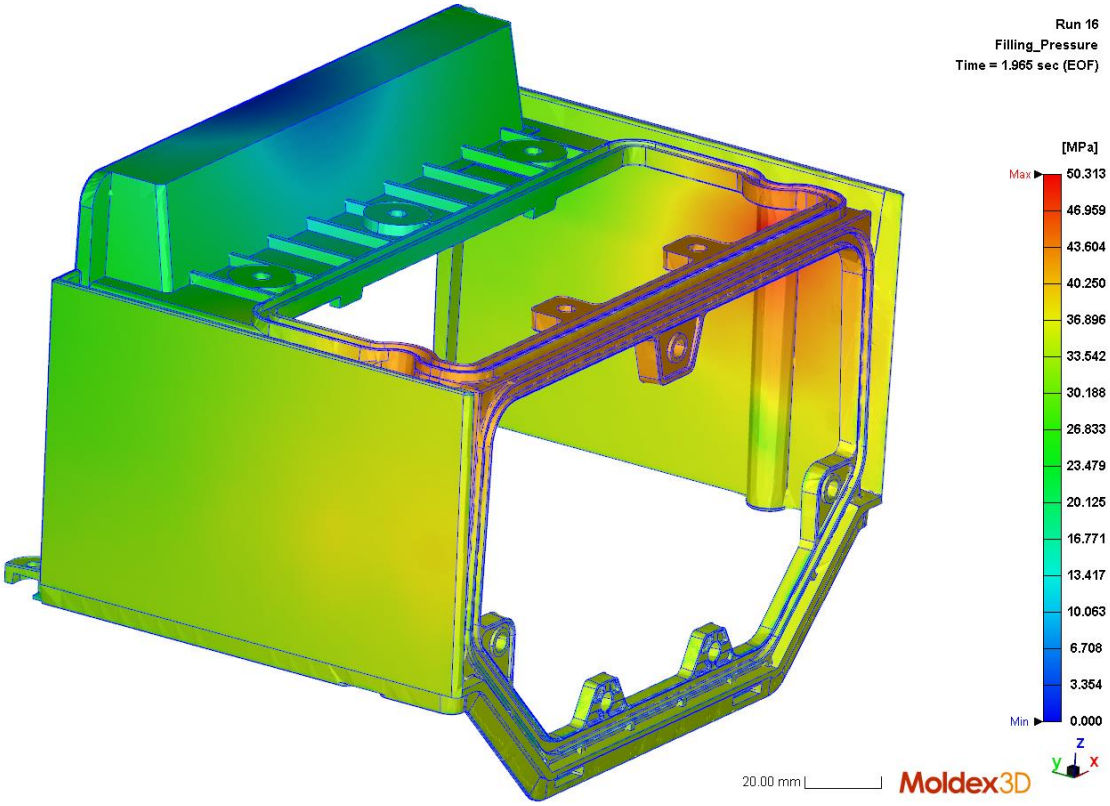


*Figure 115 Filling pressure is 50 MPa and filling time 1,965 s.*

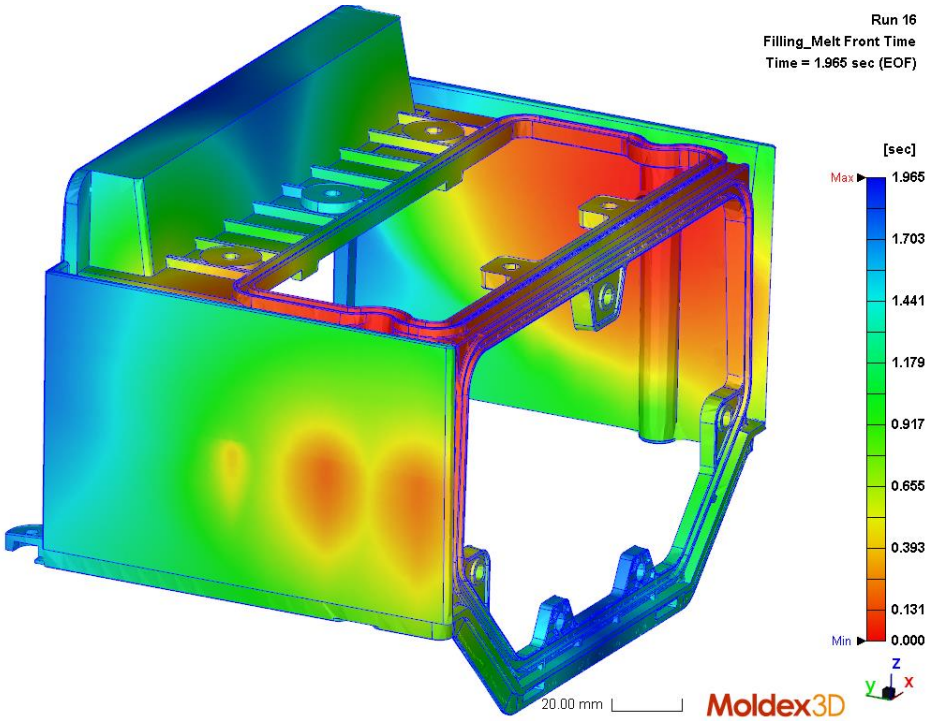


*Figure 116 Melt front time.*

To study the pressure differences during filling, 12 probe pairs (shown in figure 117) are attached to the part to see the pressure variation. Only half of the part is studied as the part is symmetrical. Probes 1 to 5 are attached on the tool insert base area and probes 6 to 12 further away from the tool insert's fixed surface. As these probes are further from the fixed point, smaller load will bend the insert easier. Furthermore, insert tip area has multiple cuts due to ribs in the part which weakens the insert tip. Probes named "IN" are attached on part's inner wall which is in contact with tool insert's inner surface. "OUT" named probes are on the opposite side on the outer wall of the part, and on its outer surface. "OUT" probes are attached on the outer surface as the pressure difference through the wall can be assumed to be negligible.

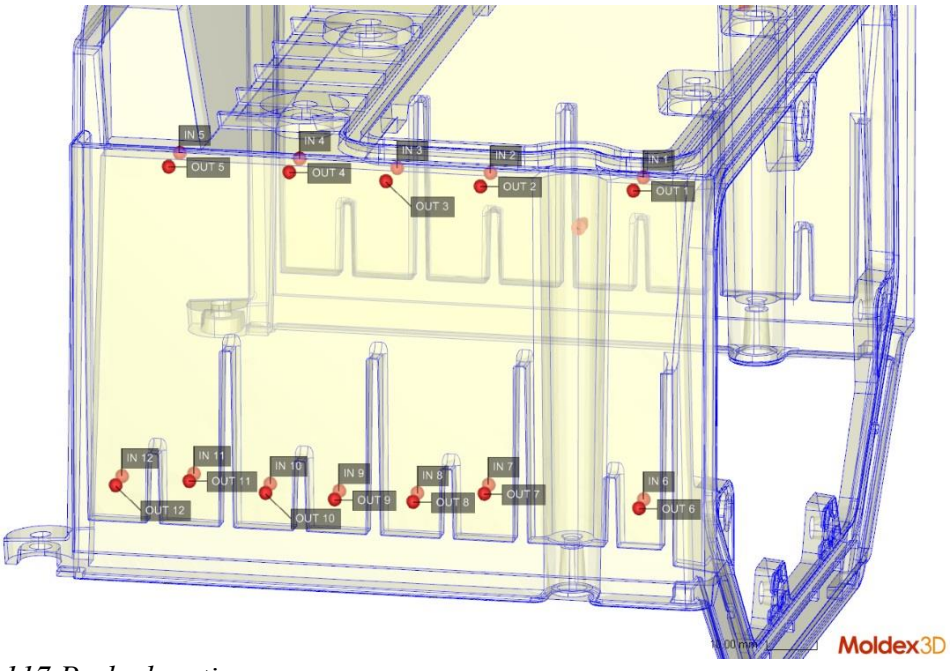


*Figure 117 Probe locations.*

During the first 0,482 s (figure 118), melt has travelled almost to the bottom of the inner wall and started to flow through the ribs on the outer wall. However, melt hasn't yet reached on the gating area in the outer wall, which generates pressure difference of 13,4 MPa at worst on the insert base. After 0,809 s (figure 119), melt flow on the outer wall has become more uniform and flow fronts on both inner and outer wall are moving on similar phase in horizontal direction. Thus, pressure differences on probes 6-8 are small, approximately 0,001-0,2 MPa. On the contrary, on vertical direction flow in the outer wall is behind and pressure difference near the insert base has increased to 21,7 MPa.

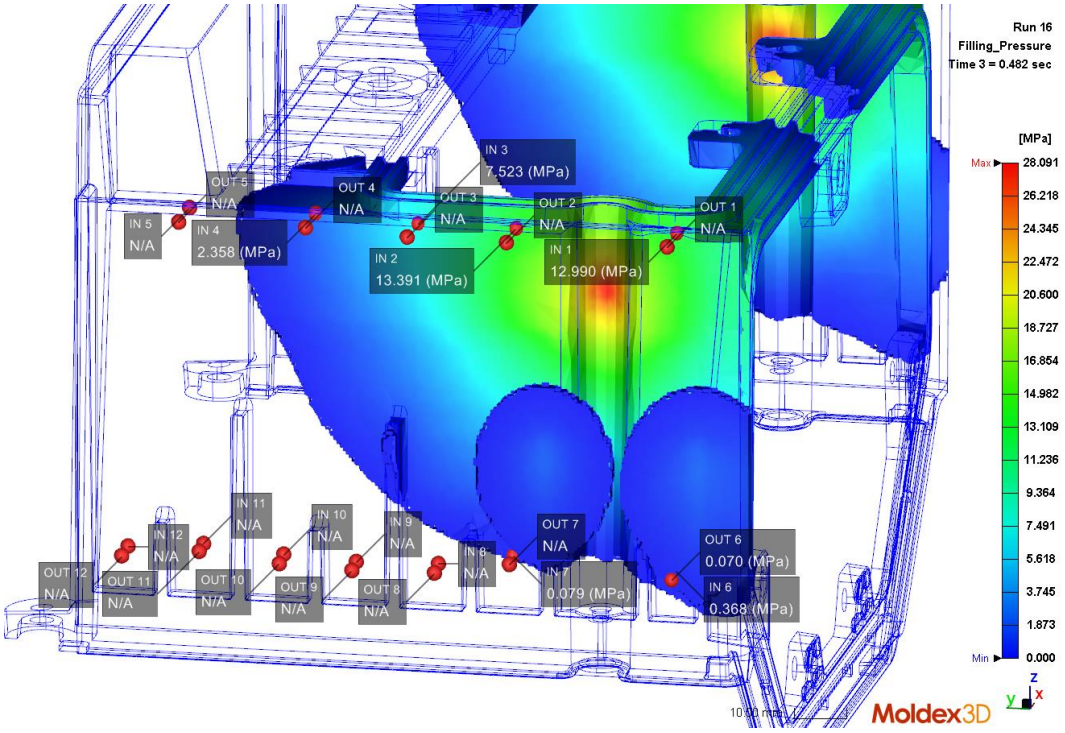


*Figure 118 Pressures on probes at 0,482 s.*

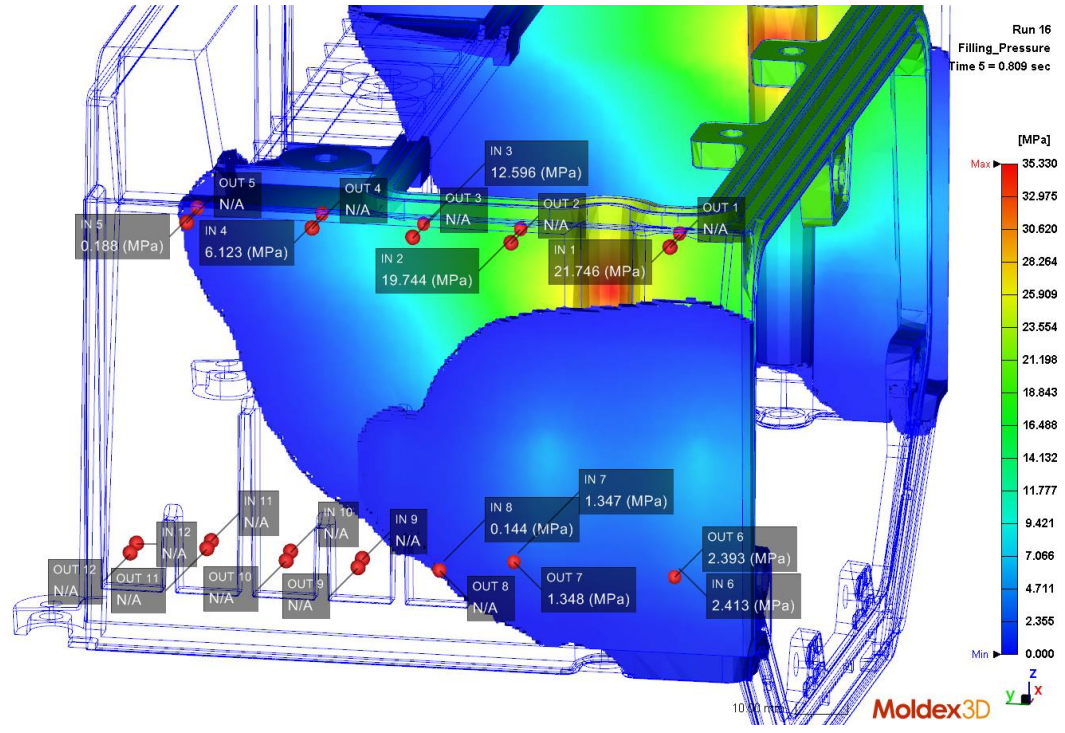


*Figure 119 Pressures on probes at 0,809 s.*

At 1,137 s, flow on the outer wall has just reached the probes OUT 1 and OUT 2 but pressure difference near insert base is still 22,4 MPa, at highest (see figure 120). On the area of probes 6-9, melt is flowing on similar phase as the pressure differences are only 0,004-0,2 MPa. Noticeable is, that pressure on the outer wall has increased over pressure on the inner wall, which indicates that inner wall has already been filled on those locations. After 1,436 s, only the leftmost part is yet not filled (figure 121). Pressure differences on probes 1-3 have slightly decreased as the outer wall has started to fill more. For probes 4 and 5, differences have increased as the outer wall isn't yet filled. Pressure differences on probes 6-11 are 0,001-0,4 MPa, thus like before.

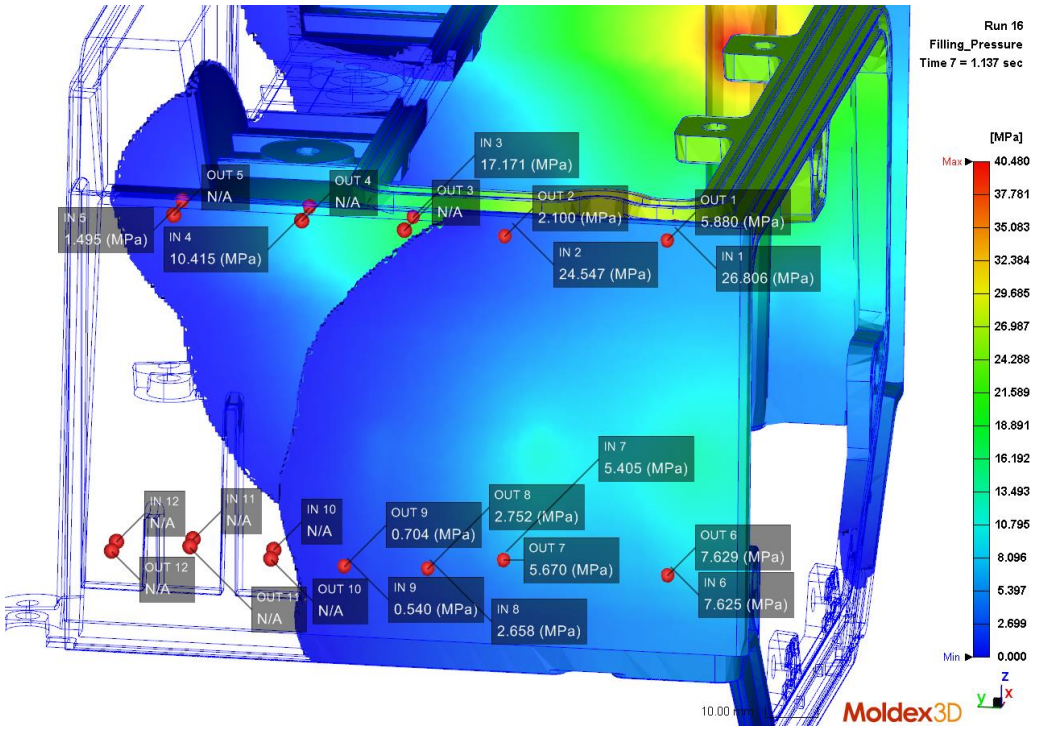


*Figure 120 Pressures on probes at 1,137 s.*

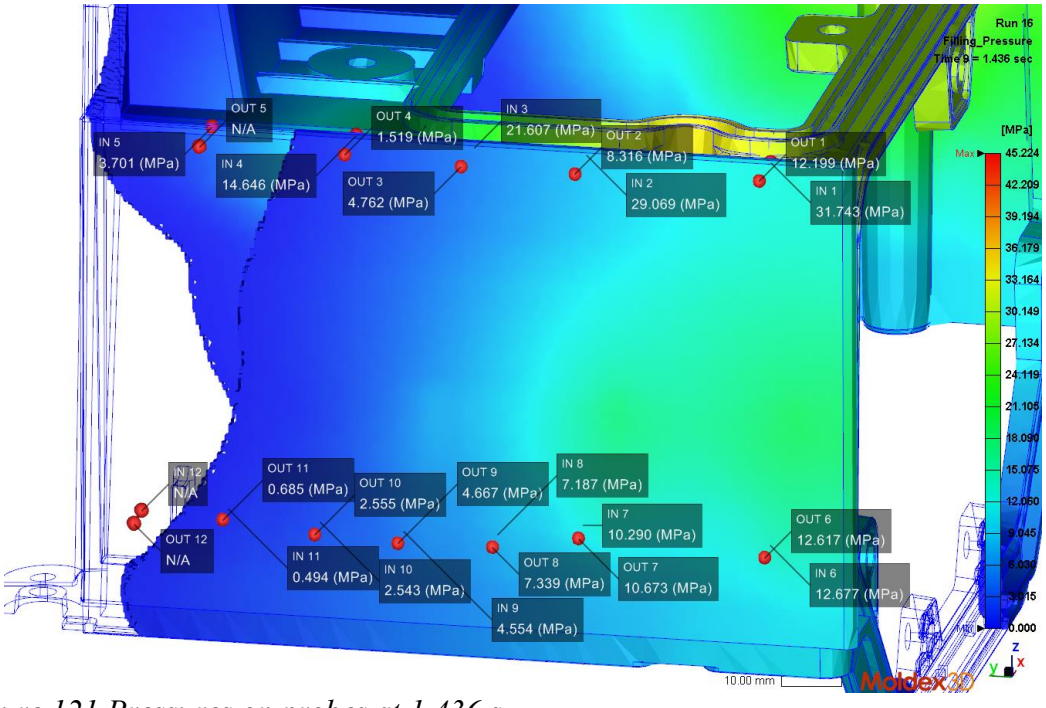


*Figure 121 Pressures on probes at 1,436 s.*

At 1,610 s, small area on both inner and outer wall is still not filled (figure 122). Pressure differences on probes 1-5 are between 5,7 MPa and 20,5 MPa. For probes 6-12 corresponding values are 0,001-0,4 MPa. At the end of filling (figure 123), pressure differences on probes 1-5 have decreased to 0,7-7,0 MPa as both walls are filled. For probes 6-12 pressure differences are 0,01-0,09 MPa.

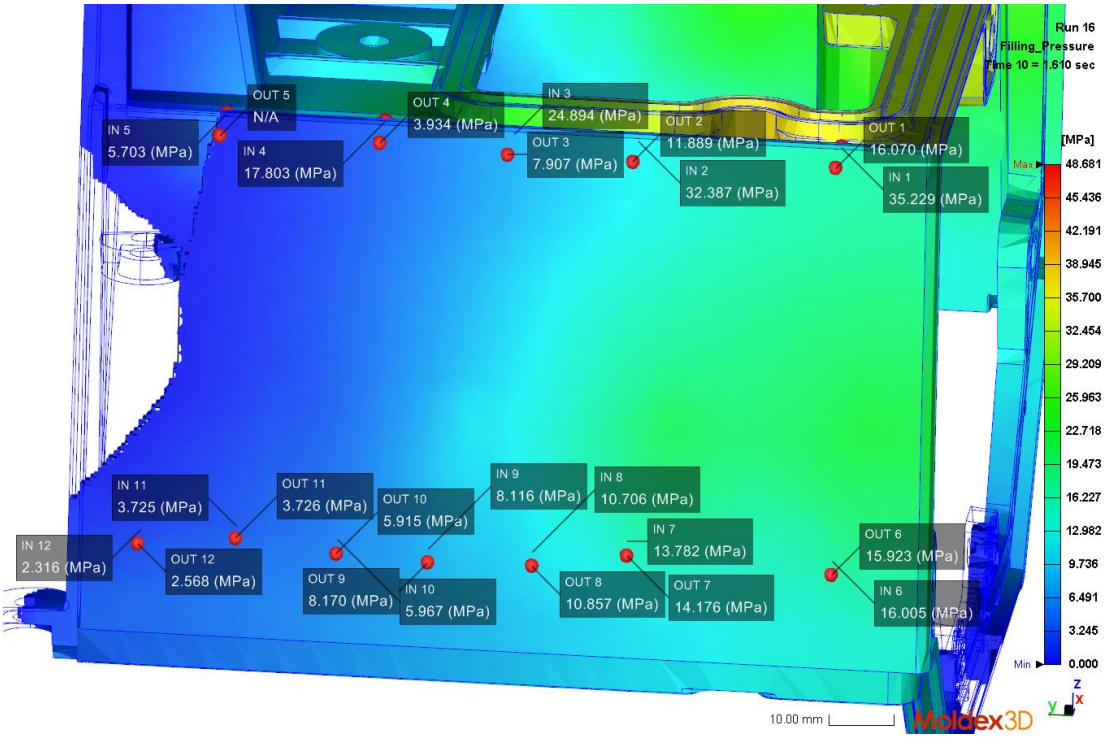


*Figure 122 Pressures on probes at 1,610 s.*

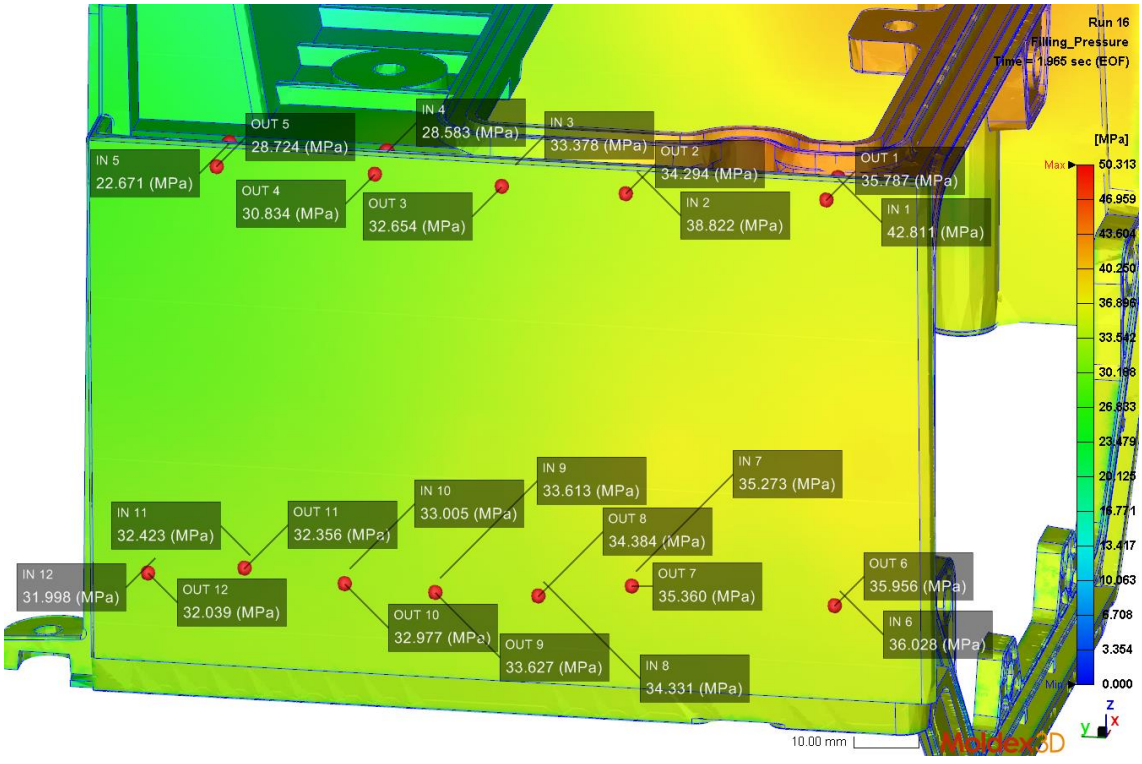


*Figure 123 Pressures on probes at end of filling.*

Pressure differences during filling are collected to table 15 based on figure 118 - figure 123. Negative values mean that pressure in the outer wall is higher than in the inner wall. Table shows that between 0,809-1,610 s, pressure difference over the tool insert in the base area is slightly below or above 20 MPa. Based on simulation results of the two initial designs this can lead to insert cracking. On the contrary, pressure differences on probes 6-12 are small throughout the filling, which indicates that melt is flowing on both inner and outer wall at the same phase in the insert tip area.

*Table 15 Pressure differences (in MPa) on probes 1-12 at six different time steps. Table is collected base on figure 118 - figure 123. Positive values mean that pressure in the inner wall is higher than pressure in outer wall. EOF refers to end of filling.*

| | **t = 0,482 s** | **t = 0,809 s** | **t = 1,137 s** | **t = 1,436 s** | **t = 1,610 s** | **t = EOF** |
|---|---|---|---|---|---|---|
| **$\Delta P_1$** | 13,0 | 21,7 | 20,9 | 19,5 | 19,2 | 7,0 |
| **$\Delta P_2$** | 13,4 | 19,7 | 22,4 | 20,8 | 20,5 | 4,5 |
| **$\Delta P_3$** | 7,5 | 12,6 | 17,2 | 16,8 | 17,0 | 0,7 |
| **$\Delta P_4$** | 2,4 | 6,1 | 10,4 | 13,1 | 13,9 | -2,3 |
| **$\Delta P_5$** | N/A | 0,2 | 1,5 | 3,7 | 5,7 | -6,1 |
| **$\Delta P_6$** | 0,3 | 0,02 | -0,004 | 0,06 | 0,08 | 0,07 |
| **$\Delta P_7$** | 0,08 | -0,001 | -0,3 | -0,4 | -0,4 | -0,09 |
| **$\Delta P_8$** | N/A | 0,1 | -0,09 | -0,2 | -0,2 | -0,05 |
| **$\Delta P_9$** | N/A | N/A | -0,2 | -0,1 | -0,05 | -0,01 |
| **$\Delta P_{10}$** | N/A | N/A | N/A | -0,01 | 0,05 | 0,03 |
| **$\Delta P_{11}$** | N/A | N/A | N/A | -0,2 | -0,001 | 0,07 |
| **$\Delta P_{12}$** | N/A | N/A | N/A | N/A | -0,3 | -0,04 |

### 5.2.3.4 Modified part design, 4 gating points

A comparative study with four gating points is made for the model presented in section 5.2.3.3. The exact same meshed model was used but with two additional gating points (see figure 124). These gating points are in the same location as the initial design in section 5.2.3.2 presented.

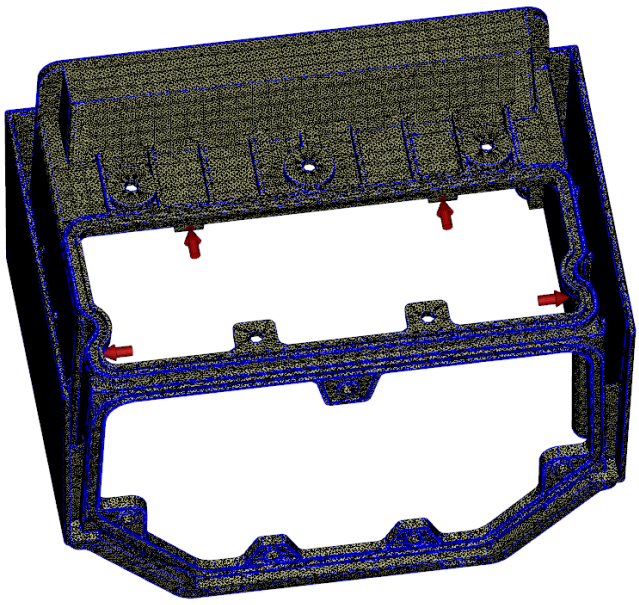

*Figure 124 Meshed model with four gating points in the initial locations.*

## Results

With four gating points, filling pressure required to fill the part is 80,287 MPa and filling time 1,815 s. Figure 125 shows pressure distribution in the part at the end of filling. Outer and inner wall seem to have quite even pressure distribution at the end of filling. In figure 126, melt front time is shown. This shows that melt flows first on the inner wall until approximately at 0,5 s, melt starts to flow on the outer wall through the higher ribs. Also, another melt front from the two gating points in y-direction reaches the outer wall at 0,9 s. Overall, melt flow seems to be uneven and the upper part of the outer wall is one of last places to fill. This will cause high pressure differences on the tool insert base, as the filling pressure is higher than with two gating points and can result as insert cracking.

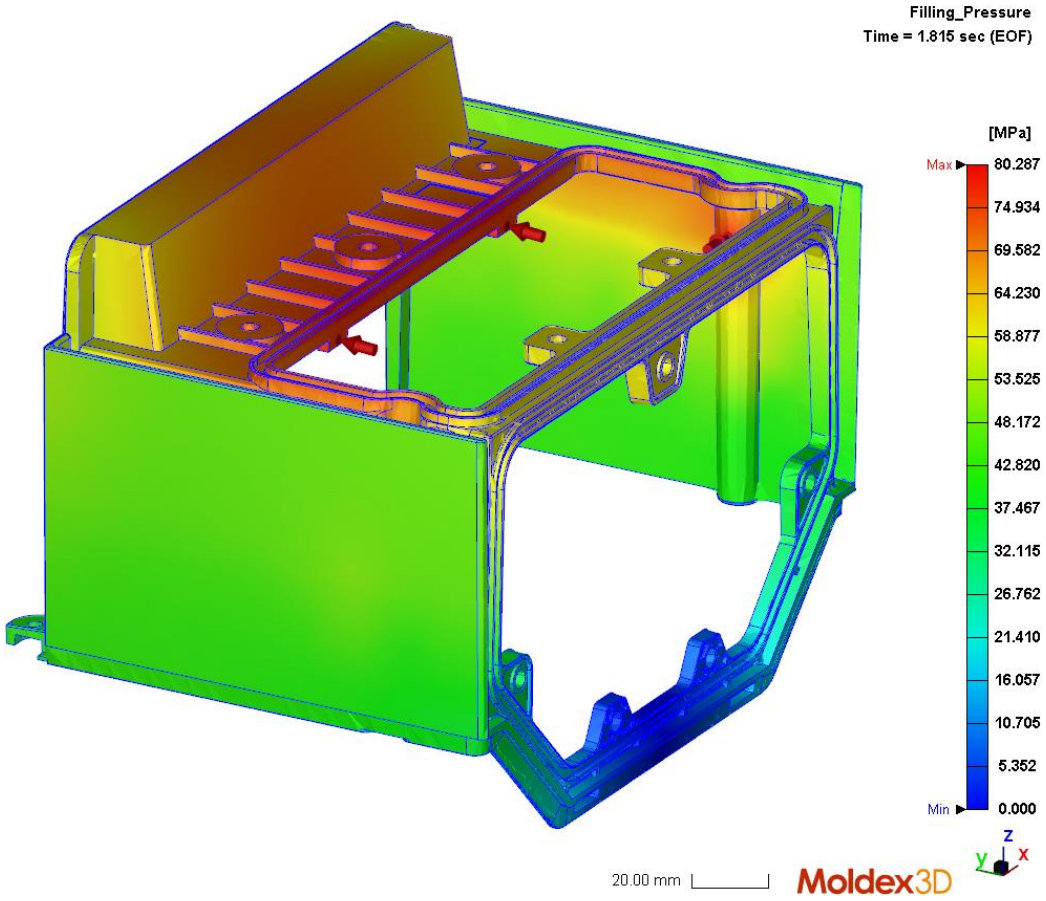


*Figure 125 Filling pressure required to fill the part is 80 MPa.*

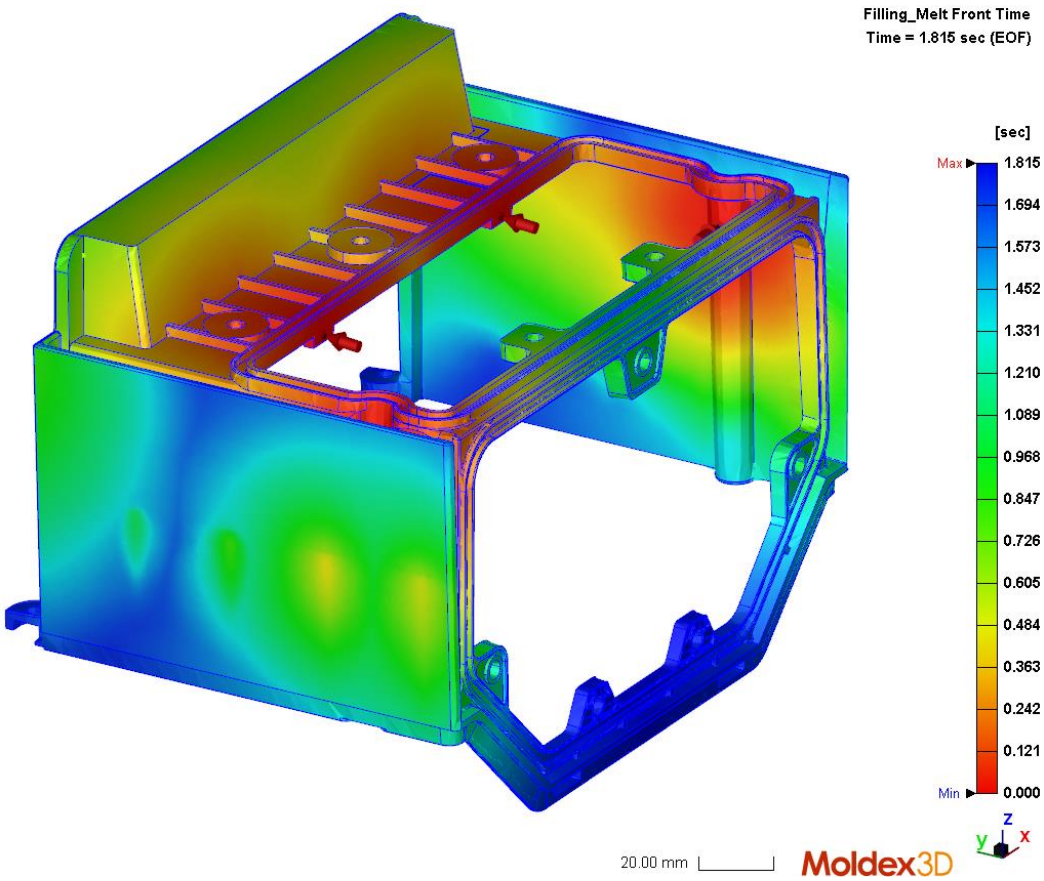


*Figure 126 Melt front time.*

To study more the pressure differences concentrating on the tool insert, 12 probe pairs, shown in figure 127, are attached to the part. Only half of the part is studied as the part is symmetrical. Probes 1 to 5 are attached on the tool insert base area and probes 6 to 12 further away from the tool insert's fixed surface. As these probes are further from the fixed point, smaller load will bend the insert easier. Furthermore, insert tip area has multiple cuts due to ribs in the part which weakens the insert tip. Probes named "IN" are attached on part's inner wall which is in contact with tool insert's inner surface. "OUT" named probes are on the opposite side on the outer wall of the part, and on its outer surface. "OUT" probes are attached on the outer surface as the pressure difference through the wall can be assumed to be negligible.

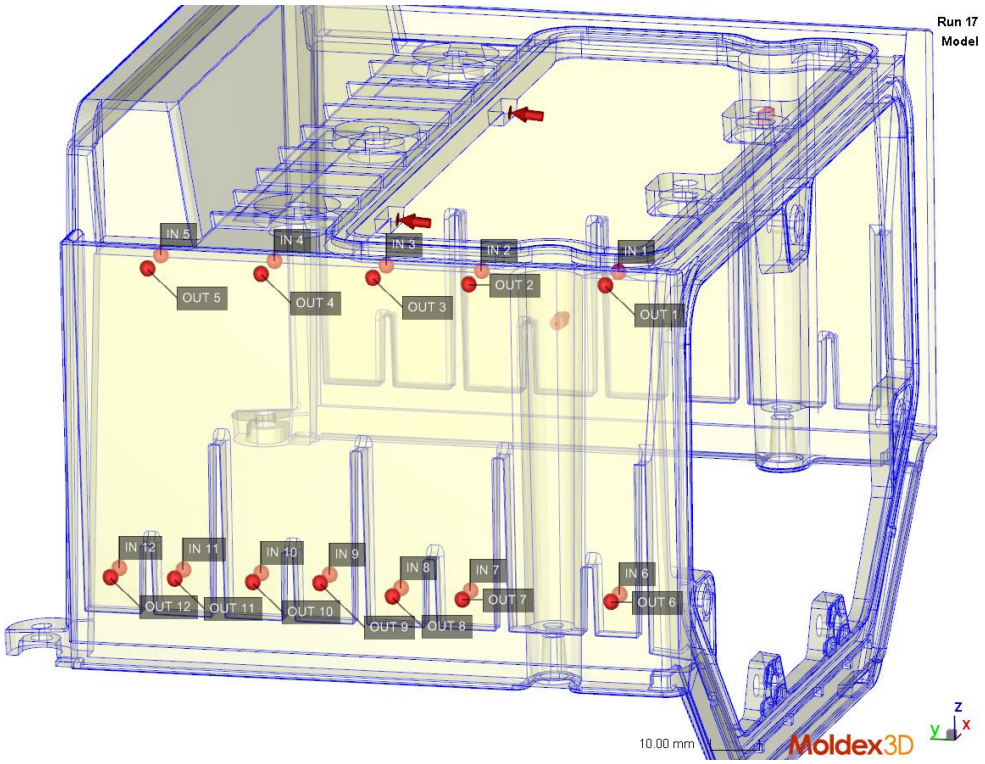


*Figure 127 Probe locations.*

During the first 0,484 seconds of filling (figure 128), melt has started to flow in the inner wall and has just reached the high ribs. At 0,807 s, melt has flown on the outer surface through two of the ribs (figure 129). At 0,484 s, pressure difference in the insert base is 8,2 MPa at maximum (in probe 2) when at 0,807 s this pressure difference has increased to 16,3 MPa.

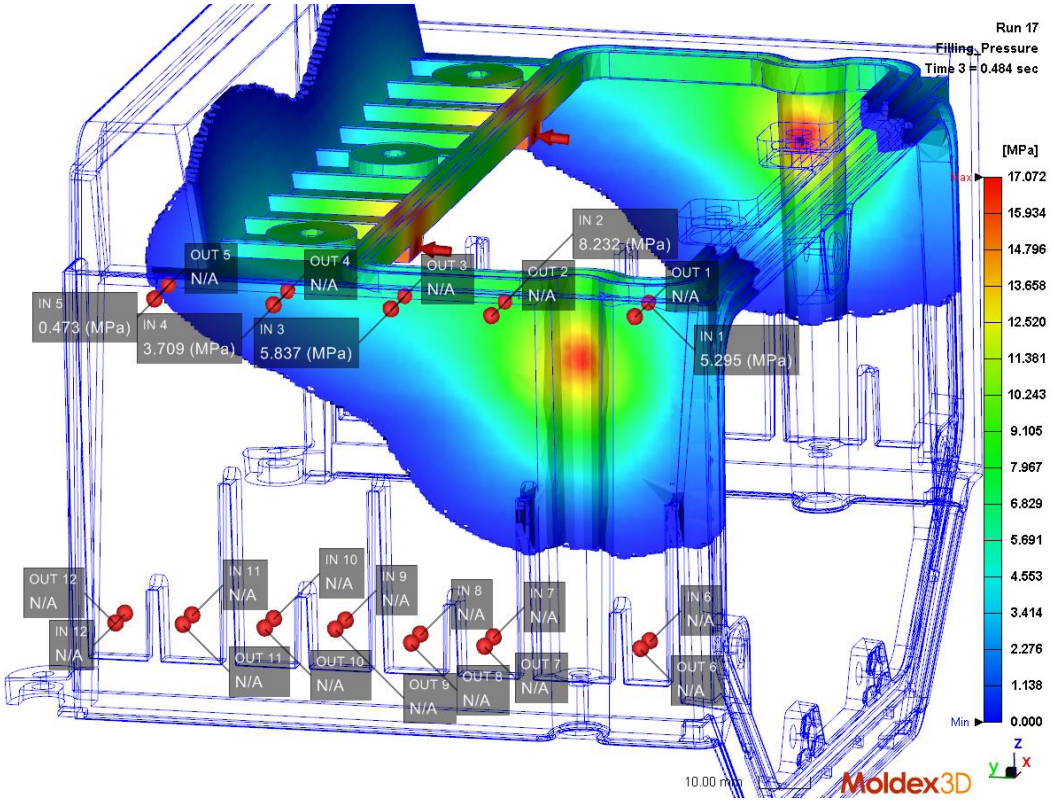


*Figure 128 Pressures on probes at 0,484 s.*

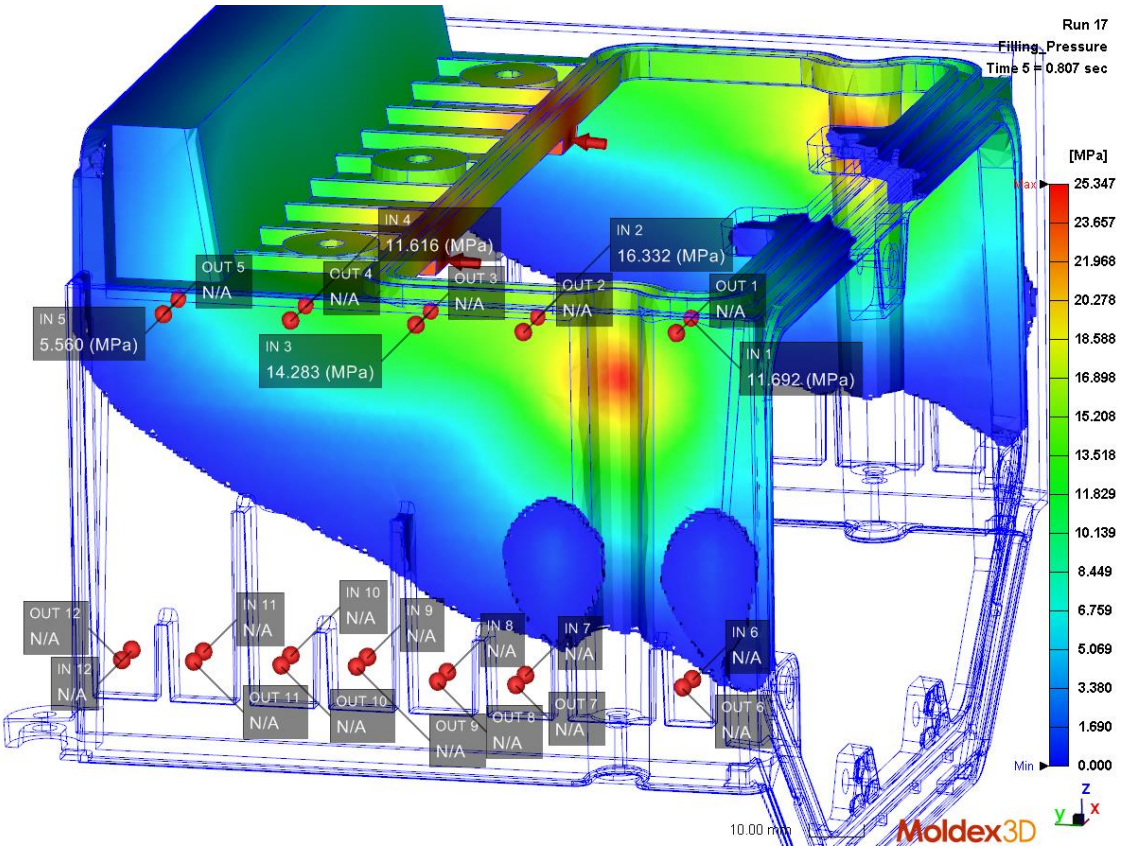


*Figure 129 Pressures on probes at 0,807 s.*

At 1,123 s (figure 130), maximum pressure difference at the insert base has increased to 31,6 MPa (in probe 2) and probes 1, 3, 4 and 5 have also high pressure differences, from 16,4 MPa to 29,2 MPa. Another melt front from gating points in y-direction has also reached the outer wall. Pressure differences at probes 6 and 7 are small, only 0,3 MPa and 0,02 MPa, which indicates that flows in the inner and outer wall are moving on same phase at the tip of the insert. Figure 131 shows melt front and pressures on probes at 1,458 s. Melt has spread more on the outer wall but hasn't yet reached the upper part, and pressure differences on area of probes 1-5 are still from 16,1 MPa to 30,8 MPa. On the contrary, pressure differences of probes 6-8 are small, approximately 0,2 MPa.

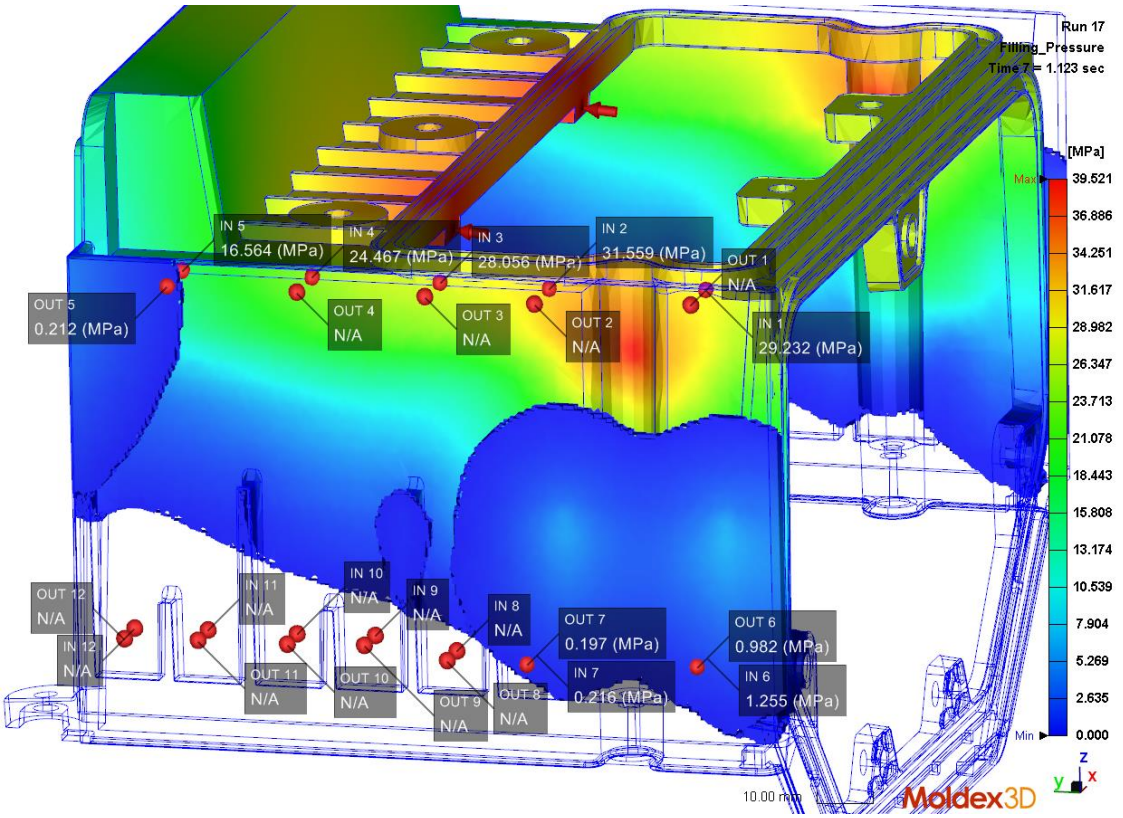


*Figure 130 Pressures on probes at 1,123 s.*

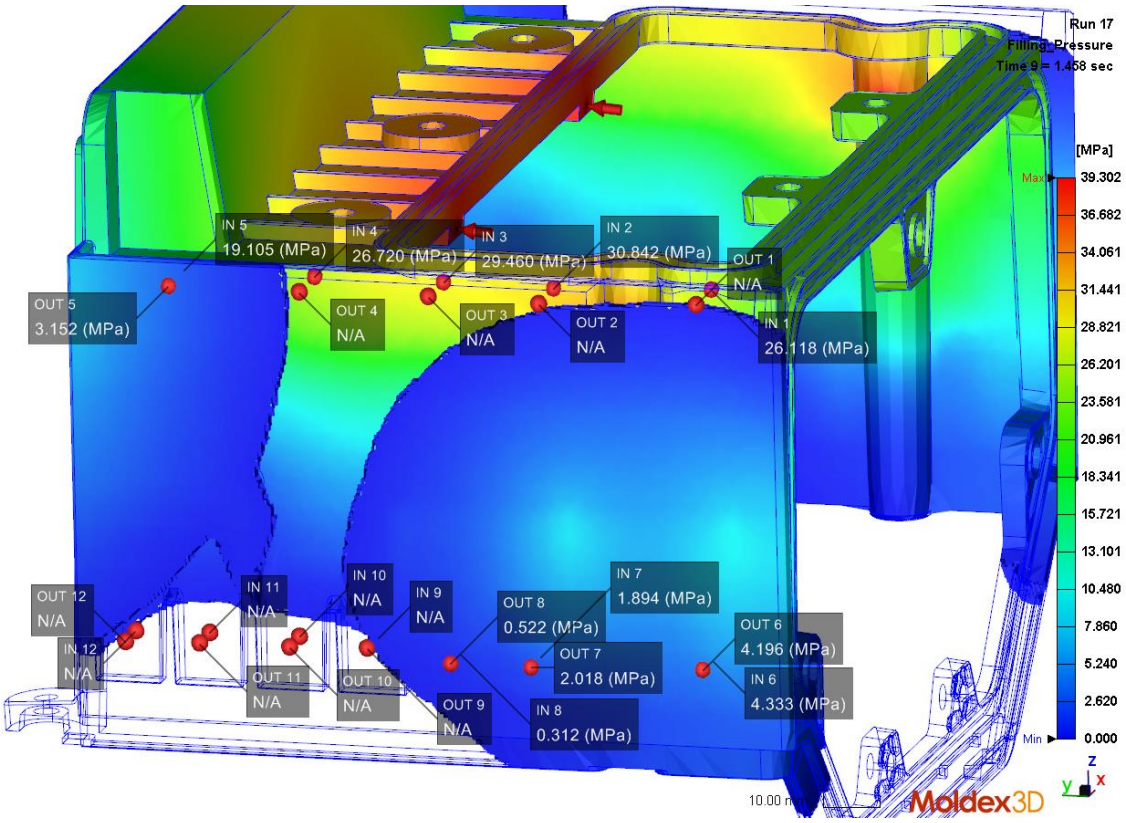


*Figure 131 Pressures on probes at 1,458 s.*

Figure 132 shows that the two melt fronts on outer wall are starting to reach each other at 1,592 s. As well, melt has started to fill the upper part of the outer wall but pressure differences there are still high, from 16,8 MPa to 32,4 MPa. For probes 6-12, pressure

differences haven't much changed but only probes 10 and 11 are still not filled. When the part is filled (figure 133), pressure differences at probes 1-5 have decreased to 11,5-21,8 MPa. For probes 6-12 corresponding values are 0,1-0,5 MPa.

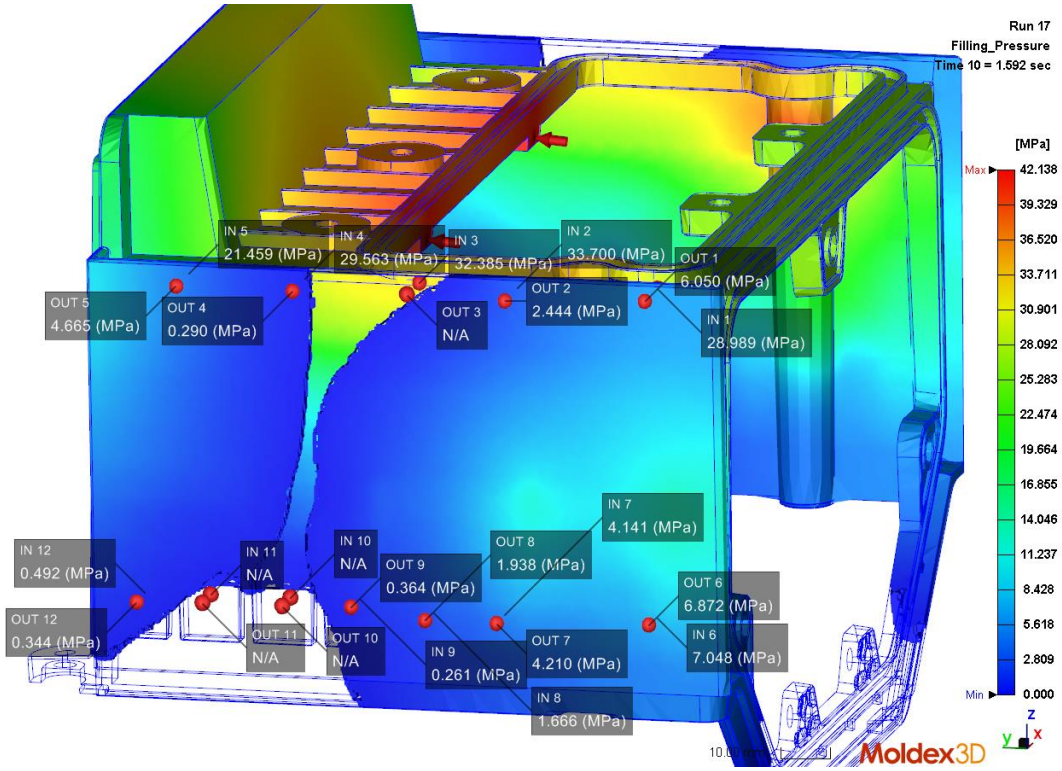


*Figure 132 Pressures on probes at 1,592 s.*

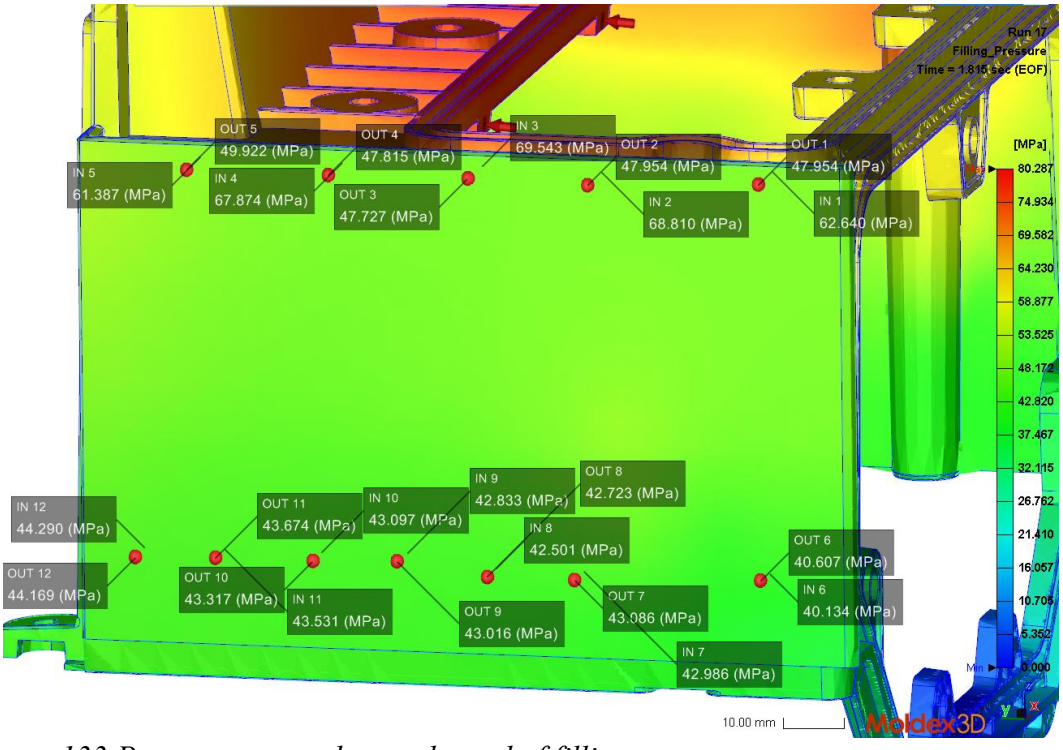


*Figure 133 Pressures on probes at the end of filling.*

Table 16 shows pressure differences on probes 1-12 during the filling. Positive values mean that pressure in the inner wall is higher than pressure in the outer wall. Table shows

that from 1,123 s until the end of filling, pressure differences between 20,1 MPa and 32,4 MPa concentrate on the tool insert base at the area of probes 1-4. This indicates uneven filling and might break the insert, as based on results from initial design, it is known that pressure differences over 20 MPa will most likely cause cracking of the insert. Pressure differences on the area of probes 6-12 are small and flows in both inner and outer wall are there well balanced.

*Table 16 Pressure differences (in MPa) on probes 1-12 at six different time steps. Values are calculated based on figure 128 - figure 133. Positive values mean that pressure in the inner wall is higher than in outer wall. EOF refers to end of filling.*

| | **t = 0,484 s** | **t = 0,807 s** | **t = 1,123 s** | **t = 1,458 s** | **t = 1,592 s** | **t = EOF** |
|---|---|---|---|---|---|---|
| **$\Delta P_1$** | 5,3 | 11,7 | 29,2 | 26,1 | 22,9 | 14,7 |
| **$\Delta P_2$** | 8,2 | 16,3 | 31,6 | 30,8 | 31,3 | 20,9 |
| **$\Delta P_3$** | 5,8 | 14,3 | 28,1 | 29,5 | 32,4 | 21,8 |
| **$\Delta P_4$** | 3,7 | 11,6 | 24,5 | 26,7 | 29,3 | 20,1 |
| **$\Delta P_5$** | 0,5 | 5,6 | 16,4 | 16,0 | 16,8 | 11,5 |
| **$\Delta P_6$** | N/A | N/A | 0,3 | 0,1 | 0,2 | -0,5 |
| **$\Delta P_7$** | N/A | N/A | 0,02 | -0,1 | -0,07 | -0,1 |
| **$\Delta P_8$** | N/A | N/A | N/A | -0,2 | -0,3 | -0,2 |
| **$\Delta P_9$** | N/A | N/A | N/A | N/A | -0,1 | -0,2 |
| **$\Delta P_{10}$** | N/A | N/A | N/A | N/A | N/A | -0,2 |
| **$\Delta P_{11}$** | N/A | N/A | N/A | N/A | N/A | -0,1 |
| **$\Delta P_{12}$** | N/A | N/A | N/A | N/A | 0,1 | 0,1 |

#### 5.2.3.5 Two higher ribs, gating from the rib area

In order to ease the plastic flow to the part's outer wall, two of the original ribs in the initial part design were made higher, as shown in figure 134. In addition to this, the gating points were moved on the area of the higher ribs to ensure plastic flowing to the other side of the insert, already in the beginning of the injection and decreasing the pressure difference over the insert, especially at the insert base.

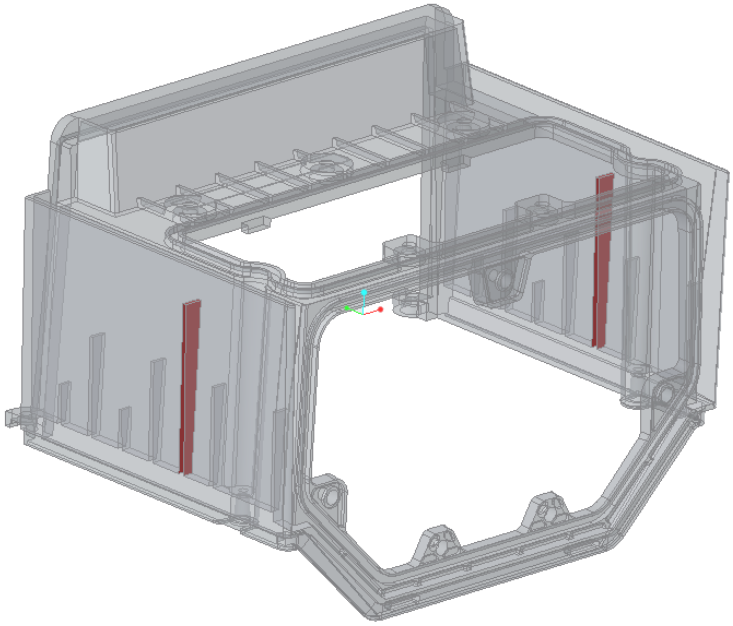

*Figure 134 Two ribs were made higher (highlighted with red) to ease the plastic flow on part's outer wall. Height of these ribs is 62 mm.*

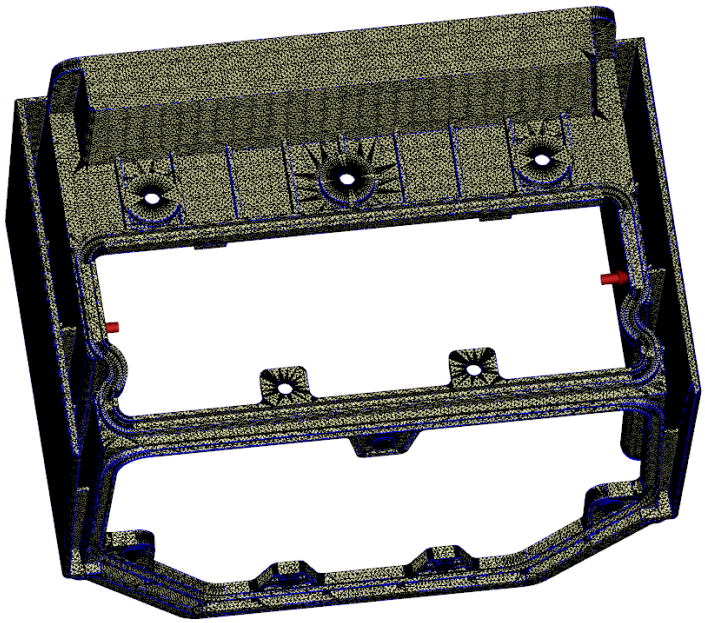

*Figure 135 Meshing of the modified part geometry. Two gating points on the area of the higher ribs (red arrows).*

## Results

Filling pressure required to fill the part is 49,843 MPa and filling time 1,912 s. Highest pressures are found near the gating points as shown in figure 136. Noticeable is that the highest pressures are near the tool insert base where the insert cracked in the molding trials with initial design. Figure 137 shows the melt front time during the filling. Figure shows that straight in the beginning of the filling, melt starts to flow on the outer wall as well. From there, the flow front starts to spread on both vertical and horizontal direction. Melt's fast movement on vertical direction should be seen as decreased pressure difference in the insert base area. As well, flows in the inner and outer wall seem to be well balanced, as the melt fronts move on similar phase on both walls.

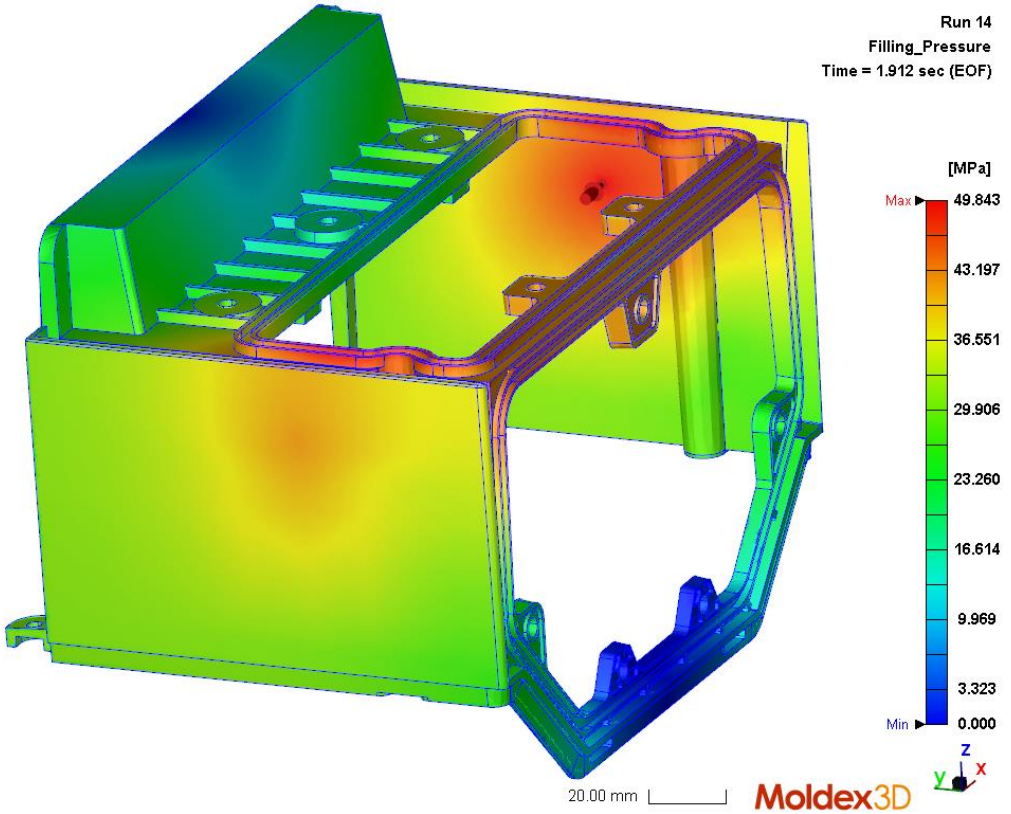


*Figure 136 Filling pressure required to fill the part is approximately 50 MPa with filling time of 1,912 s.*

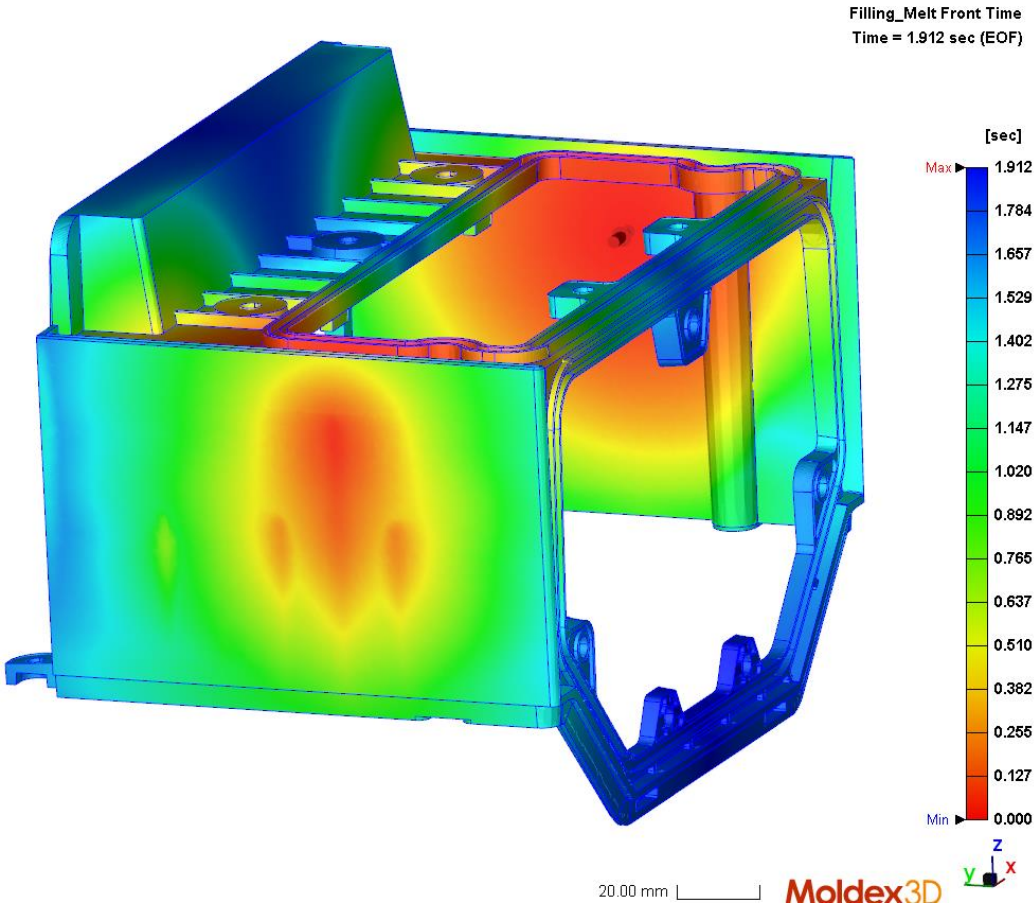


*Figure 137 Melt front time.*

To study the filling pressure differences more, 12 probe pairs are attached to the part. Only half of the part is studied as the part is symmetrical. Figure 138 shows locations of the probes, which pressure values during filling are analyzed. Probes 1 to 5 are attached on the tool insert base and probes 6 to 12 are further away from the tool insert's fixed surfaces. As these probes are further from the fixed points, smaller load will bend the insert easier. Furthermore, insert tip area has multiple cuts due to ribs in the part which weakens the insert tip. Probes named "IN" are attached on part's inner wall which is in contact with tool insert's inner surface. "OUT" named probes are on the opposite side on the outer wall of the part, and on its outer surface. "OUT" probes are attached on the outer surface as the pressure difference through the wall can be assumed to be negligible.

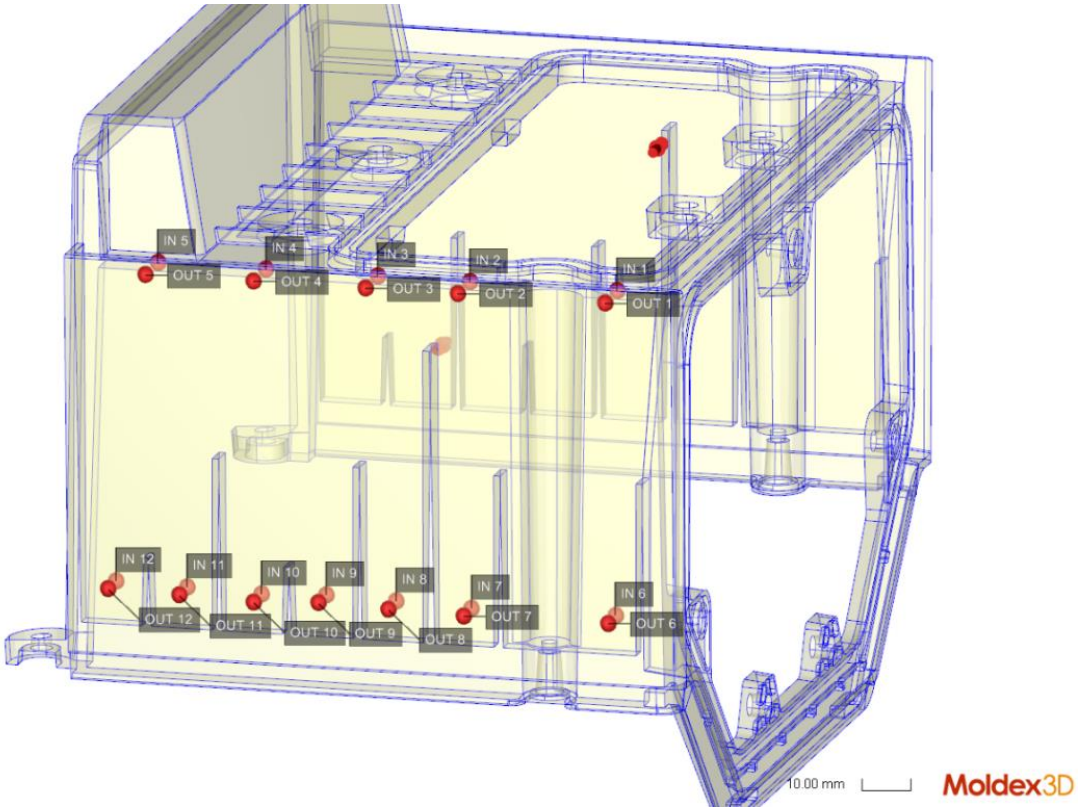


*Figure 138 Probe locations.*

Figure 139 shows melt flow at 0,505 s. Melt has already flown to outer wall through the high rib at the gating area and melt front has almost reached to the insert base area. Nevertheless, flow in outer wall is bit behind flow in inner wall. Pressure differences on probes 1-4 are from 1,8 MPa to 9,6 MPa when melt hasn't yet reached probes 5. At 0,828 s (figure 140), melt has flown in the upper part of the outer wall and pressure differences on probes 1-5 are 1,2-10,4 MPa. Melt has also reached probes 7-10 and pressure differences there are 0,1-0,6 MPa.

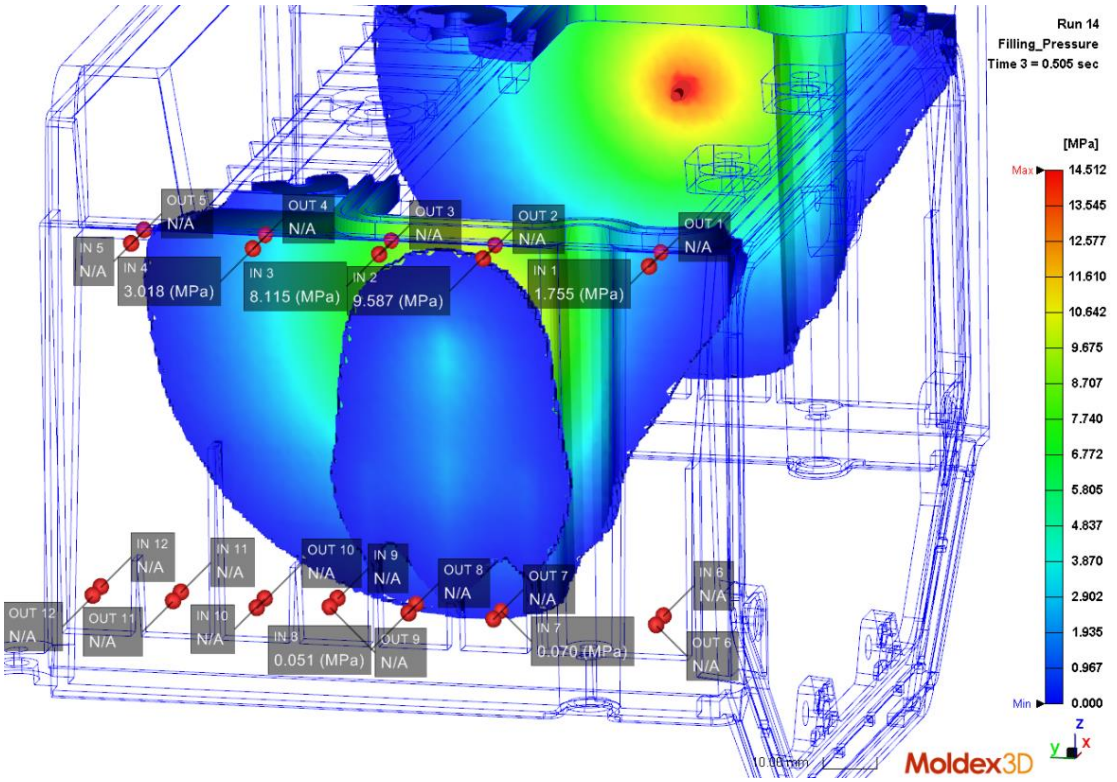


*Figure 139 Filling pattern and filling pressures at time 0,505 s.*

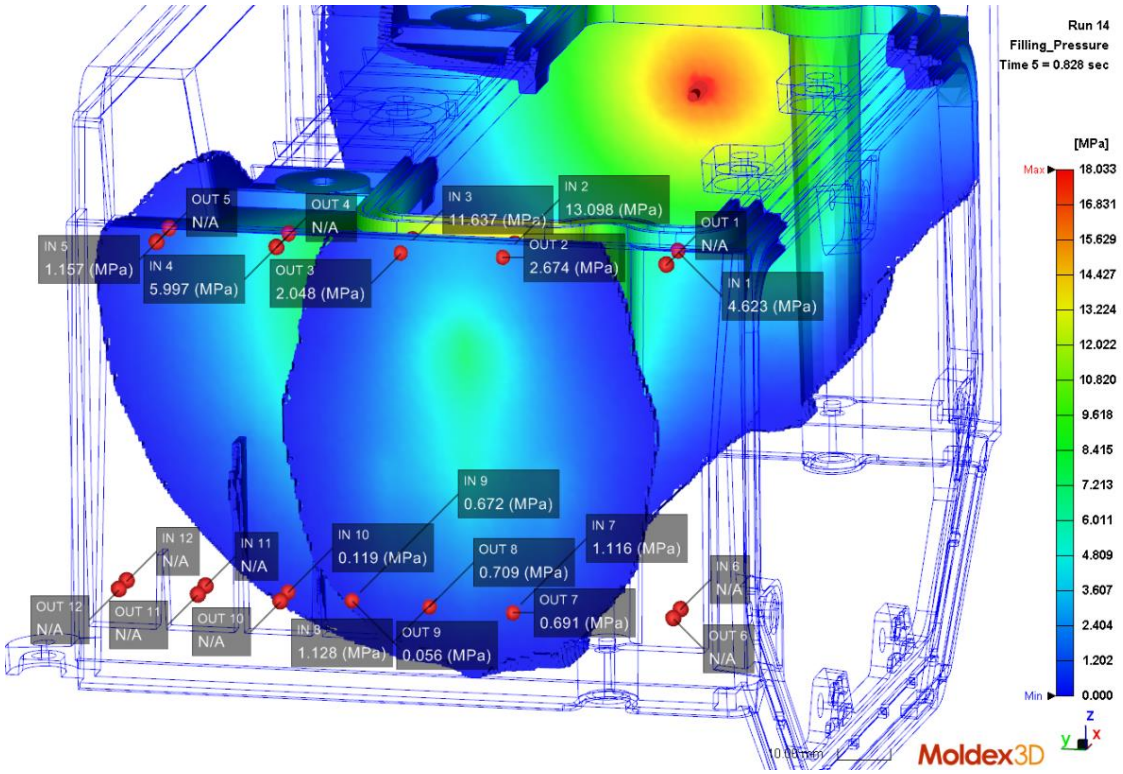


*Figure 140 Filling pattern and filling pressures at time step 0,828 s.*

At 1,164 s and 1,486 s melt has almost completely filled the outer wall (see figure 141 and figure 142) and pressure differences on probes 1-5 are 10,1 MPa or below. Flows in the lower areas of the walls are well balanced as the pressure differences on probes 7-12 are 0,9 MPa or lower. Probe 6 has slightly higher pressure difference, 2,1 MPa.

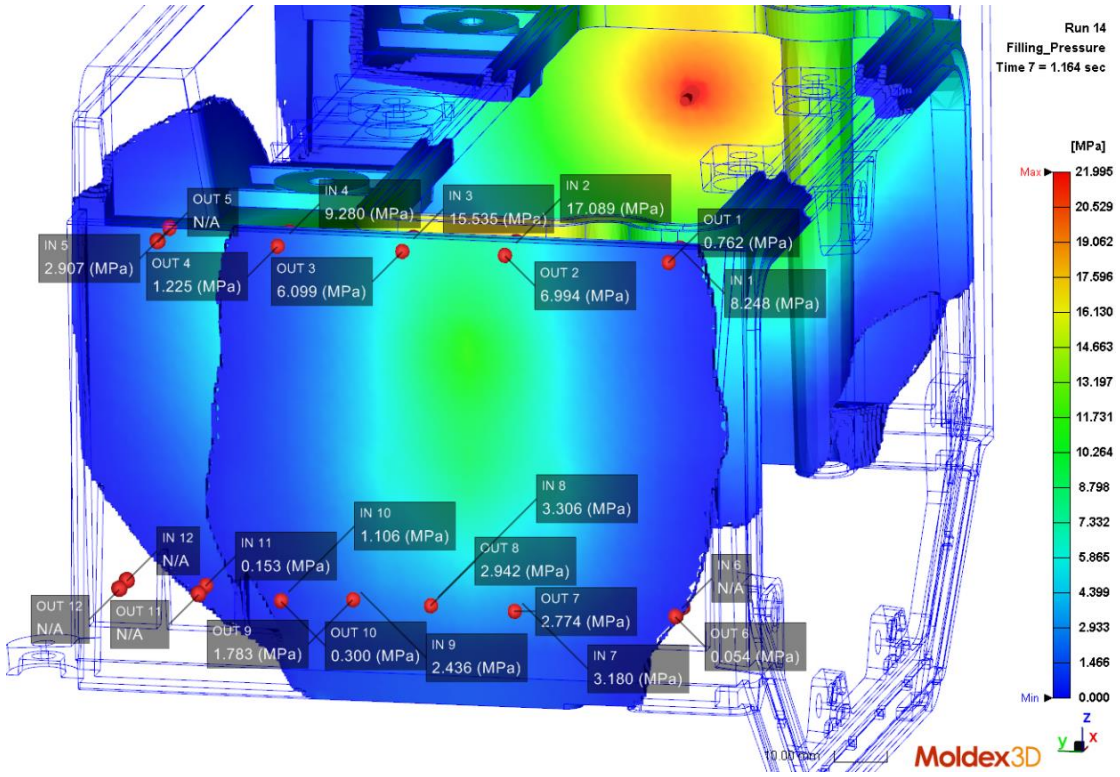


*Figure 141 Filling pattern and filling pressures at time step 1,164 s.*

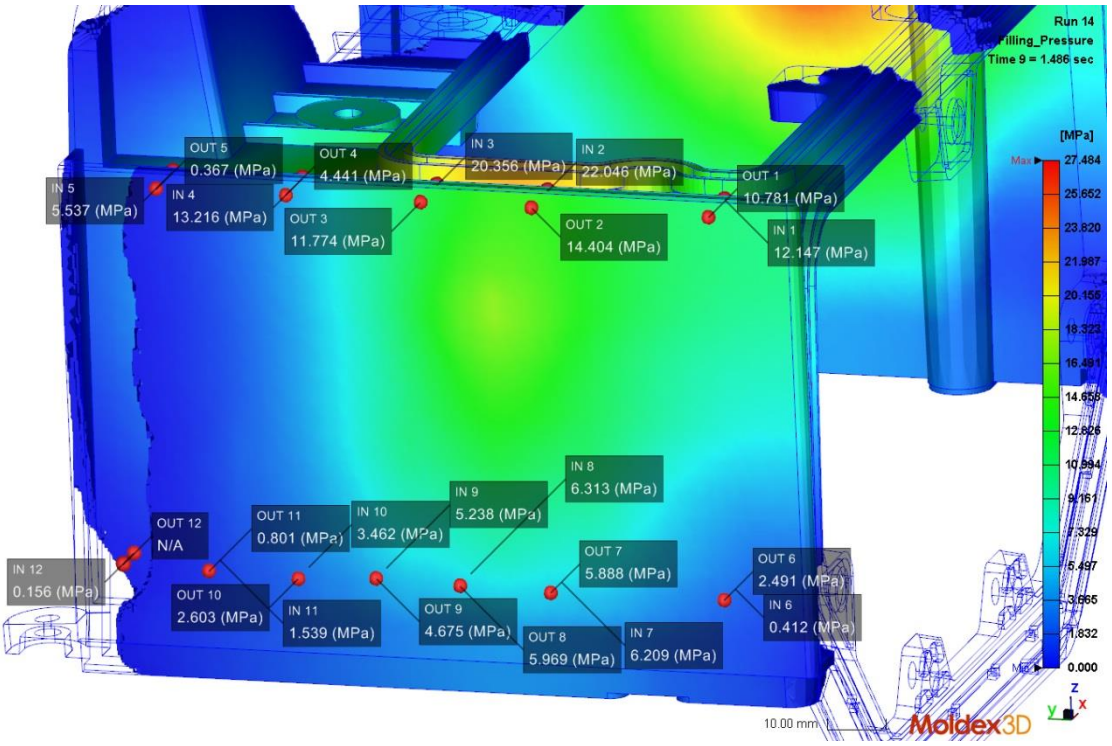


*Figure 142 Filling pattern and filling pressures at time step 1,486 s.*

During 1,648-1,912 s last areas fill, and pressure differences on most probes decrease (figure 143 and figure 144). At the end of filling, maximum pressure difference, 7,3 MPa, is found from probe 2.

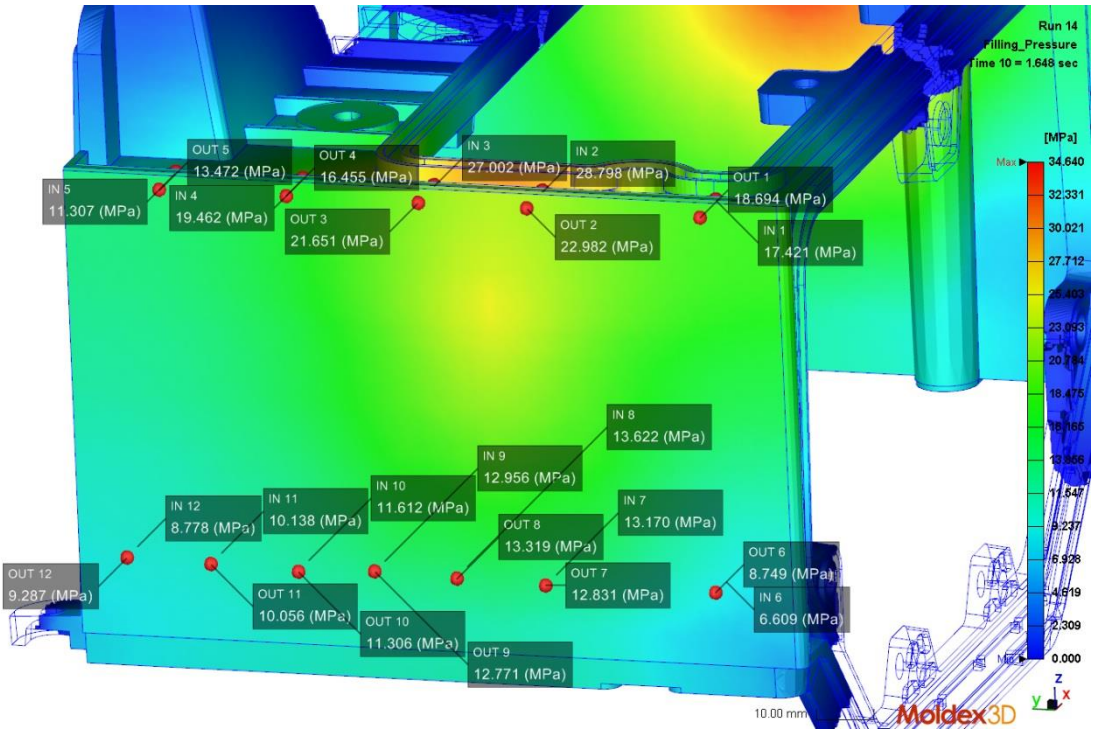


*Figure 143 Filling pattern and filling pressures at time step 1,648 s.*

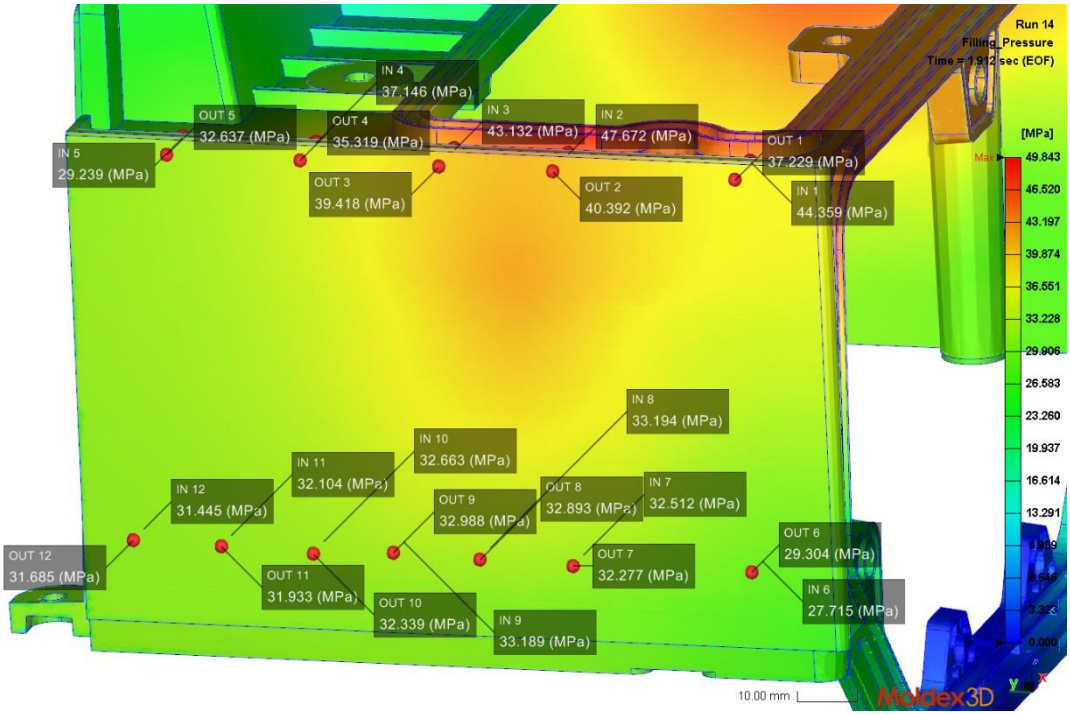


*Figure 144 Filling pattern and filling pressures at time step 1,912 s (=End of Filling).*

Pressure differences on probes during filling are collected to table 17. Positive values indicate that pressure in the inner wall is higher than pressure in the outer wall. Table shows that maximum pressure difference over the insert is 10,4 MPa during the filling. Reason for this is that melt flows to the outer wall already at the beginning of the filling through the raised rib, which prevents formation of high pressure differences on the insert base. Also, as the gating points were moved on the rib area, not only the melt flow was balanced but the pressure concentrating on the insert base was decreased as the gating points locate further away from the insert base. Pressure difference around 10 MPa is

improvement to previous cases where pressure difference was between 20 MPa and 30 MPa. On the insert tip area, pressure difference is below 1 MPa on probes 7-12 during the filling which indicates balanced flow on both inner and outer wall.

*Table 17 Pressure differences (in MPa) between probe pairs 1-12 at six different time steps based on figure 139 - figure 144. Positive value means that pressure in the inner wall is higher than in the outer wall. EOF refers to end of filling.*

| | **t = 0,505s** | **t = 0,828 s** | **t = 1,164 s** | **t = 1,486 s** | **t = 1,648 s** | **t = EOF** |
|---|---|---|---|---|---|---|
| **$\Delta P_1$** | 1,8 | 4,6 | 7,5 | 1,4 | -1,3 | 7,1 |
| **$\Delta P_2$** | 9,6 | 10,4 | 10,1 | 7,6 | 5,8 | 7,3 |
| **$\Delta P_3$** | 8,1 | 9,6 | 9,4 | 8,6 | 5,4 | 3,7 |
| **$\Delta P_4$** | 3,0 | 6,0 | 8,1 | 8,8 | 3,0 | 1,8 |
| **$\Delta P_5$** | N/A | 1,2 | 2,9 | 5,2 | -2,2 | -3,3 |
| **$\Delta P_6$** | N/A | N/A | -0,05 | -2,1 | -2,1 | -1,6 |
| **$\Delta P_7$** | 0,07 | 0,4 | 0,4 | 0,3 | 0,3 | 0,2 |
| **$\Delta P_8$** | 0,05 | 0,4 | 0,4 | 0,3 | 0,3 | 0,3 |
| **$\Delta P_9$** | N/A | 0,6 | 0,7 | 0,6 | 0,2 | 0,2 |
| **$\Delta P_{10}$** | N/A | 0,1 | 0,8 | 0,9 | 0,3 | 0,3 |
| **$\Delta P_{11}$** | N/A | N/A | 0,2 | 0,7 | 0,08 | 0,2 |
| **$\Delta P_{12}$** | N/A | N/A | N/A | 0,2 | -0,5 | -0,2 |

## Core shift analysis

In addition to the filling analysis, core shift analysis was conducted with Moldex3D to analyze if the cracking and bending problems would be solved with this design. For a core shift analysis, a separate simulation model consisting part and tool insert was constructed. Part and insert were imported to Moldex3D as assembly stp -file. In order to run a core shift analysis, the part and tool insert model need to have correspond meshing at the surfaces which are in contact with each other. This was done by copying the surface mesh from the insert and attaching it to the part model. Noticeable is that tool insert need to be defined as part insert to run the core shift analysis. In the end, insert and part model consists of 1 873 804 solid mesh elements. Boundary conditions for the core shift simulation are shown in figure 145. Insert is fixed from the top and side surfaces as highlighted with light blue arrows in the figure. Top surface is fixed in z-direction and side surfaces in x- and y-direction.

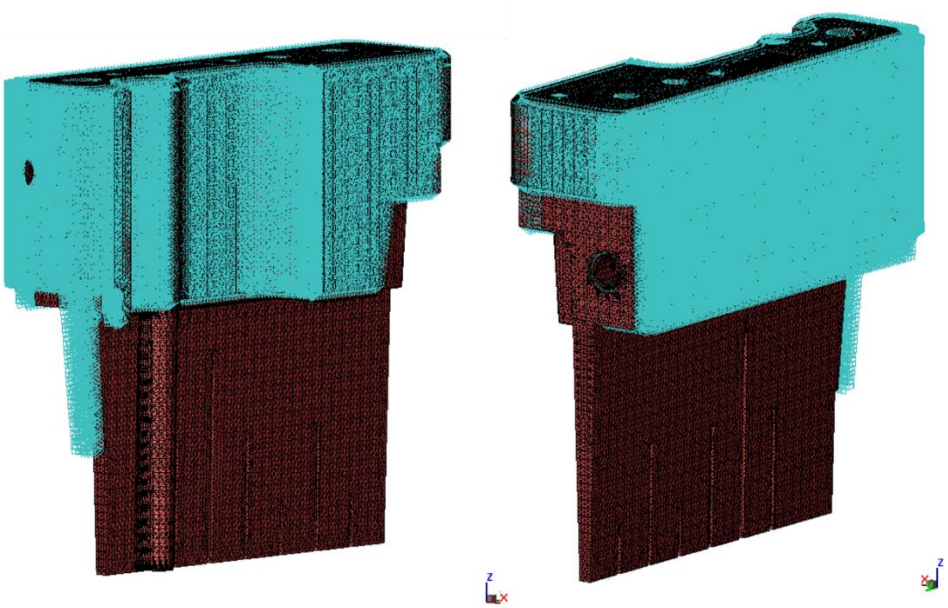

*Figure 145 Fixed surfaces highlighted with light blue arrows.*

Figure 146 and figure 147 shows Von Mises stress and stress distribution in the insert at 1,819 s. At 1,819 s, maximum stress (2196,518 MPa) is found from the tip of one round in insert (see figure 146). This high maximum value is probably due to inaccurate mesh element(s) as the maximum value is concentrated on a location where there is small round and based on figure 148, this high stress is found in less than 0,00% of the part. Scale for the results of Von Mises stress is adjusted to be from 0,1 MPa to 500 MPa as values over 439 MPa are found only from 0,02% of the part (refer to figure 148). Figure 146 shows that high stresses (500 MPa or over) are found near the gating point at the insert base on the round surface. As with the maximum stress, some of these high stresses can be due to small round on the insert base and because of the meshing accuracy of small shapes. Otherwise near the gating area and near the rib cuts, stresses are slightly below and above 200 MPa. These values are reasonable as there aren't any rounds on the rib cuts and as the fatigue stress limit of the beryllium copper is 330 MPa.

On the second surface of the insert (see figure 147), highest stresses are located on the same area as in the first side. Here the highest values are about 320 MPa. Otherwise stresses are between 230 MPa and 300 MPa near the gating point and on the insert base area. Also, on the second side, rib cuts have high stress concentrations due to sharp corners. Based on figure 148, only 0,60 % of the part undergoes stress over 219,742 MPa and average stress is 18,604 MPa. As the stress concentrations based on figure 146-figure 148 are such local, they can be due to meshing inaccuracy of small features.

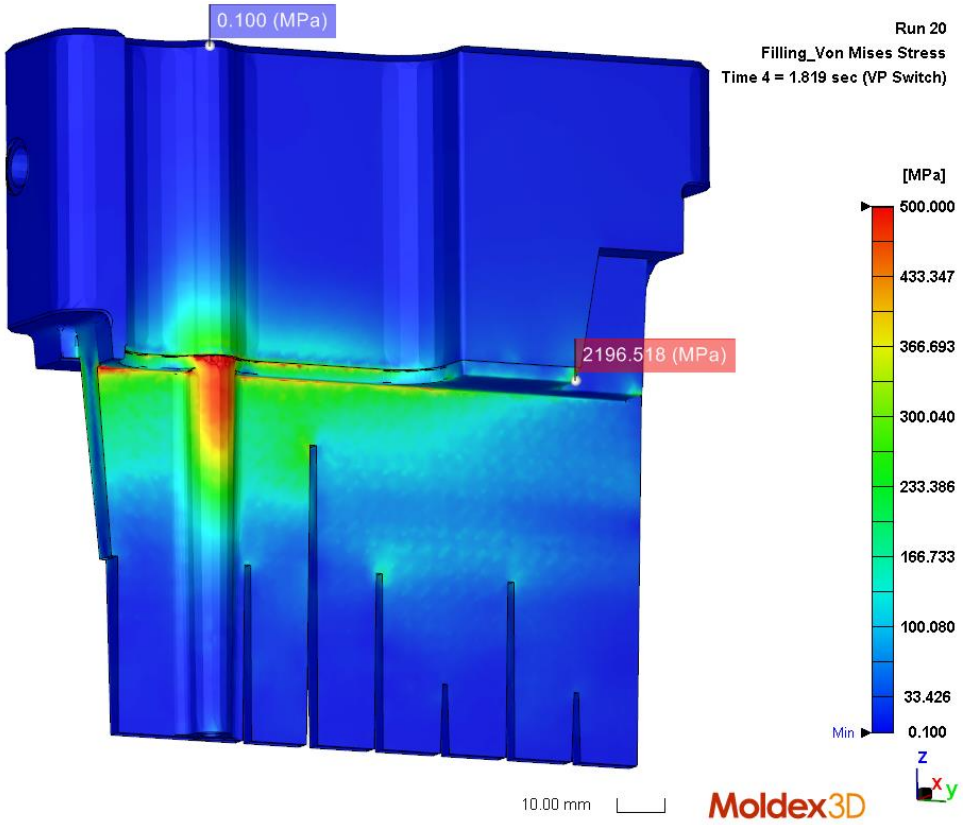


*Figure 146 Von Mises stress on the copper tool insert (side 1) at 1,819 s.*

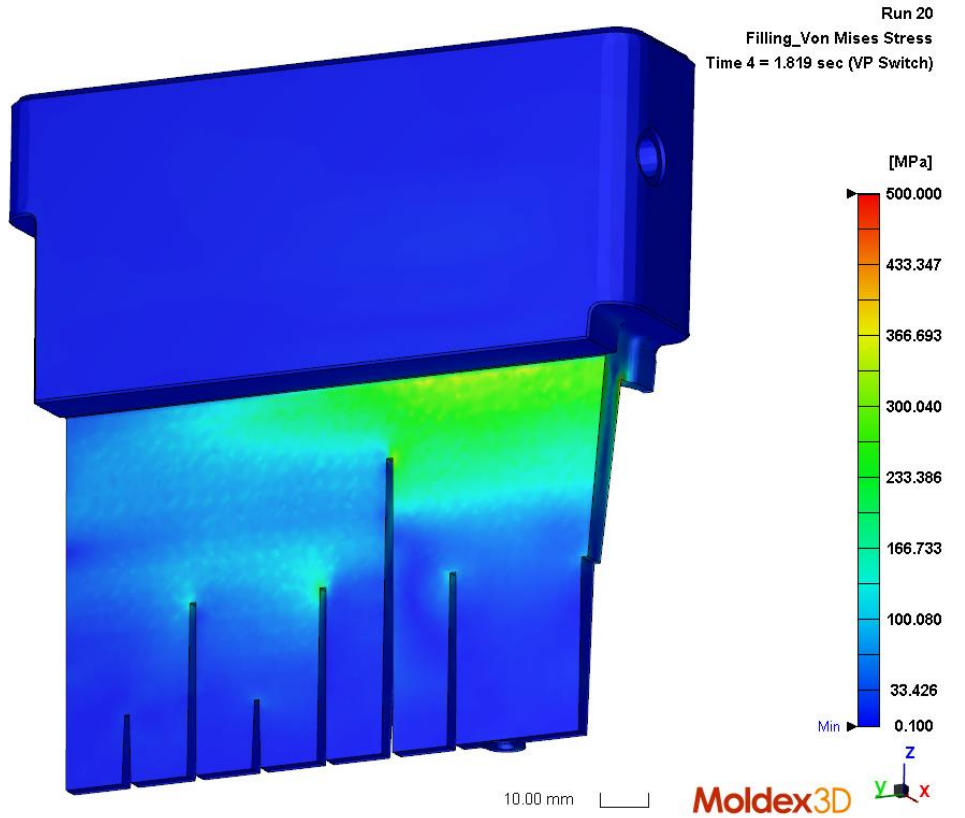


*Figure 147 Von Mises stress on the copper tool insert (side 2) at 1,819 s.*

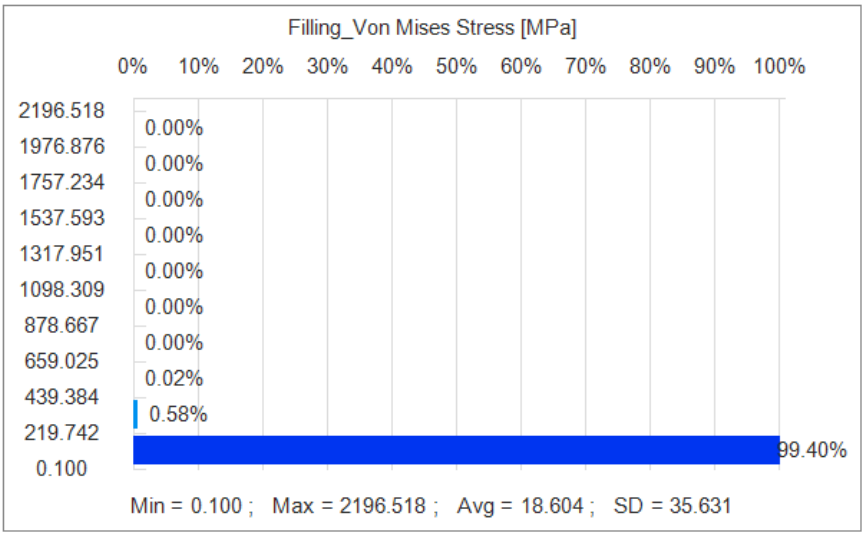


*Figure 148 Von Mises stress distribution in the tool insert at 1,819 s (refers to figure 146 and figure 147).*

Figure 149 and figure 150 show the Von Mises stresses at the end of filling on a range from 0,121 MPa to 500 MPa. Maximum stress value is located on same place as previously at 1,819 s and it has increased to 3115,269 MPa. Noticeable is that otherwise stresses near the gating point are lower (compare figure 146 and figure 149). Still on the insert base (on side 1) stresses are in some points slightly below or above 500 MPa. Otherwise on the base area, stresses are approximately between 250 MPa and 400 MPa. At the second side, stresses are close to ones at 1,819 s and mostly below 300 MPa. In some locations near the base area, stresses increase near 320 MPa. Distribution of Von Mises stresses are illustrated in figure 151 which shows that stresses over 311,636 MPa are found in only 0,11 % of the insert. Average stress at the end of filling is low, only 18,887 MPa. As mentioned already, high local values can be due to meshing inaccuracy of small features.

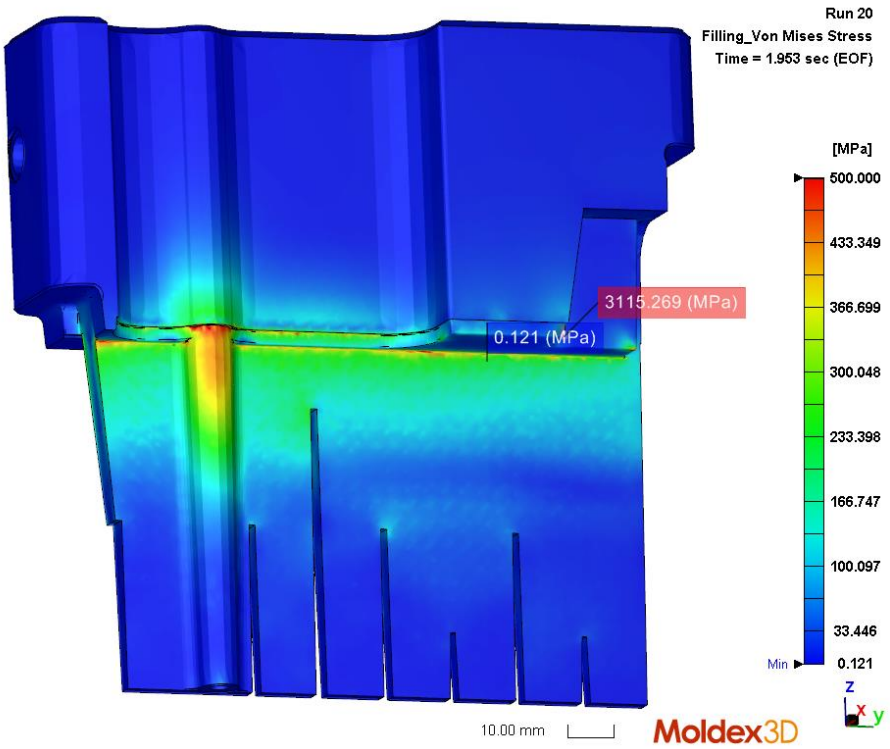


*Figure 149 Von Mises stress on side 1 at the end of filling.*

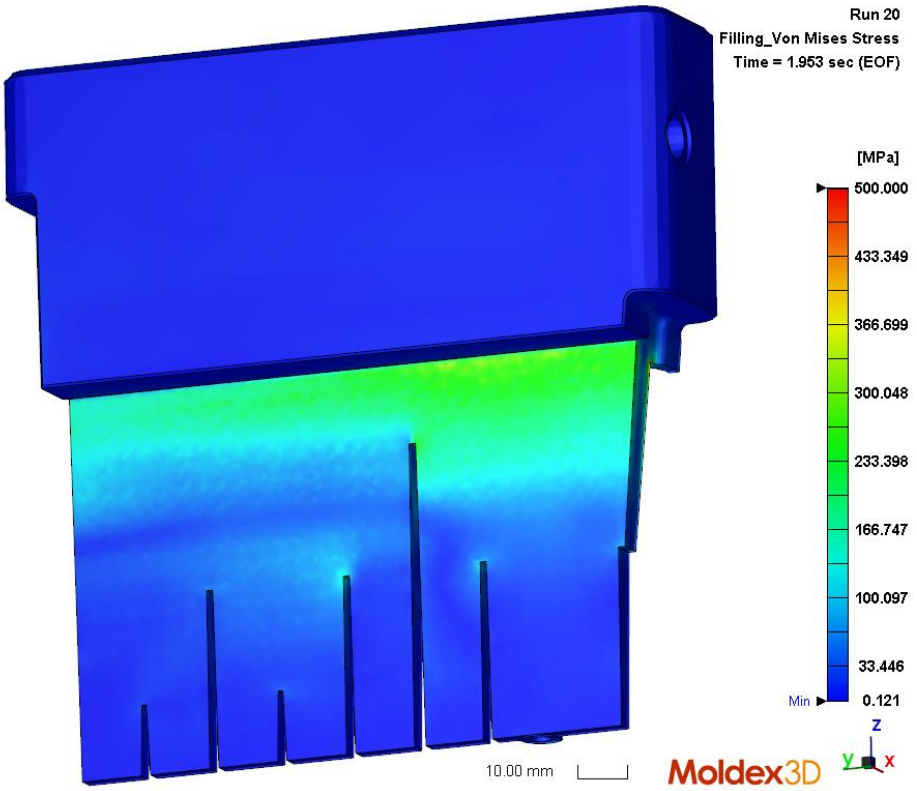


*Figure 150 Von Mises stress on side 2 at the end of filling.*

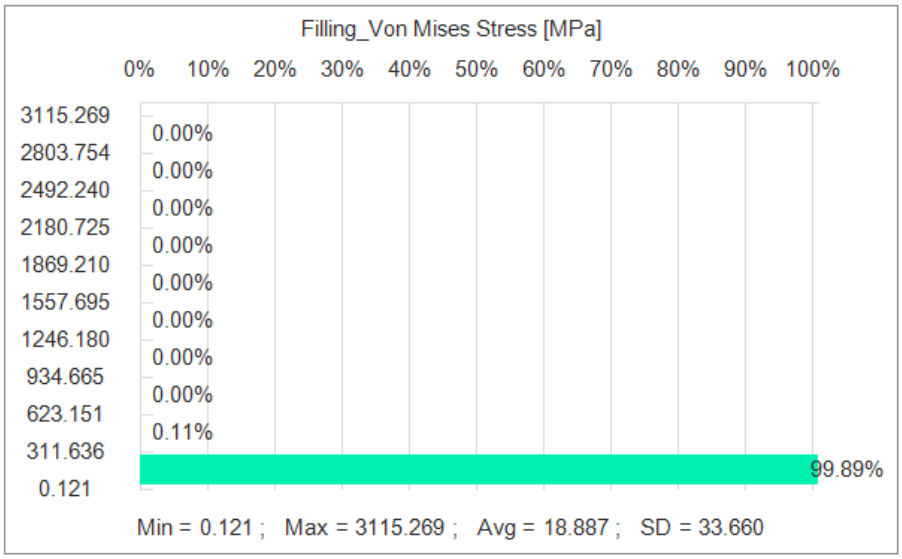


*Figure 151 Von Mises stress distribution at the end of filling (refers to figure 149 and figure 150).*

Displacement values in x-direction for the tool insert at 1,819 s are shown in figure 152. Maximum displacement value is 0,004 mm and minimum value -1,161 mm. Negative value indicates that it affects the opposite direction from the positive x-axel. Based on figure 152, area around the high rib bends towards the outer wall of the plastic part, which indicates that pressure on the inner wall is higher than on the outer wall. Figure 153 shows how these displacement values are distributed as percentage. 90,27 % of the part has displacement value between 0,004 mm and -0,113 mm. Average displacement value is -0,042 mm. Displacement values from -0,462 mm to -1,161 mm covers 3,08 % of the part. This high displacement would be from 18 to 46 % of the part's wall thickness and be seen

in the product. As the rib area had high stress values on the corners, at least partly due to excluded rounds, displacement values can also be slightly affected by that matter. Also, some very high Von Mises stress values were seen in figure 146 and figure 147 which can affect to the accuracy of displacement values.

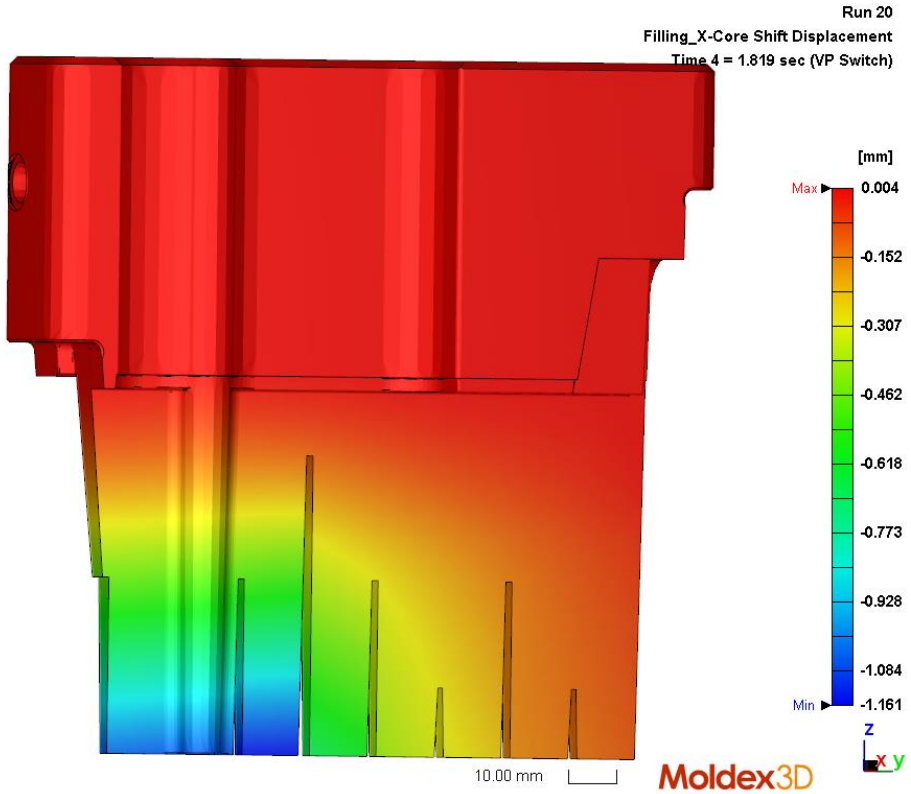


*Figure 152 Core shift displacement in x-direction at 1,819 s.*

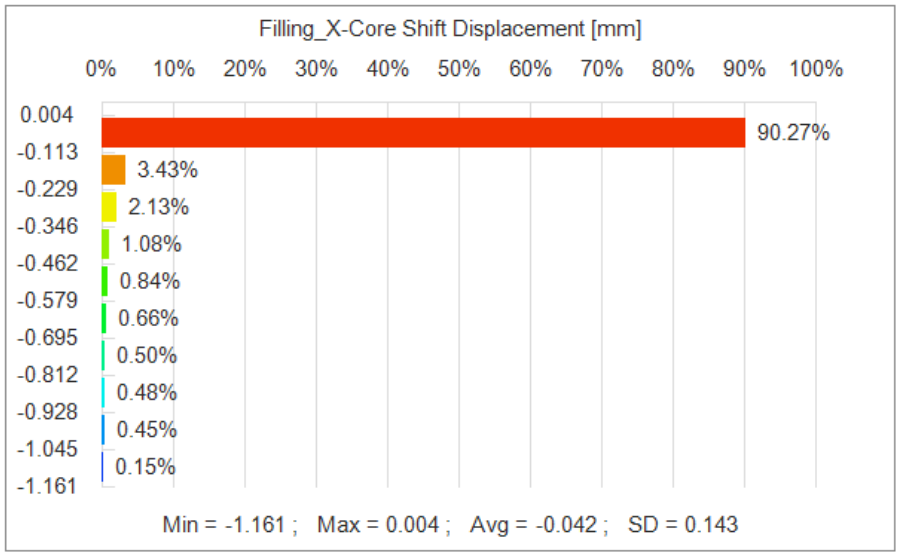


*Figure 153 Displacement (in x-direction) distribution of the insert at 1,819 s (refers to figure 152).*

Displacement values in x-direction at end of filling are shown in figure 154. Minimum value is -1,025 mm and maximum 0,005 mm. Range of displacements is slightly smaller than it was at 1,819 s but displacements are noticed to be in same locations. Figure 155 shows how displacement values are distributed as percentage. 88,09 % of the part has

displacement values between 0,005 mm and -0,098 mm. Values between -0,407 mm and -1,025 mm cover 4,42 % of the insert. These values represent 16-41 % of the part's wall thickness. These displacement values can be slightly affected by the inaccuracy of meshing small features, as mentioned before when analyzing results of Von Mises stresses. As rounds of rib cuts were excluded from the simulation model, high stress concentrations were found on the rib cuts which can also affect to the displacement values.

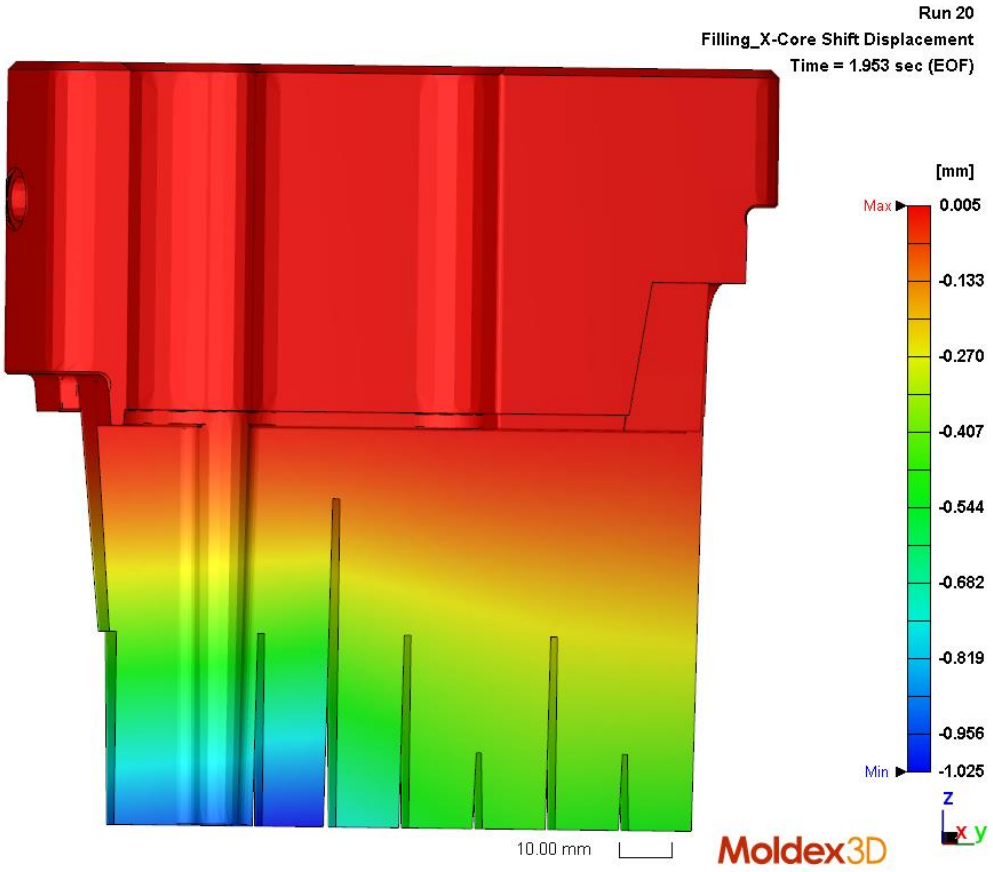


*Figure 154 Displacement in x-direction at end of filling.*

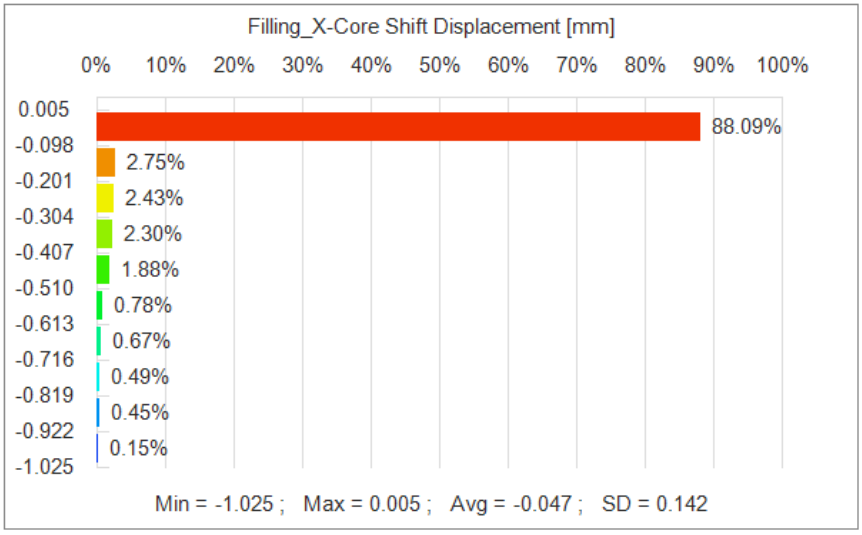


*Figure 155 Displacement (x-direction) distribution at end of filling.*

Probe 2 located close to the area where highest Von Mises stress were seen in figure 146 and figure 149. Based on table 17, probe 2 also has the highest pressure difference during the filling, which supports results from core shift analysis. As the insert has multiple rib cuts, possibility for insert bending as figure 152 and figure 154 showed, is probable and can occur without extremely high pressure differences.

#### 5.2.3.6 Two higher ribs, thinner inner wall and gating from the rib area

Compared to previous case presented in section 5.2.3.5, changes were made to product design. To restrict the plastic flow in the inner wall, its wall thickness was decreased by 0,5 mm (figure 156). Object of this change was to achieve more simultaneous flow on both sides of tool inserts to decrease the pressure differences over them. Reducing wall thickness of the inner wall also gives freedom to make the tool insert 0,5 mm thicker, which will increase its strength and decrease the risk of breaking or bending. Gating points are in the same place as in the previous study and mesh consist of 33 096 surface mesh elements and 1 455 594 solid mesh elements (figure 157).

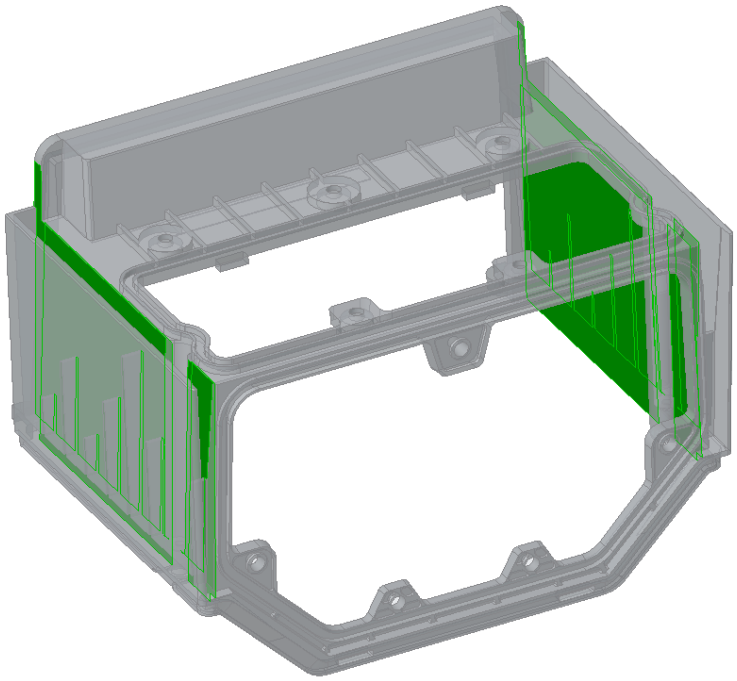

*Figure 156 Wall thickness of the inner wall (highlighted with green) decreased by 0,5 mm.*

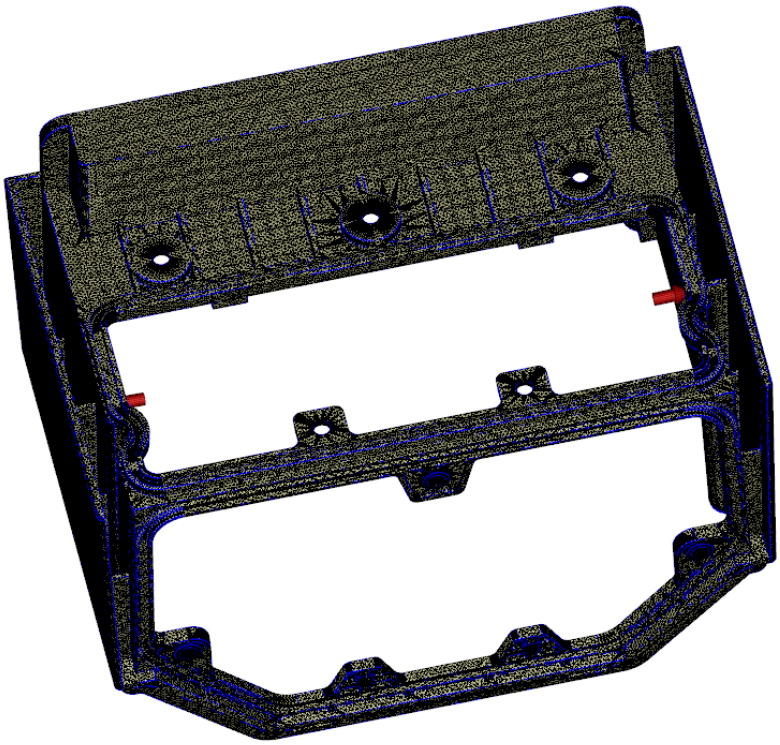

*Figure 157 Meshed part. Gating points (illustrated with red arrows) are in the same places as they were in the previous study in section 5.2.3.5.*

## Results

Filling pressure required to fill the part is 72,552 MPa and filling time 1,974 s. Highest pressure values are seen near the gate (figure 158). Melt flow pattern is shown in figure 159, which shows that melt starts to flow to the outer wall straight after beginning of filling. From there, melt starts to flow on the insert base area which will even the pressure difference on that area. Melt flow seems to be flowing on both inner and outer wall at quite same phase which indicates that pressure differences over the insert should be small.

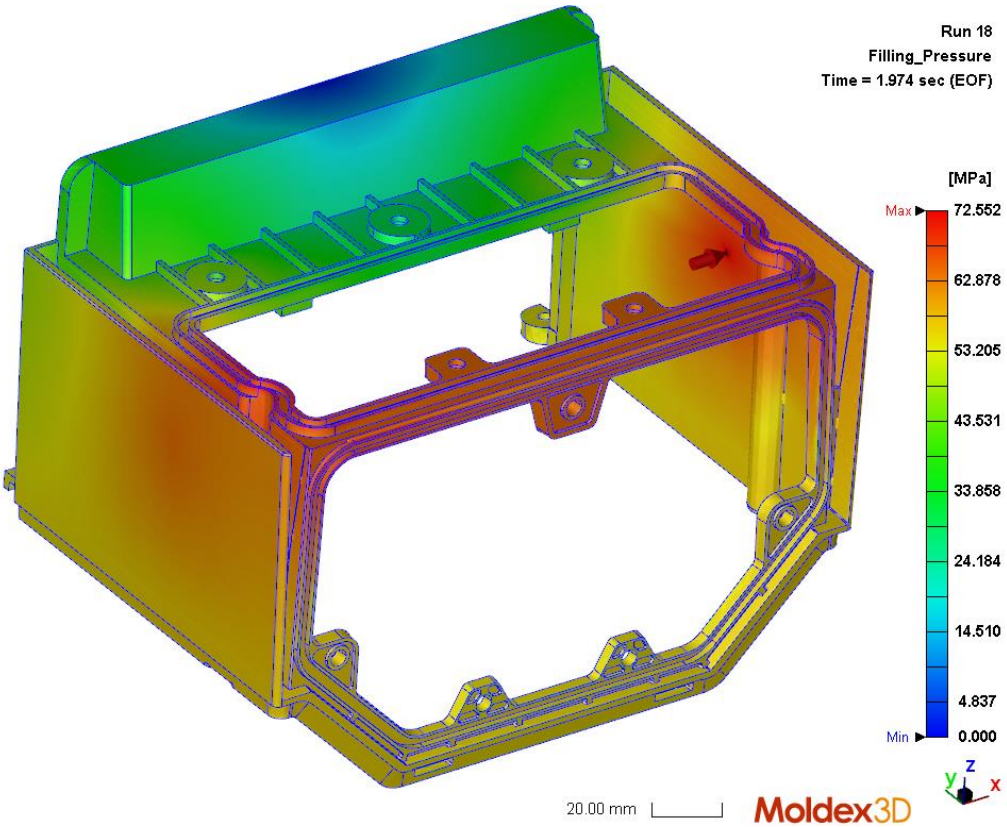


*Figure 158 Filling pressure required to fill the cavity is approximately 73 MPa.*

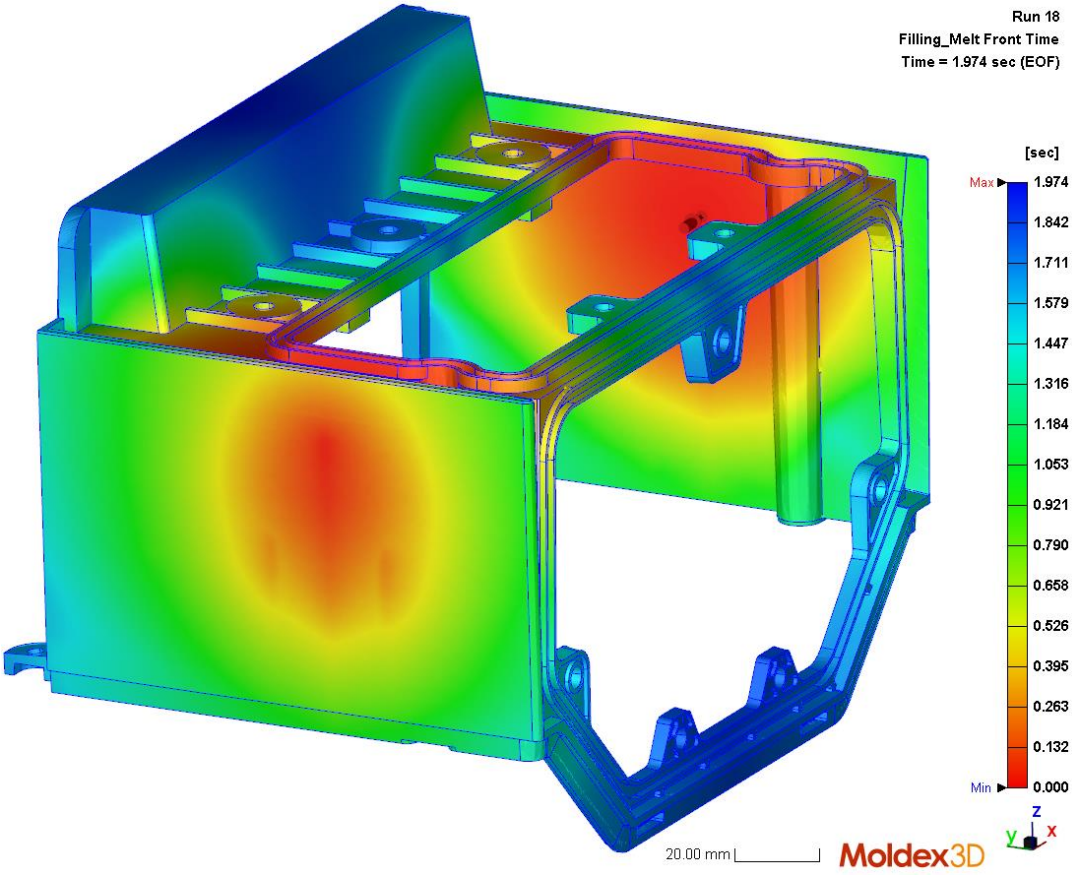


*Figure 159 Melt front time.*

To study the pressure differences during filling, 12 probe pairs are attached to the model to see how pressure changes in those locations during filling (see figure 160). Only half of the part is studied as the part is symmetrical. Probes 1 to 5 are placed on the tool insert base area where the cracking occurred and probes 6 to 12 further away to the area where the tool insert isn't fixed. As these probes are further from the fixed points, smaller load will bend the insert easier. Furthermore, insert tip area has multiple cuts due to ribs in the part which weakens the insert tip. Probes named "IN" are attached on part's inner wall which is in contact with tool insert's inner surface. "OUT" named probes are on the opposite side on the outer wall of the part, and on its outer surface. "OUT" probes are attached on the outer surface as the pressure difference through the wall can be assumed to be negligible.

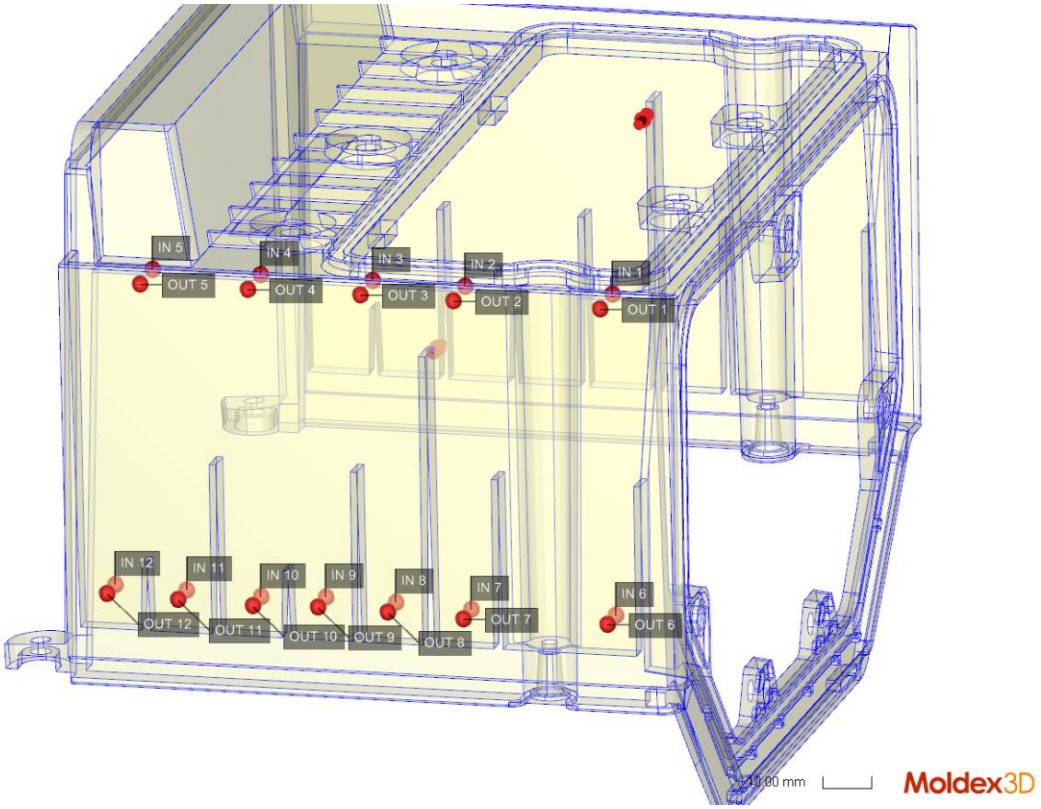


*Figure 160 Probe locations.*

As the figure 159 already predicted, melt starts to flow on the outer wall straight at the beginning of filling. After 0,506 s (figure 161), melt has already spread on quite wide area on the outer wall and reached the insert base area. Due to this, pressure differences on probes 1-4 are between 2,8 MPa and 10,7 MPa. At 0,839 s, melt has spread more in the outer wall and reached also on probes 5, 7, 8 and 9 (figure 162). Pressure difference on probes 1-5 are from 1,1 MPa to 10,4 MPa and on probes 7-9 0,2-0,3 MPa.

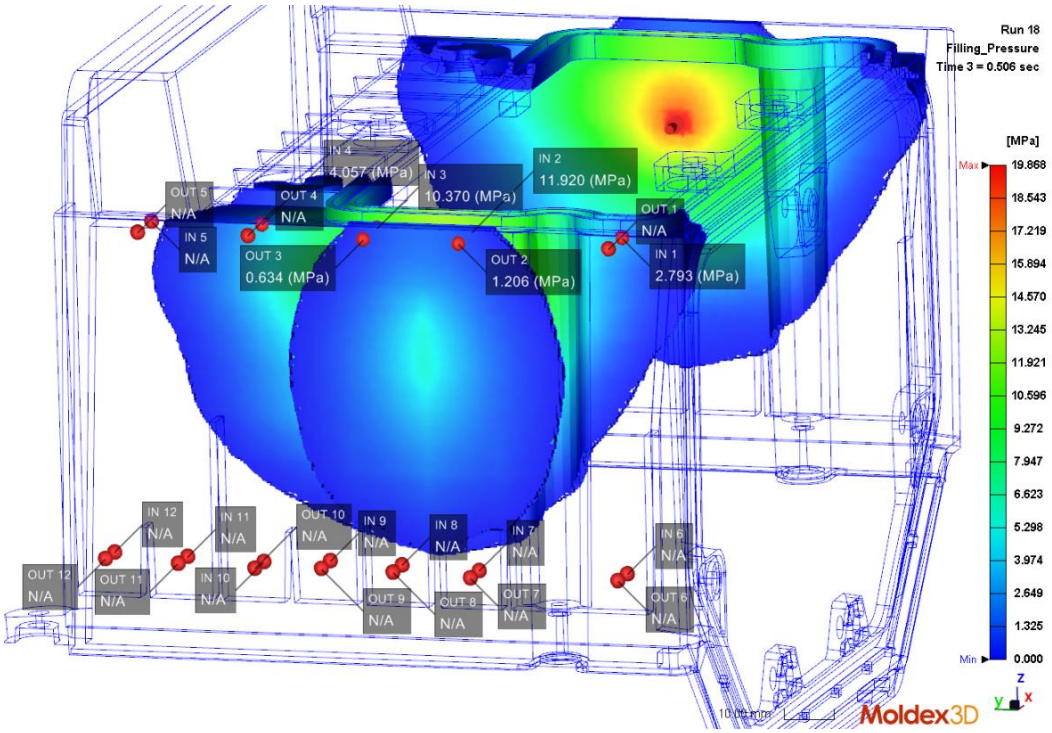


*Figure 161 Melt flow and filling pressures at time step 0,506 s.*

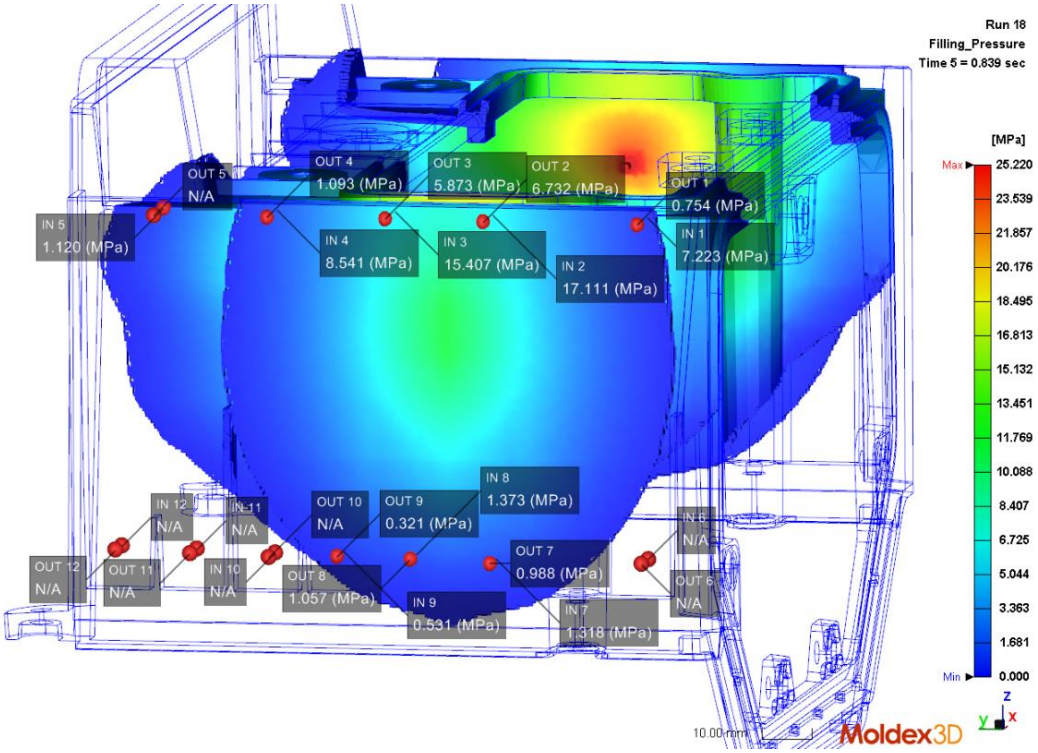


*Figure 162 Melt flow and filling pressures at time step 0,839 s.*

After 1,155 s (figure 163), melt has reached also probes 6 and 10. Pressure differences on probes 1-5 are 2,0-9,0 MPa. On probes 6-10 pressure differences are small, 0,1-0,7 MPa, which indicates that melt is flowing on same phase in both inner and outer wall. Melt in the outer wall is slightly ahead at the location of probe 6, which is due to the thinner inner wall. At 1,493 s (figure 164), melt has reached also probe 11 and probe 12 on the outer wall. Pressure differences in the insert base are from 0,3 MPa to 8,2 MPa and in the insert tip, from 0,02 MPa to 1,9 MPa.

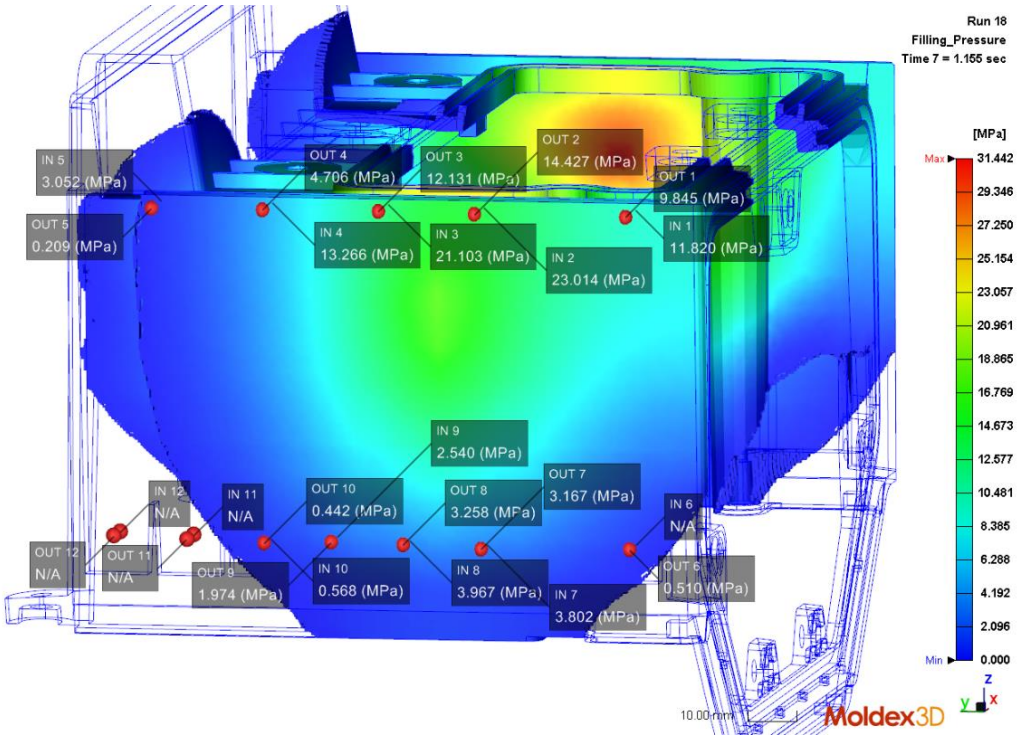


*Figure 163 Melt flow and filling pressures at time step 1,155 s.*

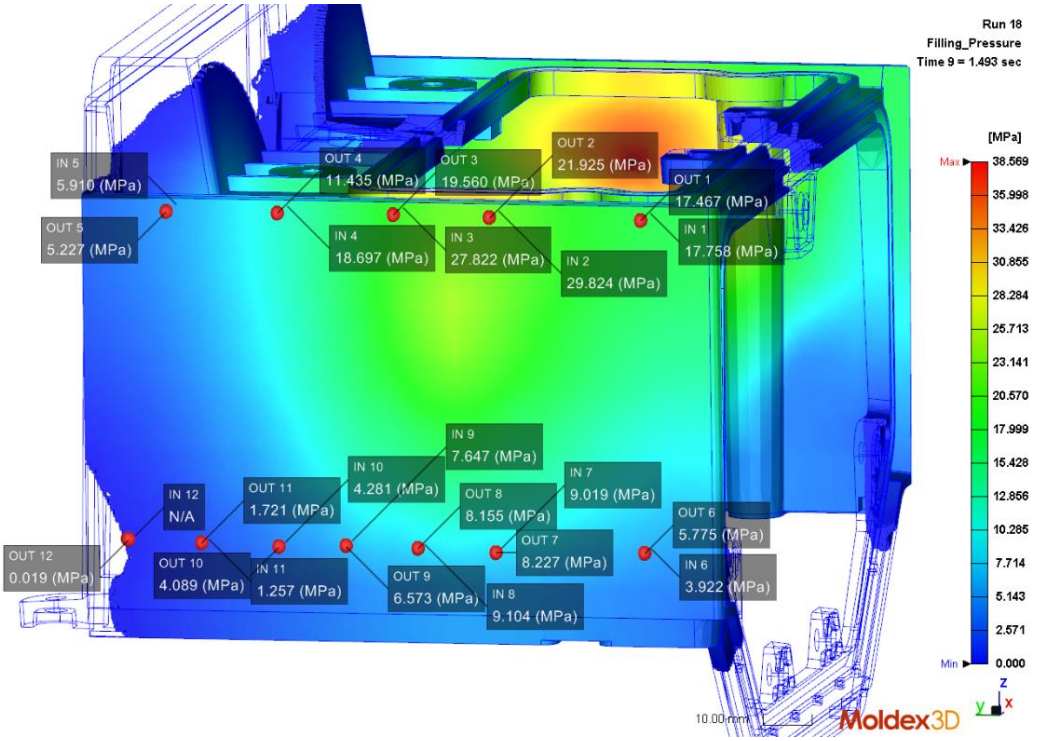


*Figure 164 Melt flow and filling pressures at time step 1,493 s.*

After 1,655 s outer wall is filled and pressure differences between inner and outer wall are starting to decrease on most probes (figure 165). Probes 1-5 have pressure differences from 0,1 MPa to 8,0 MPa. For probes 6-12, values are from 0,3 MPa to 2,5 MPa. Noticeable is, that on probes 1, 5, 6, 11 and 12, pressure in the outer wall is higher than in the inner wall. This results from the filling pattern, as flow in the outer wall has been ahead of flow in the inner wall. Melt flows better in the outer wall as it is thicker than the inner wall, which is why it takes more time for the pressure difference to even out. At the

end of filling (figure 166), pressure differences on probes 1-5 are between 0,03 MPa and 8,4 MPa. Highest value is found from probe 5 where pressure on the outer wall is 8,4 MPa higher than on the inner wall. This is probably due to filling pattern, as probes 4 are close to the gating point but as the inner wall is thinner, it takes more time for the flow to reach to the probe on the inner wall. On probes 6-12 pressure differences are from 0,08 MPa to 0,7 MPa.

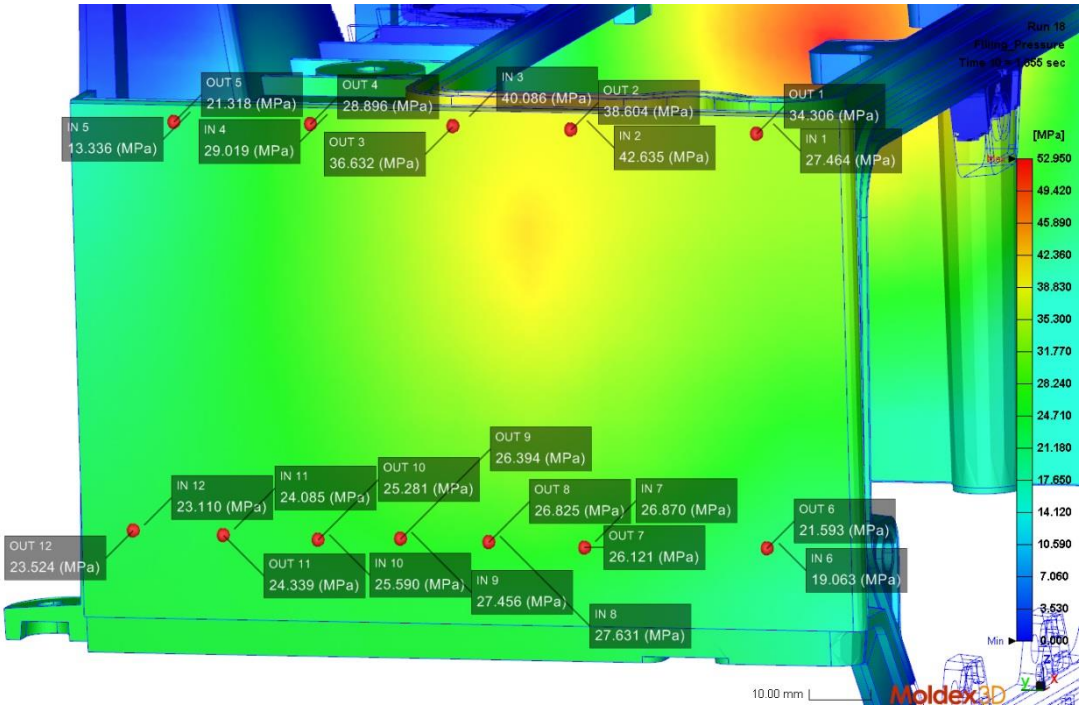


*Figure 165 Melt flow and filling pressures at time step 1,655 s.*

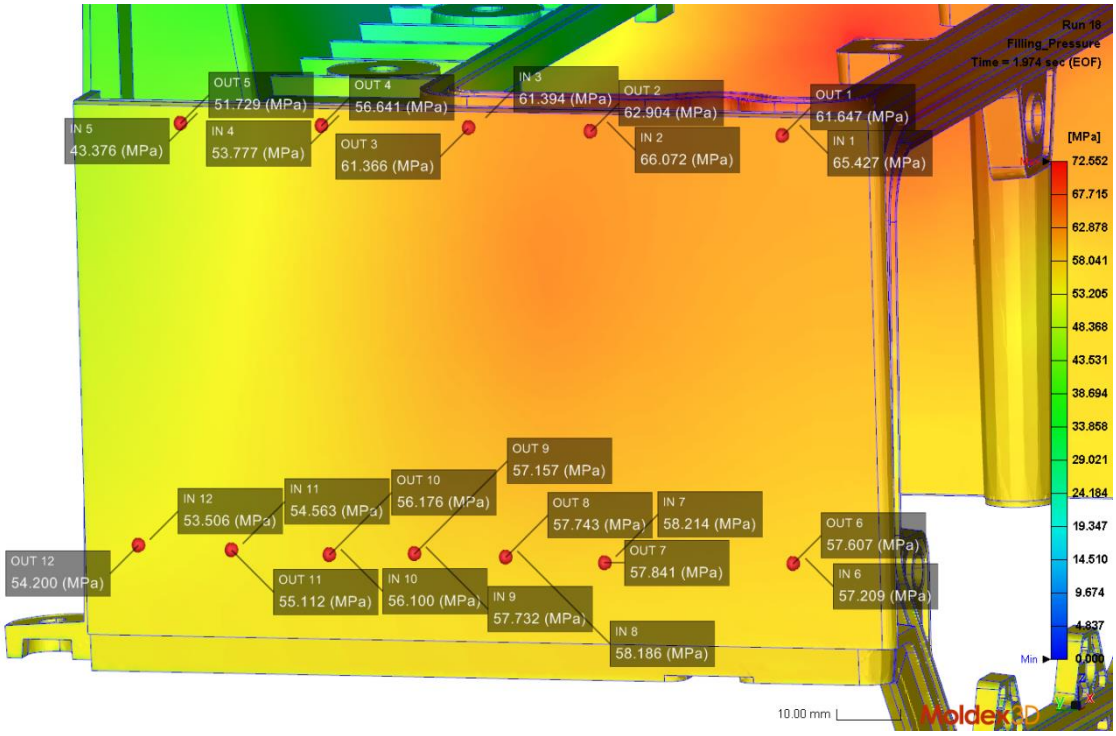


*Figure 166 Melt flow and filling pressures at the end of filling.*

Thickness of the inner wall was decreased to slow down the flow on the inner wall and this way give more time for plastic to flow to the outer wall. Figure 161 - figure 166 showed how melt flows into the part. Figures illustrated that melt starts to flow to the outer surface at the beginning of the filling, which evens the pressure difference over the tool insert. Melt flows in the inner and outer walls seem to be moving on quite similar phase in the vertical direction. In the horizontal direction, melt flow in the inner wall is slightly ahead melt flow at the outer wall in the beginning of filling. During filling, melt flow in the inner wall starts to be behind flow in the outer wall, as melt flows better in the thicker outer wall. Therefore, outer wall is the first to be filled completely. Pressure values of probes 1-12 throughout the filling are collected to table 18 based on figure 161-figure 166. Negative values indicate that pressure in outer wall is higher than in inner wall.

Based on table 18, pressure differences near the tool insert base are 10,7 MPa, at maximum (at 0,506 s, in probe 2). Highest values are found near the gating area, but as the gating points are located slightly further away from the tool insert base, pressure differences over the insert on probes, are 10,7 MPa or smaller. When more melt flows in the outer wall, pressure difference near the gate starts to decrease. On probes 6-12, pressure differences are small throughout the filling which indicates that inner and outer walls are filling quite evenly. One exception for this is noticed in probe 6. There the pressure difference increases to -2,5 MPa at 1,655 s. Noticeable is also that the outer wall has higher pressure then than the inner wall, which is due to restricted flow oín the thinner inner wall. On probes 7-12, pressure differences are between -0,7 MPa and 1,1 MPa throughout filling. Pressure difference is negative on probes 6, 11 and 12 which is due to filling pattern. These probes 6, 11 and 12 locate on rightmost and leftmost corners of the part which means that plastic has the longest way to reach them. As the inner wall is thinner and plastic has longer way to the probes, melt flow in the inner wall leaves behind.

*Table 18 Pressure differences (MPa) between probe pairs 1-12 at six different time steps based on figure 161 - figure 166. Positive value means that pressure in the inner wall is higher than in the outer wall. EOF refers to end of filling.*

| | **t = 0,506s** | **t = 0,839s** | **t = 1,155s** | **t = 1,493s** | **t = 1,655s** | **t = EOF** |
|---|---|---|---|---|---|---|
| **$\Delta P_1$** | 2,8 | 6,5 | 2,0 | 0,3 | -6,8 | 3,8 |
| **$\Delta P_2$** | 10,7 | 10,4 | 8,6 | 7,9 | 4,0 | 3,2 |
| **$\Delta P_3$** | 9,7 | 9,5 | 9,0 | 8,2 | 3,5 | 0,03 |
| **$\Delta P_4$** | 4,1 | 7,4 | 8,6 | 7,2 | 0,1 | -2,9 |
| **$\Delta P_5$** | N/A | 1,1 | 2,8 | 0,7 | -8,0 | -8,4 |
| **$\Delta P_6$** | N/A | N/A | -0,5 | -1,9 | -2,5 | -0,4 |
| **$\Delta P_7$** | N/A | 0,3 | 0,6 | 0,8 | 0,7 | 0,4 |
| **$\Delta P_8$** | N/A | 0,3 | 0,7 | 0,9 | 0,8 | 0,4 |
| **$\Delta P_9$** | N/A | 0,2 | 0,6 | 1,1 | 1,1 | 0,4 |
| **$\Delta P_{10}$** | N/A | N/A | 0,1 | 0,2 | 0,3 | 0,6 |
| **$\Delta P_{11}$** | N/A | N/A | N/A | -0,5 | -0,3 | -0,08 |
| **$\Delta P_{12}$** | N/A | N/A | N/A | -0,02 | -0,4 | -0,7 |

## Core shift analysis

In addition to the filling analysis, core shift analysis was conducted with Moldex3D to analyze possibility for insert cracking or bending. For a core shift analysis, a separate simulation model consisting part and tool insert was constructed. As the model used for core shift analysis is different from the one used in the part filling simulation, there might be some difference in filling times and pressure levels which affect results. This should

be noted when results from the core shift analysis are compared to ones from the part filling study. Part and insert were imported to Moldex3D as assembly stp -file. In order to run a core shift analysis, the part and tool insert model need to have correspond meshing at the surfaces which are in contact with each other. This was done by copying the surface mesh from the insert and attaching it to the part model. Noticeable is that tool insert need to be defined as part insert to run the core shift analysis. In the end, insert and part model consists 1 877 679 solid mesh elements. Boundary conditions for the core shift simulation are similar to ones presented in figure 145. Insert is fixed from the top and side surfaces as highlighted with light blue arrows in the figure. Top surface is fixed in z-direction and side surfaces in x- and y-direction.

Highest Von Mises stresses during filling are found at 1,817 s when filling is changed to packing stage and at the end of filling. Figure 167 and figure 168 show Von Mises stress distribution in the insert at 1,817 s. Maximum stress at 1,817 s is 1279,485 MPa in one of the insert corners (exact location shown in figure 167). However, this high stress concentration is very local, as based on figure 169, it is found in less than 0,00 % of the insert. Otherwise, high stresses are found near the rib cuts and from the insert base area. Few points, in these locations undergo stress higher than the fatigue limit, 330 MPa, of the material. On the second side of the insert (shown in figure 168), high stresses are found on the rib cuts but otherwise stresses are below 300 MPa. Figure 169 shows that 99,31 % of the insert undergoes stress between 0,079 MPa and 128,020 MPa. And stresses above 255,96 MPa are found on 0,01 % of the part.

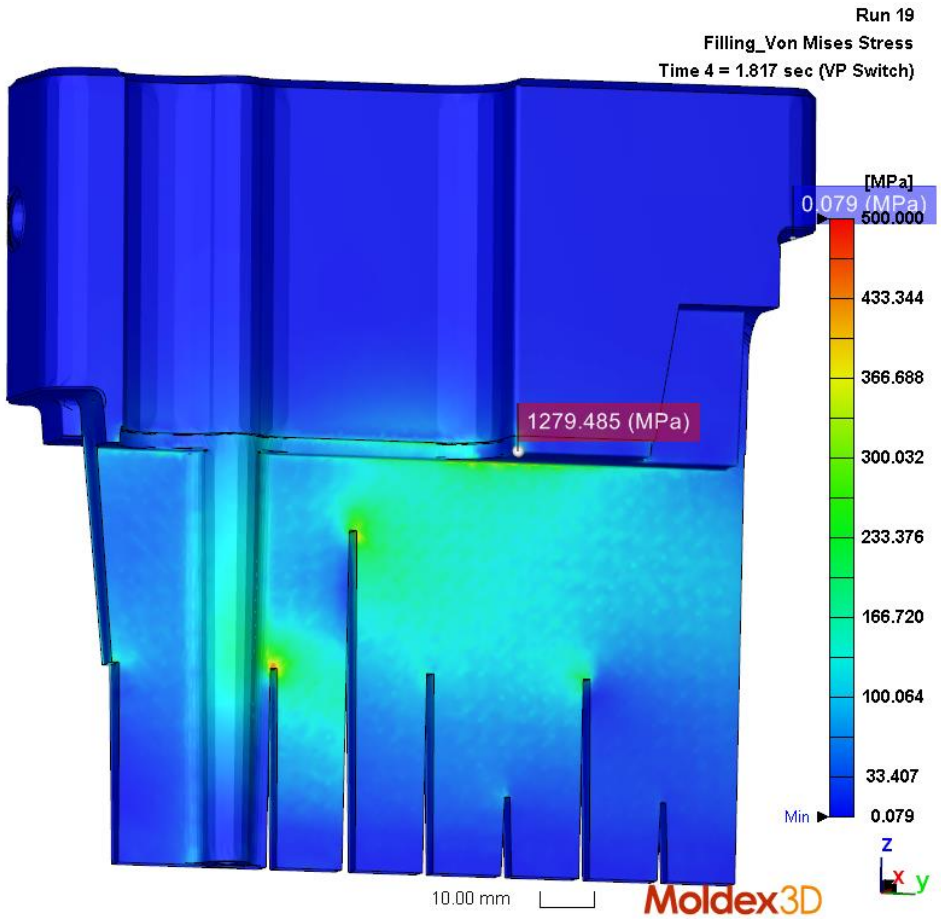


*Figure 167 Von Mises stress in the tool insert side 1 at 1,817 s. Scale is adjusted to be between 0,079 MPa and 500 MPa to visualize better stress distribution inside the insert.*

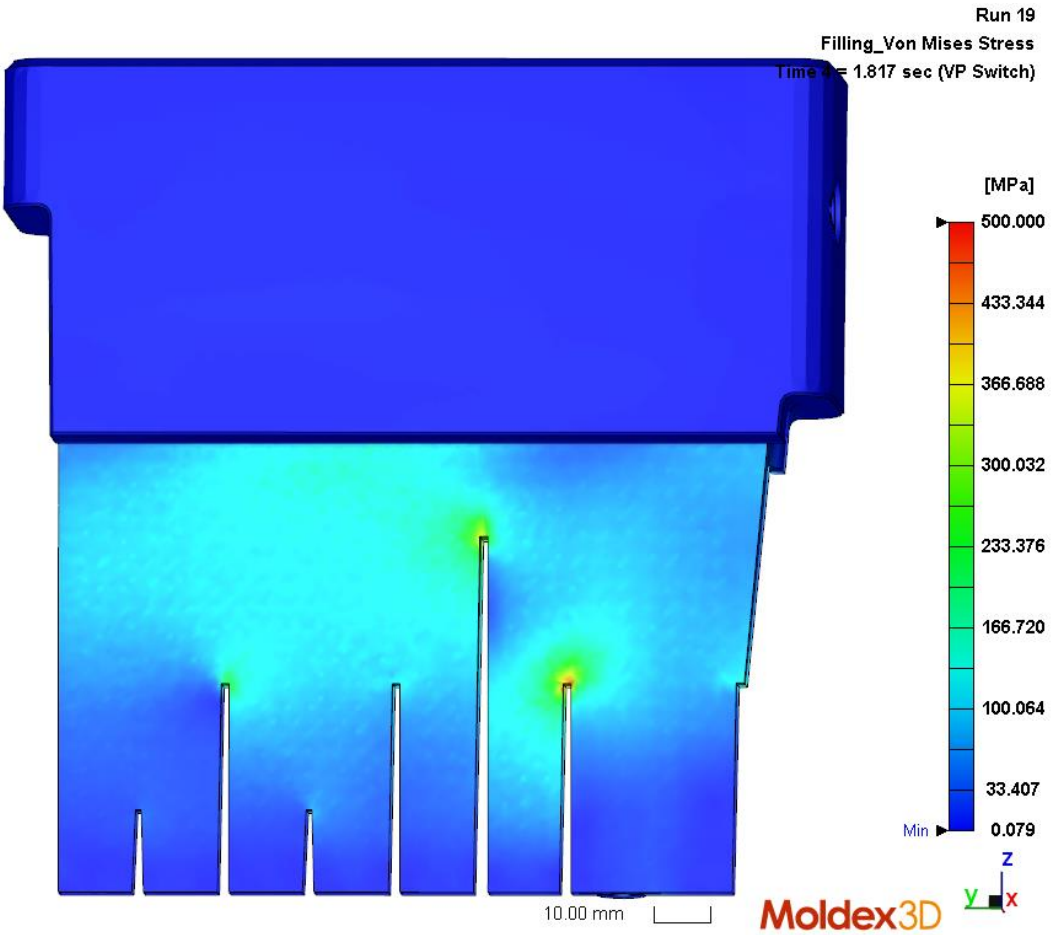


*Figure 168 Von Mises stress in the tool insert side 2 at 1,817 s. Scale is adjusted to be between 0,079 MPa and 500 MPa to visualize better stress distribution inside the insert.*

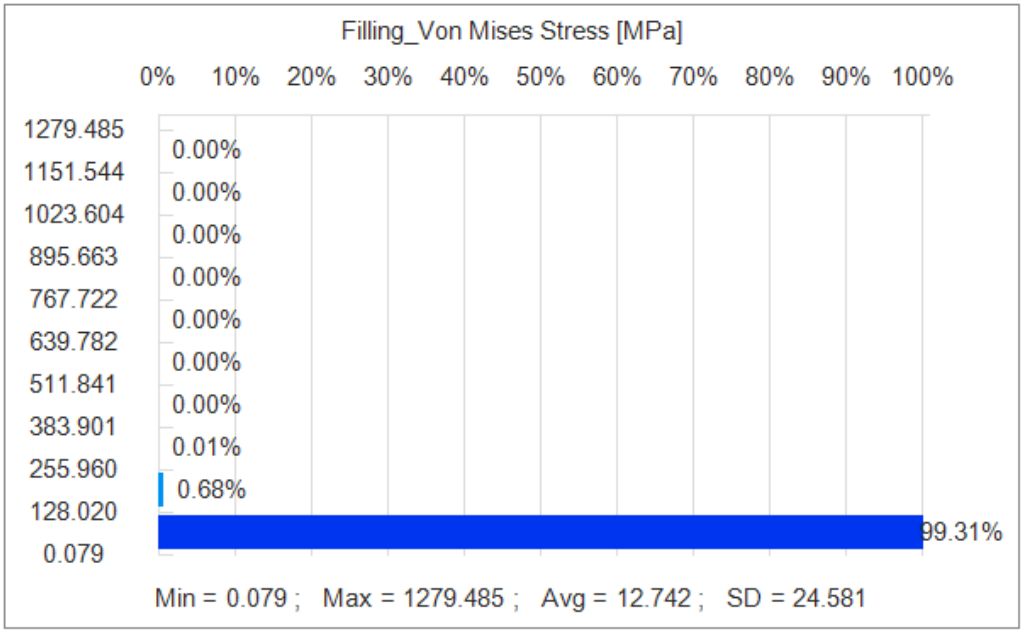


*Figure 169 Distribution of Von Mises stress in the tool insert (at 1,817 s). Maximum stress 1279,485 MPa is noted to be local as it appears in less than 0,00% of the part. 99,31 % of the part has stress below 128,020 MPa and average stress is 12,742 MPa.*

Figure 170 and figure 171 show Von Mises stress in the insert at the end of filling. At the end of filling, maximum stress has increased to 1356,150 MPa. Location of the maximum stress is same as before and that high value can result from meshing inaccuracy of small features. High stresses are found near rib cuts and on the base area but otherwise stresses have slightly decreased from the situation at 1,817 s. At the end of filling, stresses only on the first rib cut (the leftmost rib cut in figure 170) exceeds material's fatigue limit, 330 MPa. 99,72 % of the part undergoes stress between 0,180 MPa and 135,777 MPa, and only 0,01 % exceeds 271,374 MPa (see figure 172).

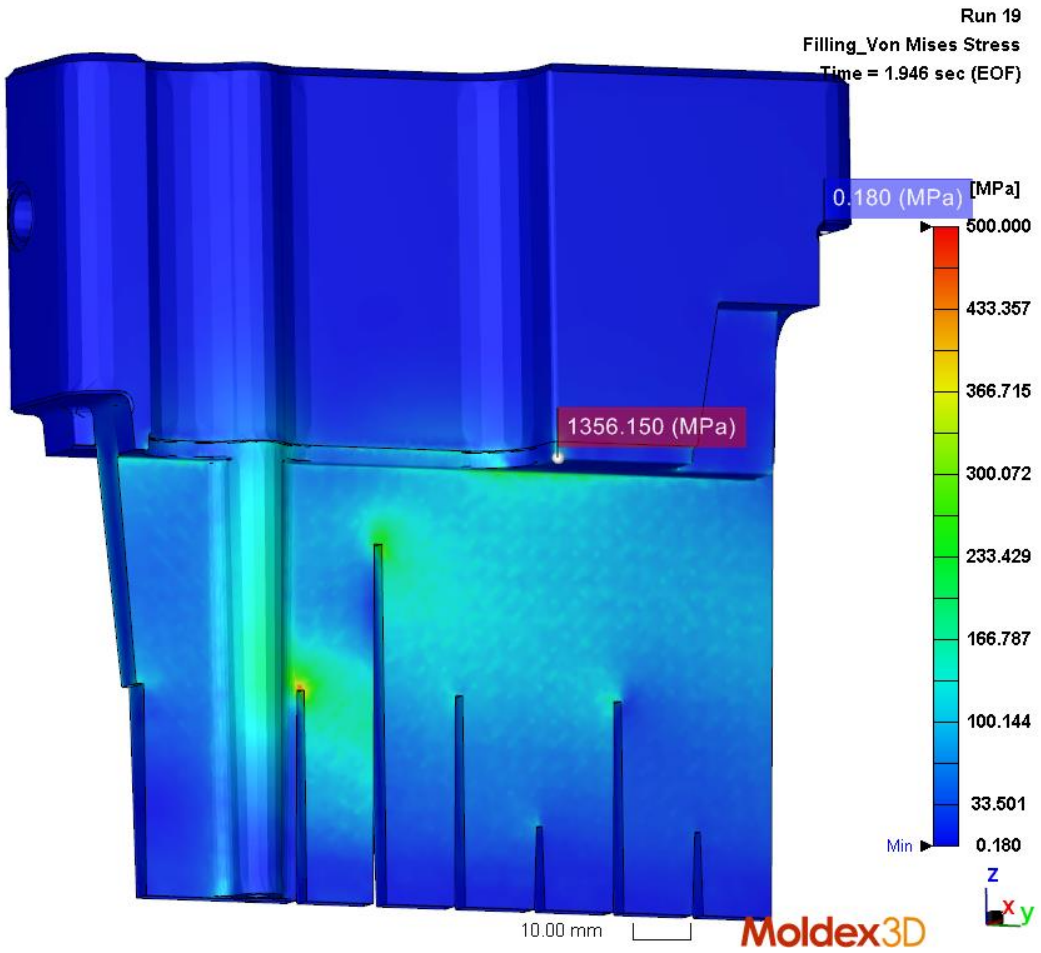


*Figure 170 Von Mises stress at the end of filling (side 1). Maximum value is 1356,150 MPa.*

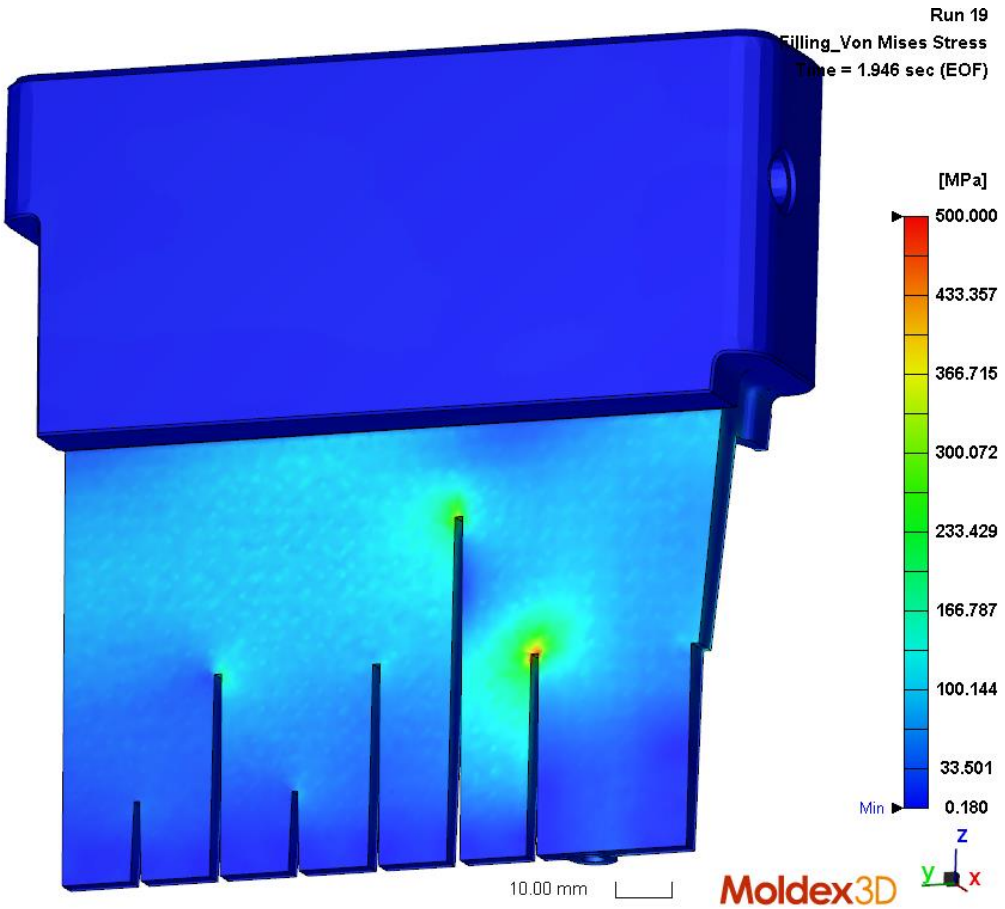


*Figure 171 Von Mises stress at the end of filling (side 2).*

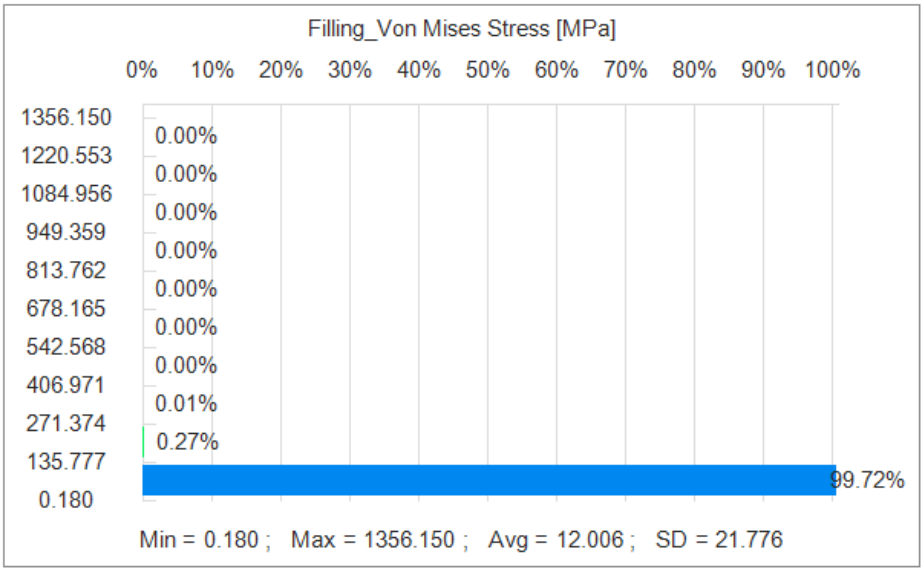


*Figure 172 Distribution of Von Mises stress at the end of filling.*

As discussed previously, highest stresses in the insert were found at 1,817 s. Due to this, it is consistent that highest displacement values are as well found at 1,817 s. Figure 173 shows displacement in x-direction at 1,817 s and figure 175 at the end of filling. Distribution (as percentage) of displacement in x-direction at corresponding time steps are shown in figure 174 and figure 176. At 1,817 s, maximum displacement is 0,386 mm and minimum -0,947 mm (figure 173). Positive value means that insert bends towards plastic part's inner wall. This is noted to happen on the leftmost part of insert (refer to

figure 173). Highest negative values are concentrated on the area next to the high rib. As the high rib cut decreases strength of the insert and as high stresses were found near it (refer figure 167 and figure 168), it's logical that highest values are found from that area. Most of the part (87,94 %) experiences displacement of -0,014-0,120 mm. However, displacements above 0,253 mm and below -0,280 mm are found from 0,63 % and 3,48 % of the insert. These high displacements represents over 10 % of the part's wall thickness.

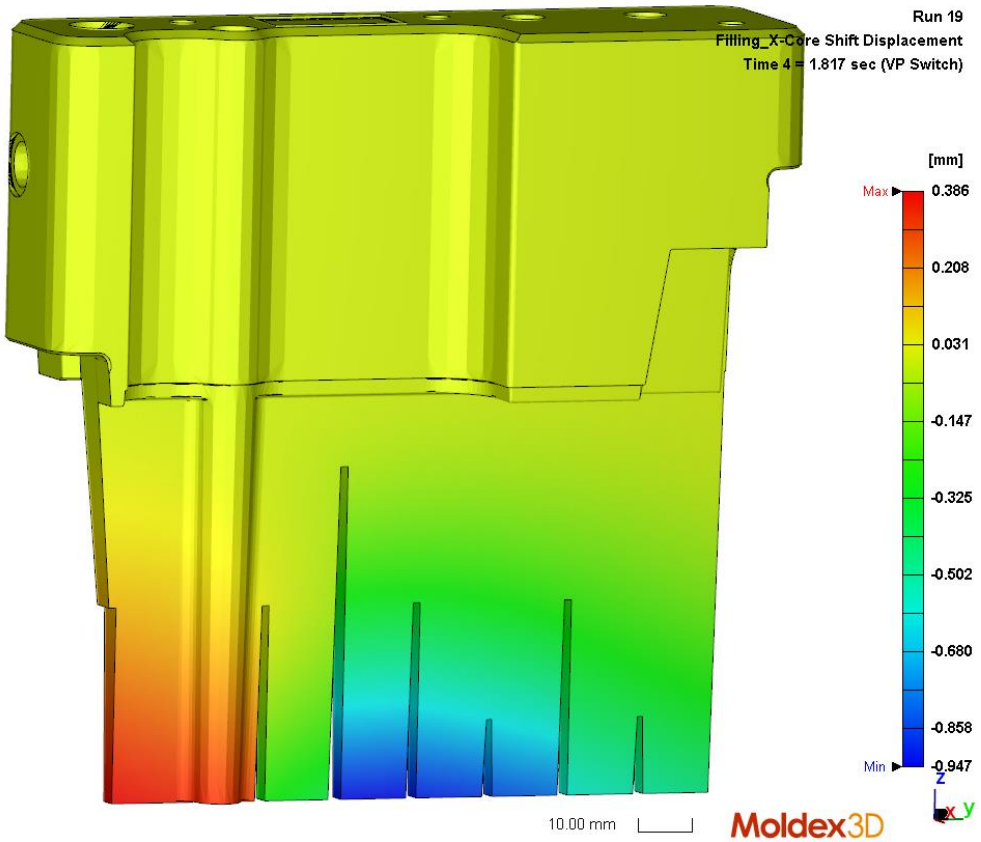


*Figure 173 Displacement in x-direction, at 1,817 s.*

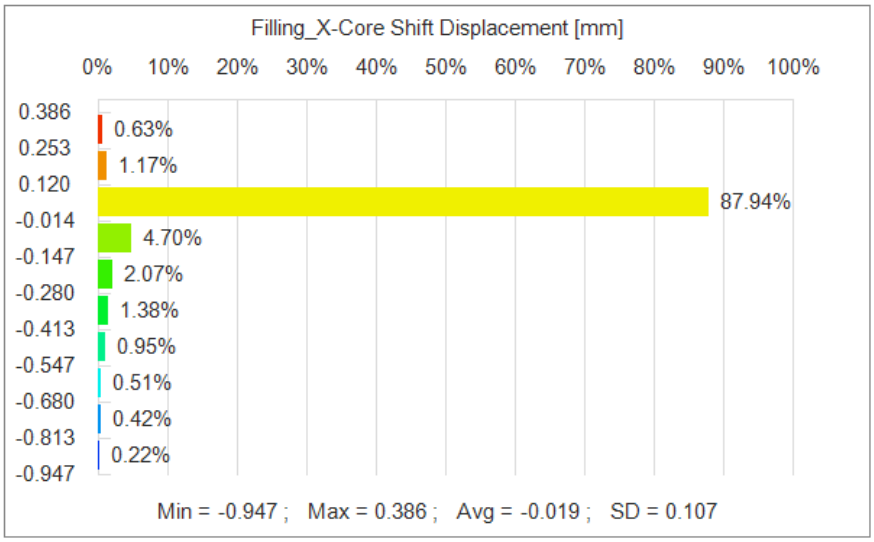


*Figure 174 Displacement (x-direction) distribution in the insert at 1,817 s.*

At the end of filling, maximum displacement is 0,432 mm and minimum -0,771 mm (see figure 175). Maximum and minimum values are located on the same areas as at 1,817 s.

As stresses at the end of filling were lower than at 1,817 s, it is logical that minimum displacement is smaller than it was at 1,817 s. 89,81 % of the part experiences displacement between -0,049 mm and 0,071 mm (see figure 176). Displacement values over 0,312 mm and below -0,290 mm are found from 0,58 % and 2,69 % of the insert.

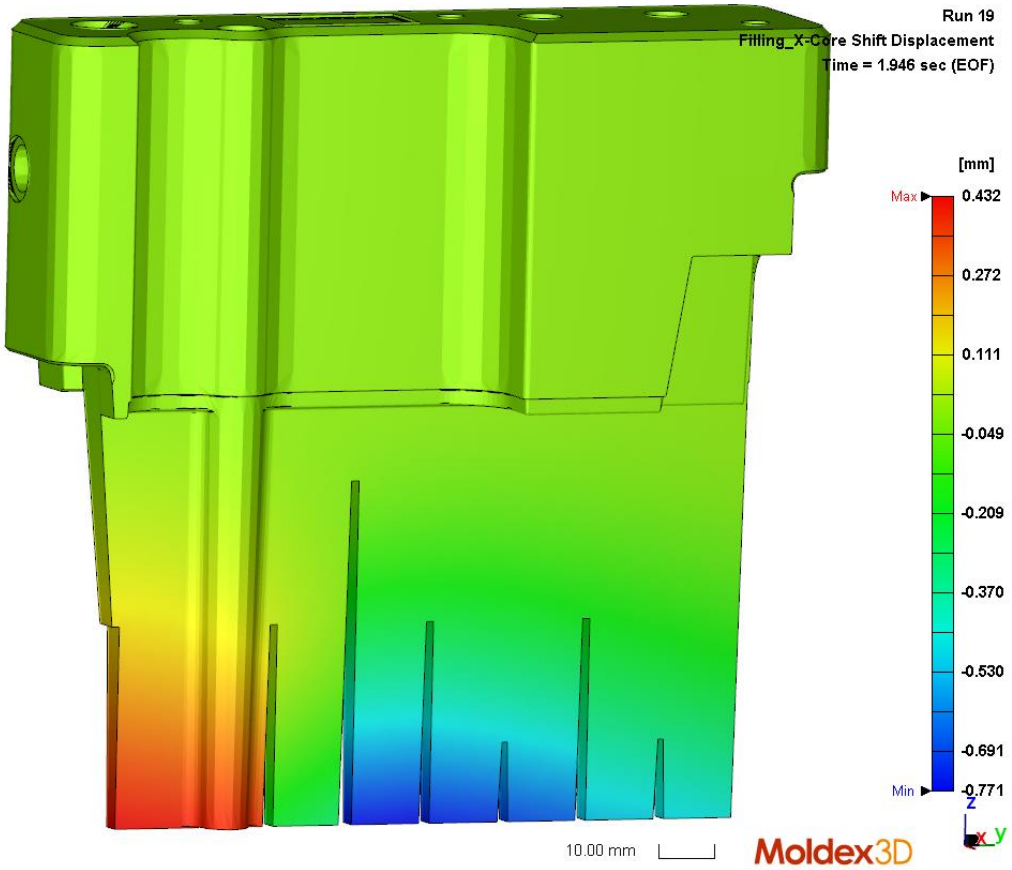


*Figure 175 Displacement in x-direction, at the end of filling.*

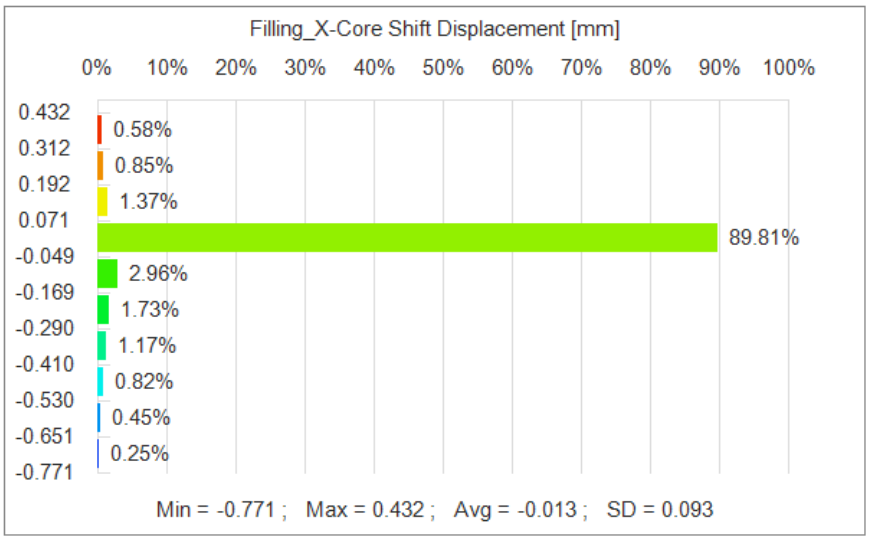


*Figure 176 Displacement (x-direction) distribution in the insert at the end of filling.*

If these results of core shift displacement are compared to previously discussed pressure differences in table 18, it is noted that pressures, at the area shown with red in figure 173, are higher on the outer wall of the part which bends the insert towards the part's inner

wall. Area shown with blue corresponds to probes 8-10 at table 18, and on that area pressure differences are 0,3-1,1 MPa at 1,655 s. Consequently, pressure in the inner wall is higher which starts to bend the insert towards part's outer wall and negative values are seen in figure 173. At the end of filling, pressure differences (based on table 18) on probes 6-10 are 0,4-0,6 MPa and not such high that they would cause high displacements.

### 5.2.4 Comparison of designs

First two cases, presented in sections 5.2.3.1 and 5.2.3.2, were simulated with the initial part design and gating locations. These two cases have been molded before these simulations and in the molding trials, insert cracking and bending was noticed. Filling simulations were done to see the pressure levels in these designs, which gave some estimation of the pressure values causing the insert failure. Four other cases were studied to find out the best design to decrease the pressure levels during filling, and to minimize the probability for insert cracking or bending. Table 19 shows maximum pressure differences at the insert base and tip collected from all six cases, based on the probes attached to the models. Notable is that probes aren't in exact same locations, but they give reference of the pressure level in the area near them.

*Table 19 Comparison of pressure differences in different designs.*

| | **Max pressure difference at insert base** | **Max pressure difference at insert tip** |
|---|---|---|
| **Initial design, 2 gating points** | 24,8 MPa | 1,7 MPa |
| **Initial design, 4 gating points** | 27,9 MPa | 1,3 MPa |
| **Modified part design, 2 gating points** | 22,4 MPa | 0,4 MPa |
| **Modified part design, 4 gating points** | 32,4 MPa | 0,5 MPa |
| **Two higher ribs, gating from the rib area** | 10,4 MPa | 2,1 MPa |
| **Two higher ribs, thinner inner wall and gating from the rib area** | 10,7 MPa | 2,5 MPa |

Initial part designs with two and four gating points showed pressure differences over 20 MPa during the filling in the insert base area. With two gating points maximum values at insert base was 24,8 MPa at 1,150 s and with four gating points, maximum value was 27,9 MPa at 1,650 s. At the insert tip area, pressure differences were 1,7 MPa with two gating points, and 1,3 MPa with four gating points. Pressure difference exceeded 20 MPa for 0,5 s when two gating points were used, and with four gating points it lasted 0,2 s.

Modifications presented in sections 5.2.3.3 and 5.2.3.4 decreased the pressure differences in the insert tip area. Modified part geometry with two gating points decreased the maximum pressure difference at the insert base slightly to 22,4 MPa. However, pressure difference over 20 MPa affects the insert base for 0,8 s which is more than with the initial design. Though, pressure differences at the insert tip are small, as the maximum value is 0,4 MPa.

Modified part design with four gating points made pressure differences at the insert base worse than in the beginning with initial design. Now the maximum pressure difference was 32,4 MPa and insert base had pressure difference over 30 MPa for 0,4 s. Pressure differences at the insert tip area were on the same level as with two gating points but the high pressure differences at the insert base, most likely induces similar cracking problems as before. As the modified design improved the filling pattern on the insert tip area, and decreased pressure differences there, pressure differences at the insert base are close to values which caused insert cracking in the molding trials with the initial design. Therefore, neither of these designs was chosen for the new molding trials.

Two of the original ribs were modified to be 62 mm high and gating points were moved on the rib area to ease the melt flow to the outer wall. This was done to decrease the pressure differences at the insert base, which were in all previous cases over 20 MPa. A significant change was noticed in the filling pattern, as the melt started to flow to the outer wall of the part straight after beginning of filling. Flows on inner and outer walls moved on quite similar phase, flow on the inner wall being slightly ahead. Pressure differences at insert base were decreased to 10,4 MPa at maximum, and pressure differences exceed 10 MPa only for 0,3 s. Pressure differences also in the insert tip were quite well balanced and only exception for this was noticed in locations of probes 6 (refer to figure 138 and table 17) where pressure difference increases to -2,1 MPa during filling. As the value is negative, pressure in the outer wall is higher than in the inner wall, which indicates that melt flows better in the outer wall. This is reasonable as shape of the outer wall is straight and inner wall has more shapes which slows the melt flow. Core shift analysis indicated that high stress concentrations would be on the insert base at the round surface (refer to figure 146 and figure 149). Some of high stresses (slightly below or over 500 MPa) can result from small rounds on the insert base, and from meshing accuracy of small shapes. Otherwise near the gating area and near the rib cuts, stresses are slightly below and above 200 MPa. These values are reasonable as there aren't any rounds on the rib cuts and fatigue stress limit for the insert material is 330 MPa. Maximum displacement (in x-direction), -1,161 mm, occurred near location of probe 6 where pressure difference was 1,6-2,1 MPa.

In order to even the melt flow in inner and outer wall, thickness of plastic part's inner wall was decreased by 0,5 mm. Due to this, higher filling pressure is required but pressure differences should decrease. Filling pattern was improved from the previous case as the melt had flown already after 0,506 s to upper part of the outer wall. Pressure differences were like ones before but slightly higher due to higher filling pressure. Pressure differences at the insert base were above 10 MPa for the first 0,8 seconds from where they started to decrease as plastic filled more the outer wall. Pressure differences on the insert tip were higher than in the previous study but still in a reasonable level as the maximum value, -2,5 MPa, was found from probe 6 at 1,655 s (refer to table 18). Core shift analysis for this design showed that Von Mises stress acting on the insert during filling exceeds material's fatigue limit only in few local positions (in 0,01% of the insert). Also, displacement values showed improvement when compared to previous case, as the maximum displacement (in x-direction) was decreased to -0,947 mm. Displacement values over -0,413 mm was noticed in 2,1 % of the part (see figure 174) which is relative small percentage and high displacements can be assumed to be local.
Based on more balanced melt flow in inner and outer walls, and decreased Von Mises stresses and displacements, last option was chosen as the design to be used in the new molding trials. Core shift analysis showed that Von Mises stress increased materials fatigue limit in only 0,01 % of the insert, which is assumed to decrease risk for insert

cracking. Based on this, material of the inserts was kept as beryllium copper. As more balanced melt flow was achieved with this design, possibility for insert bending is assumed to be smaller than with the initial designs. As the simulation model didn't have any rounds, results from core shift analysis (Von Mises stress and displacements) are expected to be lower in the real molding experiences where inserts have rounds. To decrease the risk for insert breaking, radius of the rounds at insert base were increased from the initial design. Also, to improve melt flow to the outer wall, one additional rib was added to the design. Location of this rib is the same as presented in figure 113 in section 5.2.3.3.

First molding trials with the new inserts were made in November 2019, and inserts weren't noticed to bend or have cracks after the trials. Duration of this test was four hours and new inserts seem to be working better than the initial ones, which failed straight after few molding cycles. Based on these preliminary results from the molder, design changes for the part and gate locations seem to have even the melt flow and decreased the pressure differences over tool inserts, as the simulation results indicated.

### 5.2.5 Conclusions

Injection molding simulation was used to study melt pattern and pressure levels during filling in different designs. Furthermore, pressure differences affecting over the tool inserts were calculated based on the filling simulation. Core shift analyses were conducted for two designs to estimate stresses concentrating on inserts and to estimate displacement of the inserts. However, forming simulation model for core shift analysis took more time than preparing model for filling analysis. With simulation, different designs were easy to compare, and decision of the best design was done based on the simulation results. New molding trials showed that results from simulation correlated to the ones seen in the trials, as the inserts bore four-hour test run, whereas the initial inserts cracked.

This case study showed that possible risk areas in mold can be identified by studying pressure levels and differences based on filling analysis. With core shift analysis estimation of stress levels on inserts can be calculated to analyze if stresses are below material's strength. As these simulation studies were made after the mold failure, it is noticeable that problems might have been avoided if simulation would be used before the mold construction. During the work of this case study, it was noticed that mold manufacturer wasn't aware of that the high pressure differences present in the initial design, could cause cracking of the insert. It was helpful to have simulation results also on ABB's side to compare results with ones provided by the mold manufacturer as there were matters that the mold manufacturer hasn't taken into account. Based on results from this case study, it is recommended to run at least filling analysis to study the filling pattern and pressure levels. If part has shapes that will require use of thin and high inserts, more attention should be put on studying also pressure differences over the inserts.

### 5.2.6 Possible error sources

Simplified simulation model was used to this study as the runner system was excluded from the simulation and only gating points were specified. This can cause difference between pressure levels predicted by the simulation, and pressures seen in the real molding process. However, excluding the runner system affect the pressure levels and not the pressure differences inside the part. Part models used for simulation were also

simplified by excluding most of the rounds. This was done to ease the meshing and to make it more accurate as the rounds in the part are small. In cases presented in sections 5.2.3.3 and 5.2.3.4, all of the rounds couldn't be excluded which decreased meshing quality in the areas having small rounds.

Filling studies were made to different simulation models than the core shift analyses as it requires also insert model. This can cause differences between results from filling studies and core shift analyses. Results from core shift analyses showed some high Von Mises stress values on few locations. As these stresses were noticed to be local, based on the figures showing stress distribution in insert as percentages, extremely high displacements were assumed to result from inaccurate meshing of small rounds.

Results from filling studies between different designs were compared with 12 probe pairs. These probe pairs didn't locate in exactly same locations in all the cases, which can cause variation between values of different cases. However, probes represent pressure level on the area near them which is why they are used to compare different designs.

# 6 Conclusions and discussion

Object of this thesis was to assure product quality and its manufacturability by injection molding simulation. This consisted of studying how well the results from simulation correspond to results seen in real molding process, and as another study, gaining more information by simulation what causes a premature mold break and how it can be prevented.

First case study analyzed the equivalence of simulation results and real molding process by simulating a product which behavior in injection molding is known. Product for this case was chosen to be IP21 cover of R1 sized drive as its mold model and process parameters were known. Constructing the simulation model was noticed to be quite laborious as the cooling channels needed first to be copied from the mold model into a separate file in Creo. After this, cooling channels were imported to Moldex3D environment where channels needed to be remodeled based on the imported channels. If channels aren't modelled in the Moldex3D environment, simulation software doesn't handle the channels correctly. Overall, as the cooling channels need to be remodeled in the Moldex3D environment, it is recommended to model simplified cooling channels in Moldex3D, by its own cooling channel tools, if the real cooling channel design isn't necessarily needed. Process parameters used for simulation were got from the part's injection molder, which reported the parameters as machine-depended. This required some additional work as the pressures needed to be converted from hydraulic to absolute pressures. Also, parameters were reported quite unclearly and solving these matters took some time. To improve this communication about the process parameters, it would be recommended to make a process parameter form by ABB, which would be sent to injection molder to be filled. Process parameters in the form shouldn't be machine-related and require any conversions to absolute values.

Simulation results showed higher warpage values than is seen in the real molding process, although simulation model was constructed to be equivalent with the real mold. Also process parameters were the same as used by the injection molder. One possible cause for high displacements can be in the cooling system, which handled all cooling channels as separate channels. In a real mold these channels would be chained together outside the mold by hoses, in order to have fewer cooling circuits. According to representatives of Moldex3D, high displacements can result from an inaccurate material data in Moldex3D material bank. Due to this, simulation was conducted with an alternative material, but results from warpage analysis showed displacement values similar to earlier ones. However, alternative material was from same manufacturer as the initial one, which can explain why similar displacements occurred. As simulation results of this case showed higher displacements than tolerances allow, more study should be done to find out what reasons are causing the displacements. One possibility would be to do comparative studies with a few different materials from different manufacturers, to see if the displacements are as high.

Effects of cooling channel design, molding parameters and molding material were also studied in the first case. Results showed that no big differences were seen when using simplified cooling channels instead of real cooling channels. Use of default process parameters from Moldex3D resulted slightly higher displacement values than simulation with real process parameters. However, difference wasn't big, which indicates that quite accurate results can be achieved with the default parameters. This gives confidence to make decisions based on simulation results. One study was made with polypropylene to

see how it behaves in a mold designed for PC-ABS. Results showed that displacement values were slightly higher than with PC-ABS, as polypropylene has higher shrinkage than PC-ABS. However, by adjusting the process parameters, polypropylene could most likely be used in the same mold. One object for future study would be to find the process window for polypropylene.

In the second case study, dynamic loads causing a tool insert failure were studied. This case study was based on real case in which mold inserts failed during the first molding trials. In order to find out the causes for the insert cracking and bending, molded part was simulated with Moldex3D. Filling studies showed that there were over 20 MPa pressure differences over the tool insert which were most likely the cause of cracking at the insert base. These high pressure differences over the tool inserts were noticed to result from uneven filling pattern, where one side of the insert filled much before the other. To even the pressure differences on the insert base, design changes were made to the part. These changes were noticed to increase the pressure differences even more, which was assumed to cause another insert failure. In order to balance the flow pattern, two of the original ribs on the part were made higher to ease the melt flow to other side of the insert. To ensure that melt starts to flow on the other side at the beginning of filling, gating locations were changed to be in direct connection with the high ribs. These changes balanced the flows on both sides better than what was the case with previous designs. To improve this design more, inner walls of the part were made 0,5 mm thinner. As this slowed the melt front on the inner wall of the part, plastic had more time to flow on the outer wall, which balanced the filling pattern. Furthermore, results from core shift analysis showed that Von Mises stresses were mostly below the beryllium copper's fatigue strength, 330 MPa, which indicated that cracking problems should be avoided. Values higher than the fatigue strength limit were noticed only on few locations, which were assumed to be due to meshing inaccuracy of small rounds or due to exclusion of small rounds. For the design to be used in the new molding trials, bigger radius was set for the insert base and to the ribs to decrease the risk for high stresses. Displacements of core shift analysis showed values of 0,947 mm, maximum, but they were noticed to be very local. Based on these reasons, this design was analyzed to have the smallest risks for insert cracking and it was chosen for the new molding trials.

First molding trials with the new inserts were made in November 2019 and inserts weren't noticed to bend or have cracks after molding. Duration of the test was four hours and results from it indicate that the chosen design works better than the initial design, where the problems were noticed straight after few molding cycles. Based on results from simulation and new molding trials, design changes of the part and changed gate locations balanced melt flows and decreased pressure differences over the tool inserts, thus reducing the risk for insert breaking.

Core shift analysis requires the tool insert to be defined as a part insert. Also, insert mesh needs to match with the part mesh in places where they are in contact. This was solved by copying the mesh from the insert and attached it to the part. Quality of mesh was noticed to have great impact on the core shift analysis. If the meshes of part and insert don't match each with other, core shift analysis couldn't be simulated. Another crucial matter affecting the results were the boundary conditions defined for the insert. If high number of boundary conditions were defined, core shift calculation didn't succeed even though limitations were set based on real conditions. Probably too many boundary conditions make the computing too complex to be solved, especially when the number of meshed elements is high. Overall, use of core shift analysis requires more work than basic

filling simulation, but it can give rough estimation of insert deflection and stresses affecting the inserts.

Dynamic loads on mold inserts were planned to study also with practical molding experiments to verify the findings from the simulation. These studies were planned to have a test part which would be manufactured with high and thin tool inserts. Tool inserts were planned to have sensors to measure the forces affecting the inserts during injection molding. These experiments couldn't be carried out during this thesis work due to problems regarding the practical arrangements with the mold, which arose in the last minutes of the thesis work. Therefore, the test part case study was excluded from this thesis, and the practical problem case presented as case 2 was studied instead. However, practical experiments of the dynamic loads on the mold inserts are recommended to be studied in a future work. This could be carried out by adding sensors to the mold and measuring insert deflection or forces during injection molding. One possibility could be to use strain gauges measuring the deflection. Tool inserts could have small drillings, which are equipped with separate inserts like ejector pins having strain gauges on their surfaces. This way deflection of the tool insert could be measured without the strain gauges touching the plastic melt.

During the work of case 2, problems were solved together with the mold manufacturer. It was noticed to be useful to have also own simulation results to compare with the ones provided by the mold manufacturer. In the meetings, there were noticed to be some things that the mold manufacturer hadn't considered, which could have led to selection of solution causing another insert failure. Having the simulation software available gives an easy tool to check the changes suggested by the mold manufacturer or injection molder, and to analyze the possible problem areas causing high loads and stresses to tool inserts.

Studies in this thesis provided information on simulation tools available and their advantages. By injection molding simulation, analysis of a product design and its manufacturability can easily be done. Also, in case of having features which require use of high and thin tool inserts, simulation can help predict the pressure loads concentrating on the insert. Furthermore, with a core shift analysis, amount of stresses and locations of them can be reviewed.

Studies in this thesis showed that simulation is a helpful tool to estimate pressure levels during injection molding and with more specifies analysis stresses concentrating on mold inserts can also be estimated. Simulation should be used to check product's filling pattern and pressure levels. If product geometry requires inserts, pressure levels over them should be reviewed to prevent mold failures in the future. Based on the results of this thesis, experienced mold failure case could have been avoided completely, if more attention had been put into pressure loads on the area of tool inserts. Additionally, simulation should be used to analyze effects of changes to product or mold geometry, to have grounds for decision making. When considering possible mold-related changes, it would be recommended to have simulation-based results on ABB's side also, as it helps to understand influences of them. In a future work, inconsistency in results of IP21 cover should be analyzed more and practical study to measure real dynamic pressure loads on mold should be conducted.

# References

**ABB Oy. 2019.** ABB Oy, Drives. [Online] 2019. [Cited: September 26, 2019.] https://new.abb.com/fi/abb-lyhyesti/suomessa/liiketoiminnat/drives.

**ABB Oy. 2019.** ACS580-01 quick installation and start-up guide for frames R1 to R5. 3AXD50000044838 Rev D. [Online] 30 June 2019. [Cited: 12 July 2019.] https://search.abb.com/library/Download.aspx?DocumentID=3AXD50000044838&LanguageCode=da&LanguageCode=de&LanguageCode=en&LanguageCode=es&LanguageCode=fi&LanguageCode=fr&LanguageCode=it&LanguageCode=nl&LanguageCode=pl&LanguageCode=pt&LanguageCode=ru&Languag.

**ARBURG. 2018.** Product range ALLROUNDERs. [Online] September 2018. [Cited: July 18, 2019.] https://www.arburg.com/fileadmin/redaktion/mediathek/prospekte/arburg_product_range_allrounders_680652_en_gb/#.

**Bryce, Douglas M. 1996.** *Plastic Injection Molding, Volume I - Manufacturing Process Fundaments.* Dearborn, Michigan: Society of Manufacturing Engineers (SME), 1996. 268 p. ISBN (electronic) 978-1-61344-976-9.

**Burkhardt, Gert, et al. 2012.** *Plastics Processing, 1. Processing of Thermoplastics*. In Ullmann's Encyclopedia of Industrial Chemistry. Weinheim: Wiley-VCH Verlag GmbH & Co. KGaA, 2011. P. 367-388. DOI 10.1002/14356007.a20_663.pub2.

**Calhoun, Allison R. and Golmanavich, Jerry. 2004.** *Plastics Technician's Toolbox.* Brookfield, Ct : Society of Plastics Engineers, 2004. 831 p. ISBN (electronic) 1-59124-995-3.

**Campo, E. Alfredo. 2006.** *The complete part design handbook - For injection molding of thermoplastics.* Munich: Cincinnati : Hanser Publishers; Hanser Gardner Publications cop., 2006. 891 p. ISBN (electronic) 978-1-60119-152-6.

**CustomPart.net. 2019.** Injection Molding. [Online] 2019. [Cited: February 28, 2019.] https://www.custompartnet.com/wu/InjectionMolding.

**DIN 16742. 2013.** *Plastics moulded parts - tolerances and acceptance conditions.* Berlin : Plastics Standards Committee (FNK). 72 p.

**Dong-Gyu, A., Dae-Won, K. and Yeol-Ui, Y. 2010.** Optimal injection molding conditions considering the core shift for a plastic battery case with thin and deep walls. *Journal of Mechanical Science and Technology.* February 2010. Vol. 24:1. P. 145-148. DOI 10.1007/s12206-009-1126-5.

**Fischer, Jerry M. 2003.** *Handbook of Molded Part Shrinkage and Warpage.* Norwich, N.Y. : Plastics Design Library: William Andrew Pub cop., 2003. 263 p. ISBN (electronic) 1-59124-592-3.

**Francis, Lorraine F., Stadler, Bethanie J.H. and Roberts, Christine C. 2016.** *Materials Processing - A Unified Approach to Processing of Metals, Ceramics and Polymers.* Amsterdam : Elsevier, 2016. 614 p. ISBN (electronic) 978-0-12-385133-8.

**Gelotte, Ryan and Broadbent, Matthew. 2007.** *Validation of Injection Molding Simulation Results to Actual Molded part.* In Annual Technical Conference - ANTEC, Conference Proceedings. Cincinnati, Ohio, USA: 6-11.5.2007. Society of Plastics Engineers Annual Technical Conference: Plastics Encounter at ANTEC 2007, 2007. Vol. 4, pp. 2456-2460. ISBN (electronic) 978-1-60119-877-8.

**Goodship, Vanessa. 2017.** *ARBURG Practical Guide to Injection Moulding.* 2nd edition. Shewsbury : Smithers Rapra Technology, 2017. 380 p. ISBN 978-1-91024-294-0.

**Goodship, Vanessa, Middleton, Bethany and Cherrington, Ruth. 2016.** *Design and manufacture of plastic components for multifunctionality - structural composites, injection molding, and 3D printing.* Amsterdam : Elsevier, 2016. 236 p. ISBN (electronic) 978-0-323-35384-7.

**Kalpakjian, Serope, Schmid, Steven R. and Musa, Hamidon. 2010.** *Manufacturing engineering and technology.* 6th edition. 1216 p. Singapore : Prentice Hall, 2010. ISBN 978-981-06-8144-9.

**Kalpakjian, Serope, Schmid, Steven, R. and Sekar, K. S. Vijay. 2014.** *Manufacturing engineering and technology.* 7th edition. 1216 p. Singapore : Pearson cop., 2014. ISBN 978-981-06-9406-7.

**Kazmer, David. 2007.** *Injection mold design engineering.* Munich: Cincinnati : Hanser; Hanser Gardner, 2007. 444 p. ISBN (electronic) 978-1-61344-296-8.

**Kazmer, David O. 2016.** *Injection mold design engineering (2nd edition).* Munich: Cincinnati : Hanser; Hanser Publications, 2016. 466 p. ISBN (electronic) 978-1-5231-0587-8.

**Kelly, A.L., et al. 2011.** *The effect of copper alloy mold tooling on the performance of the injection molding process*. In Polymer Engineering and Science. 2011. Vol. 51:9, pp. 1837-1847. DOI 10.1002/pen.21975.

**Kim, J.K. and Lee, C.S. 2013.** Fatigue life estimation of injection mold core using simulation-based approach. *International Journal of Automotive Technology.* October 2013, Vol. 14:5, pp. 723-729. DOI 10.1007/s12239−013−0079−y.

**Kulkarni, Suhas. 2017.** *Robust process development and scientific molding - theory and practice.* 2nd edition. Munich: Cincinnati : Hanser Publishers, 2017. 272 p. ISBN (electronic) 978-1-5231-1186-2.

**Kulkarni, Suhas. 2010.** *Robust Process Development and Scientific Molding - Theory and Practice.* Munich: Cincinnati : Hanser Publications, 2010. 272 p. ISBN (electronic) 978-1-61344-298-2.

**Kutz, Myer. 2017.** *Applied Plastics Engineering Handbook - Processing, Materials, and Applications.* 2nd edition. Amsterdam: Boston : William Andrew cop., 2017. 784 p. ISBN (electronic) 978-0-323-39041-5.

**Mennig, Günter and Stoeckhert, Klaus. 2013.** *Mold-making handbook.* 3rd edition. Munich: Cincinnati : Hanser Publishers, 2013. 700 p. ISBN (electronic): 978-1-68015-483-2.

**Moldex3D. 1995-2019.** 4. Warp Tab. *Moldex3D R17 Help.* [Online] Moldex3D, 1995-2019. [Cited: November 7, 2019.] file:///C:/Moldex3D/R17/Help/en/index.html#2-6-4_warptab.html.

**Moldex3D. 1995-2019.** Core shift. *Moldex3D R17 Help.* [Online] 1995-2019. [Cited: September 12, 2019.] file:///C:/Moldex3D/R17/Help/en/index.html#3-6-5-1_coreshift.html.

**Mäkelä, Mika and Palojoki, Vesa. 2019.** *How much ABB produces plastic parts yearly.* Helsinki: Pitäjänmäki, August 7, 2019.

**Palojoki, Vesa. 2019.** *Amount of plastic parts designed at ABB and their materials.* Helsinki: Pitäjänmäki, August 7, 2019.

**Palojoki, Vesa. 2019.** Photos of beryllium copper inserts. 2019.

**Pentagon Plastics LTD. 2019.** Pentagon Plastics LTD. [Online] 2019. [Cited: February 14, 2019.] https://www.pentagonplastics.co.uk/injection-moulding-process/.

**Rosato, Dominick V, Rosato, Donald V and Rosato, Marlene G. 2000.** *Injection molding handbook.* 3rd edition. Boston : Kluver Academic, 2000. 1460 p. ISBN 0-7923-8619-1.

**Selke, Susan E.M. and Culter, John D. 2016.** *Plastics packaging - properties, processing, applications, and regulations.* 3rd edition. Munich: Cincinnati : Hanser; Hanser Publications, 2016. 448 p. ISBN (electronic) 978-1-5231-0586-1.

**UL Prospector. 2013.** Industeel P20. [Online] December 12, 2013. [Cited: August 8, 2019.] https://materials.ulprospector.com/en/profile/default?e=215226.

**UL Prospector. 2017.** SLM 1.2344 (H13). [Online] December 19, 2017. [Cited: August 8, 2019.] https://materials.ulprospector.com/en/profile/default?e=252409.

**UL Prospector. 2013.** Uddeholm Elmax. [Online] December 12, 2013. [Cited: August 8, 2019.] https://materials.ulprospector.com/en/profile/default?e=215226.

**Wang, Maw-Ling, Chang, Rong-Yeu and Hsu, Chia-Hsiang (David). 2018.** *Molding Simulation: Theory and Practice.* Ohio : Hanser Publications, 2018. 531 p. ISBN (electronic) 978-1-56990-620-0.

**Yang, Yi, et al. 2016.** *Injection molding process control, monitoring, and optimization.* Munich: Cincinnati : Hanser Publishers, 2016. 413 p. ISBN (electronic) 978-1-5231-0590-8.